United States
Environmental Protection
Agency

Environmental Research
Laboratory
Athens GA 30613

EPA/600/3-89/048a
July 1989

Research and Development

EPA

Risk of Unsaturated/Saturated Transport and Transformation of Chemical Concentrations (RUSTIC)

Volume I: Theory and Code Verification

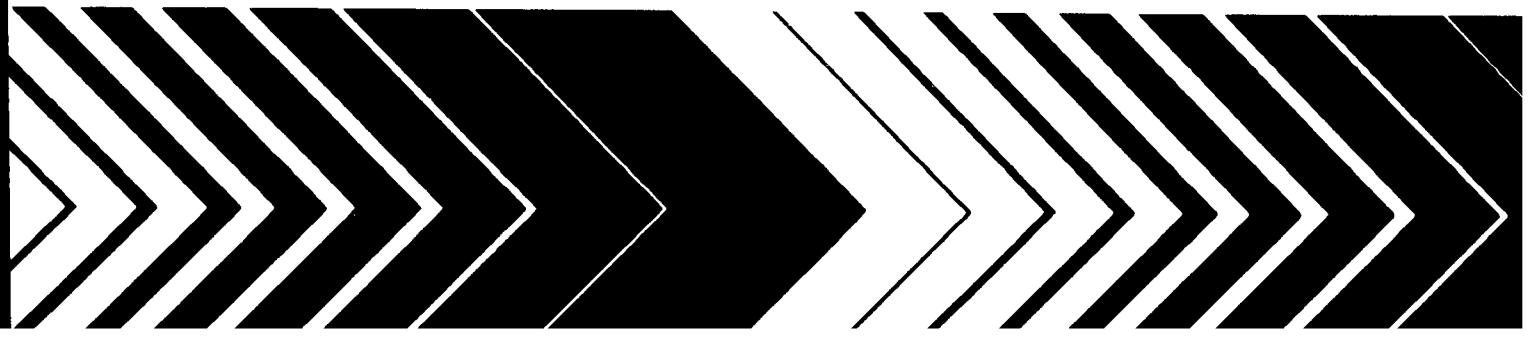

EPA/600/3-89/048a

RISK OF UNSATURATED/SATURATED TRANSPORT AND TRANSFORMATION OF CHEMICAL CONCENTRATIONS (RUSTIC)

Volume I: Theory and Code Verification

by

J.D. Dean,[1] P.S. Huyakorn,[2] A.S. Donigian, Jr.,[3]
K.A. Voos,[1] R.W. Schanz,[1] Y.J. Meeks[1], and R.F. Carsel[4]

Woodward-Clyde Consultants[1]
Oakland, CA 94607

HydroGeologic[2]
Herndon, VA 22070

AQUA TERRA Consultants[3]
Mountain View, CA 94043

Contract No. 68-03-6304

Project Officer
Robert F. Carsel
Assessment Branch
Environmental Research Laboratory[4]
U.S. Environmental Protection Agency
Athens, GA 30613

ENVIRONMENTAL RESEARCH LABORATORY
OFFICE OF RESEARCH AND DEVELOPMENT
U.S. ENVIRONMENTAL PROTECTION AGENCY
ATHENS, GA 30613

DISCLAIMER

The information in this document has been funded wholly or in part by the United States Environmental Protection Agency under Contract No. 68-03-6304 to Woodward-Clyde Consultants. It has been subject to the Agency's peer and administrative review, and it has been approved for publication as an EPA document. Mention of trade names of commercial products does not constitute endorsement or recommendation for use by the U.S. Environmental Protection Agency.

FOREWORD

As environmental controls become more costly to implement and the penalties of judgment errors become more severe, environmental quality management requires more efficient analytical tools based on greater knowledge of the environmental phenomena to be managed. As part of this Laboratory's research on the occurrence, movement, transformation, impact, and control of environmental contaminants, the Assessment Branch develops management or engineering tools to help pollution control officials reach decisions on the registration and restriction of pesticides used for agricultural purposes.

The pesticide regulatory process requires that the potential risk to human health resulting from the introduction or continued use of these chemicals be evaluated. Recently much of this attention has been focused on exposure through leaching of pesticides to groundwater and subsequent ingestion of contaminated water. To provide a tool for evaluating this exposure, the RUSTIC model was developed. RUSTIC simulates the transport of field-applied pesticides in the crop root zone, the unsaturated zone, and the saturated zone to a drinking water well, taking into account the effects of agricultural management practices. The model further provides estimates of probable exposure concentrations by taking into account the variability in the natural systems and the uncertainties in system properties and processes.

Rosemarie C. Russo, Ph.D.
Director
Environmental Research Laboratory
Athens, Georgia

ABSTRACT

This publication contains documentation for the RUSTIC model. RUSTIC links three subordinate models in order to predict pesticide fate and transport through the crop root zone, unsaturated zone, and saturated zone to drinking water wells: PRZM, VADOFT, and SAFTMOD. PRZM is a one-dimensional finite-difference model which accounts for pesticide fate and transport in the crop root zone. This release of PRZM incorporates several features in addition to those simulated in the original PRZM code: specifically, soil temperature simulation, volatilization and vapor phase transport in soils, irrigation simulation and a method of characteristics (MOC) algorithm to eliminate numerical dispersion. PRZM is now capable of simulating fate and transport of the parent compound and up to two daughter species. VADOFT is a one-dimensional finite-element code which solves the Richard's equation for flows in the unsaturated zone. The user may make use of constitutive relationships between pressure, water content, and hydraulic conductivity to solve the flow equations. VADOFT may also simulate the fate and transport of two parent and two daughter products. SAFTMOD is a two-dimensional finite-element model which simulates saturated solute flow and transport in either an X-Y or X-Z configuration. The codes are linked together with the aid of a flexible execution supervisor which allows the user to build models which are tailored to site-specific situations. In order to perform exposure assessments, the code is equipped with a Monte Carlo pre- and post-processor.

This report on the RUSTIC modeling system was submitted in fulfillment of two separate work assignments under Contract No. 68-03-6304 by Woodward-Clyde Consultants under the sponsorship of the U.S. Environmental Protection Agency. RUSTIC was developed by a Project Team headed by Woodward-Clyde Consultants as the prime contractor, with AQUA TERRA Consultants and HydroGeologic, Inc. as subcontractors. This report describes the work performed from January 1986 through September 1988. The final manuscript was prepared for publication and printing by AQUA TERRA Consultants under EPA Contract No. 68-03-3513.

TABLE OF CONTENTS

TABLE OF CONTENTS (continued)

TABLE OF CONTENTS (concluded)

FIGURES

FIGURES (continued)

FIGURES (continued)

FIGURES (continued)

FIGURES (continued)

TABLES

TABLES (concluded)

ACKNOWLEDGMENTS

A number of individuals contributed to this effort. Their roles are acknowledged in the following paragraphs.

Mr. Voos of Woodward-Clyde Consultants (WCC) programmed the execution supervisor and linked the models within the overall model architecture and design of RUSTIC developed by Mr. Jack Kittle of Aqua Terra Consultants. The model linkage was conceived by Mr. Dean and Dr. Atul Salhotra of WCC, Mr. Kittle, and Dr. Huyakorn. Dr. Huyakorn and his staff wrote the time/space bridging subroutines for the linkage.

Release II - PRZM was written by Dr. J. Lin and Mr. S. Raju of Aqua Terra Consultants under the direction of Mr. Donigian. Mr. Schanz (WCC) and Ms. Meeks (WCC) wrote the irrigation and MOC algorithms. Mr. Dean wrote the daughter products algorithms which were implemented by Dr. Lin.

The VADOFT code was written and documented by Dr. Huyakorn, H. White, J. Buckley, and T. Wadsworth of HydroGeologic. Mr. John Imhoff of Aqua Terra performed many useful testing simulations with VADOFT. SAFTMOD was written and documented by Dr. Huyakorn and J. Buckley.

The Monte Carlo pre- and post-processors were written by Dr. Salhotra, Mr. Phil Mineart, and Mr. Schanz of Woodward-Clyde. Final model assembly of the code and documentation and model testing was performed by Woodward-Clyde Consultants. Drs. Salhotra and P. Mangarella (WCC) peer reviewed the final documentation. The support of the editorial and graphics staff of WCC is appreciated.

The final manuscript was prepared for publication, incorporating review comments, by Ms. Susan Sharp-Hansen, Mr. S. Raju, and Ms. Dorothy Inahara of Aqua Terra Consultants.

The authors would like to acknowledge the support of the U.S. Environmental Protection Agency, and Mr. Lee Mulkey, Chief, Assessment Branch; Mr. Bob Carsel, Project Officer; and Dr. Rudy Parrish for their suggestions, input, and helpful comments.

SECTION 1

INTRODUCTION

This publication contains documentation for a linked model, known as RUSTIC, for contaminant transport in the root, vadose and saturated zones. A brief section on background and objectives for the model development effort follows in this introduction (Section 1.1). Section 1.2 gives a synopsis of risk and exposure assessment concepts. The reader who has sufficient background in these concepts may proceed to Section 1.3, which provides an overview of the RUSTIC linked modeling system, including major features and limitations. The documentation consists of two volumes, and Section 1.4 gives a synopsis of the contents of each. This introduction is common to both volumes.

1.1 BACKGROUND AND OBJECTIVES

The U.S. Environmental Protection Agency is continually faced with issues concerning the registration and restriction of pesticides used for agricultural purposes. Each of these regulatory processes requires that the potential risk to human health resulting from the introduction or continued use of these chemicals be evaluated. Recently, much of this attention has been focused on exposure through leaching of pesticides to groundwater and subsequent ingestion of contaminated water.

The capability to simulate the potential exposure to pesticides via this pathway has two major facets:

- Prediction of the fate of the chemical, after it is applied, as it is transported by water through the crop root zone, the vadose zone, and saturated zone to a drinking water well

- Evaluation of the probability of the occurrence of concentrations of various magnitudes at the drinking water well

There are a number of models which are capable of simulating the fate and transport of chemicals in the subsurface and in the root zone of agricultural crops. However, none of these models have been linked together in such a way that a complete simulation package, which takes into account the effects of agricultural management practices on fate and transport, is available for use either by the Agency or the agricultural chemical industry to address potential groundwater contamination problems. Without such a package, the decision maker must rely on modeling scenarios that are either incomplete or potentially incorrect. Each time a new scenario arises, recurring questions must be answered:

- What models should be used?

- How should mass transfer between models be handled?

The resolution of these issues for each scenario is both expensive and time consuming. Furthermore, it precludes consistency of approach to evaluation of contamination potential for various scenarios.

The modeling package described in this report seeks to overcome these problems by providing a consistent set of linked models which have the flexibility to handle a wide variety of hydrogeological, soils, climate, and pesticide scenarios. However, the formulation of the risk analysis problem requires more than a simple, deterministic evaluation of potential exposure concentrations. The inherent variability of force, capacitance and resistance in natural systems, combined with the inability to exactly describe these attributes of the system, suggests that exposure concentrations cannot be predicted with certainty. Therefore, the uncertainty associated with the predictions must be quantified. Consequently, this simulation package also seeks to provide this capability by utilizing Monte Carlo simulation techniques.

Stated more concisely, the objectives of this model development effort were to provide a simulation package which can:

- Simulate the fate and transport of field-applied pesticides in the crop root zone, the unsaturated zone, and the saturated zone to a drinking water well, taking into account the effects of agricultural management practices

- Provide probabilistic estimates of exposure concentrations by taking into account the variability in the natural systems and uncertainty in system properties and processes

Furthermore, it was desirable that the simulation package be easy to use and parameterize, and execute on the Agency's DEC/VAX machines. As a result, considerable effort has gone into providing parameter guidance for both deterministic and probabilistic applications of the model and software development for facile model implementation.

1.2 CONCEPT OF RISK AND EXPOSURE ASSESSMENT

Exposure assessment, as defined in the Federal Register (1984) for human impacts, is the estimation of the magnitude, frequency, and duration at which a quantity of a toxicant is available at certain exchange boundaries (i.e., lungs, gut, or skin) of a subject population over a specified time interval. Exposure assessment is an element of the larger problems of risk assessment and risk management, as demonstrated in Figure 1.1. The concentration estimates generated during an exposure assessment are combined with demographic and toxicological information to evaluate risk to a population--which can be used, in turn, to make policy decisions regarding the use or disposal of the chemical.

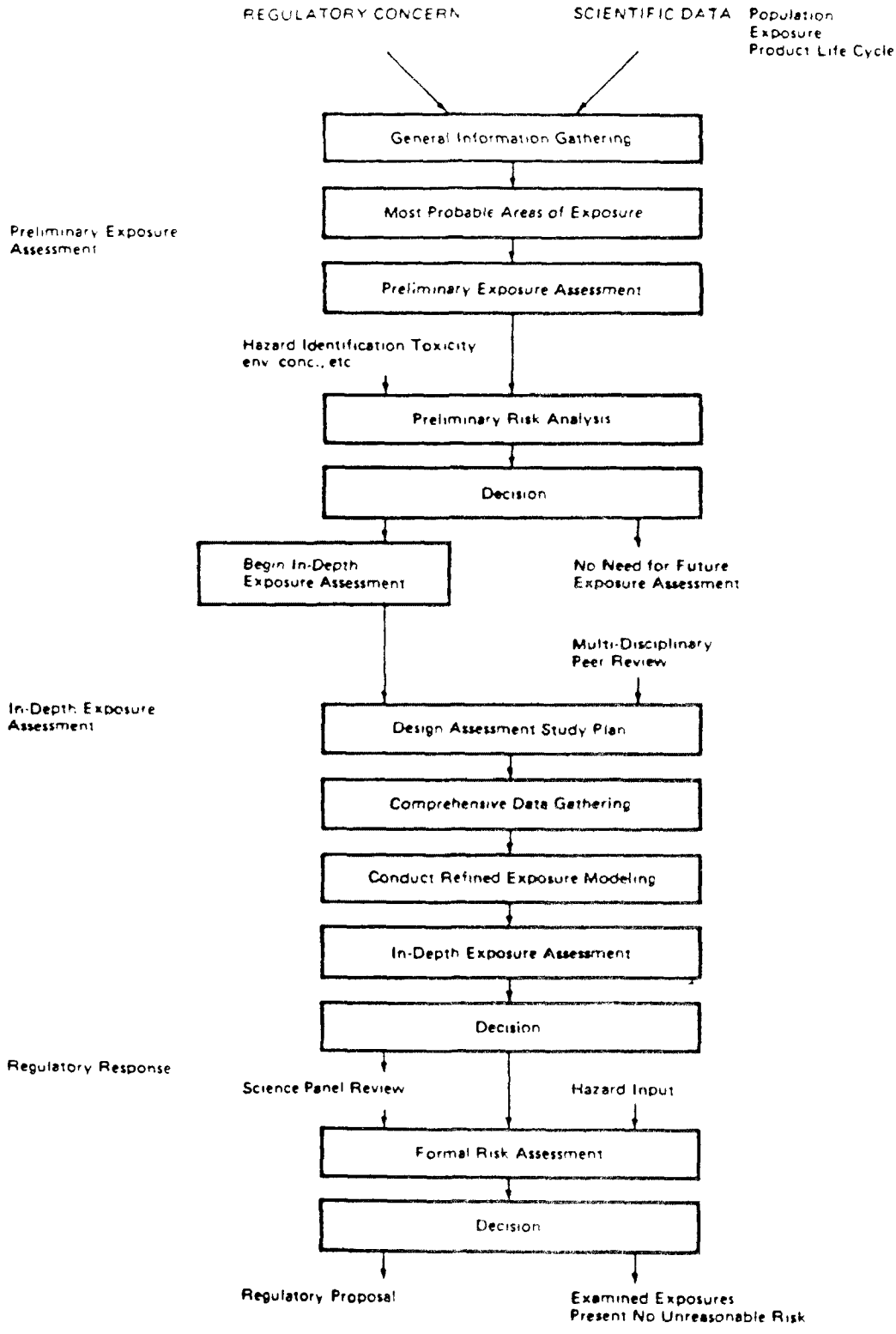

Figure 1.1. Decision path for risk assessment.

Major components of risk assessment are indicated below. Of these, the first three constitute the important steps for exposure assessment and are discussed in detail here.

- Characterization and quantification of chemical sources
- Identification of exposure routes
- Quantification of contaminant movement through the exposure routes to the receptor population/location
- Characterization of the exposed population
- Integration of quantified environmental concentrations with the characteristics of the exposed populations to yield exposure profiles

Characterization of sources(s) requires in a broad sense the estimation of the loading of a chemical into various environmental media. For the groundwater contamination problem, on a regional scale, this requires data on chemical uses and distribution of those uses (spatially and temporally). It also requires information on the crops being grown, registered or proposed chemical uses of those crops, and regional management practices. For a specific field-scale area, similar data would be needed to support an assessment; however, greater detail may be necessary.

The identification of exposure pathways involves a qualitative (or semiquantitative) assessment of how the chemical is thought to move from the source to the exposed population. Important fate processes which may serve to reduce the concentration of the chemical(s) along various pathways in different environmental media are also identified. For the case of groundwater exposure, important pathways and processes are predefined to a large extent in the models to be used.

The quantification of concentrations in a medium, given the source strength, pathways, and attenuation mechanisms along each pathway, is the next step, and is the major benefit of using models such as RUSTIC. The guidelines are very specific in the requirement that concentrations be characterized by duration and frequency as well as magnitude. These characteristics can be determined through the analysis of time series exposure data generated by the model.

The model produces a time series of toxicant concentrations in groundwater such as appears in Figure 1.2. The time series can be compared to a critical value of the concentration y. (This might be, for instance, the ADI [average daily intake level].) This type of analysis easily shows whether the criterion is exceeded and gives a qualitative feel for the severity of the exceedance state. A frequency distribution of the values of y (Figure 1.3) can be created by determining how often y is at a particular level or within a specific range. By choosing any value of y in Figure 1.2 and determining the area under the curve to the right of that value, Figure 1.4, which is a cumulative frequency distribution of the toxicant

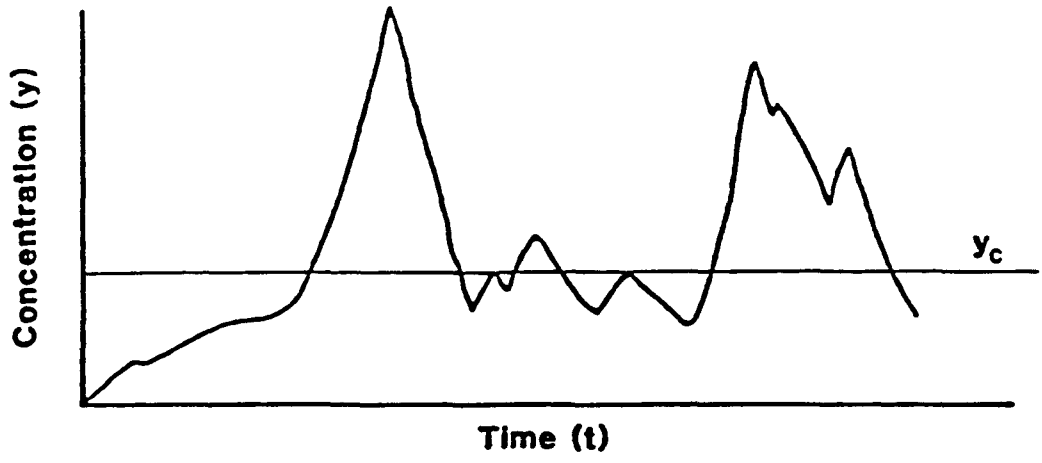

Figure 1.2. Time series plot of toxicant concentrations.

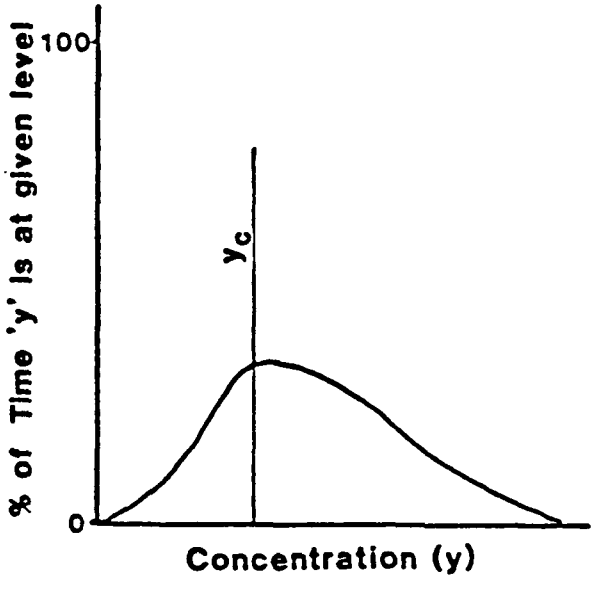

Figure 1.3.
Frequency distribution of toxicant concentrations.

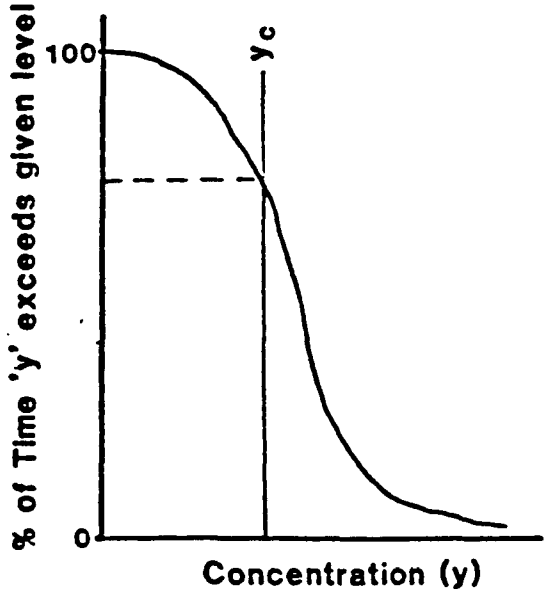

Figure 1.4.
Cumulative frequency distribution of toxicant concentrations.

concentration can be plotted. The cumulative frequency distribution shows the chance that any given value y will be exceeded. If the example time series is long enough, then the "chance" approaches the true "probability" that y will be exceeded.

Thus far, only the concentration to which the organism will be exposed has been discussed and nothing has been said concerning the duration of the event. If a window of length "t" is imposed on the time series at level y_c (Figure 1.5), and moved incrementally forward in time, a statement can be made concerning the toxicant concentration within the duration window. Normally, the average concentration within the window is used. The resulting cumulative frequency distribution shows the chance that the moving average of duration t_c will exceed the critical value of y, y_c. The moving average window should be the same length as that specified for y_c. For instance, in the case of cancer risk, a 70-year (lifetime) window is normally used to average the data in the simulated time series. The use of the moving window for averaging the time series allows us to compare both the concentration and duration against the standard. The chance or probability that the moving average concentration exceeds the standard is the essence of the exposure assessment. This type of information provides a precursor to the estimates of risk taken in using this chemical under the conditions of the model simulation. The use of models like RUSTIC which provide data of environmental concentrations and probability of occurrence ends here.

The next step in exposure assessment involves the characterization of the exposed population. Such factors as habits, age, sex, and location with respect to the source are of importance. The integration of concentration estimates and population characteristics makes possible the counting of the conditional events of concentration in an environmental medium and the opportunity for the population to be exposed to these concentrations. The exposure assessment ends at this point. The actual intake of chemicals, their fate within the human body (e.g., pharmacokinetics, toxicology), and their effects on the exposed population are not considered. These, however, are elements of the risk assessment.

Although the concepts underlying an exposure assessment are relatively simple, the actual application of these concepts is complicated because of large variations in source-specific and environment-specific characteristics and the necessity to integrate specialized knowledge from a number of different fields. This variability underscores the need to use a model such as RUSTIC in the evaluation of exposure concentrations.

1.3 OVERVIEW OF RUSTIC

This section gives an overview of the RUSTIC model highlighting the features and limitations of the simulation package as a whole and the component models PRZM, VADOFT, and SAFTMOD. The RUSTIC code was designed to provide state-of-the-art deterministic simulation of the fate and transport of pesticides, applied for agricultural purposes, in the crop root zone, the vadose zone, and the saturated zone. The model is capable of simulating multiple pesticides or parent/daughter relationships. The model is also

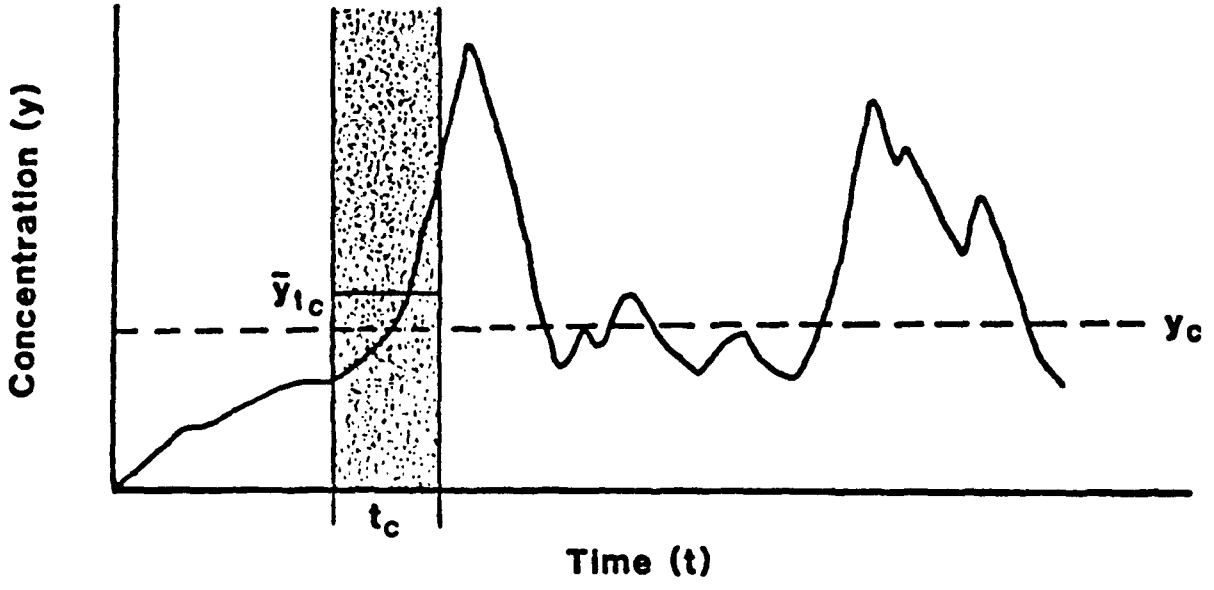

Figure 1.5. Time series of toxicant concentrations with moving average window of duration t_c.

capable of estimating probabilities of concentrations or fluxes in or fromthese various media for the purpose of performing exposure assessments.

To avoid writing an entirely new computer code, it was decided to make use of existing codes and software to the extent possible. Thus, due to its comprehensive treatment of important processes, its dynamic nature, and its widespread use and acceptability to the Agency and the agricultural chemical industry, the Pesticide Root Zone model (PRZM) (Carsel et al., 1984) was selected to simulate the crop root zone.

Having selected PRZM, several options were evaluated for developing the RUSTIC linked model to meet the objectives stated in Section 1.1. The first involved use of PRZM and a saturated zone model only. In this configuration, PRZM would be used to simulate both the root zone and the vadose zone. This option was eliminated because the assumptions of the elementary soil hydraulics in PRZM (i.e., drainage of the entire soil column to field capacity in one day) were considered inadequate for simulating flow in a thick vadose zone. The second involved the use of PRZM and a 2-D or 3-D variably saturated flow model. In this configuration, the latter model would represent both the vadose and saturated zones. Although the interface between the unsaturated and saturated zones would be more rigorously simulated, it was felt that the resulting code would be computationally too intensive for the intended application scenarios, and especially for use in a Monte Carlo (probabilistic) mode. Therefore, this option was also dropped.

The option finally selected is depicted in Figure 1.6. In this configuration, an enhanced version of PRZM is linked to a two-dimensional (single or two-layer) saturated zone model either directly or through a one-dimensional vadose zone flow and transport model. Both the vadose and saturated zone models simulate water flow and solute transport. A new code (VADOFT) was written to perform the flow and transport simulation in the vadose zone, and an existing code was modified to produce the two-dimensional X-Y, X-Z or axisymmetric simulation model for the saturated zone (SAFTMOD).

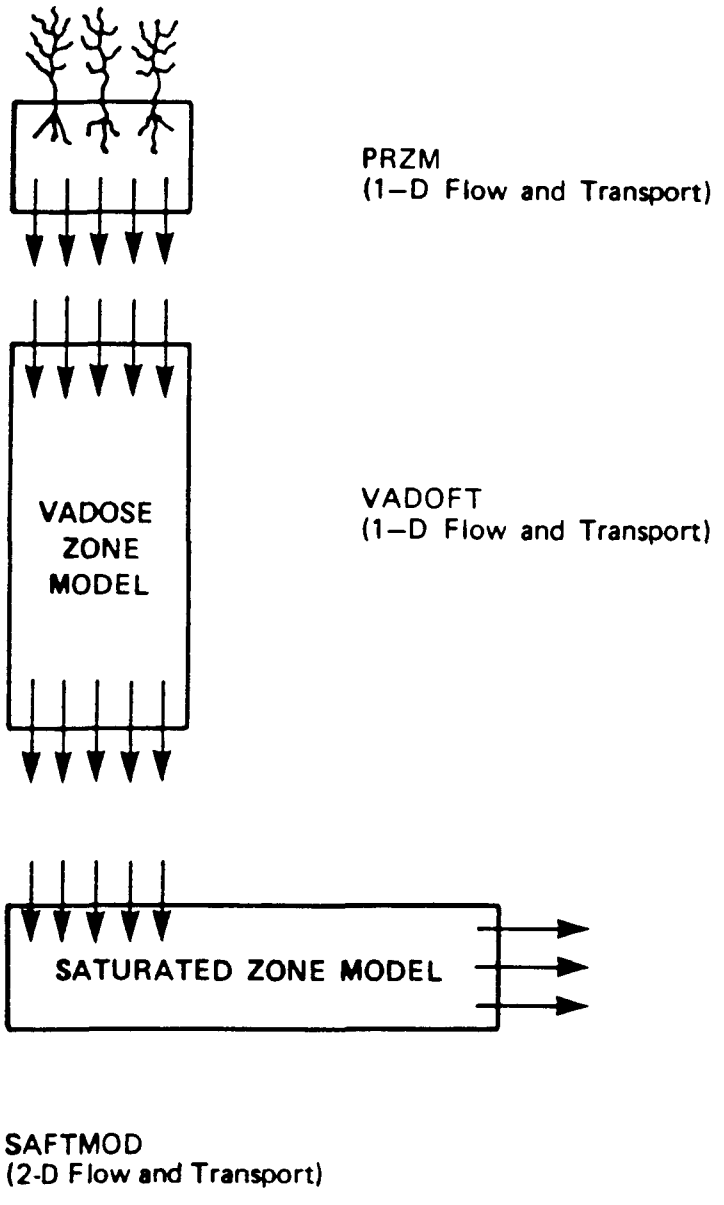

Figure 1.6. Linked modeling system configuration.

A significant problem associated with this type of linkage is the difference in time scales of the individual models. While the vadose zone models are required to operate on a daily or less-than-daily time step, the time step of the saturated zone model could vary from days to months. A second problem is the correct interfacing of the vadose and saturated zone models, especially for the case of a fluctuating water table. This requires special handling of the spatial discretizations in the two models. The solution to these linkage problems is discussed in detail in Section 5.

1.3.1 Overview of PRZM

1.3.1.1 Features--

The Pesticide Root Zone Model (PRZM) is a one-dimensional, dynamic, compartmental model that can be used to simulate chemical movement in unsaturated soil systems within and immediately below the plant root zone. It has two major components: hydrology (and hydraulics) and chemical transport. The hydrologic component for calculating runoff and erosion is based on the Soil Conservation Service curve number technique and the Universal Soil Loss Equation. Evapotranspiration is estimated either directly from pan evaporation data, or based on an empirical formula. Evapotranspiration is divided among evaporation from crop interception, evaporation from soil, and transpiration by the crop. Water movement is simulated by the use of generalized soil parameters, including field capacity, wilting point, and saturation water content. With a newly added feature, irrigation may also be considered.

The chemical transport component can simulate pesticide application on the soil or on the plant foliage. Dissolved, adsorbed, and vapor-phase concentrations in the soil are estimated by simultaneously considering the processes of pesticide uptake by plants, surface runoff, erosion, decay, volatilization, foliar washoff, advection, dispersion, and retardation. Two options are available to solve the transport equations: (1) the original backwards-difference implicit scheme that may be affected by excessive numerical dispersion at high Peclet numbers, or (2) the 'method of characteristics' algorithm which eliminates numerical dispersion while increasing model execution time.

Predictions are made on a daily basis. Output can be summarized for a daily, monthly, or annual period. Daily time series values of various fluxes or storages can be written to sequential files during program execution for subsequent analysis. In addition, a 'Special Action' option allows the user to output soil profile pesticide concentrations at user-specified times. With the Special Action option, the user can also change the values of certain parameters during the simulation period.

1.3.1.2 Limitations--

There were significant limitations in the original (Release I) version of PRZM. A few were obvious to the developers, while others were pointed out subsequently by model users. These are broken into four categories:

- Hydrology
- Soil hydraulics
- Method of solution of the transport equation
- Deterministic nature of the model

The Release II version of PRZM has been suitably modified to overcome many of these limitations.

Hydrologic and hydraulic computations are still performed in PRZM on a daily time step even though for some of the processes involved (evaporation, runoff, erosion) finer time step might be used to ensure greater accuracy and realism. For instance, simulation of erosion by runoff depends upon the peak runoff rate, which is in turn dependent upon the time base of the runoff hydrograph. This depends to some extent upon the duration of the precipitation event. PRZM retains its daily time step primarily due to the relative availability of daily versus shorter time step meteorological data. This limitation has in part been mitigated by enhanced parameter guidance.

In PRZM, Release I, the soil hydraulics were simple--all drainage to field capacity water content was assumed to occur within 1 day. (An option to make drainage time dependent was also included, but there is not much evidence to suggest that it was utilized by model users to any great extent.) This had the effect, especially in deeper soils, of inducing a greater-than-anticipated movement of chemical through the profile. While this representation of soil hydraulics has been retained in PRZM, the user has the option of coupling PRZM to VADOFT. PRZM is then used to represent the root zone, while VADOFT, with a more rigorous representation of unsaturated flow, is used to simulate the thicker vadose zone. The code VADOFT is discussed in more detail in a subsequent section. For short distances from soil surface to the water table, PRZM can be used to represent the entire vadose zone without invoking the use of VADOFT as long as no layers which would restrict drainage are present.

The addition of algorithms to simulate volatilization has brought into focus another limitation of the soil hydraulics representation. PRZM simulates only advective, downward movement of water and does not account for diffusive movement due to soil water gradients. This means that PRZM is unable to simulate the upward movement of water in response to gradients induced by evapotranspiration. This process has been identified by Jury et al. (1984) as an important one for simulating the effects of volatilization. However, the process would seem less likely to impact the movement of chemicals with high vapor pressures. For these chemicals, vapor diffusion would be a major process for renewing the chemical concentration in the surface soil.

Another limitation of the Release I model was the apparent inadequacy of the solution to the transport equation in advection-dominated systems. The backward difference formulation of the advection term tends to produce a high degree of numerical dispersion in such systems. This results in overprediction of downward movement due to smearing of the peak and subsequent overestimation of loadings to groundwater. In this new release, a new formulation is available for advection-dominated systems. The advective terms are decoupled from the rest of the transport equation and solved separately using the Method of Characteristics (MOC). The remainder of the transport equation is then solved as before, using the fully implicit scheme. This approach effectively eliminates numerical dispersion with,

however, an increase in the computation time. In low-advection systems, the MOC approach reduces to the original PRZM solution scheme, which becomes exact as velocities approach zero.

The final limitation is the use of field-averaged water and chemical transport parameters to represent spatially heterogeneous soils. Several researchers have shown that this approach produces slower breakthrough times than are observed using stochastic approaches. This concern has been addressed by adding the capability to run PRZM in a Monte Carlo framework. Thus, distributional, rather than field-averaged, values can be utilized as inputs which will produce distributional outputs of the relevant variables (e.g., flux to the water table).

1.3.2 Overview of the Vadose Zone Flow and Transport Model (VADOFT)

VADOFT is a finite-element code for simulating moisture movement and solute transport in the vadose zone. It is the second part of the three-component RUSTIC model for predicting the movement of pesticides within and below the plant root zone and assessing subsequent groundwater contamination. The VADOFT code simulates one-dimensional, single-phase moisture and solute transport in unconfined, variably saturated porous media. Transport processes include hydrodynamic dispersion, advection, linear equilibrium sorption, and first-order decay. The code predicts infiltration or recharge rate and solute mass flux entering the saturated zone. Parent/daughter chemical relationships may be simulated. The following description of VADOFT is adapted from Huyakorn et al. (1988a).

1.3.2.1 Features--

The code employs the Galerkin finite-element technique to approximate the governing equations for flow and transport and allows for a wide range of nonlinear flow conditions. Boundary conditions of the variably saturated flow problems may be specified in terms of prescribed pressure head or prescribed volumetric water flux per unit area. Boundary conditions of the solute transport problem may be specified in terms of prescribed concentration or prescribed solute mass flux per unit area. All boundary conditions may be time dependent. An important feature of the algorithm is the use of constitutive relationships for soil water characteristic curves based on soil texture.

1.3.2.2 Limitations--

Major assumptions of the flow model are that the flow of the fluid phase is one-dimensional, isothermal and governed by Darcy's law and that the fluid is slightly compressible and homogeneous. Hysteresis effects in the constitutive relationships of relative permeability versus water saturation, and water saturation versus capillary pressure head, are assumed to be negligible.

Major assumptions of the solute transport model are that advection and dispersion are one-dimensional, and fluid properties are independent of contaminant concentrations. Diffusive/dispersive transport in the porous-medium system is governed by Fick's law. The hydrodynamic dispersion coefficient is defined as the sum of the coefficients of mechanical

dispersion and molecular diffusion. Adsorption and decay of the solute is described by a linear equilibrium isotherm and a lumped first-order decay constant. Steady-state transport can not be simulated when decay is considered.

The code handles only single-phase flow (i.e., water) and ignores the presence of a second phase--i.e., air. The code does not take into account sorption nonlinearity or kinetic sorption effects which, in some instances, can be important. The code considers only single-porosity (granular) soil media. It does not simulate flow or transport in fractured porous media or structured soils.

1.3.3 Overview of the Saturated Zone Flow and Transport Model (SAFTMOD)

SAFTMOD is a finite element code for simulating groundwater flow and solute transport in the saturated zone. It is the third part of the three-component RUSTIC model for predicting the movement of pesticides within and below the plant root zone and assessing subsequent groundwater contamination. SAFTMOD performs two-dimensional simulations in an areal plane or a vertical cross section. In addition, the code can also perform axisymmetric simulations. Both single (unconfined or confined) and leaky two-aquifer systems can be handled. Transport of dissolved contaminants may also be simulated within the same domain. Transport processes accounted for include hydrodynamic dispersion, advection, linear equilibrium sorption, and first-order decay. Parent/daughter chemical relationships may be simulated. The following description of SAFTMOD is adapted from Huyakorn et al. (1988b).

1.3.3.1 Features--

The two dimensional analyses can be done in a transient or steady-state mode using SAFTMOD. The code employs the Galerkin finite-element technique to approximate the governing equations for flow and transport. For groundwater flow simulations the code accommodates water table conditions, recharge by infiltration or precipitation, and well pumping or injection. Boundary conditions of the saturated flow problem are specified in terms of prescribed hydraulic head (defined as the sum of pressure head and elevation), or prescribed volumetric water flux. Boundary conditions of the solute transport problem are specified in terms of prescribed concentration or prescribed solute mass flux. All boundary conditions can be time dependent.

1.3.3.2 Limitations--

The SAFTMOD code contains both saturated flow and solute transport models. Major assumptions of the flow model are that: Darcy's law is valid and hydraulic head gradients are the only significant driving mechanism for fluid flow, the porosity and hydraulic conductivity are constant with time, and gradients of fluid density, viscosity, and temperature do not affect the velocity distribution. For areal flow simulation in two-aquifer systems, vertical leakage is assumed in aquitards.

Major assumptions of the transport model are that fluid properties are independent of concentrations of contaminants. Contaminants are miscible

with in-place fluids. For areal transport simulations, advection in aquitards is assumed to be negligible. Diffusive/dispersive transport in the porous medium system is governed by Fick's law. The hydrodynamic dispersion coefficient is defined as the sum of the coefficients of mechanical dispersion and molecular diffusion. Adsorption and decay of the solute may be described by a linear equilibrium isotherm and a first-order decay constant. Steady-state transport can not be simulated when decay is considered.

Other limitations of the SAFTMOD code are that it simulates only single-phase water flow and solute transport in saturated porous media. It does not consider unsaturated or fractured media. Non-Darcy flow that may occur near pumping wells is neglected. The code does not take into account sorption nonlinearity or kinetic sorption effects which, in some instances, can be important.

1.3.4 Model Linkage

One of the more challenging problems in this model development effort was the temporal and spatial linkage of the component models. In the section which follows, these linkages are discussed.

1.3.4.1 Temporal Model Linkage--

The resolution of the temporal aspects of the three models was straightforward. PRZM runs on a daily time step. The time step in VADOFT is dependent upon the properties of soils and the magnitude of the water flux introduced at the top of the column. In order for the nonlinear Richards' equation to converge, VADOFT may sometimes require time steps on the order of minutes. The SAFTMOD time step, on the other hand, would normally be much longer than one day.

For simplicity, it was decided that the time step of SAFTMOD would always be an integer multiple of PRZM's daily time step. This makes the direct linkage of PRZM to SAFTMOD in a temporal sense very straightforward. PRZM is simply run for the number of days of the SAFTMOD time step, SAFTMOD is then run, and so forth. The water and pesticide fluxes from PRZM are summed and averaged over the length of the SAFTMOD time step. SAFTMOD receives the time-averaged fluxes as input.

For the linkage of PRZM, through VADOFT, to SAFTMOD, the resolution of time scales is also straightforward. VADOFT is prescribed to simulate to a "marker" time value, specifically to the end of a day. The last computational time step taken by VADOFT is adjusted so that it coincides with the end of the day. PRZM's daily water fluxes are used as input to VADOFT. VADOFT utilizes this flux as a constant over the day and adjusts its internal computational time step in order to converge. PRZM and VADOFT execute for the number of days corresponding to the SAFTMOD time step. The output from VADOFT is then time averaged and used as input to SAFTMOD.

1.3.4.2 Spatial Linkages--

The spatial linkages utilized for the models are more complex. The principal problem is the presence of a fluctuating water table, which complicates the interfacing of the vadose (or root zone) and saturated zone

codes. A second problem is that of the incompatibility between the hydraulics in PRZM and VADOFT. Of course, any linking scheme utilized must provide a realistic simulation of the flow of water and transport of solutes at the interfaces and must ensure mass balance.

PRZM and VADOFT--The major problem with the interfacing of these two models is that while VADOFT solves the Richards' equation for water flow in a variably saturated medium, PRZM uses simple "drainage rules" to move water through the soil profile. Because of this incompatibility, there may be times when PRZM produces too much water for VADOFT to accommodate within one day. This is very likely to happen in agricultural soils, where subsoils are typically of lower permeability than those of the root zone, which have been tilled and perforated by plant roots and soil biota. The result of this would be water ponded at the interface which would belong neither to PRZM or VADOFT.

The solution was to prescribe the flux from PRZM into VADOFT so that VADOFT accommodates all the water output by PRZM each day. This eliminates the problem of ponding at the interface. However, it does force more water into the vadose zone than might actually occur in a real system, given the same set of soil properties and meteorological conditions. The consequence is that water and solute are forced to move at higher velocities in the upper portions of the vadose zone. If the vadose zone is deep, then this condition probably has little impact on the solution. If it is shallow, however, it could overestimate loadings to groundwater, especially if chemical degradation rates are lower in the vadose zone than in the root zone.

VADOFT and SAFTMOD--The principal problem here is that of the presence of a dynamic boundary (rising and falling water table) between these models. Two approaches were considered to handle the problem. The first was to expand or contract the spatial domains of the models to accommodate the moving boundary. This is not a particularly insurmountable problem for the vadose zone model; however, for the saturated zone model it would require the addition of nodes at the upper boundary. This would require a constant evaluation and switching of the set of nodes receiving fluxes from the vadose zone. This appeared undesirable.

The second option was to overlap the spatial domains of the models and interpolate values for fluxes based upon the position of the water table. This latter approach was ultimately utilized. It has the additional feature of eliminating the effects of the bottom boundary conditions prescribed for the vadose zone model on the simulation of solute transport just above the water table. A detailed discussion of these spatial linkages is given in Section 5.

1.3.5 Monte Carlo Processor

RUSTIC can be run in a Monte Carlo mode so that probabilistic estimates of pesticide loadings to the saturated zone or concentrations in a well downgradient from the source area can be made. The input preprocessor allows the user to select distributions for key parameters from a variety of

distributions; the Johnson family (which includes the normal and lognormal), uniform, exponential and empirical. If the user selects distributions from the Johnson family, he may also specify correlations between the input parameters. The Monte Carlo processor reads the standard deterministic input data sets for each model, then reads a Monte Carlo input file which specifies which parameters are to be allowed to vary, their distributions, the distribution parameters, and correlation matrix. The model then executes for a prespecified number of runs.

The output processor is capable of preparing statistics of the specified output variables including mean, maximum values and quantiles of the output distribution. The output processor also can tabulate cumulative frequency histograms of the output variables and send them to a line printer for plotting.

1.3.6 Overview Summary

A modeling system (RUSTIC) has been developed for the U.S. Environmental Protection Agency which is capable of simulating the fate and transport of pesticides, following application, through the crop root zone, vadose zone and saturated zone and into drinking water wells. The model is envisioned for use in simulating farms or small communities, and was designed to handle a variety of geometries likely to be encountered in performing evaluations for pesticide registration or special reviews. A major objective was also to keep the model simple and efficient, yet allow use in a Monte Carlo mode to generate probabilistic estimates of pesticide loadings or well water concentrations. The model consists of three major computational modules; PRZM, which performs fate and transport calculations for the crop root zone and is capable of incorporating the effects of management practices; VADOFT, which simulates one-dimensional flow and transport within the vadose zone; and SAFTMOD, which simulates two dimensional flow and transport in the saturated zone. SAFTMOD is capable of simulating a variety of aquifer geometries (water table, confined and leaky two-aquifer systems) and can perform areal, cross-sectional and axisymmetric simulations. Linkage of these models is accomplished through the use of simple bridging algorithms which conserve water and solute mass.

1.4 OVERVIEW OF VOLUMES I AND II

Documentation for RUSTIC has been produced in two volumes. The subject of Volume I is model theory and code verification or testing. It contains a description of the theory underlying the PRZM, VADOFT, and SAFTMOD codes. The description of each code includes a brief overview highlighting the features and limitations of each code. This is followed by detailed descriptions of the algorithms involved in each code and how they are solved numerically. The description of each of these models concludes with a section on algorithm testing. The fifth section of Volume I contains a description of the theory behind the linkage of the three codes to provide a cohesive simulation of the movement of pesticides following application, through the root zone, the vadose zone, and the saturated zone to a drinking water well. Section 6 of Volume I covers the theory behind the uncertainty preprocessor. Volume I concludes with model development references and appendices.

Volume II is a model user's guide. It opens with an introduction and a section on the installation of the code on the target computer systems. Section 3 has a user-directed overview of the model software, simulation modules, and a description of data bases for simulation support and parameter estimation. The fourth section takes the user through problem definition and model setup, and module input sequence building. Section 5 covers parameter estimation for the execution supervisor and each computational module. Section 6 takes the user through an example problem. Following the references (Section 7), Section 8 contains appendices which include a listing of error messages and warnings, a variable glossary, and sample input and output for the example problem of Section 6.

SECTION 2

PESTICIDE ROOT ZONE MODEL (PRZM RELEASE II)

2.1 INTRODUCTION AND BACKGROUND

This section describes the theoretical background for a mathematical simulation model (PRZM) that has been developed and partially tested to evaluate pesticide leaching from the crop root zone under field crop conditions.

Following this short introduction, Section 2.2 describes the features and limitations of the model. A description of the theory, including a detailed description of the equations solved, is provided in Section 2.3. An outline of the numerical implementation techniques used by the model to apply the theory to the simulation of physical problems follows. This section concludes with a discussion of testing results for new algorithms which have been added in this release.

2.1.1 Introduction

Pesticide leaching from agricultural fields as nonpoint source loads can lead to groundwater contamination. Nonpoint source contamination is characterized by highly variable loadings, with rainfall and irrigation events dominating the timing and magnitude of the loading of pesticides leaching below the root zone. The potentially widespread, areal nature of resulting contamination makes remedial actions difficult because there is no single plume emanating from a "point source" (the more common groundwater problem) that can be isolated and controlled. In any case, a more prudent approach to prevention or reduction of pesticide groundwater contamination must be based on understanding the relationships among chemical properties, soil system properties, and the climatic and agronomic variables that combine to induce leaching. Knowledge of these relationships can allow a priori investigation of conditions that lead to problems, and appropriate actions can be taken to prevent widespread contamination.

Many investigators have studied the factors contributing to pesticide leaching. These investigations have shown that chemical solubility in water, sorptive properties, volatility, formulation, and soil persistence determine the tendency of pesticides to leach through soil. Similarly, the important environmental and agronomic factors include soil properties, climatic conditions, crop type, and cropping practices. In short, the hydrologic cycle interacts with the chemical characteristics to transform and transport pesticides within and out of the root zone. Vertical movement out of the

root zone can result in groundwater contamination and is the problem which the model is designed to investigate.

Numerical models for the movement of solutes in porous media for steady-state, transient, homogenous, and multi-layered conditions have been previously developed. Included in such studies have been linear and nonlinear sorption, ion exchange, and other chemical-specific reactions. These investigations have proven valuable in interpreting laboratory data, investigating basic transport processes, and identifying controlling factors in transport and transformation. As noted in a recent review of models for simulating the movement of contaminants through groundwater flow systems, however, the successful use of such models requires a great deal of detailed field data. This unfortunate conclusion arises from the scaling problems associated with laboratory experiments and the traditional solution of the appropriate partial differential equations at points or nodes in a finite-difference or finite-element grid network. Each spatial segment modeled must be properly characterized--a most expensive, if not impossible, task for many modeling problems.

Such problems in modeling pesticide leaching with existing procedures are discouraging when one considers the need to evaluate future problems arising from pesticides not yet widely distributed or used. Models used to perform such evaluations should conform to the maximum possible extent to known theory, but must be structured to enable efficient analysis of field situations with minimal requirements for specialized field data. In short, the goal is to integrate the essential chemical-specific processes for leaching with reasonable estimates of water movement through soil systems. Data input requirements must be reasonable in spatial and temporal requirements and generally available from existing data bases. This model attempts to meet these objectives.

2.1.2 Background

The Pesticide Root Zone Model (PRZM) (Carsel et al., 1984; Carsel et al., 1985) was selected as the code to provide the capability to simulate the fate and transport of agriculturally applied pesticides in the crop root zone. PRZM was initially designed for this purpose and has attained a degree of acceptability in both the regulatory community and in the agricultural chemical industry. Therefore, its utility in accomplishing the objective of this model development effort is obvious.

2.2 FEATURES AND LIMITATIONS

2.2.1 Features

The Pesticide Root Zone Model (PRZM Release II) is a one-dimensional, dynamic, compartmental model for use in simulating chemical movement in unsaturated soil systems within and immediately below the plant root zone (see Figure 2.1). PRZM allows the user to perform simulations of potentially toxic chemicals, particularly pesticides, that are applied to the soil or to plant foliage. Dynamic simulations allow the consideration of pulse loads, the prediction of peak events, and the estimation of time-varying mass

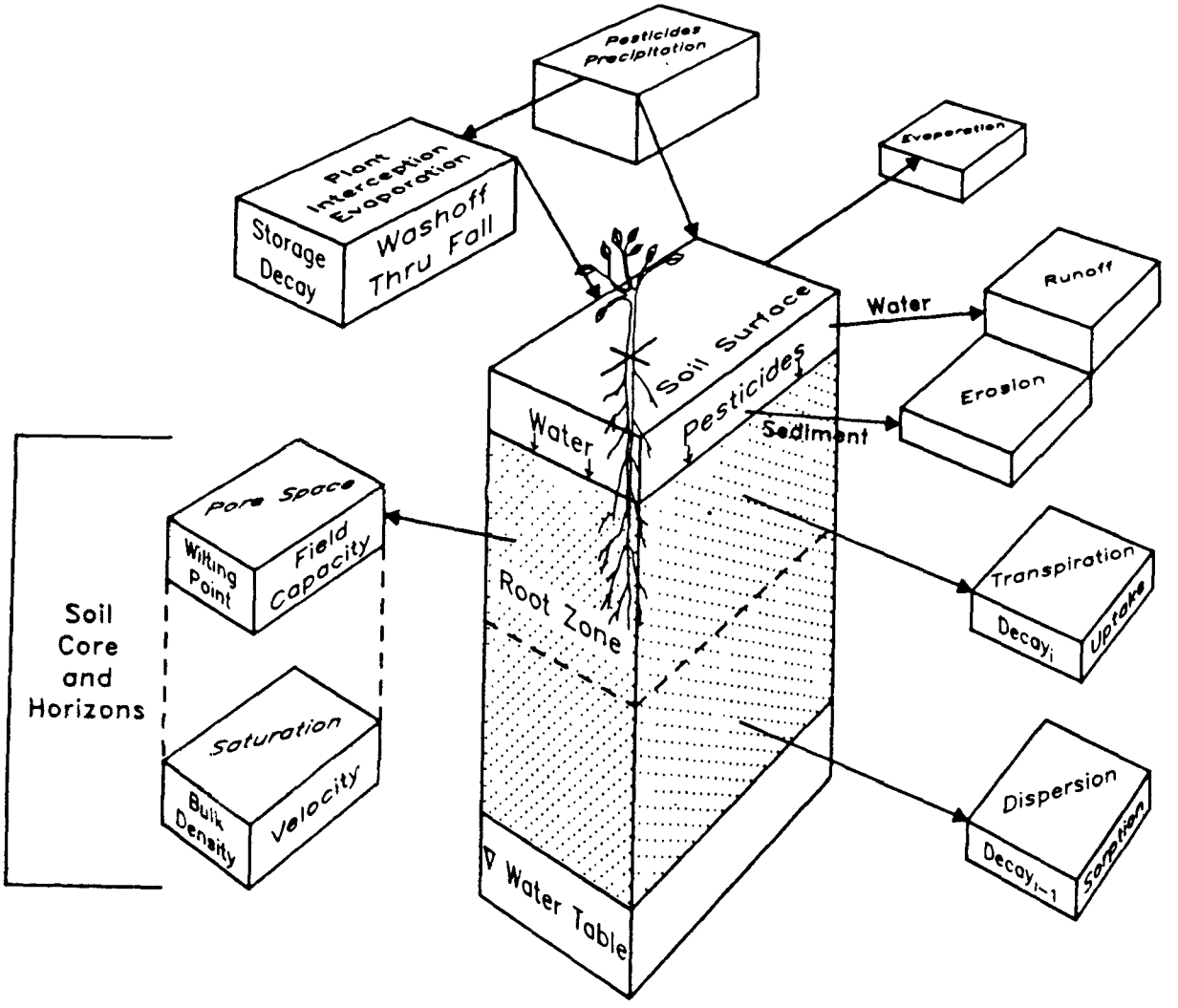

Figure 2.1. Pesticide root zone model.

emission or concentration profiles, thus overcoming limitations of the more commonly used steady-state models. Time-varying transport by both advection and dispersion in the dissolved phase or diffusion in the gas phase are represented in the program.

PRZM has two major components: hydrology and chemical transport. The hydrologic component for calculating runoff and erosion is based on the Soil Conservation Service curve number technique and the Universal Soil Loss Equation. Evapotranspiration is estimated from pan evaporation data, or by an empirical formula if input pan data are unavailable. Evapotranspiration is divided among evaporation from crop interception, evaporation from soil, and transpiration by the crop. Water movement is simulated by the use of generalized soil parameters, including field capacity, wilting point, and saturation water content. Irrigation may also be considered.

Dissolved, adsorbed, and vapor-phase concentrations in the soil are estimated by simultaneously considering the processes of pesticide uptake by plants, surface runoff, erosion, decay, volatilization, foliar washoff, advection, dispersion, and retardation. The user may elect to solve the transport equations using one of two finite-difference numerical solutions, the original backwards-difference implicit scheme featured in the first release, or a Method of Characteristics algorithm which greatly reduces numerical dispersion, but increases model execution time.

The hydrologic components of pesticide transport equations (i.e., moisture content and soil-water velocities) are decoupled, solved separately, and used to numerically integrate the equation in succeeding time steps. Predictions are made on a daily basis. Output can be summarized on a daily, monthly, or annual period. A daily time series value for various fluxes or storages can be written to sequential files during program execution.

2.2.2 Limitations

There were severe limitations of the PRZM Release I Code, some which were obvious to the developers and some which were pointed out subsequently by model users. These are broken into four categories:

- Hydrology
- Soil hydraulics
- Method of solution of the transport equation
- Deterministic nature of the model

In Release II, many of these limitations have, to an extent, been overcome.

Hydraulic computations are performed in PRZM on a daily time step; however, some of the processes involved (evaporation, runoff, erosion) are clearly among those which might be simulated on a finer time step to ensure greater accuracy and realism. For instance, simulation of erosion by runoff depends upon the peak runoff rate, which is in turn dependent upon the time base of the runoff hydrograph. This depends to some extent upon the duration of the precipitation event. PRZM retains its daily time step in this release primarily due to the relative availability of daily versus shorter time step

meteorological data. Hopefully, a portion of this limitation has been mitigated by enhanced parameter guidance.

The method of computing potential evapotranspiration using Hamon's formula, in the absence of some evaporation data, has also been retained. Evapotranspiration from irrigated citrus in Florida was found to be substantially underpredicted when using this method to estimate potential evapotranspiration (Dean and Atwood 1985). Users should carefully check the model's hydrologic simulation when using this option.

The capability to simulate soil temperature has been added to this release of PRZM in order to correct Henry's constant for the temperature occurring in various depths in the soil when performing vapor-phase calculations. Removal of water by evaporation versus transpiration from the profile may have a pronounced effect on soil temperature. This is due to the fact that more heat is removed during the process of evaporation because the energy necessary to vaporize water leaves the system, producing a cooling effect. No differentiation is made between evaporation and transpiration in PRZM at this time.

In PRZM, Release I, the soil hydraulics were simple--all drainage to field capacity water content was assumed to occur within 1 day. (An option to make drainage time dependent was also included, but there is not much evidence to suggest that it was utilized by model users to any great extent). This had the effect, especially in larger soil cores, of inducing a greater-than-anticipated movement of chemical through the profile. While this representation of soil hydraulics has been retained in PRZM, the user has the option, with the linked modeling system, of coupling PRZM to VADOFT. PRZM is then used to represent the root zone, while VADOFT, with a more rigorous representation of unsaturated flow, is used to simulate the thicker vadose zone. The difficulties in parameterizing the Richards equation for unsaturated flow in VADOFT is overcome by using the technique of van Genuchten to generate soil water characteristic curves using soil textural information. For short soil cores, PRZM can obviously be used to represent the entire vadose zone.

The addition of algorithms to simulate volatilization has brought into focus another limitation of the soil hydraulics representation. PRZM simulates only advective, downward movement of water and does not account for diffusive movement due to soil water gradients. This means that PRZM is unable to simulate the upward movement of water in response to gradients induced by evapotranspiration. This process has been identified by Jury et al. (1984) as an important one for simulating the effects of volatilization. However, the process would seem less likely to impact the movement of chemicals with high vapor pressures. For these chemicals, vapor diffusion would be a major process for renewing the chemical concentration in the surface soil.

Another limitation of the Release I model was the inadequacy of the solution to the transport equation in advection-dominated systems. The backward difference formulation of the advection term tends to produce a high degree of numerical dispersion in such systems. This results in overprediction of downward movement due to smearing of the peak and subsequent overestimation

of loadings to groundwater. In this new release, a new formulation is available for advection-dominated systems. The advective terms are decoupled from the rest of the transport equation and solved separately using a Method of Characteristics (MOC) formulation. The remainder of the transport equation is then solved as before, using the fully implicit scheme. This approach effectively eliminates numerical dispersion, but with some additional overhead expense in computation time. In low-advection systems, the MOC approach reduces to the original PRZM solution scheme, which is exact for velocities approaching zero.

The final limitation is the use of field-averaged water and chemical transport parameters to represent spatially heterogeneous soils. Several researchers have shown that this approach produces slower breakthrough times than are observed using stochastic approaches. This concern has been addressed by adding the capability to run PRZM in a Monte Carlo framework. Thus, distributional, rather than field-averaged, values can be utilized as inputs which will produce distributional outputs of the relevant variables (e.g., flux to the water table).

2.3 DESCRIPTION OF THE EQUATIONS

The mathematical description of the processes simulated by PRZM are broken down in the following discussion into five categories:

- Transport in Soil
- Water Movement
- Soil Erosion
- Volatilization
- Irrigation

The first three categories were simulation options previously available in PRZM Release I. Since the capability to simulate ponding is new, the mathematical basis of the ponding algorithms is described in detail. The final process, volatilization, was not available in previous releases of PRZM, and its theoretical basis is also described in detail.

2.3.1 Transport in Soil

The PRZM model was derived from the conceptual, compartmentalized representation of the soil profile as shown in Figure 2.2. From consideration of Figure 2.2, it is possible to write mass balance equations for both the surface zone and the subsurface zones. Addition of the vapor phase and ponded water compartments in PRZM require the consideration of additional terms. The surface zone expressions for each of the dissolved, adsorbed, and vapor phases can be written as:

$$\frac{A\ \Delta z\ \partial(C_w\theta)}{\partial t} = J_D - J_V - J_{DW} - J_U - J_{QR} + J_{APP} + J_{FOF} \pm J_{TRN} \qquad (2\text{-}1)$$

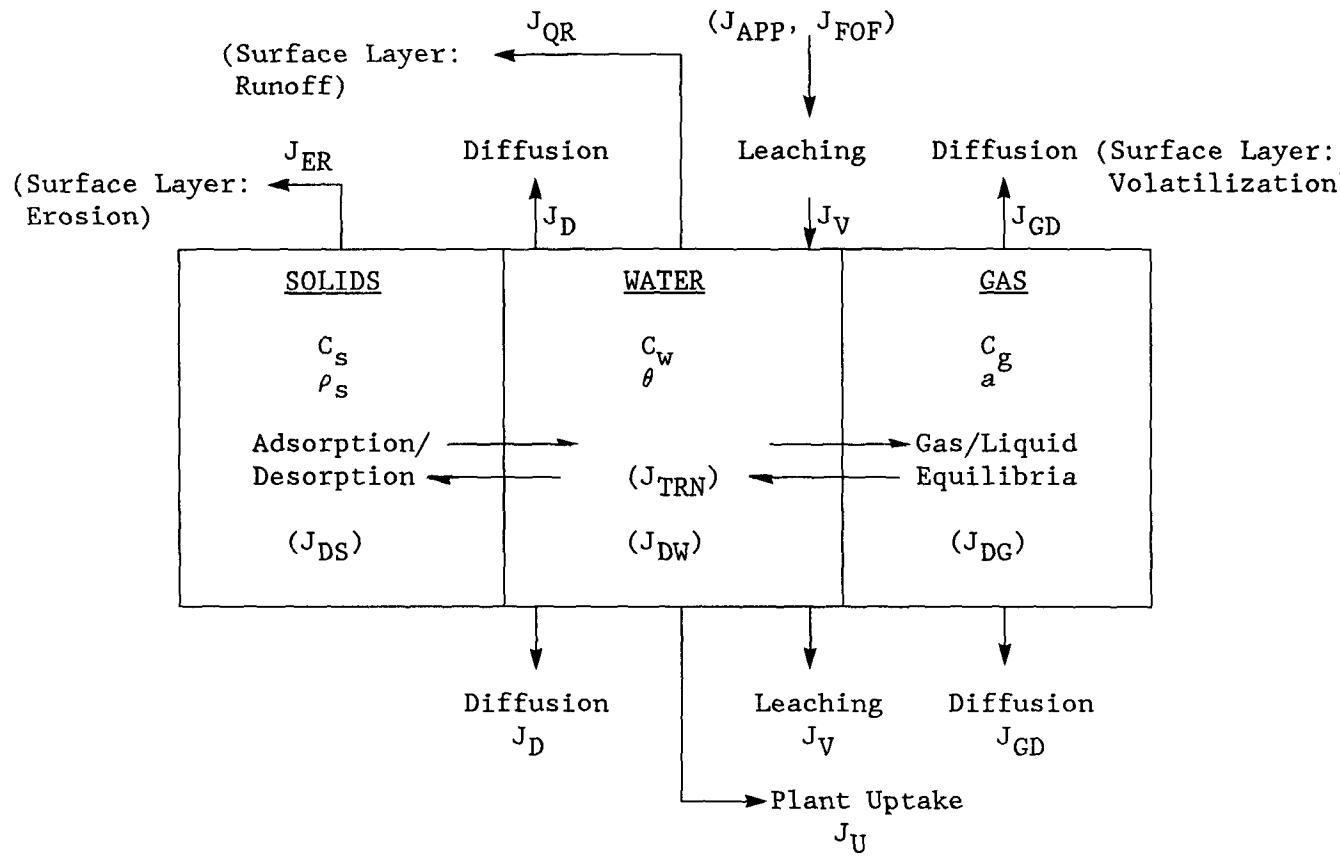

Figure 2.2. *Schematic representation of a single chemical in a soil layer.*

$$\frac{A\ \Delta z\ \partial(C_s \rho_s)}{\partial t} = -\ J_{DS} - J_{ER} \qquad (2\text{-}2)$$

$$\frac{A\ \Delta z\ \partial(C_g a)}{\partial t} = J_{GD} - J_{DG} \qquad (2\text{-}3)$$

where

A = cross-sectional area of soil column (cm^2)

Δz = depth dimension of compartment (cm)

C_w = dissolved concentration of pesticide ($g\ cm^{-3}$)

C_s = sorbed concentration of pesticide ($g\ g^{-1}$)

C_g = gaseous concentration of pesticide ($g\ cm^{-3}$)

θ = volumetric water content of soil ($cm^3\ cm^{-3}$)

a = volumetric air content of the soil ($cm^3\ cm^{-3}$)

ρ_s = soil bulk density ($g\ cm^{-3}$)

t = time (d)

J_D = represents the effect of dispersion and diffusion of dissolved phase ($g\ day^{-1}$)

J_V = represents the effect of advection of dissolved phase ($g\ day^{-1}$)

J_{GD} = represents the effect of dispersion and diffusion in vapor phase ($g\ day^{-1}$)

J_{DW} = mass loss due to degradation in the dissolved phase ($g\ day^{-1}$)

J_{DG} = mass loss due to degradation in the vapor phase ($g\ day^{-1}$)

J_U = mass loss by plant uptake of dissolved phase ($g\ day^{-1}$)

J_{QR} = mass loss by removal in runoff ($g\ day^{-1}$)

J_{APP} = mass gain due to pesticide deposition on the soil surface ($g\ day^{-1}$)

J_{FOF} = mass gain due to washoff from plants to soil ($g\ day^{-1}$)

J_{DS} = mass loss due to degradation of sorbed phase chemical ($g\ day^{-1}$)

J_{ER} = mass loss by removal on eroded sediments ($g\ day^{-1}$)

J_{TRN} = mass gain or loss due to parent/daughter transformations

Equations for the subsurface zones are identical to Equations (2-1), (2-2), and (2-3) except that J_{QR}, J_{FOF}, and J_{ER} are not included. J_{APP} applies to subsurface zones only when pesticides are incorporated into the soil. For subsurface layers below the root zone, the term J_U is also not utilized.

Note that terms representing phase transfers (e.g., volatilization) are neglected in Equations (2-1) through (2-3) because they cancel when the equations are added (see Equation (2-19) below).

Each term in Equations (2-1) through (2-3) are now further defined. Dispersion and diffusion in the dissolved phase are combined and are described using Fick's law as

$$J_D = - \frac{A \, \Delta z \, D_w \, \partial^2 (C_w \theta)}{\partial z^2} \tag{2-4}$$

where

D_w = diffusion-dispersion coefficient for the dissolved phase, assumed constant (cm^2 day^{-1})

C_w = dissolved concentration of pesticide (g cm^{-3})

θ = volumetric soil water content (cm^3 cm^{-3})

x = soil depth dimension (cm)

In a similar manner, dispersion and diffusion in the vapor phase are described by Fick's law as

$$J_{GD} = - \frac{A \, \Delta z \, D_g \, \partial^2 (C_g a)}{\partial z^2} \tag{2-5}$$

where

D_g = Molecular diffusivity of the pesticide in the air-filled pore space (cm^2 day^{-1})

C_g = vapor-phase concentration of pesticide (g cm^{-3})

a = volumetric air content (cm^3 cm^{-3})

The dependence of the molecular diffusivity of the pesticide in air-filled pore space on the volumetric air content is described by the Millington-Quirk expression (Jury et al., 1983a)

$$D_g = \frac{a^{10/3}}{n^2} D_a$$

where

a = the air-filled porosity ($cm^3\ cm^{-3}$)

ϕ = total porosity ($cm^3\ cm^{-3}$)

D_a = molecular diffusivity of the chemical in air, assumed constant ($cm^2\ day^{-1}$)

The mathematical theory underlying the diffusive and dispersive flux of pesticide in the vapor phase within the soil and into the overlying air can be found in the section describing volatilization.

The advective term for the dissolved phase, J_V, describes the movement of pesticide in the bulk flow field and is written as

$$J_V = \frac{A\ \Delta z\ V\ \partial(C_w \theta)}{\partial z} \qquad (2\text{-}6)$$

where

V = velocity of water movement ($cm\ day^{-1}$)

Vapor-phase advection has not been included as a flux in the transport equation. A number of researchers have indicated a consensus that vapor-phase advection is not likely to be significant for agricultural situations (W. Jury, W. Spencer, W. Farmer, L. Thibodeaux - personal communications, 1987). Early studies of water vapor movement suggested that the fluctuation of barometric pressure at the soil surface could act as a pumping mechanism for vapor-phase advective transport (Fukuda 1955; Farrell et al., 1966; Scotter and Raats 1970). However, using models for vapor emissions from landfills, Thibodeaux et al. (1982) found that atmospheric pressure fluctuations increased the total emission rate for benzene by only 15%, compared to constant pressure conditions. Therefore, it appears to be a reasonable assumption at this time to neglect vapor-phase advection in modeling chemical migration for agricultural situations.

Degradation of a pesticide in or on soil may be due to such processes as hydrolysis, photolysis, and microbial decay. If these processes follow pseudo first-order kinetics, the rate coefficients may be combined into a single decay coefficient. Assuming the same rate constants for the solid and dissolved phases, the rate of change of chemical out of each phase due to decomposition may be written as:

$$J_{DW} = K_s\ C_w\ \theta\ A\ \Delta z \qquad (2\text{-}7)$$

$$J_{DS} = K_s \; C_s \; \rho_s \; A \; \Delta z \tag{2-8}$$

$$J_{DG} = K_g \; C_g \; a \; A \; \Delta z \tag{2-9}$$

where

K_s = lumped, first-order decay constant for solid and dissolved phases (day^{-1})

K_g = lumped, first-order decay constant for vapor phase (day^{-1})

C_s = solid-phase concentration of pesticide ($g \; g^{-1}$)

Plant uptake of pesticides is modeled by assuming that uptake of a pesticide by a plant is directly related to transpiration rate. The uptake is given by:

$$J_U = f \; C_w \; \theta \; \epsilon \; A \; \Delta z \tag{2-10}$$

where

J_u = uptake of pesticide ($g \; day^{-1}$)

f = the fraction of total water in the zone used for transpiration (day^{-1})

ϵ = an uptake efficiency factor or reflectance coefficient (dimensionless)

Erosion and runoff losses as well as inputs to the surface zone from foliar washoff are considered in the surface layer. The loss of pesticide due to runoff is

$$J_{QR} = \frac{Q}{A_w} \; C_w \; A \tag{2-11}$$

in which

J_{QR} = pesticide loss due to runoff ($g \; day^{-1}$)

Q = the daily runoff volume ($cm^3 \; day^{-1}$)

A_w = watershed area (cm^2)

and the loss of pesticide due to erosion is

$$J_{ER} = \frac{p\ X_e\ r_{om}\ C_s\ A}{A_w} \qquad (2\text{-}12)$$

where

J_{ER} = the pesticide loss due to erosion (g day^{-1})

X_e = the erosion sediment loss (metric tons day^{-1})

r_{om} = the enrichment ratio for organic matter (g g^{-1})

p = a units conversion factor (g $tons^{-1}$)

Soil erosion is discussed in more detail in Section 2.3.3.

Pesticides can be applied to either bare soil if pre-plant conditions prevail or to a full or developing crop canopy if post-plant treatments are desired. The pesticide application is an input mass rate which is calculated by one of the application/deposition models discussed in Section 3.1. It is partitioned between the plant canopy and the soil surface, and the rate at which it reaches the soil surface is designated J_{APP}.

Pesticides applied to the plant canopy can be transported to the soil surface as a result of rainfall washoff. This term, J_{FOF}, is defined as:

$$J_{FOF} = E\ P_r\ M\ A \qquad (2\text{-}13)$$

where

E = foliar extraction coefficient (cm^{-1})

P_r = daily rainfall depth (cm day^{-1})

M = mass of the pesticide on the plant surface projected area basis (g cm^{-2})

The foliar pesticide mass, M, is further subject to degradation and losses through volatilization. Its rate of change is given by

$$\frac{AdM}{dt} = -\ K_f MA - J_{FOF} + A_F\ b\ A \qquad (2\text{-}14)$$

where

K_f = lumped first-order foliar degradation constant (day^{-1})

A_F = application rate to the plant (g ha^{-1} day^{-1})

b = a units conversion factor (ha)

Adsorption and desorption in Equations (2-1) through (2-3) are treated as instantaneous, linear, and reversible processes. Using this assumption, the sorbed phase concentration can be related to the dissolved-phase concentration by:

$$C_s = K_d\ C_w \tag{2-15}$$

where

K_d = partition coefficient between the dissolved and solid phases ($cm^3\ g^{-1}$)

A similar expression can be developed to express the vapor phase concentration in terms of the dissolved-phase concentration as follows

$$C_g = K_H C_w \tag{2-16}$$

where

K_H = Henry's constant, i.e., distribution-coefficient between liquid phase and vapor phase ($cm^3\ cm^{-3}$)

The transformation of parent to daughter is assumed to be first order and takes place according to

$$J_{TRN} = -\ K_{TRN}\ C_w\ A\ \Delta z\ \theta \tag{2-17}$$

where

K_{TRN} = the transformation rate constant (day^{-1})

When simulating an end-of-chain daughter, J_{TRN} may also be a source term equal to the sum of the first-order transfers from any and all parents.

$$J_{TRN} = \sum_k K_{TRN}^k\ C_w^k\ A\ \Delta z\ \theta \tag{2-18}$$

in which the superscript k denotes a parent compound. For intermediate products, the solute transport equation may contain terms such as those shown in both Equations (2-17) and (2-18). The transformation of parent to daughter compounds is discussed in detail in Section 2.5.4. The section includes a description of the equations used to simulate this process.

Summing Equations (2-1), (2-2), and (2-3) and utilizing (2-15) and (2-16), the following expression results for the mass balance of pesticide in the uppermost soil layer:

$$\frac{\partial[C_w(\theta + K_d\,\rho_s + aK_H)]}{\partial t} = D_w \frac{\partial^2(C_w\theta)}{\partial z^2} + D_g \frac{\partial^2(aC_wK_H)}{\partial z^2} - \frac{\partial C_w\theta V}{\partial z}$$

$$- C_w\left[K_s(\theta + K_d\rho_s) + K_g aK_H + f\theta\epsilon + \frac{Q}{A_w\Delta z} + \frac{pX_e r_{om} K_d}{A_w\Delta z}\right]$$

$$+ \frac{J_{APP}}{A\,\Delta z} + \frac{EP_r M}{\Delta z} - K_{TRN}\,C_w\theta + \sum_k K_{TRN}^k\,C_w^k\,\theta \qquad (2\text{-}19)$$

Equation (2-19) is solved in PRZM for the surface layer with $f\theta = 0$, and an upper boundary condition which allows vapor phase flux upward from the soil surface to the overlying air. This upper boundary condition is described more fully in the section on volatilization. The lower boundary condition is one which allows advection, but no diffusion, out of the bottom of the soil profile.

2.3.2 Water Movement

Because V and θ are not generally known and not generally measured as part of routine monitoring programs, it is necessary to develop additional equations for these variables. In the general case, Darcy's law can be combined with the continuity equation to yield the Richards equation (Richards 1931):

$$\frac{\partial\theta}{\partial t} = \frac{\partial}{\partial z}\left[K(\theta)\,\frac{\partial h}{\partial t}\right] \qquad (2\text{-}20)$$

where

$K(\theta)$ - hydraulic conductivity at various heads (cm sec^{-1})

θ - soil water content (cm^3 cm^{-3})

and

$$V = -\,K(\theta)\,\frac{\partial h}{\partial t} \qquad (2\text{-}21)$$

or, in simpler terms

$$\frac{\partial\theta}{\partial t} = -\,\frac{\partial V}{\partial z} \qquad (2\text{-}22)$$

where

θ = soil water content ($cm^3\ cm^{-3}$)

V = soil water velocity ($cm\ day^{-1}$)

Writing Equation (2-22) in an integrated backwards finite difference form yields

$$\Delta z\ (\theta^{t+1} - \theta^{t}) = (V_i - V_{i-1})\ \Delta t \qquad (2\text{-}23)$$

or

$$\theta^{t+1}\ \Delta z = (V_i - V_{i-1})\Delta t + \theta^{t}\Delta z \qquad (2\text{-}24)$$

In these equations, t and t+1 denote the beginning and end of time step values, respectively, and i is the soil layer index. These equations can be further simplified by substituting the nomenclature SW for $\theta\Delta z$ so that

$$SW^{t+1} = SW^{t} + (V_i - V_{i-1})\ \Delta t \qquad (2\text{-}25)$$

where

SW = soil water content (cm)

The velocities in Equation (2-25) are a function of inputs to the soil (precipitation, infiltration) and outflows from the soil (evapotranspiration, runoff).

Water balance equations are separately developed for (a) the surface zone, (b) horizons comprising the active root zones, and (c) the remaining lower horizons within the unsaturated zone. The equations are:

Surface Zone

$$(SW)_1^{t+1} = (SW)_1^{t} + INF - I_1 - E_1 - U_1 \qquad (2\text{-}26)$$

Root Zone

$$(SW)_1^{t+1} = (SW)_1^{t} + I_{i-1} - U_i - I_i \qquad (2\text{-}27)$$

Below Root Zone

$$(SW)_1^{t+1} = (SW)_1^{t} + I_{i-1} - I_i \qquad (2\text{-}28)$$

where

$(SW)_i^t$ = soil water in layer "i" on day "t" (cm)

E_i = evaporation (cm day^{-1})

U_i = transpiration (cm day^{-1})

I_i = percolation out of zone i (cm day^{-1})

INF = infiltration into layer 1 (cm day^{-1})

Daily updating of soil moisture in the soil profile using the above equations requires the additional calculations for infiltration, evaporation, transpiration, and percolation.

Infiltration is calculated as

$$INF = P + SM - Q - E \tag{2-29}$$

where, assuming a unit area of 1 cm^2,

P = precipitation as rainfall, minus crop interception (cm day^{-1})

SM = snowmelt (cm day^{-1})

Q = runoff (cm day^{-1})

E = evaporation (cm day^{-1})

The calculations of precipitation, snowmelt, and runoff on a daily time step are described below. The disaggregation of these values and the calculation of the change in the depth of ponding on a finer time step is included in Sections 2.3.5.4 and 2.4.4 describing the simulation of furrow irrigation and ponded surface water.

Input precipitation is read in and pan evaporation and/or air temperature are inputs from which potential evapotranspiration (PET) is estimated. Incoming precipitation is first partitioned between snow or rain, depending upon temperature. Air temperatures below 0°C produce snow and may result in the accumulation of a snowpack. Precipitation first encounters the plant canopy and once the interception storage is depleted, the remaining depth is available for the runoff or infiltration.

The runoff calculation partitions the precipitation between infiltrating water and surface runoff. Infiltrating water may be ponded on the soil surface for a period of time before it infiltrates, but this ephemeral process is described in a following section. Runoff is calculated by a modification of the USDA Soil Conservation Service curve number approach (Haith et al. 1979). Snowmelt is estimated on days in which a snowpack exists and above freezing temperatures occur as

$$SM = C_M T \tag{2-30}$$

where

C_M = degree-day snowmelt factor (cm $°C^{-1}$ day^{-1})

T = average daily temperature (°C)

The precipitation and/or snowmelt are inputs to the SCS runoff equation written as

$$Q = \frac{(P + SM - 0.2S)^2}{P + SM + 0.8S} \quad (2\text{-}31)$$

where S, the watershed retention parameter, is estimated by

$$S = 1000/RCN - 10 \quad (2\text{-}32)$$

where

RCN = SCS runoff curve number

Curve numbers are a function of soil type, soil drainage properties, crop type, and management practice. Typically, specific curve numbers for a given rainfall event are determined by the sum of the rainfall totals for the previous 5 days, known as the 5-day antecedent moisture condition. In this release of PRZM, as in the original version, the curve numbers are continuously adjusted each day as a function of the soil water status in the upper soil layers. These algorithms were developed and reported by Haith and Loehr (1979).

The daily evapotranspiration demand is divided among evaporation from canopy, ponded surface water, soil evaporation, and crop transpiration. Total demand is first estimated and then extracted sequentially from crop canopy storage, ponded surface water, and then from each layer until wilting point is reached in each layer or until total demand is met. Evaporation occurs down to a user-specified depth. The remaining demand, crop transpiration, is met from the active root zone. The root zone growth function is activated at crop emergence and increases stepwise until maximum rooting depth is achieved at crop maturity.

Actual evapotranspiration from a soil layer is estimated as:

$$ET_i = MIN\left[(SW_i - WP_i)\, f_{di},\ ET_p - \sum_{1}^{i-1} ET_i\right] \quad (2\text{-}33)$$

where

ET_i = the actual evapotranspiration from layer 'i' (cm)

f_{di} = depth factor for layer 'i'

WP_i = wilting point water content in layer 'i' (cm)

ET_p = potential evapotranspiration (cm)

This equation states that the transpiration from any layer 'i' is the minimum of the available water in layer 'i' or the demand remaining after extracting available water from layers above 'i' in the profile.

The depth factor, f_{di}, is internally set in the code. It linearly weights the extraction of ET from the root zone with depth. A triangular root distribution is assumed from the surface zone to the maximum depth of rooting, with the maximum root density assumed to be near the surface. This algorithm essentially views the plant as a pump and assumes that it will expend the minimum energy possible in pumping. As long as the soil water is equally available, water closest to the surface meets this criterion.

Evapotranspiration may also be limited by soil moisture availability. The potential rate may not be met if sufficient soil water is not available to meet the demand. In that case, PRZM modifies the potential rate by the following equations:

$$ET_p = ET_p; \quad \text{if } SW \geq 0.6\ FC \tag{2-34}$$

$$ET_p = SMFAC\ ET_p; \quad \text{if } WP < SW < 0.6\ FC$$

$$ET_p = 0; \quad \text{if } SW \leq WP$$

where

FC = soil moisture content at field capacity (cm)

WP = soil moisture content at wilting point (cm)

SMFAC = soil moisture factor

The SMFAC concept has been used in other similar water balance models (Haith et al. 1979; Stewart et al. 1976) and is internally set in the code to linearly reduce ET_p when soil water becomes limited. Finally, if pan evaporation input data are available, ET_p is related to the input values as

$$ET_p = C_p\ PE \tag{2-35}$$

where

PE = pan evaporation (cm day^{-1})

C_p = pan factor (dimensionless)

The pan factor is constant for a given location and is a function of the average daily relative humidity, average daily wind speed, and location of the pan with respect to an actively transpiring crop.

In the absence of pan evaporation data, ET_p is estimated by

$$ET_p = 14000\ L_d^2\ (SVD) \qquad (2\text{-}36)$$

where

L_d = possible hours of sunshine per day, in 12-hour units

SVD = saturated vapor density at the mean air temperature (g cm^{-1})

$$SVD = 0.622\ SVP/(R_g\ T_{abs})$$

where

SVP = saturated vapor pressure at the mean absolute air temperature (mb)

R_g = dry-air gas constant

T_{abs} = absolute mean air temperature (°K)

The final term in the water balance equations that must be defined is the percolation value, I. Because the Richards equation is not solved in PRZM utilizing soil water characteristic curves to predict water movement, PRZM resorts to "drainage rules" keyed to soil moisture storages and the time available for drainage. Two options are included. Although these options are admittedly simplistic representations of soil moisture redistribution, they are consistent with the objectives of PRZM and its intended uses.

2.3.2.1 Option 1--
Percolation, I, in this option is defined in the context of two bulk soil moisture holding characteristics commonly reported for agricultural soils: field capacity and wilting point. Field capacity is a somewhat imprecise measure of soil water holding properties and is usually reported as the moisture content that field soils attain after all excess water is drained from the system under influence of gravity, usually at tensions of about 0.3 bar. The difficulty with this concept is the fact that some soils will continue to drain for long periods of time, and thus field capacity is not a constant. Admitting the lack of theoretical and physical rigor, the concept remains as a useful measure of soil moisture capacity and has been successfully used in a number of water balance models (Haith et al., 1979; Stewart et al., 1976). Wilting point is a function of both the soil and plants growing in the soil. It is defined as the soil moisture content below which plants are unable to extract water, usually at tensions of about 15 bar.

Field capacity and wilting point are used operationally to define two reference states in each soil layer for predicting percolation. If the soil

water, SW, is calculated to be in excess of field capacity, then percolation is allowed to remove the excess water to a lower zone. The entire soil profile excess is assumed to drain within 1 day. The lower limit of soil water permitted is the wilting point. One outcome of these assumed "drainage rules" is that the soil layers below the root zone tend to quickly reach field capacity and remain at that value. When this condition is reached, all water percolated below the root zone will displace the water within the lower soil layer simulated, and so on. There is no allowance for lateral water movement. Water balance accounting in this manner should be most accurate for sandy soils in which water movement is relatively unimpeded and is least accurate for clay soils (Stewart et al., 1976).

2.3.2.2 Option 2--
The second option is provided to accommodate soils having low permeability layers that restrict the "free drainage" assumed in Option 1. In the context of the field capacity reference condition, two things may occur. First, conditions may prevail that raise the soil moisture levels above field capacity for periods of time because the water is "backed up" above a relatively impermeable layer. Second, the excess water may not drain during the 1-day period assumed in Option 1. To accommodate these conditions, two additional parameters are needed. Maximum soil moisture storage, θ_s is added to represent moisture contents under saturated conditions. The drainage rate also must be modified to allow drainage to field capacity over periods in excess of 1 day (one time step). The drainage rate is assumed to be a first-order function of the water content above field capacity and is modeled by

$$\frac{d\ (\theta - \theta_{fc})}{dt} = -\ \alpha\ (\theta - \theta_{fc}) \qquad (2\text{-}37)$$

which has the solution

$$\theta_i^{t+1} = (\theta_i^{t*} - \theta_{fc_i})\ \exp(-\alpha\Delta t) + \theta_{fc_i} \qquad (2\text{-}38)$$

where

θ = soil layer water content ($cm^3\ cm^{-3}$)

θ_{fc}= water content at field capacity ($cm^3\ cm^{-3}$)

α = drainage rate parameter (day^{-1})

In this equation, t and t+1 denote beginning and end of time step values, respectively, and i is the soil layer index. The value t* denotes a value of time between beginning and end of time step. The variable θ_i^{t*} here denotes current storage plus any percolation from the next layer above, before the occurrence of any drainage from the current layer. Because Equation (2-38) is solved independently for each layer in the profile, there is a possibility of exceeding the storage capability (saturation water content, θ_s) of a low-

permeability layer in the profile if a more permeable layer overlies it. At each time step, once redistribution is complete, the model searches the profile for any $\theta_i > \theta_{s_i}$. If this condition is found, the model redistributes water back into overlying layers, as if the percolation of additional water beyond that necessary to saturate the low-permeability layer had not occurred. This adjustment is necessary due to the nature of Equation (2-38) and the fact that these equations for each layer are not easily coupled. The difficulty in coupling the equations for the entire profile arises from the dichotomy that one of two factors limits percolation from a stratum in the profile: either the rate at which that stratum can transmit water, or the ability of the stratum below it to store or transmit water. This dichotomy leads to an iterative (or at least corrective) approach to the explicit solution of a system of equations for θ_i represented by Equation (2-38). It should be noted, however, that the value of α selected by this approach is only relevant if the permeability of the soil materials, and not storage considerations in the profile (i.e., the presence of a water table), is the limiting factor for percolation of water.

2.3.3 Soil Erosion

Removal of sorbed pesticides on eroded sediments requires estimates for soil erosion. The Modified Universal Soil Loss Equation (MUSLE) as developed by Williams (1975) is used to calculate soil loss:

$$X_e = a\ (V_r\ q_p)^{0.56} K\ LS\ C\ P \qquad (2\text{-}39)$$

where

X_e = the event soil loss (metric tons day^{-1})

V_r = volume of event (daily) runoff (m^3)

q_p = peak storm runoff ($m^3\ sec^{-1}$)

K = soil erodability factor

LS = length-slope factor

C = soil cover factor

P = conservation practice factor

a = units conversion factor

Most of the parameters in Equation (2-39) are easily determined from other calculations within PRZM (e.g., V_r), and others are familiar terms readily available from handbooks. However, the peak storm runoff value, q_p, can vary widely depending upon rainfall and runoff characteristics. A trapezoidal hydrograph is assumed in PRZM. From the assumed hydrograph shape and the storm duration, a peak runoff rate is calculated.

The enrichment ratio, r_{om}, is the remaining term which needs to be defined to estimate the removal of sorbed pesticides by erosion. Because erosion is a

selective process during runoff events, eroded sediments become "enriched" in smaller particles. The sediment transport theory available to describe this process requires substantially more hydraulic spatial and temporal resolution than used in PRZM, leading to the adoption of an empirical approach (Mockus 1972). The enrichment ratio for organic matter is calculated from

$$\ln(r_{om}) = 2 + 0.2 \ln(X_e/A_w) \quad (2\text{-}40)$$

2.3.4 Volatilization

As volatilization was not available in the previous releases of PRZM, its theoretical basis is discussed in detail here. The following key processes have been identified as important in volatilization algorithms to simulate vapor-phase pesticide transport within the soil/plant compartments:

- Vapor-phase movement of the pesticide in the soil profile
- Boundary layer transfer at the soil-air interface
- Vertical diffusion of pesticide vapor within the plant canopy
- Pesticide mass transfer between the plant (leaves) and the surrounding atmosphere
- Soil temperature effects on pesticide volatilization

The discussion of the volatilization algorithms is presented in four parts: influence of vapor phase pesticide in soil and volatilization flux, volatilization flux through the plant canopy, volatilization flux from plant surfaces, and soil temperature modeling and effects. Figure 2.3 is a schematic of the pesticide vapor and volatilization processes considered in soil and plant compartments.

2.3.4.1 Soil Vapor Phase and Volatilization Flux--

The governing equations for chemical transport in the vapor phase were introduced previously in the description of transport in the soil. Fluxes from the soil column in the vapor phase are summarized in that discussion by Equations (2-3), (2-5), and (2-9). The terms in these equations are summed with the other flux terms to produce the transport equation (2-19). In addition to these enhancements, the upper boundary of PRZM was changed from a zero-concentration boundary to a stagnant-layer boundary to allow diffusive transport upward from the soil to the overlying atmosphere. This enhancement is discussed in detail below.

Surface boundary condition--When a pesticide is incorporated into the soil, the initial volatilization rate is a function of the vapor pressure of the chemical at the surface as modified by adsorptive interactions with the soil. As the concentration at the surface of the soil changes, volatilization may become more dependent on the rate of movement of the pesticide to the soil surface (Jury et al., 1983b).

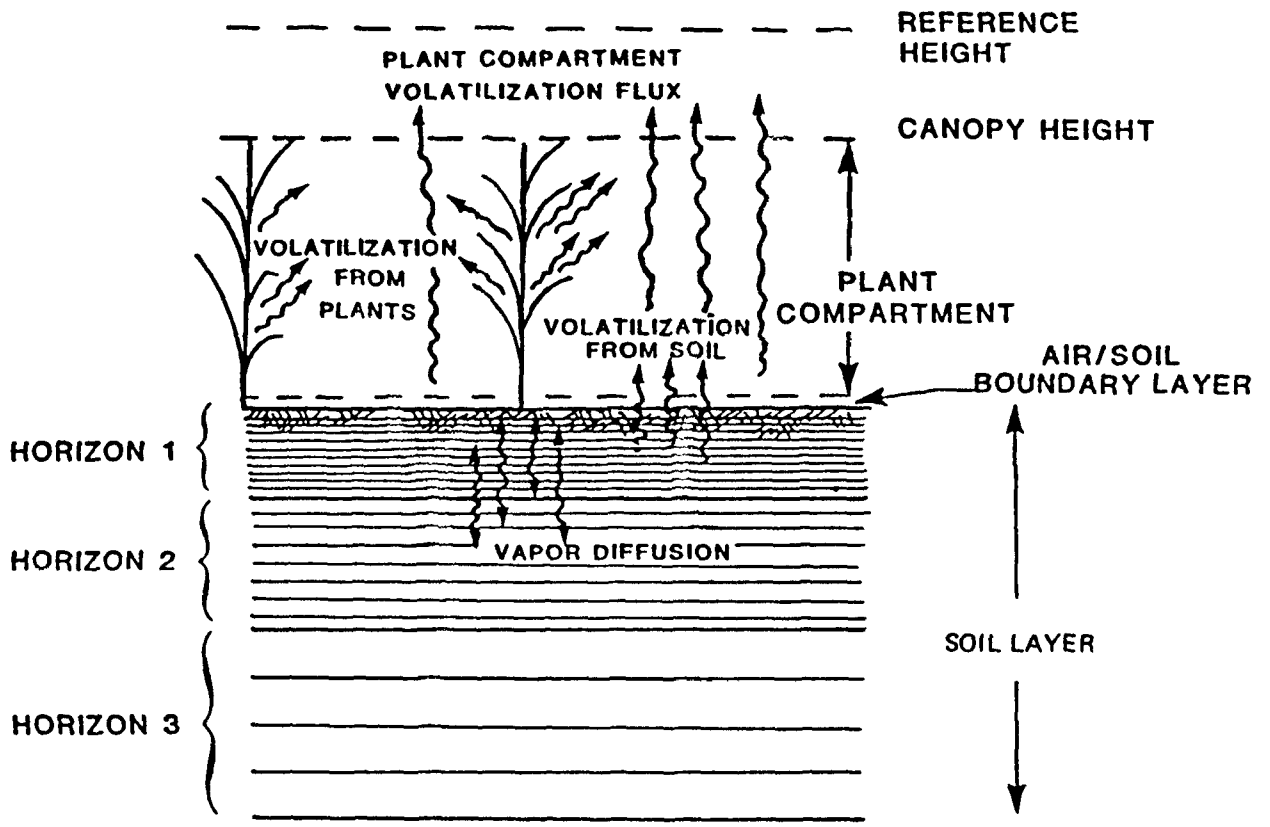

Figure 2.3. Schematic of pesticide vapor and volatilization processes.

The soil surface layer can be visualized as a membrane which only allows water to pass through and keeps the solute behind. Experimental results show that within the top centimeter of the soil surface, the pesticide concentration can increase as much as 10-fold due to the accumulation of chemical at the surface layer, resulting in higher vapor density. In order to describe these phenomena, Jury et al. (1983a, 1983b) proposed a boundary layer model which states that the controlling mechanism for pesticide volatilization is molecular diffusion through the stagnant surface boundary layer.

The layer of stagnant air may or may not form a significant barrier to volatilization loss for a given pesticide, depending on a variety of factors. In general, if the diffusion rate through the air layer is able to match the upward flux to the soil surface without having the surface concentration build up, then the stagnant layer is not acting as a barrier to loss and the volatilization flux will not depend strongly on the thickness of the boundary layer. Conversely, if the diffusion rate through the air is less than the flow to the surface by diffusion or mass flow, then the concentration at the soil surface will not be close to zero, and the thickness of the air layer will regulate the loss by volatilization. In other words, the significance of the boundary layer model depends on the ratio of the magnitudes between the upward soil pesticide flux and the boundary layer diffusion flux. Only downward, advective movement of water is treated in PRZM Release I. In this case, the sources that contribute to the upward soil pesticide flux are only the diffusion processes in the vapor and dissolved phases, but not upward water advection.

The zero chemical concentration upper boundary condition in the first release was modified in accordance with Jury's boundary layer model. The pesticide volatilization flux from the soil profile can be estimated as follows:

$$J_1 = \frac{D_a A}{d} (C_{g,1} - C^*_{g,d}) \qquad (2\text{-}41)$$

where

J_1 = volatilization flux from soil (g day^{-1})

D_a = molecular diffusivity of the chemical in air (cm^2 day^{-1})

A = cross-sectional area of soil column (cm^2)

d = thickness of stagnant air boundary layer (cm)

$C_{g,1}$ = vapor-phase concentration in the surface soil layer (g cm^{-3})

$C^*_{g,d}$ = vapor-phase concentration above the stagnant air boundary layer (g cm^{-3})

The thickness of the stagnant boundary layer can be estimated using a water vapor transport approach (Jury et al., 1983a). However, Wagenet and Biggar

(1987) assumed a constant value of 5 mm for this thickness, which is consistent with the values estimated by Jury. Consequently, the same assumption of a 5-mm thickness for the stagnant layer has been used here pending the results of further sensitivity analyses. The value of $C^*_{g,d}$ can take on a value of zero if the soil surface is bare or can be positive if a plant canopy exists.

2.3.4.2 Volatilization Flux through the Plant Canopy--
In pioneering work on this topic, Parmele et al. (1972) discuss a number of micrometeorological techniques for calculating pesticide volatilization flux from observed aerial pesticide concentrations. Their procedures are based on the assumption that the vertical diffusivity coefficient (K_z) for pesticide vapor is analogous to the vertical diffusivity for water vapor, energy, or momentum. The pesticide volatilization flux can be computed by Fick's first law of diffusion, as follows:

$$J_z(Z) = -K_z(Z)\ (dP/dZ) \qquad (2\text{-}42)$$

where

$J_z(Z)$ = pesticide flux at height Z ($g\ m^{-2}\ s^{-1}$)

(dP/dZ) = pesticide concentration gradient ($g\ m^{-2}$)

$K_z(Z)$ = the vertical diffusivity at the height Z ($m^2\ s^{-1}$)

The value of K_z depends on the turbulent flow of the atmosphere into which the pesticide vapor is dissipated. Therefore, it is a function of the prevailing meteorological conditions and not of any physical or chemical property of the pesticide.

In order to apply these concepts, pesticide concentrations at two or more heights are required to estimate the pesticide gradient and the subsequent flux. For the estimation of vertical diffusivity, more extensive meteorological information is also required. All of these data requirements pose significant limitations for a predictive modeling approach consistent with expected and current PRZM users.

In developing this PRZM module, the following approaches are proposed to circumvent the intensive data requirements. First, a relationship for K_z is derived as a function of height within the canopy. Then one need only consider the pesticide concentration gradient (or a suitable surrogate) in order to compute the pesticide volatilization flux.

Estimation of $K_z(Z)$--Mehlenbacher and Whitfield (1977) present the following formula to compute K_z at various heights within the plant canopy:

$$K_z(Z) = K_z(Z_{CH})\ \exp\left[4.0\left(\frac{Z}{Z_{CH}} - 1.0\right)\right] \qquad (2\text{-}43)$$

$$K_z(Z_{CH}) = U^* \, k \, (Z_{CH} - \underline{D})/\phi_h \tag{2-44}$$

$$U^* = \frac{k \, U_{CH}}{\ln[(Z_{CH} - \underline{D}/Z_o) + \psi_m(\phi_m)]} \tag{2-45}$$

where

$K_z(Z)$ = thermal eddy diffusivity at height Z ($m^2 \, s^{-1}$)
$K_z(Z_{CH})$ = thermal eddy diffusivity at canopy height ($m^2 \, s^{-1}$)
Z_{CH} = canopy height (m)
Z_o = roughness length (m)
$\underline{D}$ = zero plane displacement height (m)
k = von Karman's constant, 0.41
U* = friction velocity ($m \, s^{-1}$)
ϕ_h = stability function for sensible heat
$\psi_m(\phi_m)$ = integrated momentum stability parameter as a function of ϕ_m
ϕ_m = stability function for momentum
U_{CH} = wind velocity at the canopy height ($m \, s^{-1}$)

For agricultural applications, the canopy height is used as a reference height for calculating U*. The user is required to input the wind speed and the height where the measurement was made. The wind speed at the canopy height (U_{CH}) is computed based on the logarithm law. The relationship is as follows:

$$\frac{U_{CH}}{U_{measured}} = \frac{\ln\left[\frac{Z_{CH} - \underline{D}}{Z_o}\right]}{\ln\left[\frac{Z_{measured} - \underline{D}}{Z_o}\right]} \tag{2-46}$$

The friction velocity U* can be visualized as a characteristic of the flow regime in the plant canopy compartment in which the logarithmic velocity distribution law holds. As shown in Equation (2-43), U* is calculated as a function of U_{CH}, Z_{CH}, Z_o, $\underline{D}$, and ψ_m. Rosenberg (1974) describes $Z_o + \underline{D}$ as the total height at which the velocity profile above the canopy extrapolates to zero wind velocity. The values for both Z_o and $\underline{D}$ can be estimated with the following equations presented by Thibodeaux (1979). For very short crops (lawns, for example), Z_o adequately describes the total roughness length, and little adjustment of the zero plane is necessary (i.e., $\underline{D} = 0$). $\underline{D}$ is assumed

to be zero in the current code when Z_{CH} is less than 5 cm. For tall crops, Z_o is related to canopy height (Z_{CH}) by

$$\log Z_o = 0.997 \log Z_{CH} - 0.883 \quad (2\text{-}47)$$

In tall crops Z_o is no longer adequate to describe the total roughness length, and a value of $\underline{D}$, the zero plane displacement, is needed. For a wide range of crops and heights, 0.02 m < Z_{CH} < 25 m, the following equation for $\underline{D}$ has been presented by Stanhill (1969):

$$\log \underline{D} = 0.9793 \log Z_{CH} - 0.1536 \quad (2\text{-}48)$$

This equation results from a linear regression analysis based on the published data for 19 different crops with limited data measured for the same crop at different growth stages. Strictly speaking, both Z_o and $\underline{D}$ should be evaluated from experimental observations. In the calculation of K_z, the module uses these two equations for estimation of Z_o and $\underline{D}$, since there is no method available to justify any variations for crop type, row spacing, or canopy density.

With estimates of Z_o and $\underline{D}$, U* (friction velocity) can be estimated if the values of the stability parameters (ψ_m and ϕ_h) are known. These two variables are closely related to Ri, the Richardson number, which is the measure of the rate of conversion of convective turbulence to mechanical turbulence. It is defined as follows (Wark and Warner 1976):

$$Ri = \frac{(g/T)\ (\partial T/\partial Z)}{(\partial U/\partial Z)^2} \quad (2\text{-}49)$$

where

g = acceleration of gravity (m sec^{-2})

T = potential temperature (°K)

Z = elevation (m)

U = wind velocity (m s^{-1})

Potential temperature is defined as the temperature which a parcel of dry air would acquire if brought adiabatically from its initial pressure to a saturated pressure of 1000 millibars (Perkins 1974). In application of the model, the measured temperature is used in the Richardson number estimation as suggested by Rosenberg (1974).

The sign of Ri indicates the atmospheric condition, and its magnitude reflects the degree of the influence. There are several different formulas for relating Ri to the atmospheric stability parameters; for these purposes, the sign of Ri is of greater concern than its magnitude. When Ri is larger than 0.003, the atmosphere exhibits little vertical mixing, reflecting stable

conditions; when the absolute value of Ri, |Ri|, is less than 0.003, neutral stability conditions exist (Oliver 1971); and when Ri is less than -0.003, convective mixing becomes dominant and atmospheric conditions are unstable.

To relate the atmospheric stability parameters to the Richardson number, Thom et al. (1975) proposed the following formulas based on the work by Dyer (1974) and Dyer and Hicks (1970):

For stable conditions -

$$\phi_h = \phi_m = 1 + 5.2Ri \tag{2-50}$$

For unstable conditions -

$$\phi_h = \phi_m^2 = (1 - 16Ri)^{-1/2} \tag{2-51}$$

For neutral conditions -

$$\phi_h = \phi_m = 1 \tag{2-52}$$

The integrated momentum stability parameter, ψ_m, can be evaluated based on the following equation as derived by Lo (1977):

$$\psi_m = \pi/2 - 1 + \ln(8) + \phi_m + 3\ln(\phi_m) - 2\ln(\phi_m+1) - \ln(1+\phi_m^2) - 2\tan^{-1}(\phi_m) \tag{2-53}$$

Under neutral conditions, $\psi_m = 0$ and the equation is not used.

In the application of these procedures, the calculations are performed as follows:

1) Evaluate Richardson number from temperature and wind velocity gradients.

2) Determine stability condition based on calculated Ri.

3) Calculate ϕ_h and ϕ_m, based on the stability condition and associated Equations (2-50), (2-51), or (2-52).

4) Calculate ψ_m, from Equation (2-53).

5) Calculate Z_o and $\underline{D}$ from canopy height using Equations (2-47) and (2-48).

6) Estimate $K_z(Z)$ by applying Equations (2-45), (2-44), and (2-43).

The resistance approach for the estimation of volatilization flux from soil- The calculation of the volatilization flux from the soil is based on a resistance-type approach. For pre-plant pesticides, and time periods just after emergence and post-harvest, transport by volatilization from plant surfaces is much less than vapor phase transport by other mechanisms. For those conditions in which the plant leaves do not act as significant sources or sinks for pesticide vapor, the resistances of the air for the whole plant compartment can be estimated as follows (Mehlenbacher and Whitfield 1977):

$$\Sigma R = R_{bd} + R_{pc} \tag{2-54}$$

$$R_{bd} = \frac{d}{D_a} \tag{2-55}$$

$$R_{pc} = \int_{d}^{Z_{CH}} \frac{dz}{K_z(Z)} \tag{2-56}$$

where

ΣR = total vertical transfer resistance (day cm^{-1})

R_{bd} = boundary layer resistance (day cm^{-1})

R_{pc} = plant canopy resistance (day cm^{-1})

The flux is calculated as follows:

$$J_{pc} = \frac{C_{g,1}}{\Sigma R} \tag{2-57}$$

where

J_{pc} = volatilization flux from plant canopy (g cm^{-2} day^{-1})

$C_{g,1}$ = pesticide vapor concentration in top soil layer (g cm^{-3})

For those conditions in which plants can act as significant pesticide sources or sinks, another approach must be taken. The influences of plant canopy require the formulation for the surface boundary condition as described in the following two sections.

2.3.4.3 Volatilization Flux from Plant Surfaces--
A detailed description of the controlling factors for volatilization from plant surfaces has been presented by Taylor (1978). He indicated that the distribution of the pesticide residues over the plant surface appeared to be the dominant factor. This, together with the influence of the microscale climate at the plant surface, makes accurate simulation of plant volatilization processes very difficult.

For organophosphate insecticides, Stamper et al. (1979) has shown that the disappearance rates from leaf surfaces can be estimated by a logarithmic or a first-order kinetics approach. Similar observations for first-order kinetics were found for volatilization of 2,4-D iso-octyl ester from leaf surfaces by Grover et al. (1985). Thus, a simple rate constant approach is possible, which requires the user to input the first-order rate constant for volatilization. The plant leaf volatilization flux can be estimated as follows:

$$J_{pl} = M\ K_f \tag{2-58}$$

where

J_{pl} = volatilization flux from the leaf (g cm^{-2} day^{-1})
M = foliar pesticide mass (g cm^{-2})
K_f = first-order volatilization rate (day^{-1})

A resistance type approach is also applicable for volatilization flux estimation from plant leaves. The current code employs the first-order kinetics approach to calculate volatilization flux from plant leaf surfaces described above. This approach, which requires the user to specify the first-order rates constant for plant leaf volatilization, was selected because it is consistent with the foliar fate model in PRZM Release I.

Average pesticide concentration in plant canopy--Volatilization flux from plant leaves (J_{pl}) will exist only after pesticide application to the plant foliage has been specified in the model input. When a plant canopy exists, the average concentration in the air within the plant canopy can be estimated as follows:

$$C_g^* = (J_{pc} + J_{pl})\ \Sigma\ R_{0.5} \tag{2-59}$$

where

C_g^* = average concentration in the air between the ground surface and the plant canopy height (g cm^{-3})
$\Sigma R_{0.5}$ = canopy resistance from half canopy height to the top of the canopy

$$= \int_{0.5Z_{CH}}^{Z_{CH}} \frac{dz}{K_z(Z)} \tag{2-60}$$

Equation (2-59) then calculates the mean plant compartment pesticide concentration as the concentration at one-half of the canopy height. This

approach assumes a linear concentration gradient from ground surface to canopy height.

2.3.4.4 Soil Temperature Simulation--
Soil temperature is modeled in order to correct the Henry's law constant, K_H, for temperature effects. The interaction of microclimate with the soil surface which results in a given soil temperature regime is complex and dynamic. Soil surface configuration and plant residue cover, both affected by tillage, have significant impact on soil heat flux and, therefore, soil temperature. Studies of tillage and residue effects on soil temperature have been dominated by qualitative observations and site-specific measurements. The lack of mathematical evaluation and supporting field data has limited the ability of researchers to predict, beyond qualitative terms, the tillage and residue effect on soil temperature for soil and climatic conditions other than those under which data have been collected.

The objective of the soil temperature model is to provide a scientifically sound and usable approach: (i) to predict with reasonable accuracy the daily average soil temperatures at the soil surface and in and below the root zone, utilizing basic soil physical and thermal properties, and daily climatic measurements taken at weather stations; and (ii) to allow consideration of the residue, canopy, and tillage effects on soil temperature.

Several models are available to predict soil temperature under various soil surface conditions, but there are restrictions to the general use of these models because either they need large data bases which are not available at many places, or they are site specific. Existing soil temperature models form two general groups: (1) process-oriented models, which require detailed information on soil and surface characteristics, initial and boundary conditions, and inputs, and (2) semi- or non-process-oriented models, which often utilize weather station information and soil temperature information at one depth to develop empirical relationships.

Table 2-1 summarizes the key characteristics of the soil temperature models reviewed in this work. For both the process and semi-process oriented models, the two primary components are estimation of soil surface (or upper boundary) temperatures and soil profile temperature utilizing the calculated or estimated surface temperature as the upper boundary condition. A number of the models utilize the same procedure for calculating temperature in the soil profile (Gupta et al., 1981; Wagenet and Hutson 1987) and differ only in the procedures for specifying the surface boundary condition.

Van Bavel and Hillel (1975, 1976) developed a dynamic numerical procedure to link together the process-oriented simulations of heat movement in the soil and the partition of heat and energy at the soil surface. Soil surface temperature, T_o, is calculated as a factor in predicting evaporation from a bare soil. Their technique utilized simultaneous solutions of seven equations with seven unknowns: net radiative flux, evaporation rate, air sensible heat flux, soil sensible heat flux, surface soil temperature, Richardson's number, and the saturation humidity at the surface soil temperature. Heat and water (liquid) flows are each coupled at the soil surface. An iterative procedure was used at each update to find the proper

TABLE 2-1. SUMMARY OF SOIL TEMPERATURE MODEL CHARACTERISTICS

Model/Author(s)	Van Bavel and Hillel (1975)	Thibodeaux (1979)	Gupta et al. (1981, '82,'83)	Parton (1984)	Cruse et al. (1980)	Hasfurther and Burman (1974)	Williams et al. (1984)	Wagenet and Hutson (1987)	Chen et al. (1983)
1) Type of Model:									
a) Process-Oriented	X	X					X	X	X
b) Semi-Process-Oriented			X	X					
c) Non-Process-Oriented					X	X			
2) Heat Flow Process									
a) Conduction	X		X	X			X	X	X
b) Convection									X
c) Radiation	X	X			X		X		
3) Upper Boundary Temperature									AT
a) Est. by Energy Partitioning	X	X							
b) Est. by Empirical Relationship			X	X		X	ME	AVE	
4) Soil Temperature Profile: (Solving 1-D Heat Flow Eqn. Using the Procedure of:)									
a) Hanks et al. (1971)			X	EX				X	
b) Wierenga and de Wit (1970)	X*								
c) Curve Fitting					X**	X	DD		
5) Input Data Required									
a) Daily Max and Min Air Temp.			X	X	X	X	X		
b) Daily Max and Min Soil Surface Temperature			X						
c) Hourly Air Temperature	X	X	X						X
d) Hourly Solar Radiation	X	X		XX	XX		XX		
e) Surface Albedo	X	X			X		X		
f) Wind Velocity	X	X			X				
g) Humidity/Dewpoint Temp.	X	X							
h) Canopy Shadow/Ht. of Veg.	X	X							
i) Soil Water Content	X		X		at 5 cm		X	X	X
j) Soil Bulk Density	X		X		X	X	X	X	X
k) Soil Mineral Composition	X		X		X			X	X
l) Percentage Organic Matter	X		X		X			X	X
6) Soil Surface Condition									
a) Residue Cover	X		X		X		X		100%
b) Tillage Condition			X		X		X		
c) Crop Canopy	X	X	X	X			X		
7) Time Step									
a) Hourly	X	X	X	X				X	X
b) Daily					X	X	X		

* - Horton et al. (1984) used a 2-D heat flow equation.
** - Regression equation is fitted for soil temp at 5-cm depth.
DD - Damping depth parameter is used to predict soil temperature at different depths.
ME - Simplified mathematical relationship involving solar radiation, surface albedo, and daily min and max air temperatures.
AVE - "Average" measured soil surface temperatures are used.
AT - Ambient air temperature is used as upper boundary temperature.
XX - Total daily solar radiation.
EX - Explicit Finite Difference Scheme.

soil surface temperature. Soil temperatures were then estimated (Wierenga and de Wit 1970) by using these estimates of T_o as the surface boundary condition. Inputs required for this model include solar radiation, air and dewpoint temperature, wind speed, initial soil temperature profile, and the surface roughness evaluated by its effect on the aerodynamic roughness parameter. No comparisons were made between predicted and measured soil temperatures. Thibodeaux (1979) describes a similar energy-balance procedure for calculating soil surface temperatures.

For modeling soil profile temperatures, Hanks et al. (1971) used a numerical approximation for the one-dimensional soil-heat flow equation. This method requires the input of initial and boundary conditions, as well as the soil thermal conductivity and heat capacity as a function of depth and time. Predicted root zone soil temperature profiles were within 1°C of observed values for a 3-day period, but this model needs estimated or measured soil surface temperatures as upper boundary condition.

Using the Hanks et al. (1971) procedure for the root zone, Gupta et al. (1981-1984) developed a model for estimating hourly soil temperature by depth from meteorologic data. Inputs needed for this model include hourly air temperature at the 2-m height; daily maximum and minimum soil temperatures; initial soil temperature with depth; and soil thermal diffusivity, which may be estimated from soil mineral composition, organic matter percentage, bulk density, and soil water content. The upper boundary temperatures are estimated by a sine function. The amplitude of the function is equal to the difference between daily maximum temperatures of air and soil surface or daily minimum temperatures of air and soil surface. Empirical curves relating daily maximum air temperature to daily maximum soil surface temperature, and daily minimum air temperature to daily minimum soil surface temperature, were developed for different residue and tillage conditions for the specific application site. These relationships provided a means of accounting for residue and tillage effects on soil temperature, but require site-specific data.

The soil temperature model in PRZM is derived from a combination of the work by van Bavel and Hillel (1976) and Thibodeaux (1979) for estimating the soil surface/upper boundary temperature. The soil profile temperature procedures were developed by Hanks et al. (1971) and applied by Gupta et al. (1981, 1982, 1983) and Wagenet and Hutson (1987)

Estimating upper boundary temperature--An energy balance procedure is used in PRZM to estimate soil surface temperature (Thibodeaux 1979; van Bavel and Hillel, 1976). The same procedure is used in the POSSM model (Brown and Boutwell, 1986), which employs PRZM as a framework for PCB fate simulation.

The basic energy-balance equation with terms having units of cal cm^{-2} day^{-1} at the air/soil interface may be described as:

$$R_n - H_s - LE_s - G_s = \Delta TH \qquad (2\text{-}61)$$

where

R_n = net radiation (positive downward)

H_s = sensible air heat flux (positive upward)

LE_s = latent heat flux (positive upward)

G_s = soil heat flux (positive downward)

ΔTH = change in thermal energy storage in the thin soil layer (cal cm^{-2} day^{-1})

The term ΔTH can be evaluated as:

$$\Delta TH = (\rho_b d)\ s\ (T_{i+1} - T_i) \tag{2-62}$$

where

ρ_b = bulk density of soil (g cm^{-3})

d = thickness of a thin, surface soil layer (cm)

s = the specific heat capacity of soil (cal g^{-1} $°C^{-1}$)

T_i, T_{i+1} = the representative temperature for the surface layer at two consecutive time steps and can be represented as the average of temperatures at the top and bottom of the soil layers.

For evaluating the heat exchange across the air/soil interface, the thickness, d, can be set to a small value so that ΔTH may be neglected. As a result, the right side of Equation (2-61) is set equal to zero.

Net radiation flux at any surface can be represented as:

$$R_n = (R_s - R_{sr}) + (R_{la} - R_{lar}) - R_{ls} \tag{2-63}$$

where

R_n = the net radiation flux (cal cm^{-2} day^{-1})

R_s = incident short-wave solar radiation (cal cm^{-2} day^{-1})

R_{sr} = reflected short-wave solar radiation (cal cm^{-2} day^{-1})

R_{la} = incident long-wave atmospheric radiation (cal cm^{-2} day^{-1})

R_{lar} = reflected long-wave atmospheric radiation (cal cm^{-2} day^{-1})

R_{ls} = long-wave radiation emitted by the soil (cal cm^{-2} day^{-1})

The terms R_s and R_{sr} include both the direct and diffuse short-wave radiation, and are related as follows:

$$R_{sr} = \alpha R_s \quad (2\text{-}64)$$

where

α = the albedo of the surface (dimensionless)

Therefore, the short-wave radiation component of the energy balance is

$$R_s - R_{sr} = R_s(1 - \alpha) \quad (2\text{-}65)$$

The incident short-wave radiation can either be measured directly using pyranometers or else calculated using a variety of available empirical relationships or nomographs. The model requires input of a radiation time series, whether measured or calculated, in order to simulate soil temperature.

The albedo of a canopy-covered land surface can be estimated as:

$$\alpha(t) = \alpha_c \, C(t) + \alpha_s \, (1 - C(t)) \quad (2\text{-}66)$$

where

$\alpha(t)$ = albedo on day t

α_c = albedo of canopy cover (0.23 for vegetation)

$C(t)$ = canopy cover on day t (fraction)

α_s = albedo of soil surface (dimensionless)

Since the albedo of soil surface changes with the soil surface condition, it is defined by the user as 12 monthly values corresponding to the first day of each month; the albedo value for each day is interpolated between the neighboring monthly values. For snow cover less than 0.5 cm, the surface albedo is estimated using Equation (2-66), and for snow cover above 0.5 cm, the surface albedo is set equal to the snow albedo value (0.80).

The incident long-wave atmospheric radiation, R_{la}, is represented as

$$R_{la} = e_a \, \sigma \, T_a^4 \quad (2\text{-}67)$$

where

e_a = emissivity of the atmosphere [dimensionless]

α = the Stefan-Boltzmann constant [$11.7*10^{-8}$ cal cm^{-2} $°K^{-4}$ day^{-1}]

T_a = the air temperature [°K]

Wunderlich (1972) has proposed a correction to Equation (2.67) for the effects of cloud cover, which could increase R_{la} by up to 25 percent under overcast conditions. However, this correction is not included in the model because it would require input of a cloud cover timeseries, and the effect on the calculated soil surface temperature would be small.

The emissivity of the atmosphere varies from a low of 0.7 to almost unity. Numerous empirical relationships for estimating e_a have been proposed (Salhotra 1986). A simple reliable method is the use of Swinbank's formula:

$$e_a = 0.936*10^{-5}\ T_a^2 \qquad (2\text{-}68)$$

The reflected long-wave radiation, R_{lar}, can be expressed as:

$$R_{lar} = R_{la}\ (1 - \gamma) \qquad (2\text{-}69)$$

where

γ = the reflectivity of the surface for long-wave radiation [dimensionless]

The resulting net atmospheric long-wave radiation component becomes:

$$R_{la} - R_{lar} = R_{la}(1 - \gamma) = 0.936*10^{-5}\ T_a^6\ \sigma\ (1 - \gamma) \qquad (2\text{-}70)$$

The long-wave radiation component emitted by the soil surface is represented in an analogous equation to the atmospheric component, as follows:

$$R_{ls} = e_s\ \sigma\ T_s^4 \qquad (2\text{-}71)$$

where

e_s = infrared emissivity of soil (dimensionless)

T_s = soil surface temperature (°K)

Since the soil emissivity and reflectivity are related as e_s=1-γ, we can replace (1 - γ) in Equation (2-70) with e_s.

Combining the radiation components from Equations (2-65), (2-70), and (2-71), the net radiation flux is calculated as follows:

$$R_n = R_s\ (1 - \alpha) + 0.936*10^{-5}\ \alpha\ T_a^6\ e_s - e_s\ \alpha\ T_s^4 \qquad (2\text{-}72)$$

The evaporative heat flux, LE_s, is estimated by:

$$LE_s = \mu \; E \; \rho_w \tag{2-73}$$

where

μ = latent heat of vaporization/unit quantity of water (580.0 cal g^{-1})

E = evaporation rate (cm day^{-1})

ρ_w = density of water (1.0 g cm^{-3})

The evaporation rate is obtained from the evapotranspiration (EVPOTR) subroutine of PRZM. It is assumed that the calculated evapotranspiration from the top 5 cm depth of soil represents the potential evaporation energy loss at the air/soil interface. However, only a fraction of the evapotranspiration loss calculated by PRZM contributes to this heat flux. This fraction is estimated as the portion of the land surface not covered by vegetation, (i.e., 1.0 - canopy cover).

The sensible air heat flux, H_s, is given by:

$$H_s = \rho_a \; C_{pa} \; h \; (T_s - T_a) \tag{2-74}$$

where

ρ_a = air density (g cm^{-3})

$$= (-0.0042 \; T_a + 1.292)10^{-3} \tag{2-75}$$

C_{pa} = specific heat of air at constant pressure (0.2402 cal g^{-1} $°K^{-1}$)

h = heat transfer coefficient at air-soil interface (cm day^{-1})

T_a = the air temperature (°C)

The air density is computed based on the daily air temperature using a simple linear correlation (2-75) developed from data in Thibodeaux (1979). The heat transfer coefficient is given by:

$$h = K_1^2 \; V_z \left[\ln\left(\frac{Z_{RH} - D}{Z_o} \right) \right]^{-2} \tag{2-76}$$

where

K_1 = Von Karman's number (0.41)

V_z = wind velocity (cm day^{-1})

Z_{RH} = reference height at which V_z is measured (m)

$\underline{D}$ = zero plane displacement (m)

Z_o = roughness height (m)

Equation (2-76) is valid only when the air temperature does not vary greatly with height, as is often the case near sunrise or sunset or under cloudy skies or when canopy heights are relatively small. It appears to be a reasonable approximation for most agricultural crops. Correlations have been developed relating $\underline{D}$ and Z_o to the canopy height as described previously in this section by Equations (2-47) and (2-48).

From the fundamental equation of heat conduction, the soil heat flux, G_s, is given by:

$$G_s = (T_s - T_1)\ \lambda_1/D_1 \tag{2-77}$$

where

T_1 = temperature of the soil at bottom of layer 1 (°K)

T_s = soil surface temperature (°K)

λ_1 = thermal conductivity of layer 1 (cal cm^{-1} day^{-1} $°K^{-1}$)

D_1 = thickness of layer 1 (cm)

Substituting Equations (2-70), (2-71), (2-72), and (2-75) into Equation (2-59), the following fourth-order equation in terms of T_s results:

$$e\sigma T_s^4 + [\rho_a C_{pa} h + \lambda_1/D_1]\ T_s - [(1-\alpha)R_s + 0.936*10^{-5}\ \sigma\ T_a^6\ e_s$$
$$+ \rho_a C_{pa} h T_a - \mu E \rho_w + \lambda_1/D_1 T_1] = 0 \tag{2-78}$$

The value of T_s at each time step is estimated by solving the above equation using an iterative solution based on the Newton-Raphson method. The initial estimate of soil surface temperature is taken to equal measured air temperature, and R_n, LE_s, H_s, and G_s are calculated as explained above. The value for T_1 is obtained from the previous time step. These calculations are repeated until the difference between two consecutive estimates for soil surface temperature is less than the convergence criteria (set to 0.1°C).

Simulation of heat flow through soil profile--The soil profile temperature model is based on the one-dimensional partial differential equation describing heat flow in soils:

$$\frac{\partial T}{\partial t} = \frac{\partial}{\partial z}\left(d\ \frac{\partial T}{\partial z}\right) \tag{2-79}$$

where

d = the thermal diffusivity.

The thermal diffusivity is equal to the ratio of thermal conductivity and heat capacity of the soil. The procedures used to estimate soil thermal conductivity and heat capacity are taken from de Vries (1963). They are calculated from basic soil properties; soil water content, mineral composition, texture, and thermal conductivity of the individual soil particles. These parameters are either input or supplied by the model in the simulation. The thermal diffusivity is given by:

$$d = \lambda / C \tag{2-80}$$

where

d = thermal diffusivity of the soil layer ($cm^2\ day^{-1}$)

λ = thermal conductivity of the soil layer ($cal\ cm^{-1}\ day^{-1}\ °C^{-1}$)

C = heat capacity per unit volume of the soil layer ($cal\ cm^{-3}\ °C^{-1}$)

Temperature effect--A detailed discussion of the temperature effect on the volatilization behavior of pesticides is presented by Streile (1984). Two parameters that influence the vapor-phase transport in the soil profile are Henry's constant and the vapor diffusion coefficient.

The equation used to correct Henry's constant for temperature effects is (Streile 1984):

$$K_H(T) = K_{H,1} \exp\left[\frac{-\Delta H'_{vap}}{R}\left(\frac{1}{T} - \frac{1}{T_1}\right)\right] \tag{2-81}$$

where

$K_{H,1}$ = Henry's constant at the reference temperature T_1

$\Delta H'_{vap}$ = partial molar enthalpy of vaporization from solution ($J\ mole^{-1}$)

The temperature effect on the vapor phase diffusion coefficient can be estimated from the Fuller correlation as presented in Liley and Gambill (1973). However, it is not implemented in the code due to the general lack of information required to use it.

2.3.5 Irrigation Equations

PRZM irrigation algorithms determine depths of irrigation water to be applied at the soil surface. These depths are computed from the soil water deficit and are added as infiltration to the first PRZM soil compartment. Above and below canopy sprinklers, flooding, and furrow irrigation can be simulated. Methods for computing water application depths for each type of irrigation are described in the following paragraphs.

2.3.5.1 Soil Moisture Deficit--

Irrigation is triggered when the average root-zone soil moisture volume falls below a level f_c defined by the user as a fraction of the available water capacity. The soil moisture deficit, D, is then given by:

$$D = (\overline{\theta}_{fc} - \overline{\theta}_z)\, Z_r \qquad (2\text{-}82)$$

where

- D = soil moisture deficit (cm)
- $\overline{\theta}_z$ = average root-zone soil moisture content ($cm^3 cm^{-3}$)
- $\overline{\theta}_{fc}$ = average root-zone soil moisture content at field capacity ($cm^3\ cm^{-3}$)
- Z_r = root zone depth (cm)

D is the depth of water over the unit area that must be added to the soil by irrigation to bring the soil water content up to field capacity.

2.3.5.2 Sprinkler Irrigation--

Irrigation water from sprinklers may be applied either above or below the crop canopy. When applied above the crop canopy, irrigation water is intercepted by the canopy and may run off when it reaches the soil surface. The depth of water applied during a daily PRZM time step by overcanopy sprinklers is estimated from the soil moisture deficit:

$$Da = D\,(1 + LF) + I_f \qquad (2\text{-}83)$$

where

- Da = depth of irrigation water applied to the field (cm)
- I_f = crop canopy interception capacity (cm)
- LF = a factor specified by the user to allow for the practice in saline soils of adding water to leach salts out of the root zone (fraction of Da)

The water depth Da is applied as precipitation above the crop canopy, and canopy interception is computed for the current crop in the PRZM crop growth

subroutines. Sprinkler runoff from the soil surface is estimated using the SCS curve number approach, assuming that runoff characteristics of sprinkler water are similar to those of precipitation. Water that does not run off infiltrates into the first PRZM soil compartment.

Irrigation water applied below the crop canopy is not subject to canopy interception losses. The depth of water applied by undercanopy sprinklers is therefore given by:

$$Da = D\ (1 + LF) \qquad (2\text{-}84)$$

The irrigation water depth APDEP is applied as throughfall to the soil surface, and sprinkler runoff is estimated using the SCS curve number approach.

In some instances the sprinkler system may be unable, due to hydraulic limitations, to deliver water at the rate needed to meet the required daily application depth. In these cases the sprinkler application depth Da is set equal to the maximum depth that the system can deliver. The user is therefore required to input the maximum water application rate R_{max} (cm hr^{-1}) for the sprinkler system.

2.3.5.3 Flood Irrigation--
Flood irrigation in this case refers to the practice of flooding entire fields with irrigation water. Flood-irrigated fields are diked around the edges to allow water to pond and infiltrate into the soil. In the PRZM irrigation algorithm, it is assumed that this water ponds uniformly over the entire field. The amount of water applied to the soil surface is then:

$$Da = D\ (1 + LF) \qquad (2\text{-}85)$$

Since the field is assumed to be diked around the edges, no water is allowed to run off from the field.

2.3.5.4 Furrow Irrigation--
Furrow irrigation involves the release of water into numerous small channels which cut across the planted field. Infiltration depths within furrows vary due to differences in times at which water reaches various locations down the furrow, with less water infiltrating at the downstream end (Figure 2.4). Hydraulic characteristics of the furrow determine how quickly water moves down the channel, while soil characteristics determine the rate of infiltration once water reaches a location in the furrow.

The PRZM furrow irrigation model computes daily infiltration depths at various locations down the length of the furrow. This requires solution of the open channel flow equations of motion coupled with a soil infiltration model. Numerous attempts have been made in the literature to solve the furrow-irrigation advance problem, ranging in complexity from empirical

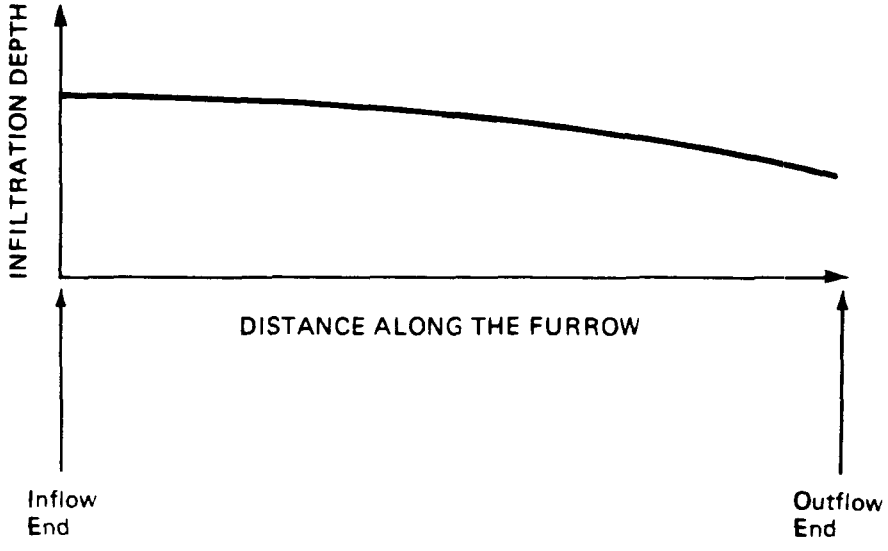

Figure 2.4. Variability of infiltration depths within an irrigation furrow.

volume-balance solutions (Wilke and Smerdon 1965; Fok and Bishop 1965) to numerical solutions of the full open channel flow equations of motion (Bassett and Fitzsimmons 1974). In general, solutions of the full equations of motion are too computationally intensive for this application, while simpler empirical models involve infiltration parameters which are not easily related to physical soil characteristics.

The PRZM furrow advance model uses the kinematic wave simplification of the equations of motion coupled with the Green-Ampt infiltration model to determine furrow infiltration depths. Kinematic-wave theory neglects inertial accelerations and assumes that the water surface slope is equal to the ground slope. The equations of motion then reduce to:

$$\frac{\partial Q}{\partial z} + \frac{\partial A}{\partial t} = \frac{-\partial q}{\partial t} \qquad (2\text{-}86)$$

where

Q = flow rate in the channel ($m^3\ s^{-1}$)

A = cross-sectional area of flow (m^2)

x = distance down the furrow (m)

q = volume infiltrated per unit length of channel ($m^3\ m^{-1}$)

The flow area A is related to the flow rate Q by Manning's equation:

$$Q = \frac{1}{n}\ AR^{2/3}\ S^{1/2} \qquad (2\text{-}87)$$

where

n = Manning's roughness coefficient

R = the hydraulic radius of flow (m)

S = the channel slope (vertical/horizontal)

Section 2.4.4 explains how the solution of the horizontal furrow irrigation equation is applied to PRZM.

2.4 NUMERICAL SOLUTION TECHNIQUES

This section describes the numerical techniques which are used to solve the differential equations introduced in the preceding section. Section 2.4.1 discusses the two numerical techniques available to solve the chemical transport equations, a backwards-difference implicit scheme, and a Method of Characteristics algorithm. The additional terms and the adjustment in the upper soil boundary which are added into these transport equations to simulate volatilization are described in Section 2.4.2. The numerical approximations used to calculate soil temperature are presented in Section

2.4.3 and the numerical solution for furrow infiltration depths are presented in Section 2.4.4.

Although the equations in this section are shown with a constant compartment depth (i.e. Δz) for simplicity and clarity, the PRZM module allows the use of variable compartment sizes so that each soil horizon can use a different compartment depth. For example, this capability allows use of smaller depths in the surface horizon for better simulation of surface processes, and larger depths in the lower horizons to minimize computational time. This is discussed in greater detail in Section 2.5.2.1.

2.4.1 Chemical Transport Equations

The second-order partial differential equation outlined in Section 2.3 must be solved with appropriate boundary conditions. The calculations for moisture contents, air contents, pore velocities, erosion, and runoff are decoupled from, and solved in advance of, the transport equation. The resulting values, treated as constant for each specific time step, are then used as coefficients in a discretized numerical approximation of the chemical transport equation.

Two techniques are currently available to solve the discretized chemical transport equation for the new dissolved pesticide concentration at the end of the time step. The available techniques are:

- A backward-difference, implicit scheme to simulate all chemical transport processes
- A method of characteristics (MOC) algorithm which simulates diffusion, decay, erosion, runoff, and uptake by the backward-difference technique, but uses the method of characteristics to simulate advective transport

The user is allowed to select the desired solution technique in the input sequence. Details of these techniques are provided below. Results from test simulations are provided in Section 2.5.1.

Identical discretizations and initial and boundary conditions are used with both numerical simulation techniques. A spatial and time discretization step is used equal to those applied in the water balance equations. For boundary conditions at the base of the soil column, the numerical technique uses

$$\frac{C_{w_{i+1}}\,\theta_{i+1} - C_{w_i}\,\theta_i}{\Delta z} = 0 \qquad (2\text{-}88)$$

in which the subscripts "i" refer to soil layer numbers.

This condition corresponds to a zero concentration gradient at the bottom of the soil profile. The upper boundary condition is discussed in more detail in Section 2.4.2.

A backwards-difference solution algorithm was the only solution option available in the original PRZM model. In this method, the first derivative in space, the advection term, is written as a backward difference (i.e., involves the difference C[i,j]-C[i-1,j]). The second spatial derivative, the diffusion term, is centered in space (i.e., based on the terms C[i-1,j]+C[i+1,j]-2C[i,j]). The time derivative is also calculated as a backward difference in the original code, (C[i,j]-C[i,j-1]). The equations are then made implicit by writing each concentration for the (j+1)th time step. The advantage of this numerical scheme is that it is unconditionally stable and convergent. However, the terms truncated in the Taylor's series expansion from which the finite difference expression are formulated lead to errors which, in the advection terms, appear identical to the expressions for hydrodynamic dispersion. In the simulation results these terms manifest themselves as "numerical dispersion," which is difficult to separate from the physical dispersion which is intentionally simulated. In systems with significant advection (i.e., high Peclet number), the artificial numerical diffusion may dominate the physical dispersion. It can be up to orders of magnitude larger, leading to difficulty in the interpretation of simulation results.

To minimize the effects of numerical dispersion in systems having high Peclet numbers, a method of characteristics solution was added as an option to PRZM. This solution method avoids the backwards-difference approximation for the advection term and the associated numerical dispersion by decomposing the governing transport equation. In advection-dominated systems, as the dispersion term becomes small with respect to the advection term, the advection-dispersion equation approaches a hyperbolic equation. According to the MOC theory, advection of the solute can be simulated separately from the other processes governing the fate and transport of that advected solute. M. Baptista et al. (1984) state that no error is introduced by this decomposition provided that the advection equation is solved first by an explicit procedure, and the diffusion equation is solved next by an implicit technique. This order was preserved in the PRZM model by utilizing a new explicit algorithm for advection which is always called first, and is immediately followed by execution of a modified version of the existing implicit algorithm for simulation of other processes. The advection algorithm employed was adapted from those described by Khalell and Reddell (1986) and Konikow and Bredehoeft (1978). These techniques were modified to allow simulation of changes in saturation and adsorption of the pesticide and variable compartment size.

In the new explicit advection algorithm, in addition to the fixed grid system, a set of moving points is introduced. These points can be visualized as carrying the chemical mass contained within a small region in space surrounding the point. Initially, these points are uniformly distributed throughout the flow domain. At each time interval, these moving points are redistributed according to the local solute velocity in each compartment. New points may enter the top of the flow domain, while old points may move out the bottom. When the moving points are transported in horizons where the compartment size is larger and numerical resolution is less, the points may be consolidated to conserve computational effort. After the new locations have been assigned to each point, the average concentration in each

compartment is computed based on the number and mass carried by the points contained within the compartment at that time. This temporary average concentration is returned to the main program, and a subroutine which assembles the terms in the transport equation (without advection) is called. Changes in concentration due to all other fate and transport processes (diffusion, decay, sources, etc.) are calculated for each compartment exactly as in the original version of PRZM. These values are then returned to the main program, and one transport step is complete.

When the MOC algorithm is called during the next time step, the exact location of each moving point has been saved. The first task is to update the masses carried by each moving point using the changes calculated during the last time step. Increases in mass are simply added equally to each point in the compartment, while decreases are weighted by the actual value at each point before subtraction to avoid simulating negative masses. The updated moving points are then relocated and the two-step process is repeated again until the end of the simulation.

Under some extreme conditions (e.g. high rainfall on soils with very low field capacity values), mass balance problems can occur when advective transport is simulated by means of the MOC option. The mass balance errors are related to the generation of extremely high velocities. Because a daily time step is used, high velocities can cause the moving points used in the MOC option to pass through several soil horizons without the properties of those horizons being considered. If significant chemical mass is in the soil column when the high velocities occur, mass balance problems can result. A statement printed in the PRZM output file warns users who are using the MOC option when high velocities are generated. If unacceptable mass balance errors are noted, the simulation should be reproduced using the backward-difference option instead of the MOC scheme.

2.4.2 Volatilization

The numerical techniques discussed in the previous section (2.4.1) are the basis of the simulation of chemical transport in all phases. However, the following modifications have been made to the upper boundary condition in order to model volatilization of chemical from the soil surface.

In order to simulate vapor-phase pesticide movement past the soil surface, the zero concentration upper boundary conditions used in the original PRZM code has to be modified. Jury's boundary layer model (1983a, 1983b) has been incorporated into the PRZM code. The model states that the controlling mechanism for pesticide volatilization is molecular diffusion through the stagnant surface boundary layer. The volatilization flux from soil profile can be estimated as follows:

$$J_1 = \frac{D_a A}{d} (C_{g,1} - C^*_{g,d}) \qquad (2\text{-}89)$$

where

J_1 = volatilization flux from soil (g day^{-1})

D_a = molecular diffusivity of the chemical in air ($cm^2 day^{-1}$)

$C_{g,1}$ = vapor-phase concentration in the surface soil layer (g cm^{-3})

$C^*_{g,d}$ = vapor-phase concentration above the stagnant air boundary layer (= 0, for the no-canopy field condition) (g cm^{-3})

$\underline{d}$ = thickness of stagnant air boundary layer (cm)

This equation defines the new flux-type boundary condition for the volatilization simulation. In order to incorporate the new flux-type boundary condition into the PRZM code, new mass balance equations were derived for the surface soil and stagnant air layers. Figure 2.5(a) is a schematic of the top two soil layers and the stagnant surface boundary layer when no plant canopy exists. Zero concentration is assumed for $C^*_{g,d}$ under the no-canopy field condition.

A mass balance equation for the uppermost soil compartment is

$$V \frac{\Delta(a\ C_{g,1})}{\Delta t} = A\ D_g \frac{\Delta C_g}{\Delta z} - A \frac{D_a}{\underline{d}} C_{g,1} - V\ a\ K_g\ C_{g,1} \qquad (2\text{-}90)$$

where

D_g = molecular diffusivity of pesticide in air filled pore space ($cm^2 day^{-1}$)

V = volume of the compartment (cm^3)

A = area of the compartment (cm^2)

a = volumetric air content ($cm^3\ cm^{-3}$)

K_g = first-order reaction rate constant (day^{-1})

The first term of the right-hand side of Equation (2-90) represents the gas diffusive flux into the surface soil layer, and the second term denotes the gas diffusive output as governed by the stagnant boundary layer above the soil surface. By using backward implicit finite differencing, the following is derived:

$$a[1,n-1]\ K_H\ C_w[1,n-1] = -\frac{\Delta t}{\Delta z^2} D_g[2,n]\ K_H\ C_w[2,n] + \left[\frac{\Delta t}{\Delta z^2} D_g[1,n]\ K_H + a[1,n]\ K_H\ (1 + K_g) + \frac{\Delta t\ D_a}{\Delta z\ \underline{d}} K_H\right] C_w[1,n] \qquad (2\text{-}91)$$

where

n = time index

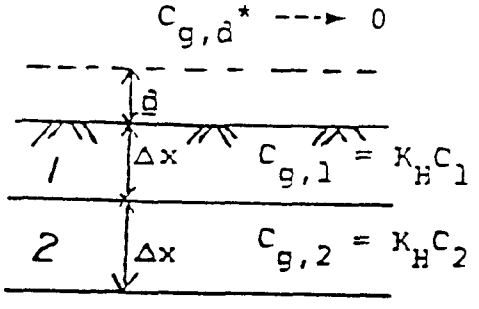

(a) without plant canopy

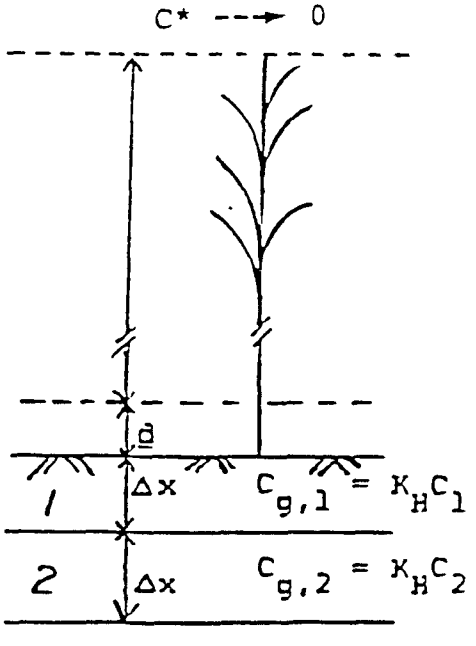

(b) with plant canopy

Figure 2.5. Schematic of the top two soil compartments and the overlying surface compartment (a) without plant canopy, (b) with plant canopy.

By substituting Equation (2-91) into the overall (i.e., all phases) mass balance equation for the uppermost soil layer, a flux-type upper boundary condition is obtained. Figure 2.5(b) reflects the field situation when a plant canopy exists. Zero concentration is now assumed to exist above the top of the canopy compartment. The volatilization flux from the plant canopy is defined as follows:

$$J_{pc} = \left(\frac{1}{d/D_a + \Sigma R}\right) (C_{g,1} - C^*) \qquad (2\text{-}92)$$

where

J_{pc} = volatilization flux through the plant canopy (g cm^{-2} day^{-1})

ΣR = vertical transfer resistance (day cm^{-1}, described in Section 2.3.4.3)

C^* = concentration above the plant canopy (assumed to be zero)

By carrying out a similar mass balance using finite differences, the boundary condition which describes the field with canopy existing is obtained.

2.4.3 Soil Temperature

Soil temperature is solved for numerically. Section 2.3.4.4 describes the theoretical basis for the simulation of soil temperature. The distribution of temperature within the soil profile is summarized by Equation (2-79). This equation is solved numerically for soil temperature, T, as a function of depth, Z, and time, t, based on the input thermal diffusivity, d, for each soil compartment, and the following initial and boundary conditions:

Initial Condition:

$$T_{z,o} = T(z) \qquad (2\text{-}93)$$

Boundary Conditions:

$$T_{o,t} = T_s(t) \qquad (2\text{-}94)$$

$$T_{L,t} = T_L(t) \qquad (2\text{-}95)$$

where

$T(z)$ = initial soil temperature in each soil compartment (°C)

$T_s(t)$ = calculated soil surface temperature for each time step (°C)

$T_L(t)$ = lower boundary temperature condition at the bottom of the soil core (°C)

The lower boundary temperature is defined by the user as 12 monthly values corresponding to the first day of each month; the value for each day is interpolated between the neighboring monthly values.

The following numerical approximation used in the model is taken from Hanks et al. (1971):

$$\frac{T_{i,j} - T_{i,j-1}}{\Delta t} = \frac{(T_{i-1,j} - T_{i,j})d_{i-\frac{1}{2},j} - (T_{i,j} - T_{i+1,j})d_{i+\frac{1}{2},j}}{\Delta z^2} \qquad (2\text{-}96)$$

Equation (2-96) is solved using a modified numerical solution procedure of Hanks et al. (1971) which involves the same finite difference technique and tridiagonal matrix solver (Thomas algorithm) used in PRZM (Carsel et al. 1984).

2.4.4 Furrow Irrigation

To simplify the algebra required to calculate the furrow infiltration volume as Manning's equation is substituted into the kinematic wave model (equation 2-86), Manning's equation is approximated as follows:

$$A = \alpha Q^m \qquad (2\text{-}97)$$

α and m are constants which are estimated by the model from the parameters of Manning's equation as follows:

$$m = \frac{\ln(A_2) - \ln(A_1)}{\ln(Q_2) - \ln(Q_1)} \qquad (2\text{-}98)$$

$$\alpha = A_1/Q_1^m \qquad (2\text{-}99)$$

where

A_1, A_2= cross-sectional areas (m^2) at depths y_1 and y_2

Q_1, Q_2= flow rates ($m^3\ s^{-1}$) computed from Manning's equation [(Equation 2-75)] at depths y_1 and y_2

y_1 = 1 cm

y_2 = 10 cm

The depths y_1 and y_2 were chosen to represent the range of depths likely to occur in furrows.

Substituting Equation (2-97) into Equation (2-86):

$$\frac{\partial Q}{\partial z} + \frac{\partial(\alpha\, Q^m)}{\partial t} = - \frac{\partial q}{\partial t} \qquad (2\text{-}100)$$

No closed-form solution to the above equation is known when infiltration is time-variable. Equation (2-100) is therefore solved for Q using the backwards-space, backwards-time, finite-difference solution described by Li et al. (1975). Writing Equation (2-100) in finite-difference form:

$$\frac{Q_{i+1}^{k+1} - Q_i^{k+1}}{\Delta z} + \frac{(\alpha Q^m)_{i+1}^{k+1} - (\alpha Q^m)_{i+1}^{k}}{\Delta t} = - \frac{(q_{i+1}^{k+1} - q_{i+1}^{k})}{\Delta t} \qquad (2\text{-}101)$$

where

Q_i^k = flow rate at time k, station i

Δz = spatial step

Δt = time step

Infiltration volumes are computed using the Green-Ampt model:

$$\frac{\partial I_i^k}{\partial t} = K_s \left[1 + \frac{(H + H_s)\theta}{I}\right] \qquad (2\text{-}102)$$

where

I_i^k = infiltration depth at time k (m), station i

K_s = saturated hydraulic conductivity of the soil (m s^{-1})

H = ponded water depth (m)

H_s = suction parameter (m)

θ = available porosity (fraction)

I = total volume of infiltrated water (m)

The Green-Ampt model has long been accepted as a model of the advance of the wetting front through the soil column, and involves parameters which can be related to well-known soil properties. The volume of infiltration is

computed assuming I_i^k is an average infiltration depth for the channel at location i:

$$q_i^k = W_i^k \, I_i^k \qquad (2\text{-}103)$$

where

q_i^k = volume infiltrated at location i (m^3 m^{-1})

W_i^k = current flow width at location i (m)

Furrow channels are assumed to be trapezoidal in shape. Equation (2-87) is solved at each station at the end of each time step for the new flow rate Q_{i+1}^{n+1}. Because the equation is non-linear with respect to Q, the new value of flow is found using second-order Taylor series iteration. Given the flow rate in the furrow, infiltration depths at each location are then computed using the Green-Ampt model [Equation (2-102)].

The PRZM furrow irrigation model determines infiltration depths at various locations in the furrow. Irrigation continues until the depth of water infiltrated at the downstream end of the furrow is sufficient to meet the soil moisture deficit SMDEF. The depth of water applied as irrigation to the first PRZM soil compartment is then set equal to either the average furrow infiltration depth or the infiltration depth at a specific location in the furrow, depending upon options selected by the user. This depth of water then infiltrates through the root zone as determined by the PRZM soil hydraulic algorithms.

2.5 RESULTS OF PRZM TESTING SIMULATIONS

This section includes the results of testing the two solute transport solution techniques and the volatilization algorithm. Simulated results are compared with those from analytic solutions. Sensitivity analyses were also performed to evaluate the effects of key model parameters on the prediction of volatization rates. A test comparison of the model with field data from Georgia (soybeans) concludes the section.

The PRZM model has undergone additional performance testing with field data in New York and Wisconsin (potatoes), Florida (citrus), and Georgia (corn) (Carsel et al., 1985; Jones 1983; Jones et al., 1983). The results of these tests demonstrate that PRZM is a useful tool for evaluating groundwater threats from pesticide use. Please refer to these references for information regarding the further testing of PRZM under field conditions.

2.5.1 Transport Equation Solution Options

Currently, two numerical solution options are available to the PRZM user for the chemical transport equation. As discussed in Section 2.4.1, the finite difference option (utilizing subroutine SLPSTO) is unconditionally stable and convergent, but may result in excessive numerical dispersion in high Peclet

number systems. The MOC method of characteristics algorithm (utilizing subroutines MOC and SLPST1) eliminates or reduces that numerical dispersion. Two examples are provided which compare the alternate solutions methods at high Peclet number (greater than 5.0) and at low Peclet number (less than .5).

2.5.1.1 High Peclet Number--
Figure 2.6 presents the analytical solution (Hunt 1978) together with the SLPST0 and MOC/SLPST1 solutions at 6 days for the transport of a 69 mg cm^{-3} pesticide application in the uppermost compartment. The physical parameters are as presented in the figure--notably the Peclet number is 5.1. The following table details pertinent features of the simulation:

Method	Location of Peak	Value of Peak (mg/cm^3)	% Error at Peak	Runtime (sec)
Analytical	5.8	11.2	-	-
SLPST0	4.5	5.07	-54	88.5
MOC/SLPST1	5.5	12.09	+7	112.4

At this relatively high Peclet number, the SLPST0 algorithm shows excessive numerical dispersion, capturing only about half the amplitude of the peak concentration, while showing excessive mass in both tails. In addition, the SLPST0 algorithm does not predict the location of the peak precisely (it is lagged behind the location of the peak given by the analytical solution and the MOC/SLPST1 solution). In this example, the MOC/SLPST1 algorithm requires 27% more runtime, but errs by only 7% in the peak and shows good agreement in the tails. Users should note that the increase of runtime could be significantly high for longer simulation periods and deeper soil profiles.

2.5.1.2 Low Peclet Number--
Figure 2.7 illustrates the results of a SLPST0 and MOC/SLPST1 simulation 8 days after an incorporation of 69 mg/cm^3 in the sixth compartment using the parameters listed. The predicted concentrations at this lower Peclet number, 0.46, are very similar in the peaks and the tails, and apparently little additional resolution is gained from utilizing the MOC algorithm. However, the additional computational burden associated with the MOC algorithm is only 7% in this example.

2.5.2 Testing Results of Volatilization Subroutines

To test and validate the operation of the volatization algorithms, model results were compared with Jury's analytical solution (Jury et al., 1983a), and against field data for trifluralin from Watkinsville, GA. Sensitivity analyses were also performed to evaluate effects of key parameters on model predictions. The intent of this preliminary model testing was to evaluate model operation by comparing the results for the volatization flux from a soil surface application.

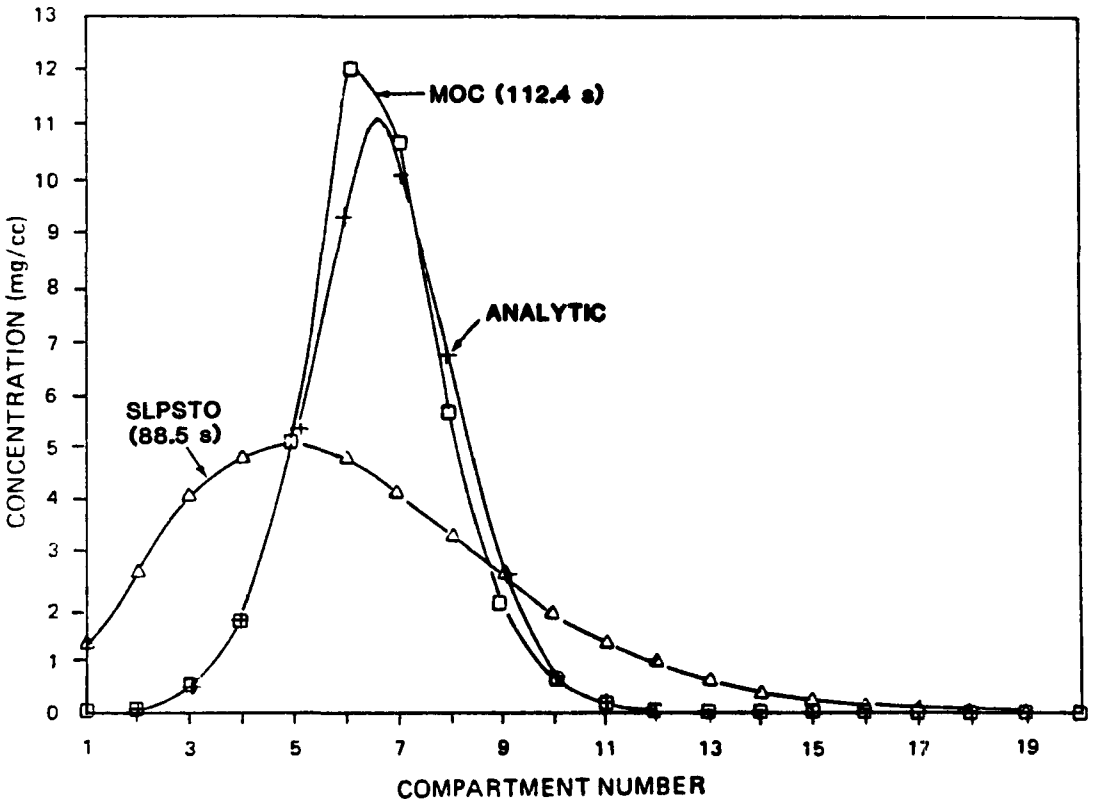

Velocity = 11.1 cm/day

Diff coef = 2.0 cm^2/day

Retardation Coef = 11.74

Decay Constant = .10 /day

Core length = 20 cm

Delta x = 1 cm

Delta t = 1 day

Peclet = 5.1

Figure 2.6. Comparison of simulation results at high Peclet number.

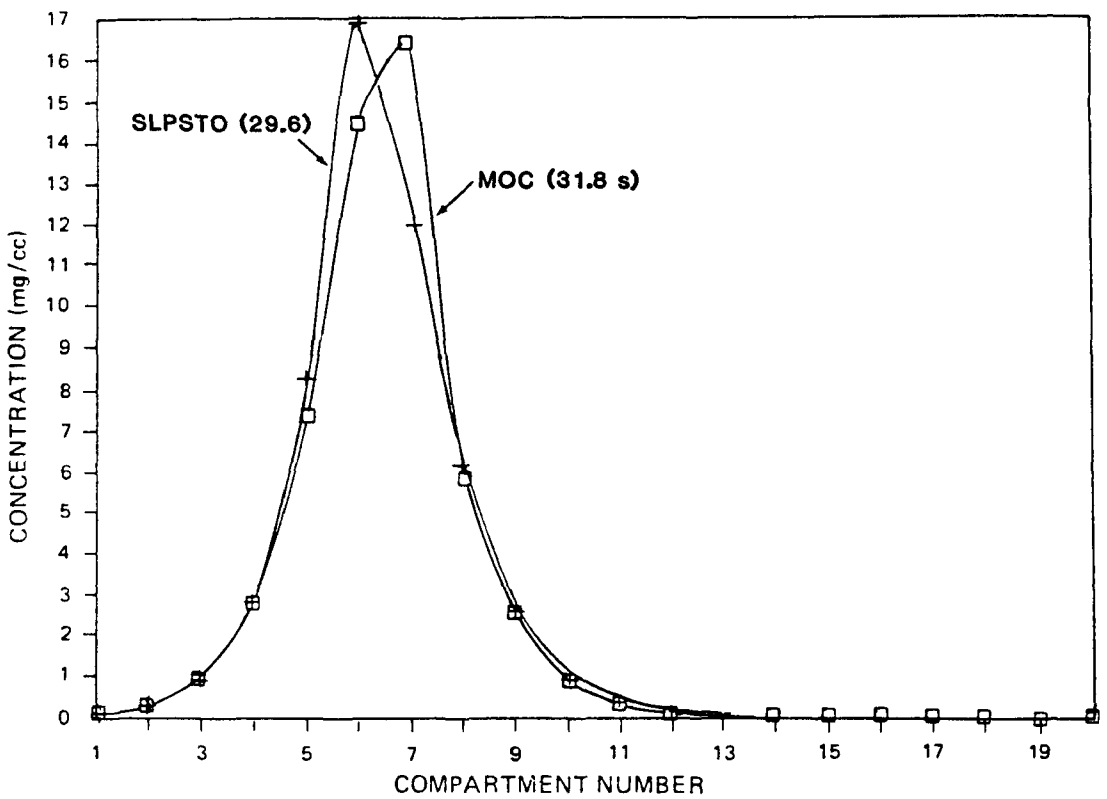

Velocity = 1.82 cm/day	Delta x = 1 cm
Diff Coef = 4.0 cm^2/day	Delta t = 1 day
Retardation Coef = 11.74	Core length = 20 cm
Decay = .1 /day	Peclet = .46

Figure 2.7. Comparison of simulation results at low Peclet number.

2.5.2.1 Comparison with Analytical Solution--
Jury et al. (1983a) presented a mathematical model for describing volatile loss and movement of soil-applied organic chemicals. By making the following assumptions, they derived an analytical solution for evaluating the chemical concentration profile within the soil and the volatilization flux at the soil surface:

1) Uniform soil properties consisting of a constant water content, bulk density, liquid water flux (either upward, downward, or zero), and a constant organic carbon fraction

2) Linear equilibrium adsorption isotherm

3) Linear equilibrium liquid-vapor partitioning (Henry's law)

4) Uniform incorporation of a quantity of chemical to a specified depth below the surface

5) Pesticide loss by volatilization through a stagnant air boundary layer at the soil surface

6) Infinite depth of uniform soil below the depth of incorporation

Assumptions 2 to 5 are satisfied by the current PRZM code. Assumption 6 defines zero concentration for the bottom layer, which is somewhat different from PRZM's zero gradient bottom boundary condition. However, as long as no chemical reaches the bottom layer, these two types of boundary conditions produce identical results. Our test runs for volatilization were designed to satisfy this requirement. In order to comply with assumption 1, the hydrological computation subroutines in PRZM were bypassed and replaced with a constant value for water flux. A positive flux value indicates a leaching condition, while a negative flux value indicates an evaporating condition. The hydrological subroutines in PRZM are based on a moisture-routing method in which daily accounting of water inflow and outflow is recorded. One limitation of the moisture-routing method is that it is unable to properly describe the upward movement of evaporating water. Evaporation loss is removed from specific surface soil layers without accounting for movement between layers.

The pesticide 2,4-D was chosen as the test compound for our simulation; the input parameters are listed in Table 2-2 and were obtained from Jury et al. (1983a). The test run results for daily volatilization flux are presented in Figures 2.8(a), 2.8(b), 2.9(a), and 2.9(b), corresponding to the four test cases listed at the bottom of Table 2-2. Two different soil compartment depths (DELX) of 1.0 and 0.1 cm were used to investigate the sensitivity of the volatilization algorithms to the spatial discretization in the surface soil horizon.

Figure 2.8(a) shows the steady state situation (i.e., no evaporation and no leaching) without any advective movement. The daily volatilization flux values predicted by the two different DELXs are almost identical. In this case, the magnitude of DELX is relatively unimportant. The simulation

TABLE 2-2. INPUT PARAMETERS FOR THE TEST CASES - ANALYTICAL SOLUTION

D_G	Air diffusion coefficient	0.43 (m^2 day^{-1})
D_L	Water diffusion coefficient	4.3×10^{-5} (m^2 day^{-1})
ϕ	Porosity	0.5
ρ	Bulk density	1.35 (kg m_{-3})
T	Temperature	25°C
f_{oc}	Organic carbon fraction	0.0125
θ	Water content	0.3
a	Air content	0.2
M	Pesticide applied	1 (kg ha^{-1})
L	Depth of incorporation	0.1 m
K_H	Henry's constant for 2,4-D	5.5×10^{-9}
K_{oc}	Organic carbon partition coefficient for 2,4-D	0.02 (m^3 kg^{-1})
u	Decay coefficient for 2,4-D	4.62×10^{-2} (day^{-1})
l	Total depth of soil column	0.3 m
t	Simulation period	30 days
J_w	Water flux	
E	Evaporation flux	

Test case #1: no evaporation and no leaching (J_w = E = 0)

Test case #2: with leaching (J_w = 0.01 cm day^{-1})

Test case #3: with evaporation (E = 0.01 cm day^{-1})

Test case #4: with evaporation (E = 0.25 cm day^{-1})

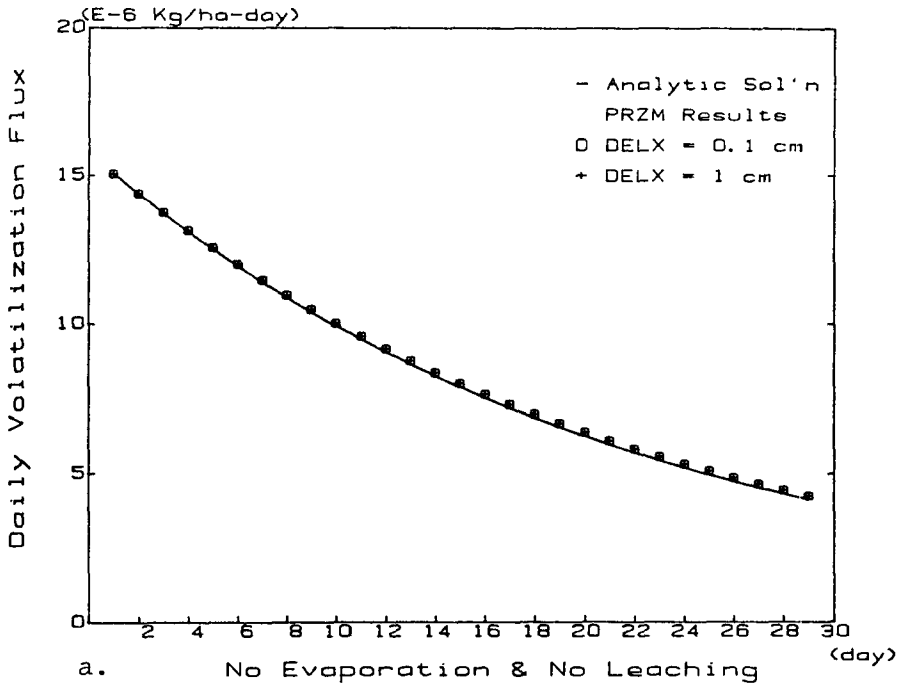

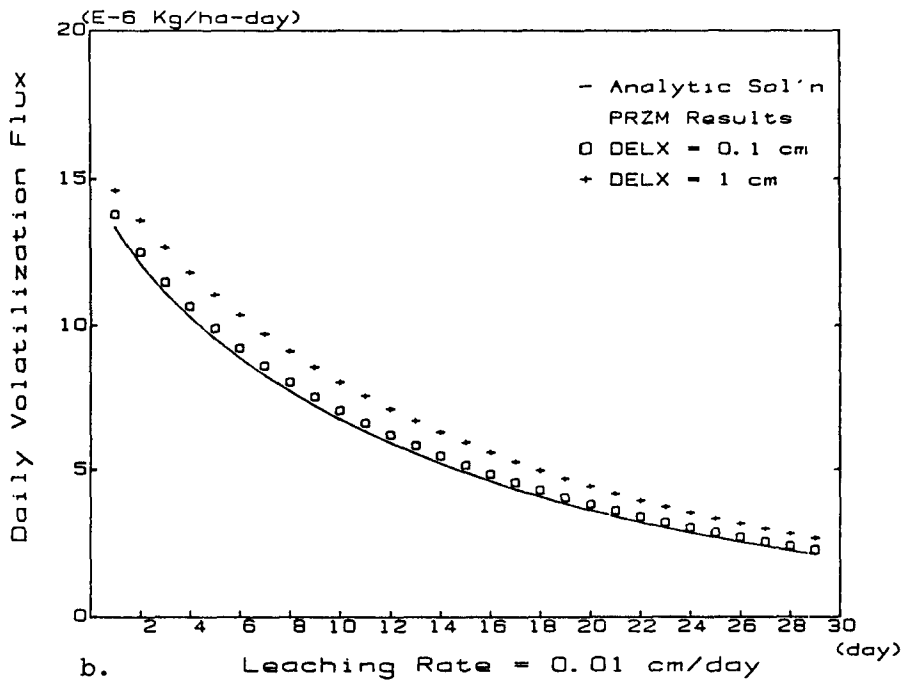

Figure 2.8. Comparison of volatilization flux predicted by PRZM and Jury's analytical solution: Test cases #1 and #2.

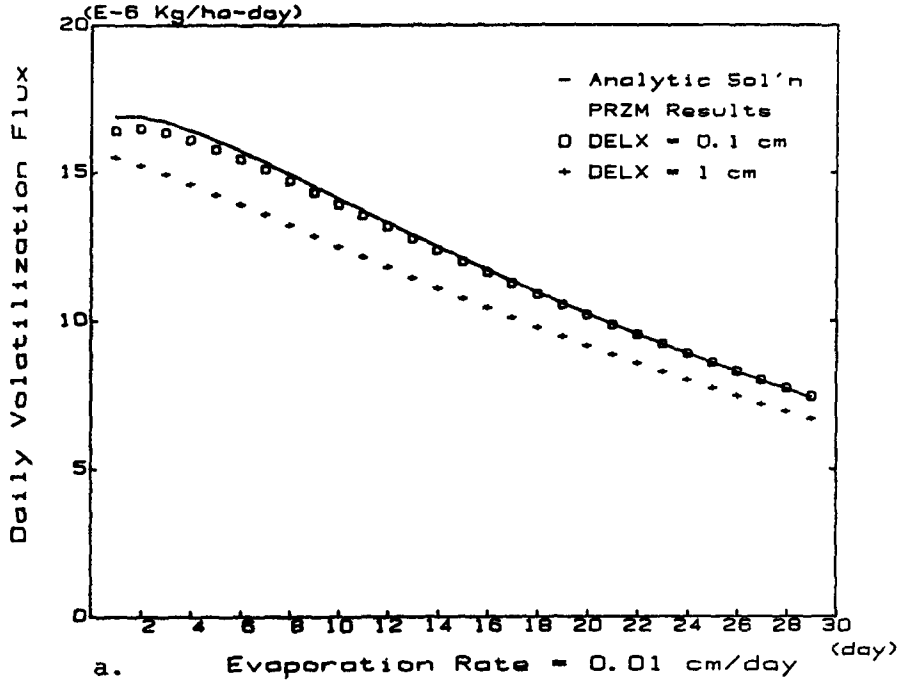

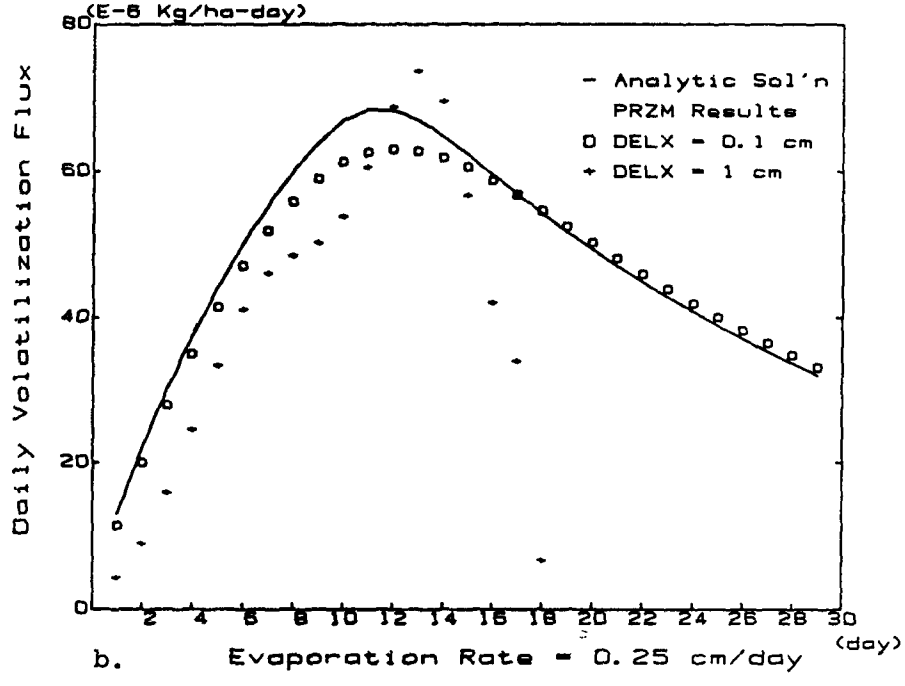

Figure 2.9. Comparison of volatilization flux predicted by PRZM and Jury's analytical solution: Test cases #3 and #4.

results with a leaching rate of 0.01 cm/day are shown in Figure 2.8(b). Because of the leaching influence, the predicted daily flux is smaller than the corresponding daily value shown in Figure 2.8(a). The differences beween the analytical solution and the PRZM predictions are due to the finite difference solution technique and the occurrence of advective movement by leaching. The simulation results using the smaller DELX (0.1 cm) more closely match the analytical solution results, and an even smaller DELX would have improved the agreement further. The slope of both DELX curves is the same as the analytical solution, and the maximum differences (for the 1.0 cm DELX) from the analytical solution are 10% or less.

Figure 2.9 shows the simulation results under evaporating conditions with the upward advective velocity at 0.01 (Figure 2.9(a)) and 0.25 (Figure 2.9(b)) cm/day. The "wick effect" phenomenon (described in Section 2.3.4) leading to enhanced upward movement of the pesticide can be observed in these two figures. The maximum daily flux occurs on the first day for the leaching conditions. Depending on the magnitude of the evaporating water velocity, the maximum daily flux no longer occurs on the first day of the pesticide application. Also the magnitude of the maximum daily flux is enhanced by the magnitude of the evaporating water velocity. The effect of DELX becomes more critical as the influence of advective movement increases. For simulations using a 1.0-cm DELX, Figure 2.9(a) shows stable numerical behavior with a small discrepancy when compared to the analytical solution result. As the advective movement becomes larger, the numerical behavior becomes more unstable, as shown in Figure 2.9(b). The smaller 0.1-cm DELX showed good agreement with the analytical solution for both test cases shown in Figure 2.9.

Based on these test cases, it appears that a finer DELX, in the range of 0.1 to 0.5 cm, is needed for top soil layers when volatilization processes are simulated with PRZM. However, this finer DELX requirements poses an additional computational burden for PRZM applications due to the increase in the number of soil compartments. To circumvent this burden, the PRZM code was modified to allow a variable compartment depth, which allows the user to select a smaller DELX for the top horizon (or any other horizon) and a bigger DELX for the rest of the soil profile. By selecting this variable compartment depth capability, a significant saving in CPU time may be achieved while a better representation is provided for calculation of the surface volatilization flux. In conjunction with field data comparisons (presented below), the results of model runs and CPU time are presented for both uniform and variable compartment depth simulation runs.

2.5.2.2 Comparison with Field Data--
Preliminary model testing with field observations was also performed to assess the ability to predict the general magnitude of volatilization losses and daily fluxes under field conditions. Based on a review of available volatilization field data sets, a USDA experimental watershed site in north-central Georgia was selected because of its use of a volatile pesticide (trifluralin), surface-applied to a major crop (soybeans), with a comprehensive micrometeorological and soil sampling plan.

The study site was located at Watkinsville, GA, on a 1.26-ha watershed comprised of Cecil soil (63.9% sand, 23.6% silt, and 12.5% clay) with 0.55% organic carbon, a pH of 6.5, and a slope of 3.0%. Harper et al. (1976) present a detailed description of the site, the equipment, and the installation procedures required for collecting microclimate data. They also summarize the method, assumptions, and calculations used for determining pesticide volatilization flux rates. Trifluralin was surface-applied as a spray to a bare soil surface, using a ground sprayer equipped with flat-fan nozzles, at a rate of 1.12 kg/ha between 1220 and 1247 eastern daylight time (EDT) on 15 June 1973.

The field results shown in Table 2-3 were obtained from White et al. (1977). The values in columns 2, 4 and 5 of Table 2-3 provide the cumulative volatilization flux, remaining pesticide in soil, and total cumulative decay losses, respectively. A discrepancy is noted for the data in column 4 of Table 2-3; the pesticide remaining in soil at the 35th day is smaller than that at the 49th day. This discrepancy is most likely due to sampling variations, although data were not available to establish accuracy limits on the data points. Meteorological data required for applying PRZM to the site, which include daily precipitation and pan evaporation, were obtained from Smith et al. (1978).

The PRZM input parameters for trifluralin and the Watkinsville site are listed in Table 2-4. Two additional key parameters which influence the volatilization results are the decay rate and the adsorption partition coefficient. The magnitude of the decay rate can be estimated from the data in column 5 of Table 2-3, assuming that decay accounts for all losses from the soil other than volatilization. A value of 0.0206 per day for the first-order decay rate constant obtained from these data points is consistent with the value of 0.0198 per day used by Donigian et al. (1986) after reviewing the literature. An initial value for K_d was obtained from the organic carbon content of 0.55% and an organic-carbon partition coefficient (Koc) value of 13,700, resulting in a K_d of 75 ml/g. Figure 2.10 shows the results of sensitivity analyses runs for K_d and the decay rate; the observed data for trifluralin from Table 2-3 is also included for comparison. Figure 2.10(a) shows a good representation of the observed cumulative volatilization curve. Figure 2.10(b) shows that a value of 40 for K_d, and a decay rate of 0.02 per day provides the best representation of the decay rate values analyzed.

The simulation results for cumulative volatilization flux and cumulative pesticide decay are shown in Figure 2.11 for four different DELX combinations. For these simulations, DELX values of 1.0, 0.5, 0.25, and 0.1 cm were chosen for the first horizon and 5-cm DELX for the rest of the profile. The field data are also included in the figures for comparison. Table 2-5 shows the total volatilization flux for each of the 4 using variable DELX, as well as for a simulation using simulations, a constant 1.0-cm DELX throughout the whole soil profile. The CPU requirements for each run are also included in Table 2-5. The predicted total volatilization flux using the smallest DELX of 0.1 cm is closest to the field-measured value; the values for DELX of 0.25 cm and 0.50 cm are also quite close to the field value. The saving of CPU time can be observed from Table 2-5. One hundred twenty-nine seconds are required for the simulation using 1.0-cm DELX for the

TABLE 2-3. TRIFLURALIN VOLATILIZATION LOSSES, AMOUNTS REMAINING IN SOIL, AND ESTIMATED LOSSES VIA OTHER PATHWAYS FOR THE 120-DAY FIELD TEST

Time, (day)	Cumulative Volatilized % of Total Applied	Cumulative Volatilized % of Total Volatilized	Remaining* in Soil, % Applied	Estimated Other Losses, % of Applied
Application	3.5	13.3	--	---
1	3.8	14.8	89	7.2
2	5.3	20.3	72	22.7
6	10.9	42.2	64	25.1
18	20.5	79.1	51	28.5
35	23.4	90.2	33	43.6
49	24.4	94.1	35	40.6
63	25.1	96.9	23	48.9
76	25.4	98.2	20	54.6
120	25.9	100.0	11	63.1

Source: White et al., 1977.

* Based on amount remaining in soil at a 0- to 7.5-cm depth as compared with an initial 1.0 μg/g level at application (rate was 1.12 kg/ha).

TABLE 2-4. INPUT PARAMETERS FOR THE TEST CASES - WATKINSVILLE SITE

Simulation start date		14 June 1973
Simulation end date		31 December 1973
Trifluralin:	Henry's constant	6.7×10^{-3}
	Diffusion coefficient in air	0.43 m^2 day^{-1}
	Application date	15 June 1973
	Amount applied	1.12 kg ha^{-1}
	Incorporation depth	5 cm

Horizon	Thickness (cm)	DELX (cm)	Field Capacity	Wilting Point	Initial Water Content
1	5	0.1	.207	.095	0.166
2	10	5.0	.207	.095	0.217
3	15	5.0	.339	.239	0.318
4	60	5.0	.320	.239	0.394

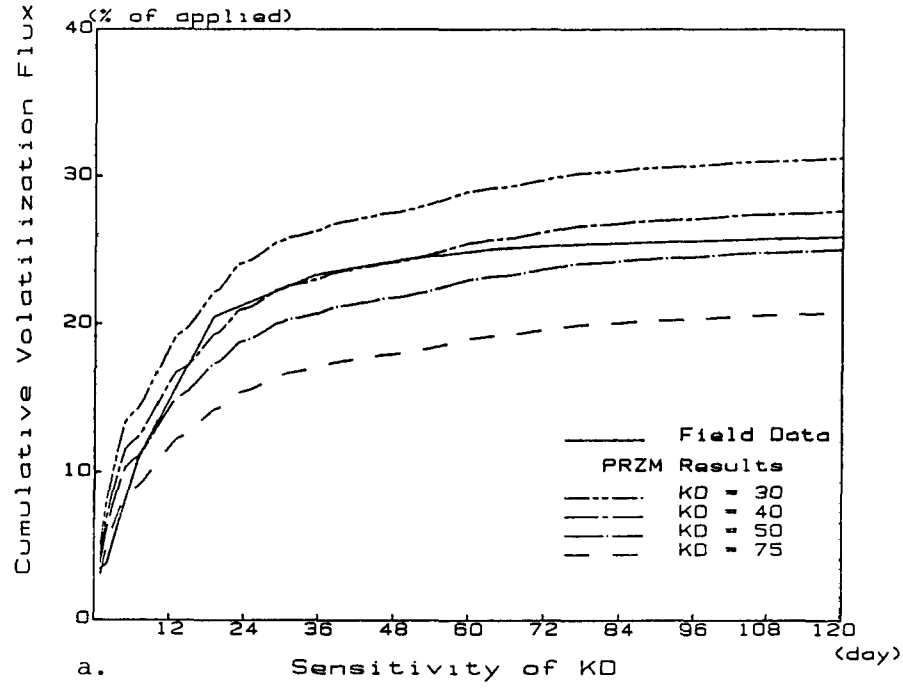

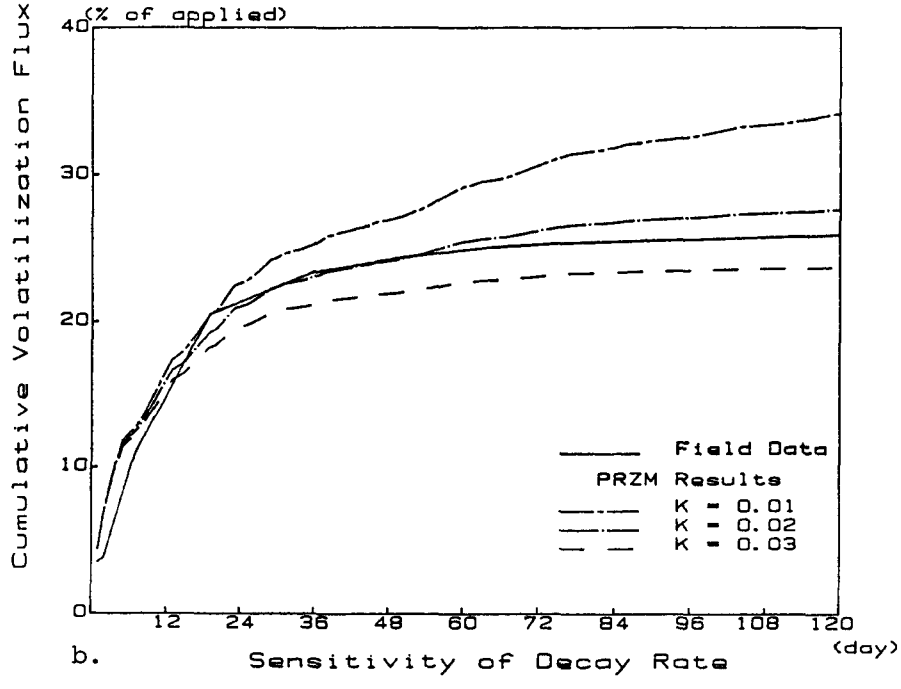

Figure 2.10. Sensitivity of cumulative volatilization flux to K_d and decay rate.

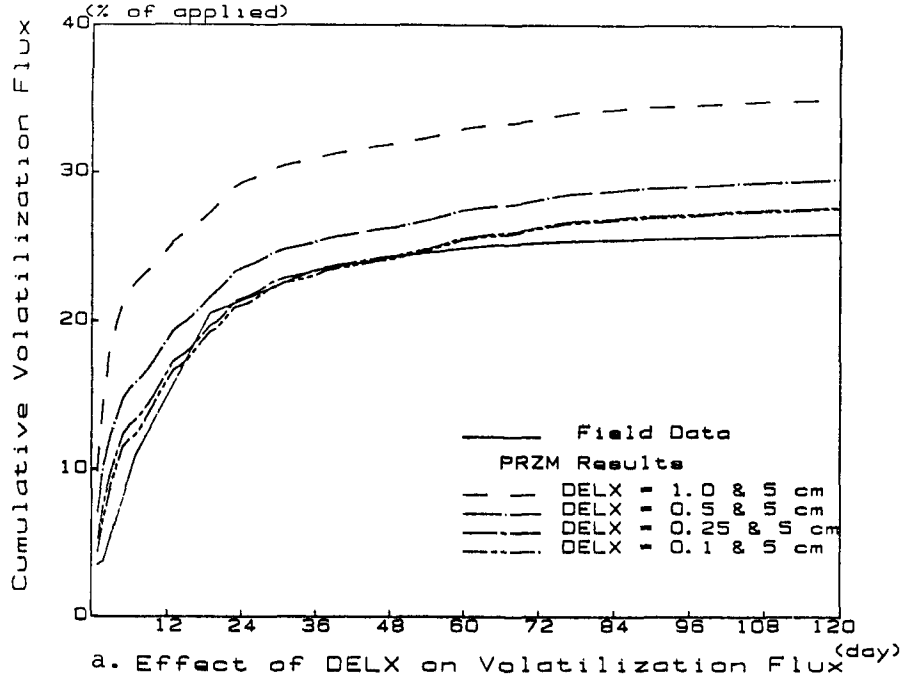

a. Effect of DELX on Volatilization Flux

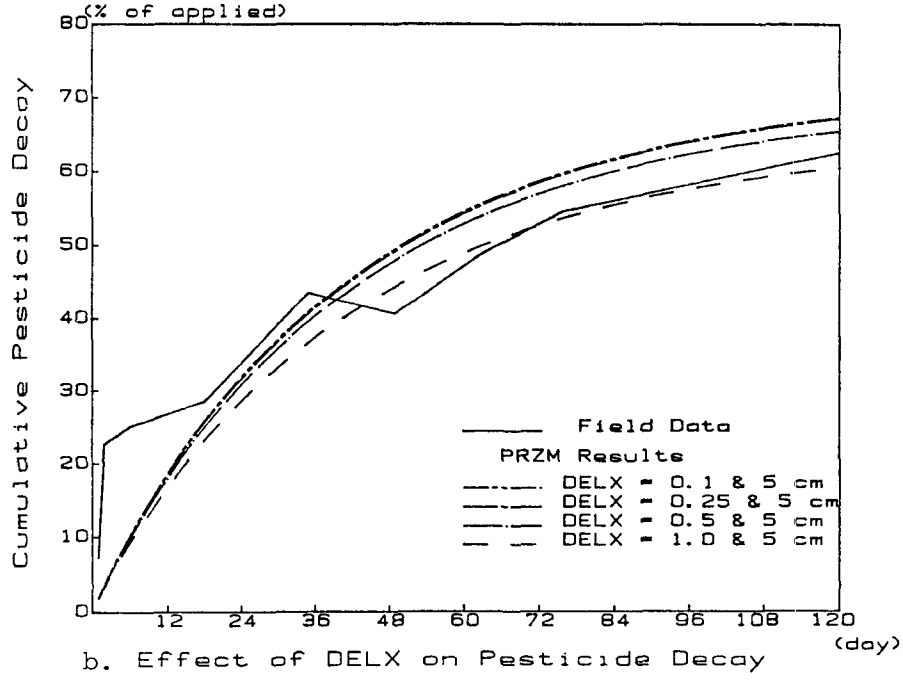

b. Effect of DELX on Pesticide Decay

Figure 2.11. Effects of DELX on volatilization flux and pesticide decay.

whole soil profile, compared with only 39 seconds for the simulation using 1.0 cm for the top horizon and 5.0 cm for the rest of the profile. The results in Table 2-5 indicate that a DELX of 0.25-0.50 cm for the top horizon may be a reasonable compromise between simulation accuracy and CPU costs.

TABLE 2-5. SIMULATION RESULTS OF USING DIFFERENT COMPARTMENT DEPTH (DELX)

Horizon	Constant DELX		Variable DELX				
	Depth (cm)	DELX (cm)	DELX (cm)	DELX (cm)	DELX (cm)	DELX (cm)	
1	5	1.0	1.0	0.5	0.25	0.1	
2	10	1.0	5.0	5.0	5.0	5.0	
3	15	1.0	5.0	5.0	5.0	5.0	
4	60	1.0	5.0	5.0	5.0	5.0	Field Value
Total Volatilization Flux (kg/ha)		0.393	0.398	0.338	0.317	0.316	0.290
CPU (Sec)		129	39	46	67	106	

Figure 2.12(a) demonstrates significant differences between the observed pesticide decay and the simulated values during the first few weeks following application. In fact, the observed data appear to indicate a much higher attenuation rate during the first few days following application, with a lower rate for the remaining period. To better match the decay characteristics, and evaluate the potential impact on the volatilization simulation, a two-step decay procedure was used with a rate of 0.1 per day for 5 days following application and a rate of 0.01 per day for the remaining period. The results of these simulations in terms of pesticide remaining in the soil, shown in Figure 2.12, indicate a much better agreement with the observed field values in Figure 2.12(b). The impact of the two-step decay on both cumulative decay and volatilization flux is shown in Figure 2.13. The cumulative pesticide decay shown in Figure 2.13(a) improves considerably (compared to Figure 2.11(b)), while the results for cumulative volatilization flux (Figure 2.13(b)) are slightly better than those in Figure 2.11(a).

2.5.2.3 Conclusions from Volatilization Model Testing--
The primary conclusions derived from this preliminary model testing are as follows:

1) Comparisons with Jury's analytical solution indicate that the volatilization algorithms are operating correctly, and that with a very small DELX (0.1 cm or less), the results are in excellent agreement.

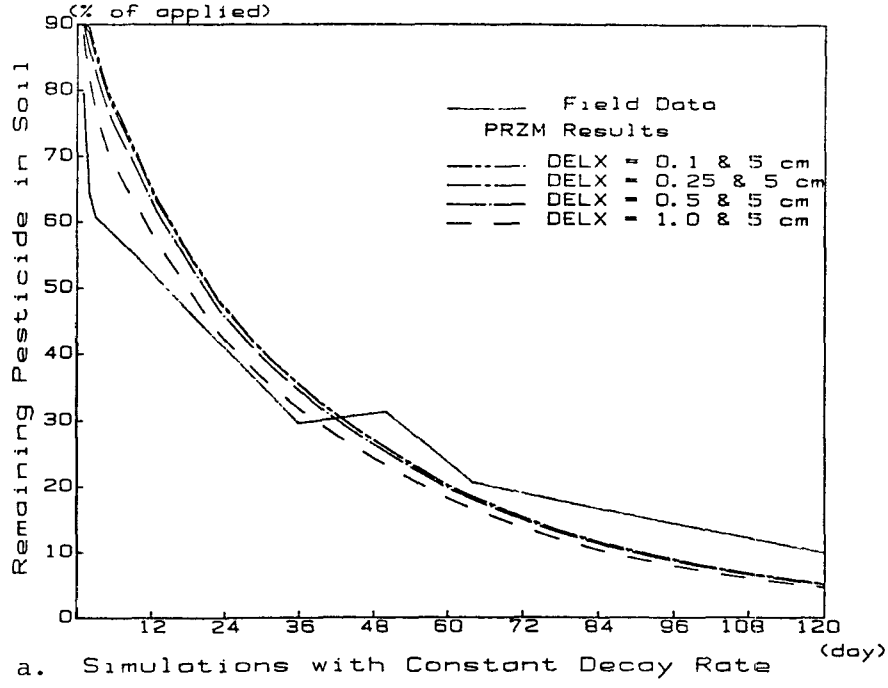

a. Simulations with Constant Decay Rate

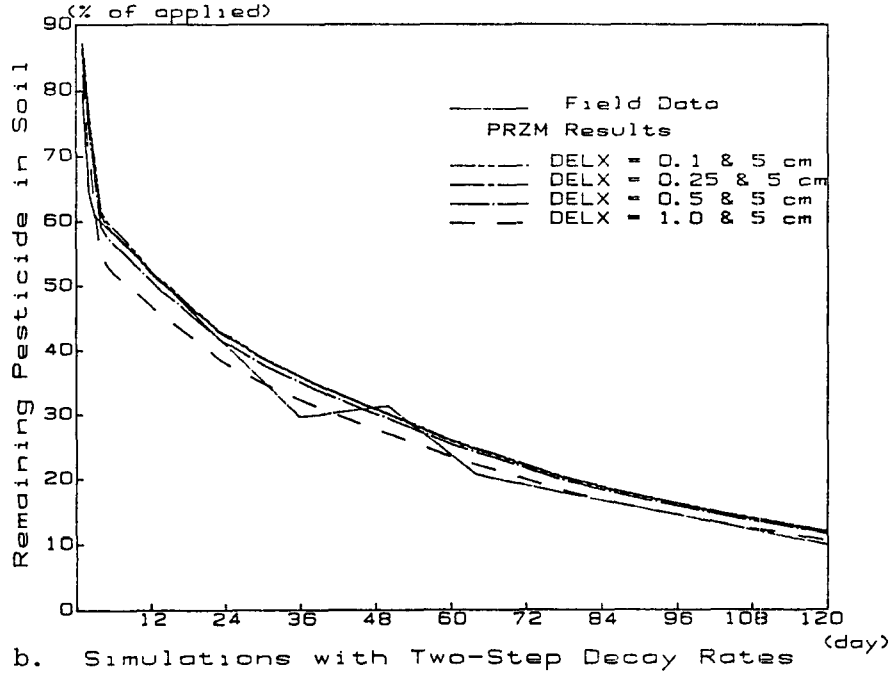

b. Simulations with Two-Step Decay Rates

Figure 2.12. Comparison of constant and two-step decay rates.

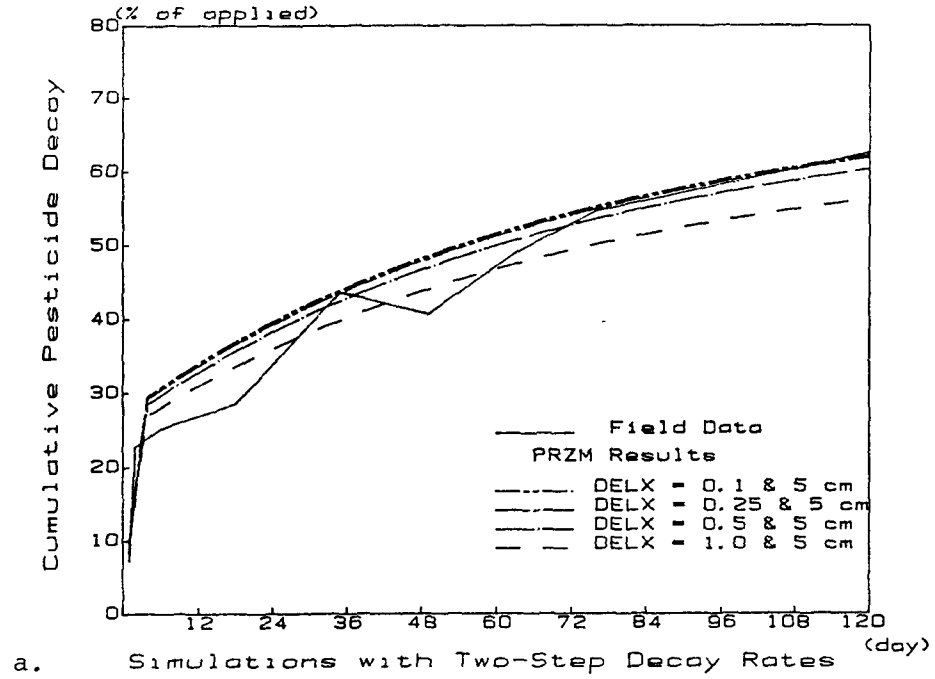

a. Simulations with Two-Step Decay Rates

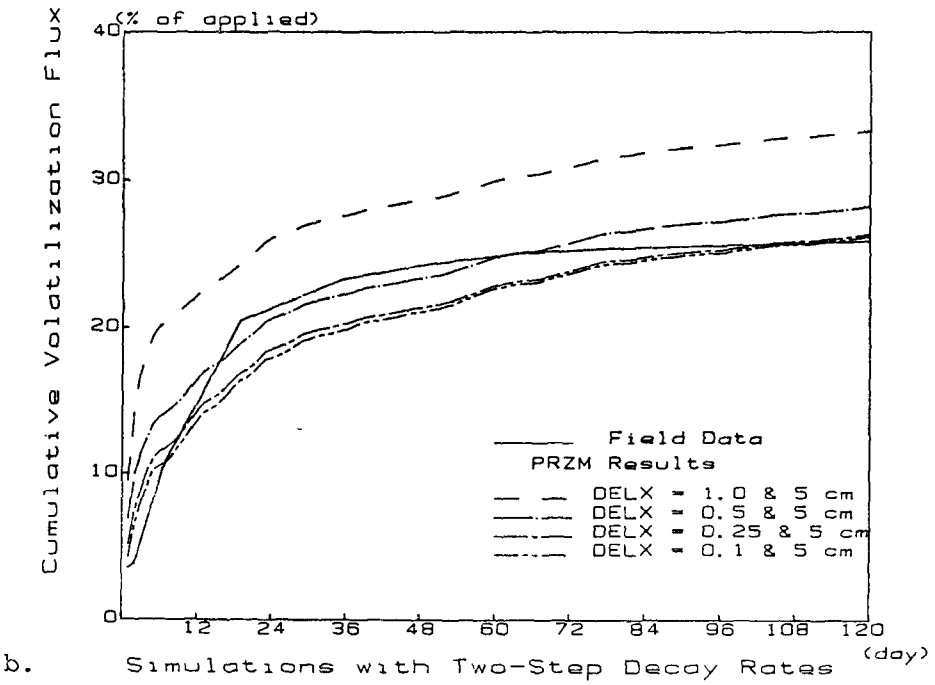

b. Simulations with Two-Step Decay Rates

Figure 2.13. Effects of two-step decay rates on volatilization flux and pesticide decay.

2) The preliminary field testing results with trifluralin in Watkinsville, GA, indicate good agreement between measured and predicted volatilization flux when measured decay rates and adjusted K_d values are used.

3) Small soil layer depths in the range of 0.25 and 0.50 cm are needed to provide the best presentation of volatilization flux at reasonable CPU times, based on the Watkinsville testing.

4) A two-step decay rate best represents the attenuation behavior of trifluralin, using a higher rate for the period immediately following application, and a lower rate for the remaining period.

Further testing of the volatilization model should be performed to evaluate its capabilities for different compounds, different regions, and other crops. In addition, the plant compartment vapor transport and concentration calculations should be tested with the additional data available from the Watkinsville site and from other field data sets (e.g., Grover et al., 1985; Willis et al., 1983).

2.5.3 Testing Results of Soil Temperature Simulation Subroutine

Preliminary testing of the soil profile temperature simulation subroutine was performed by comparing predicted values with values obtained by an analytical solution to the governing heat flow equation. These testing results are discussed in this section. Field testing of the soil surface/upper boundary temperature simulation, estimated by the energy balance procedure in the model, was not performed due to problems in obtaining observed meteorological and soil temperature data for the Watkinsville, GA, test site.

An analytical solution presented in Kreysig (1972) for the classical one-dimensional heat flow partial differential equation (described in Section 2.3.4.4) was used to calculate changes in the soil temperature profile with time, due to a change in the upper boundary temperature. In order to develop a valid comparison between the analytical and finite difference methods, the following assumptions were made:

a) Uniform properties throughout the soil profile
b) Constant lower-boundary temperature
c) Uniform initial temperatures throughout the profile

To compare the results of the analytical solution with the finite difference solution from the soil temperature model, the following parameters were used:

Depth of the soil profile	= 100 cm
Compartment thickness (DELX)	= 1.0 cm
Diffusivity of the soil profile	= 864 cm^2 day^{-1}
Upper-boundary temperature, $T_{(o,t)}$	= 30°C
Lower-boundary temperature, $T_{(L,t)}$	= 20°C
Initial temperature, $T_{(x,o)}$	= 20°C

Figures 2.14 and 2.15 show the comparison of soil temperature profiles predicted by both the analytical solution and the finite difference soil temperature model after 1 day and 5 days of simulation. In Figure 2.14 the finite difference solution is obtained by using a 1-hour time step, while in Figure 2.15 a 1-day time step is used. The following observations are evident from these testing results:

1) Comparison of the soil temperature profiles predicted by both methods indicate excellent agreement when the smaller, 1-hour time step is used in the finite difference procedure, as shown in Figure 2.14.

2) The finite difference solution obtained by using the daily time steps deviates from the analytical solution by about 1°C, in the upper and middle portions of the soil profile (Figure 2.15). This deviation is due to the assumption of a constant initial temperature profile and the abrupt change in the upper-boundary temperature from 20°C to 30°C for the first daily time step.

3) As the steady-state condition is approached, irrespective of the time step used in the finite difference solution, the soil temperature profiles predicted by both methods are in good agreement (Figures 2.14(b) and 2.15(b)).

Table 2-6 shows that reducing the depth of the compartment from 1 cm to 0.1 cm does not produce any significant change in the finite difference solution. These depths bracket the range of values for DELX (i.e., compartment thickness) likely to be used for the surface soil horizon.

These test results show that for smaller time steps the finite difference solution will be in complete agreement with the analytical solution. For a daily time step as used in PRZM, under expected environmental conditions, with a non-uniform initial temperature profile, non-uniform soil characteristics, and smaller daily changes in the upper-boundary temperature, the soil temperature profile estimated by the finite difference method used in the model is expected to be capable of providing close agreement with observed temperature profile data. In addition to further testing of the soil profile temperature model with field data, the procedure to estimate the upper-boundary temperature should be tested to evaluate and demonstrate the validity of the entire soil temperature simulation model.

2.5.4 Testing of Daughter Products Simulation

The fate of pesticides in soils is a complex issue. There are many processes (i.e., volatilization, degradation, etc.) which must be considered in order to adequately address this issue. One of these processes, which has been largely neglected in pesticide leaching models, is that of the transformation of the parent compound to various toxic daughter products. The tendency has been to lump all the toxic family into a "total toxic residue" and model the fate of this composite as a single chemical. This assumption may not be acceptable, especially if the daughters have very different decay rates or adsorption partition coefficients from the parent or from each other.

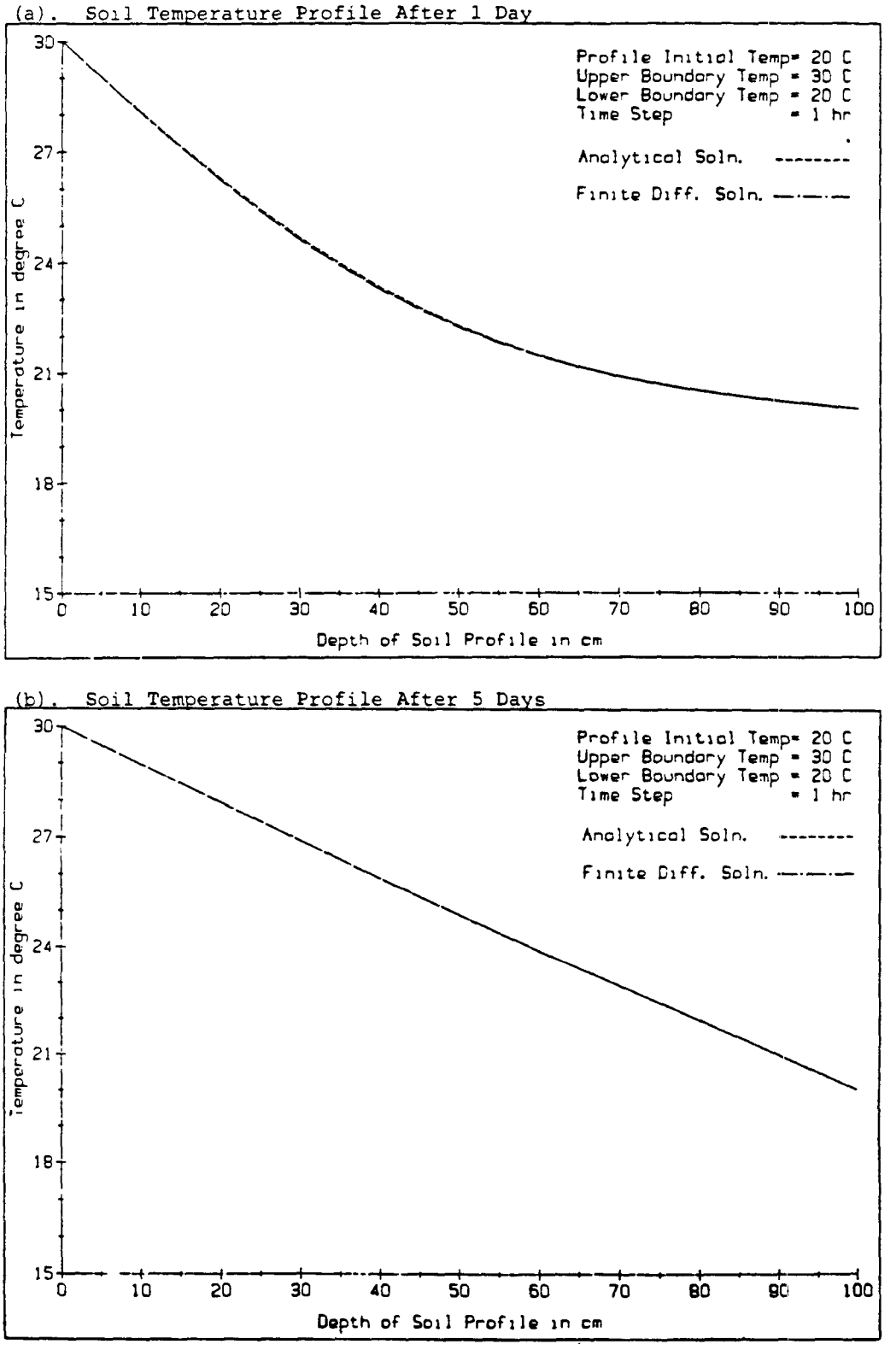

Figure 2.14. Comparison of soil temperature profiles predicted by analytical and finite difference solutions.

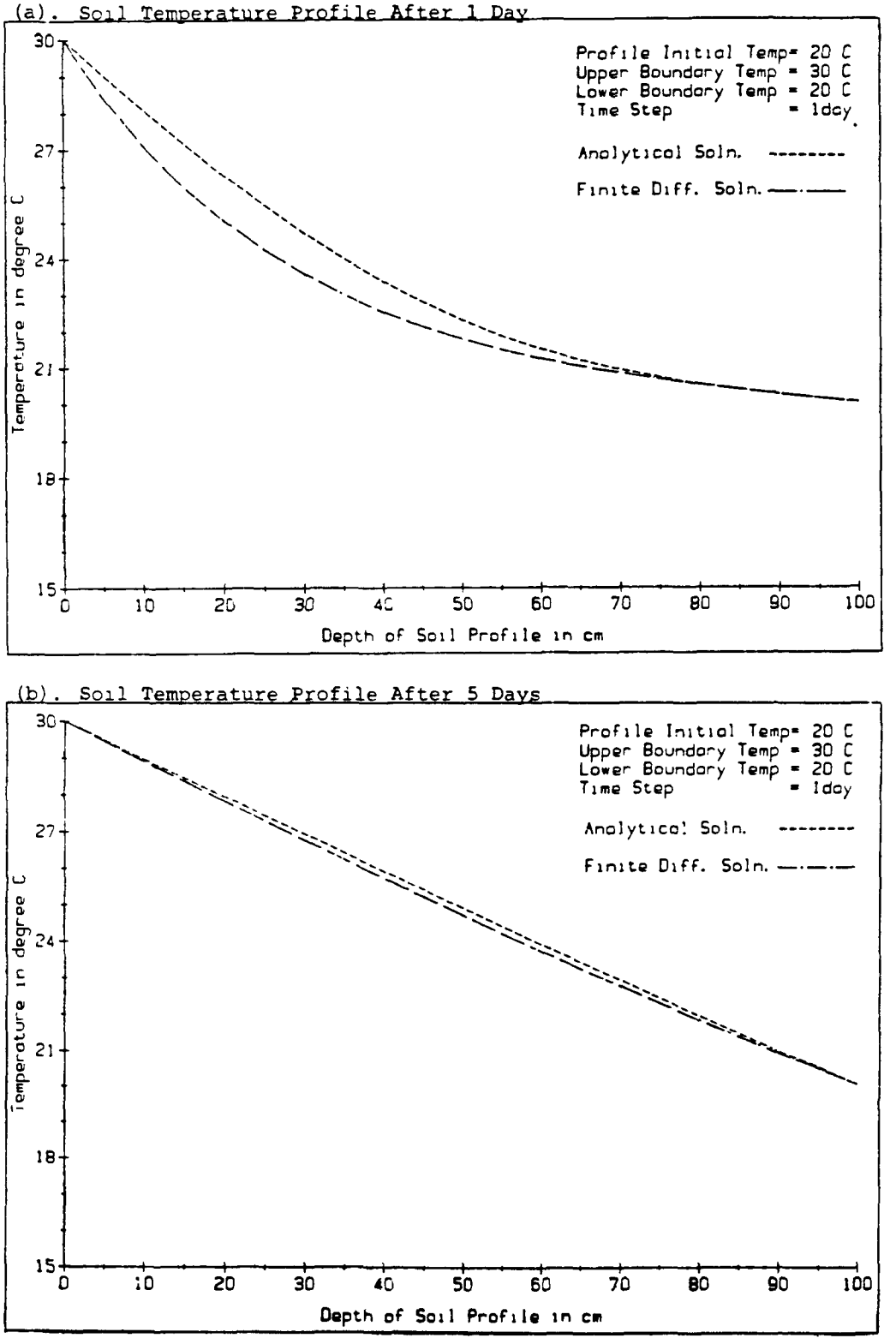

Figure 2.15. Comparison of soil temperature profiles predicted by analytical and finite difference solutions.

Table 2-6. SIMULATED SOIL TEMPERATURE PROFILE AFTER ONE DAY FOR DIFFERENT COMPARTMENT THICKNESSES (TIME STEP = 1 DAY)

Depth (cm)	DELX = 1 cm	DELX = 0.1 cm
0.0	30.000	30.000
1.0	29.665	29.664
2.0	29.341	29.340
3.0	29.028	29.026
4.0	28.725	28.723
5.0	28.432	28.431
10.0	27.109	27.106
20.0	25.048	25.045
30.0	23.577	23.574
40.0	22.524	22.520
50.0	21.766	21.760
60.0	21.215	21.206
75.0	20.638	20.627
99.0	20.023	20.020
100.0	20.000	20.000

Algorithms have been included in PRZM to simulate parent/daughter relationships. An analytical solution to the decay and transformation model was derived to check the numerical model.

The system which was modeled is shown in Figure 2.16. The C_i are dissolved concentrations and the C_i^* are adsorbed concentrations. The K_i are adsorption partition coefficients, the k_j are decay and transformation rates in the dissolved species, the k_i^* are adsorbed phase decay coefficients and θ and ρ are the water content and soil bulk densities, respectively. Notice that only the dissolved forms may be transformed from one toxic form to another. A system of first order differential equations describing this system can be written as:

$$\frac{d\ C_1\theta}{dt} = -\ (k_1 + k_2)\ C_1\theta \qquad (2\text{-}104)$$

$$\frac{d\ C_2\theta}{dt} = -\ (k_3 + k_4)\ C_2\theta + k_2\ C_1\theta \qquad (2\text{-}105)$$

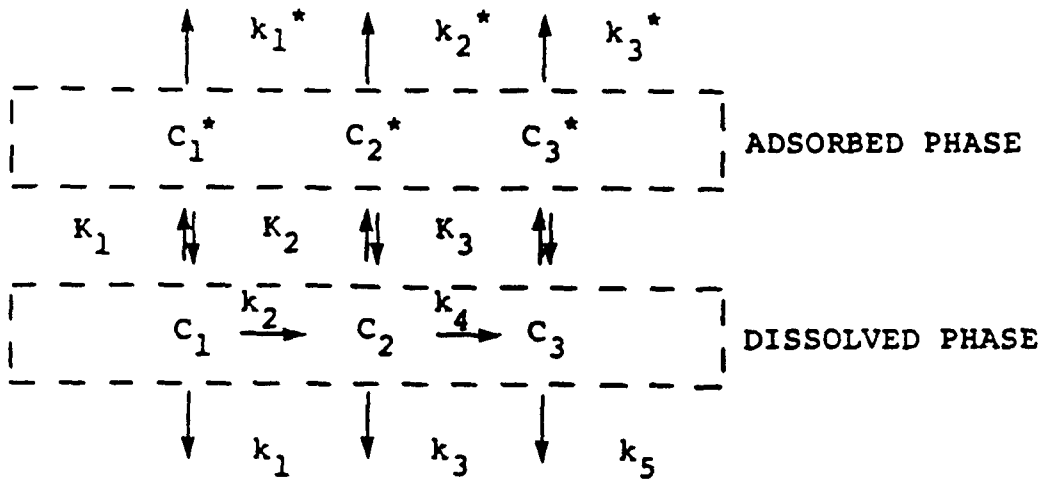

Figure 2.16. Schematic of a system of parent and daughter pesticides.

$$\frac{d\, C_3\theta}{dt} = - k_5\, C_3\theta + k_4\, C_2\theta \qquad (2\text{-}106)$$

$$\frac{d\, C_1^*\rho}{dt} = - k_1^*\, C_1^*\, \rho \qquad (2\text{-}107)$$

$$\frac{d\, C_2^*\rho}{dt} = - k_2^*\, C_2^*\, \rho \qquad (2\text{-}108)$$

$$\frac{d\, C_3^*\rho}{dt} = - k_3^*\, C_3^*\, \rho \qquad (2\text{-}109)$$

Making use of $C_i\, K_i = C_i^*$ the six equations above can be reduced to three equations in three unknowns, namely:

$$\frac{d\, C_1}{dt} = a_1\, C_1 \qquad (2\text{-}110)$$

$$\frac{d\, C_2}{dt} = a_2\, C_1 + a_3\, C_2 \qquad (2\text{-}111)$$

$$\frac{d\, C_3}{dt} = a_4\, C_2 + a_5\, C_3 \qquad (2\text{-}112)$$

in which

$$a_1 = - \frac{\theta(k_1 + k_2) - k_1^* K_1\rho}{\theta + K_1 \rho} \quad (2\text{-}113)$$

$$a_2 = \frac{k_2\theta}{\theta + K_2\rho} \quad (2\text{-}114)$$

$$a_3 = - \frac{\theta(k_3 + k_4) - k_2^* K_2\rho}{\theta + K_2 \rho} \quad (2\text{-}115)$$

$$a_4 = \frac{k_4\theta}{\theta + K_3\rho} \quad (2\text{-}116)$$

$$a_5 = - \frac{\theta k_5 - k_3^* K_3\rho}{\theta + K_3 \rho} \quad (2\text{-}117)$$

These ordinary differential equations with constant coefficients can be solved analytically for C_1, C_2 and C_3 using the initial conditions $C_1 = C_1'$ when $t = 0$ and $C_2 = C_3 = 0$ at $t = 0$. The solutions as given in Dean and Atwood (1985) are:

$$C_1 = C_1' e^{a_1 t} \quad (2\text{-}118)$$

$$C_2 = \left(\frac{a_2}{a_1 - a_3}\right) C_1' e^{a_1 t} - \left(\frac{a_2}{a_1 - a_3}\right) C_1' e^{a_3 t} \quad (2\text{-}119)$$

and

$$C_3 = \left(\frac{a_2 a_4}{(a_1 - a_5)(a_1 - a_3)}\right) C_1' e^{a_1 t} - \left(\frac{a_2 a_4}{(a_3 - a_5)(a_1 - a_3)}\right) C_1' e^{a_3 t} + \left(\frac{a_2 a_4}{(a_3 - a_5)(a_1 - a_3)} - \frac{a_2 a_4}{(a_1 - a_5)(a_1 - a_3)}\right) C_1' e^{a_5 t} \quad (2\text{-}120)$$

In PRZM, the equations are solved numerically as part of the general advection-dispersion equation for a solute in a porous medium by using an implicit scheme. A new subroutine was added to set up the transformation

(source and sink) terms for the system. The relationship $C_1 \rightarrow C_2 \rightarrow C_3$ may be modeled or the system can be configured for $C_1 \rightarrow C_2$ and $C_1 \rightarrow C_3$ or for independent C_1, C_2 and C_3 simply by selecting zero or positive values for the appropriate transformation rate constants.

Figures 2.17 through 2.19 show the results of a series of tests performed on the numerical model and checked by the analytical model. In these figures, the solid line represents the "true" or analytical solution, while the dashed line represents the approximate numerical solution. ' In Figure 2.17, there was no decay of the dissolved phase chemicals and no adsorption of any species. The rate of transformation from C_1 to C_2 was 0.2 day^{-1} and that from C_2 to C_3, 0.5 day^{-1}. After 20 days nearly all the chemical is in form C_3. The numerical model traces the decay and formation of each constituent closely, being poorer in those regions where the rate of change of the concentrations are more rapid. Figure 2.18 shows the same system with a decay rate of 0.01 day^{-1} in the dissolved phase. Figure 2.19 shows the solution for the same system except that the adsorption coefficients have been given values ($K_1 = 0.5$, $K_2 = 1.0$ and $K_3 = 5.0$) as have the adsorbed phase decay coefficients ($k_i^* = 0.01$). Notice that the transformation rate is retarded when adsorption is introduced.

Using the analytical model, the assumption of modeling the "total toxic residue" decay as a first-order process was tested. Adsorption coefficients for aldicarb, aldicarb sulfoxide and aldicarb sulfone in a Woburn sandy loam ($K_1 = 0.55$, $K_2 = 0.16$ and $K_3 = 0.185$) and decay and transformation rate constants ($k_1 = 0.07$, $k_2 = 0.55$, $k_3 = 0.01$, $k_4 = 0.031$ and $k_5 = 0.0152$) were taken from Bromilow et al. (1980). A soil bulk density of 1.45, a water content of 0.27 cm^3 cm^{-3} and an initial aldicarb parent mass of 100 mg were also used. The model was run for 90 days and the results are shown in Figure 2.20.

The results show that the decay of the sum of the dissolved aldicarb concentrations does <u>not</u> follow first-order kinetics. The reason for this is the conversion of aldicarb parent to aldicarb sulfoxide. Because the sulfoxide has a lower partition coefficient, the dissolved concentration <u>increases</u> until most of this conversion is complete. Once this happens, however, the sum of the sulfoxide and the sulfone concentrations does follow a first-order decay curve.

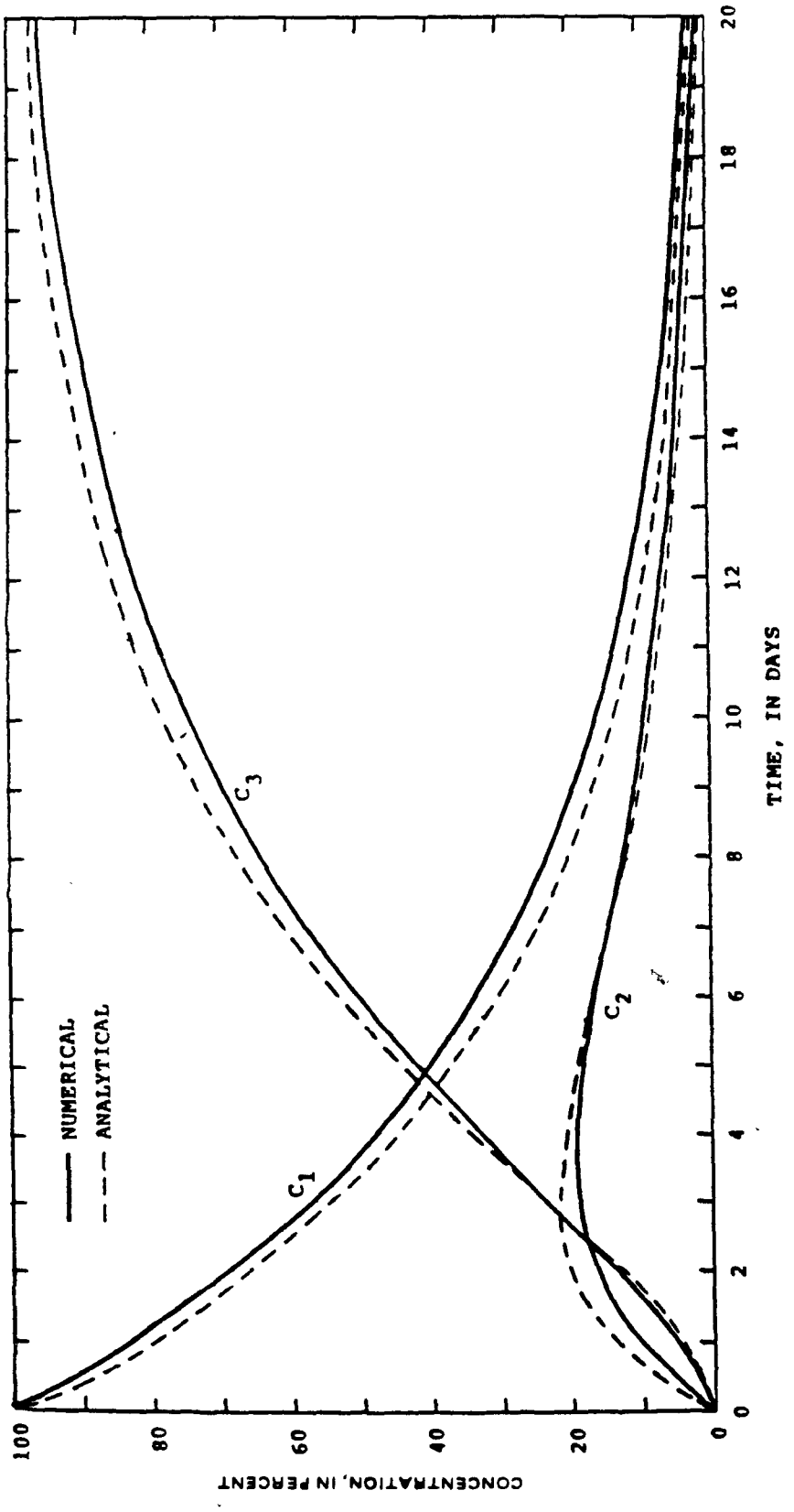

Figure 2.17. Conversion of C_1 to C_2 to C_3 with no adsorption and no decay.

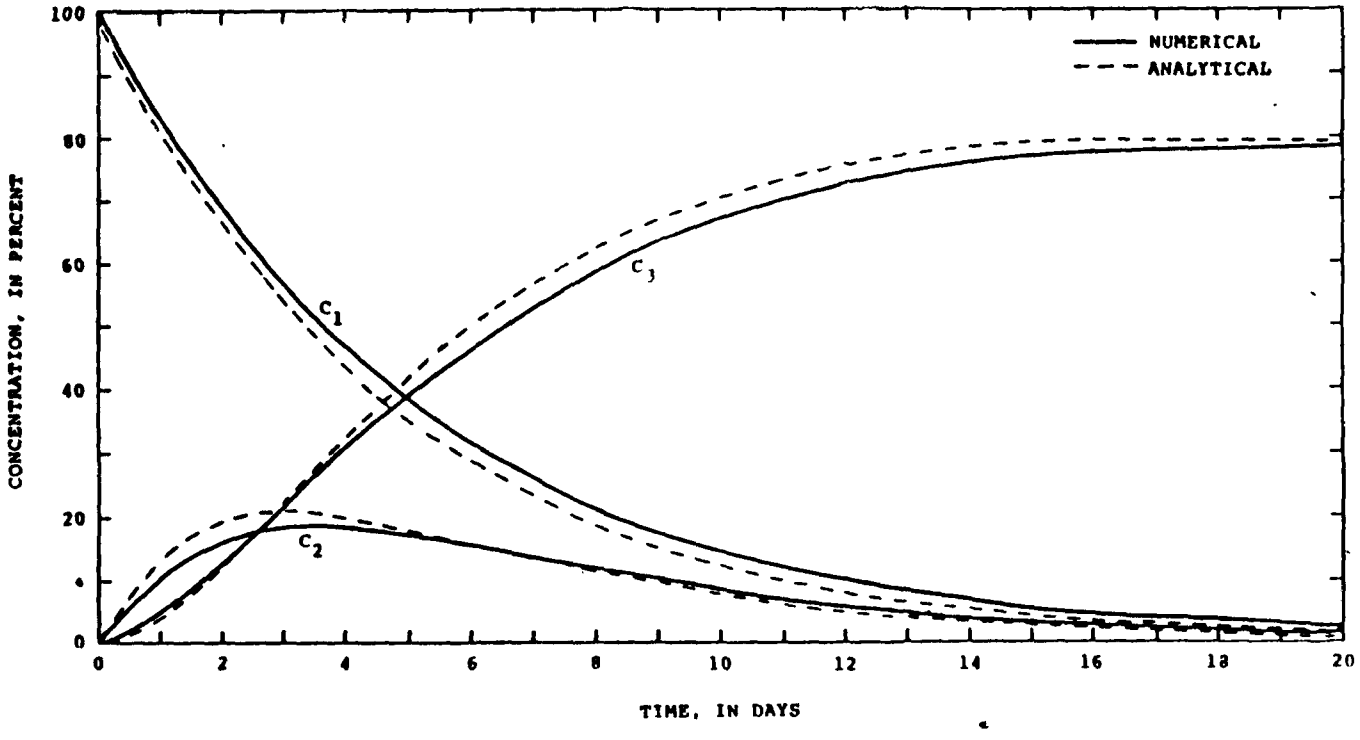

Figure 2.18. Conversion of C_1 to C_2 to C_3 with decay but no adsorption.

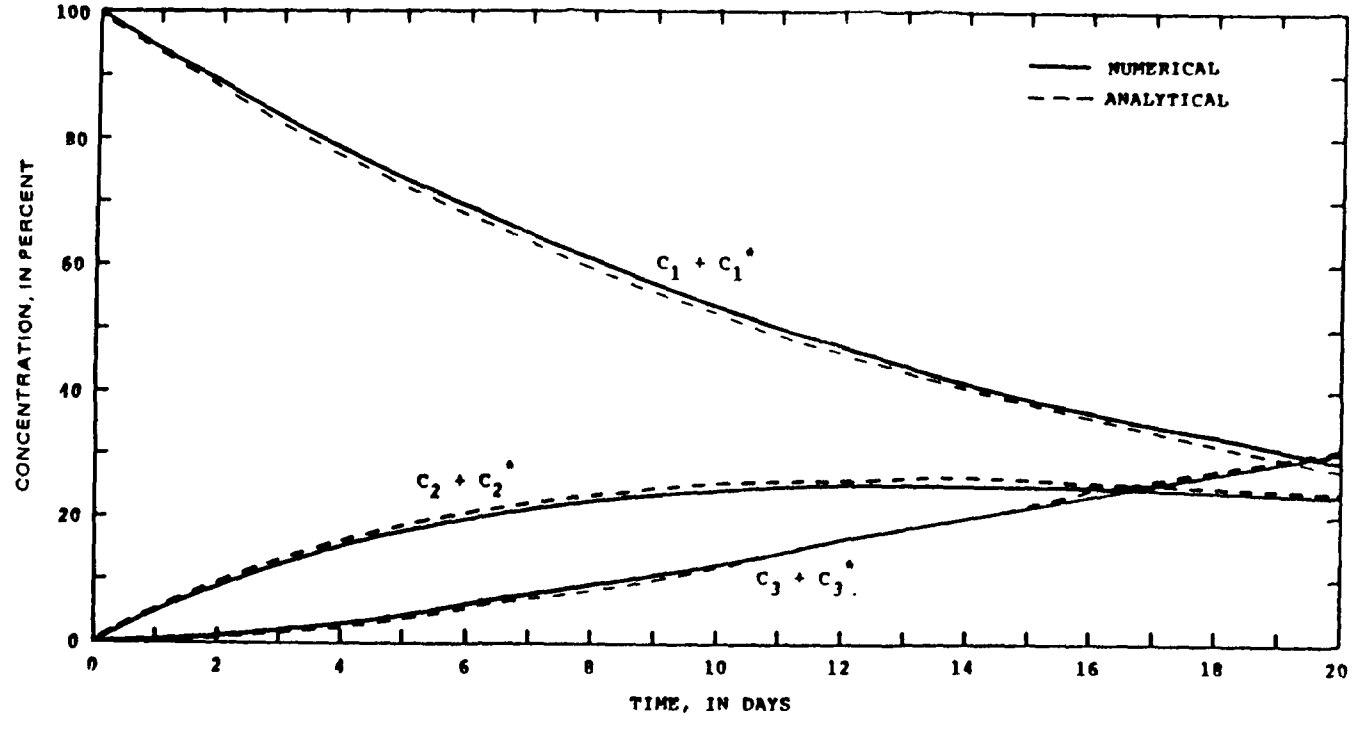

Figure 2.19. Conversion of C_1 to C_2 to C_3 with decay and adsorption.

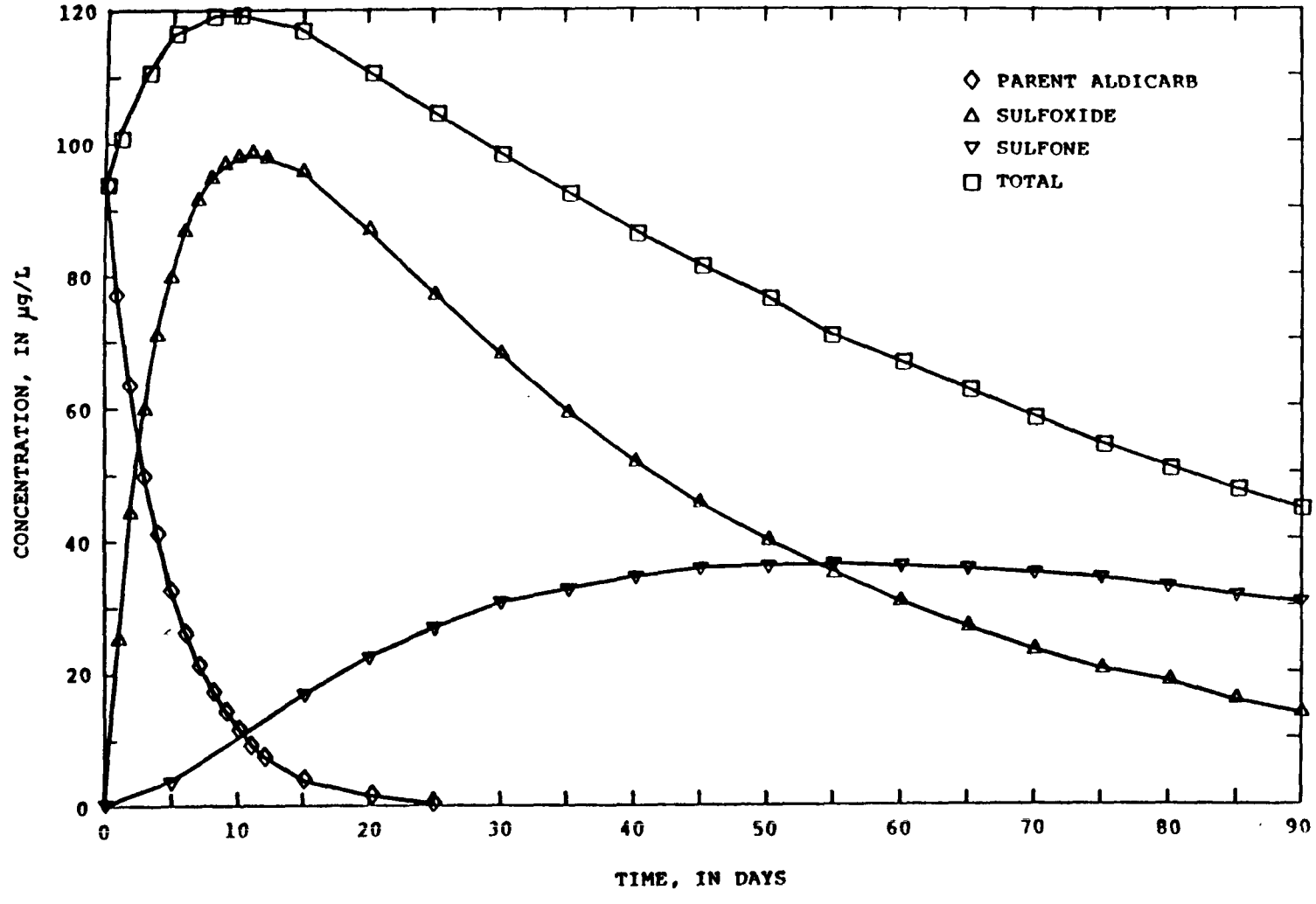

Figure 2.20. Conversion of aldicarb to aldicarb sulfoxide to aldicarb sulfone.

SECTION 3

VADOSE ZONE FLOW AND TRANSPORT MODEL (VADOFT)

3.1 INTRODUCTION

VADOFT is a finite-element code for simulating moisture movement and solute transport in the vadose zone. It is the second part of the three-component RUSTIC model for predicting the movement of pesticides within and below the plant root zone and assessing consequent groundwater contamination. The VADOFT code simulates one-dimensional, single-phase moisture movement in unconfined, variably saturated porous media. The code considers only single-porosity media and also ignores the effects of hysteresis. Transport of dissolved contaminants may also be simulated within the same domain. Transport processes accounted for include hydrodynamic dispersion, advection, linear equilibrium sorption, and first-order decay. VADOFT also simulates solute transformations in order to account for parent/daughter relationships.

3.2 OVERVIEW OF VADOFT

3.2.1 Features

3.2.1.1 General Description--

The VADOFT code can be used to perform one-dimensional modeling of water flow and transport of dissolved contaminants in variably or fully saturated soil/aquifer systems. For demonstrative purposes, we consider a scenario involving the migration of pesticide through the root zone, the vadose zone, and the saturated zone of an unconfined aquifer (Figure 3.1). VADOFT can be operated as a stand-alone code or operated in conjunction with the root zone model, PRZM, and/or the saturated-zone model, SAFTMOD. In the latter cases, boundary conditions at the interfaces of the modeled domains are established via model linkage procedures.

3.2.1.2 Process and Geometry--

VADOFT performs one-dimensional transient or steady-state simulations of water flow and solute transport in variably saturated porous media. The code employs the Galerkin finite-element technique to approximate the governing equations for flow and transport. It allows for a wide range of nonlinear flow conditions, and handles various transport processes, including hydrodynamic dispersion, advection, linear equilibrium sorption, and first-order decay. Steady-state transport can not be simulated when decay is considered. Boundary conditions of the variably saturated flow problems are specified in terms of prescribed pressure head or prescribed volumetric water flux per unit area. Boundary conditions of the solute transport problem are

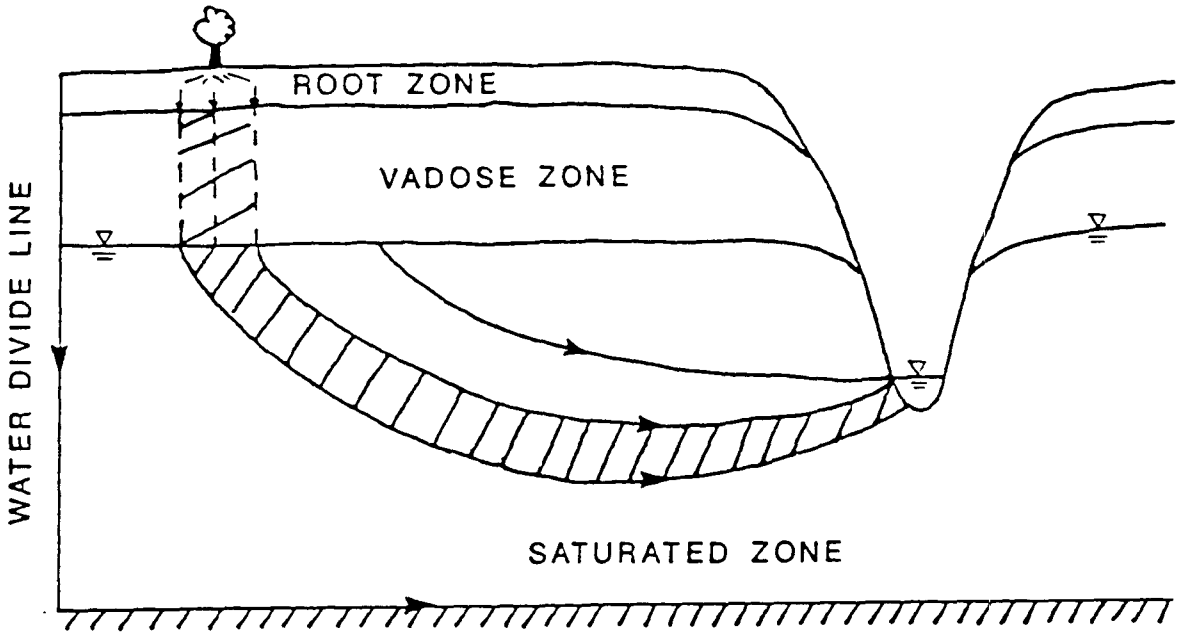

Figure 3.1. Cross-section view showing the solute migration path in the vadose and saturated zones of an unconfined aquifer.

specified in terms of prescribed concentration or prescribed solute mass flux per unit area. All boundary conditions may be time dependent.

3.2.1.3 Assumptions--
The VADOFT code contains both flow and solute transport models. Major assumptions of the flow model are as follows:

- Flow of the fluid phase is one-dimensional and considered isothermal and governed by Darcy's law.
- The fluid considered is slightly compressible and homogeneous.
- Hysteresis effects in the constitutive relationships of relative permeability versus water saturation, and water saturation versus capillary pressure head, are assumed to be negligible.

Major assumptions of the solute transport model are as follows:

- Advection and dispersion are one-dimensional.
- Fluid properties are independent of concentrations of contaminants.
- Diffusive/dispersive transport in the porous-medium system is governed by Fick's law. The hydrodynamic dispersion coefficient is defined as the sum of the coefficients of mechanical dispersion and molecular diffusion.

- Adsorption and decay of the solute may be described by a linear equilibrium isotherm and a first-order decay constant.

- Vapor transport can be neglected.

3.2.1.4 Data Requirements--
Data required for the simulation of variably saturated flow include values of the saturated hydraulic conductivity and specific storage of the porous media, the geometry and configuration of the flow region, as well as initial and boundary conditions associated with the flow equation. Soil moisture relationships are also required. These include relative permeability versus water phase saturation and capillary head versus water phase saturation. These relationships may be supplied to the code using tabulated data or functional parameters.

Data required for the simulation of solute transport in variably saturated soil include dispersivity and porosity values, retardation and decay constants, values of Darcy velocity and water saturation, as well as initial and boundary conditions associated with the transport equation.

3.2.2 Limitations

Major limitations of the VADOFT code are summarized as follows:

- In performing a variably saturated flow analysis, the code handles only single-phase flow (i.e., water) and ignores the flow of a second phase (i.e., air) which, in some instances, can be significant.

- The code ignores the effects of hysteresis on the soil moisture constitutive relations.

- The code does not take into account sorption nonlinearity or kinetic sorption effects which, in some instances, can be important.

- The code considers only single-porosity (granular) soil media. It cannot handle fractured porous media or structured soils.

- The code does not take into account transverse dispersion, which can be important for layered media.

3.3 DESCRIPTION OF FLOW MODULE

3.3.1 Flow Equation

VADOFT considers the problem of variably saturated flow in a soil column in the vadose zone of an unconfined aquifer. The code solves the Richards' equation, the governing equation for infiltration of water in the vadose zone:

$$\frac{\partial}{\partial z}\left[Kk_{rw}\left(\frac{\partial \psi}{\partial z} - 1\right)\right] = \eta \frac{\partial \psi}{\partial t} \qquad (3\text{-}1)$$

where ψ is the pressure head (L), K is the saturated hydraulic conductivity (LT^{-1}), k_{rw} is the relative permeability, z is the vertical coordinate pointing in the downward direction (L), t is time (T), and η is an effective water storage capacity (L^{-1}) defined as

$$\eta = S_w S_s + \phi \frac{dS_w}{d\psi} \tag{3-2a}$$

where S_s is specific storage (L^{-1}), S_w is water saturation, and ϕ is the effective porosity. Specific storage is defined by

$$S_s = \rho g[\phi c_f + (1 - \phi) c_s] \tag{3-2b}$$

where c_f is the fluid compressibility (LT^2M^{-1}), c_s is the solid skeleton compressibility (LT^2M^{-1}), ρ is the fluid density ML^{-3}), and g the gravitational acceleration (LT^{-2}).

The initial and boundary conditions of the one-dimensional infiltration problem may be expressed as:

$$\psi(z,0) = \psi_i \tag{3-3}$$

either

$$V(0,t) = I \tag{3-4a}$$

or

$$\psi(0,t) = \psi_o \tag{3-4b}$$

either

$$\psi(L,t) = \psi_L \tag{3-5a}$$

or

$$V(L,t) = 0 \tag{3-5b}$$

where ψ_i is the initial pressure head value (L), ψ_o is the pressure head at the upper boundary (L), ψ_L is the pressure head at the lower boundary (L), I is the rate of infiltration at the soil surface (LT^{-1}), L is the thickness of the vadose zone (L), and V the vertical Darcy velocity (LT^{-1}) (defined by Equation 3-8). The boundary condition in equation 3-5b is valid because the bottom boundary of VADOFT coincides with the bottom of the SAFTMOD aquifer (see the section on linkage).

To solve the variably saturated infiltration problem, it is also necessary to specify the relationships of relative permeability versus water saturation, and pressure head versus water saturation. Two alternative function expressions are used to describe the relationship of relative permeability versus water saturation. These functions are given by (Brooks and Corey 1966; van Genuchten 1976):

$$k_{rw} = S_e^{\,n} \tag{3-6a}$$

and

$$k_{rw} = S_e^{\,1/2}\,[1 - (1 - S_e^{\,1/\gamma})^{\gamma}]^2 \tag{3-6b}$$

where n and γ are empirical parameters and S_e is the effective water saturation defined as $S_e = (S_w - S_{wr})/(1 - S_{wr})$, with S_{wr} being referred to as the residual water saturation.

The relationship of pressure head versus water saturation is described by the following function (van Genuchten 1976; Mualum 1976):

$$\frac{S_w - S_{wr}}{1 - S_{wr}} = \begin{cases} \dfrac{1}{[1 + (\alpha|\psi - \psi_a|)^{\beta}]^{\gamma}} & \text{for } \psi < \psi_a \\ 1 & \text{for } \psi \geq \psi_a \end{cases} \tag{3-7}$$

where α and β are empirical parameters, ψ_a is the air entry pressure head value (L), and S_{wr} is the residual water phase saturation. The parameters β and γ are related by $\gamma = 1 - 1/\beta$.

Descriptive statistical values for α, β, and γ have been determined by Carsel and Parrish (1987) for 12 soil classifications (see Volume II, Section 5). Using the mean parameter values, the relationships of effective saturation versus capillary head and relative permeability versus effective saturation are plotted. Logarithmic plots are shown in Figures 3.2-3.4. To show more vividly the high degree of nonlinearities, the relationships of relative permeability versus effective saturation are also plotted on arithmetic scales and presented in Figures 3.5-3.7. It is important that the finite element flow module be capable of handling such high nonlinearities to be successful in performing a Monte Carlo study of infiltration in the unsaturated zone.

Equation 3-1 is solved using the Galerkin finite element subject to the initial and boundary conditions given in Equations 3-3 through 3-5. After the distributions of ψ and S_w have been determined, the Darcy velocity is computed from

$$V = - Kk_{rw}\left(\frac{\partial \psi}{\partial z} - 1\right) \tag{3-8}$$

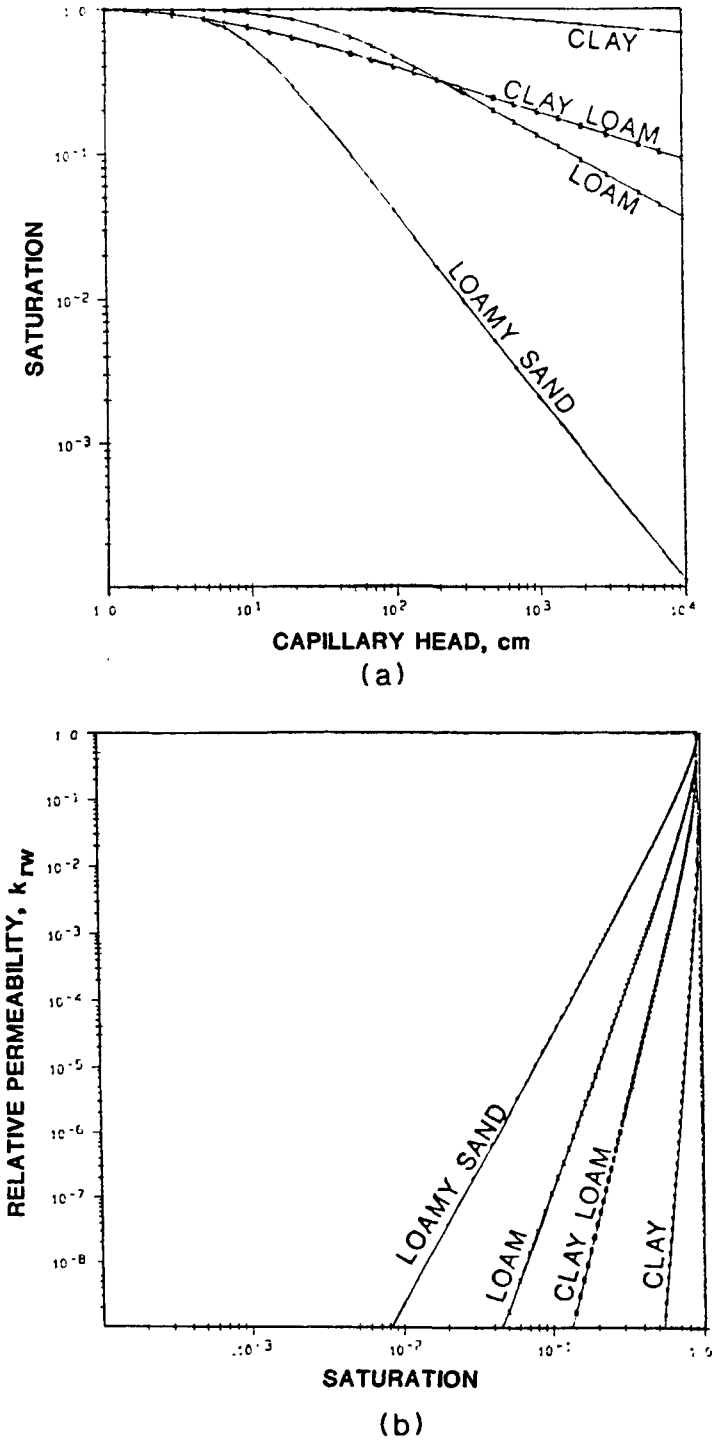

Figure 3.2. Logarithmic plot of constitutive relations for clay, clay loam, loam, and loamy sand: (a) saturation vs. capillary head and (b) relative permeability vs. saturation.

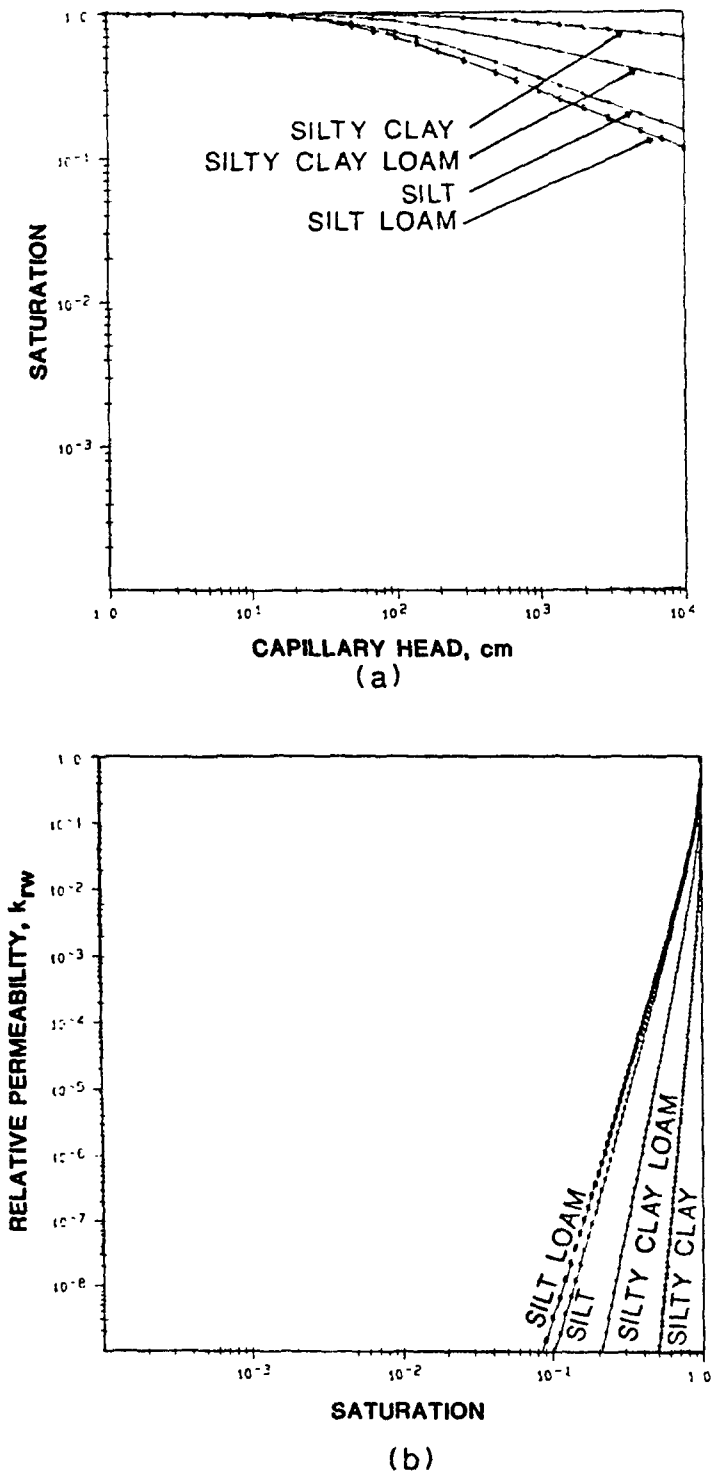

Figure 3.3. Logarithmic plot of constitutive relations for silt, silty clay loam, silty clay and silty loam: (a) saturation vs. capillary head and (b) relative permeability vs. saturation.

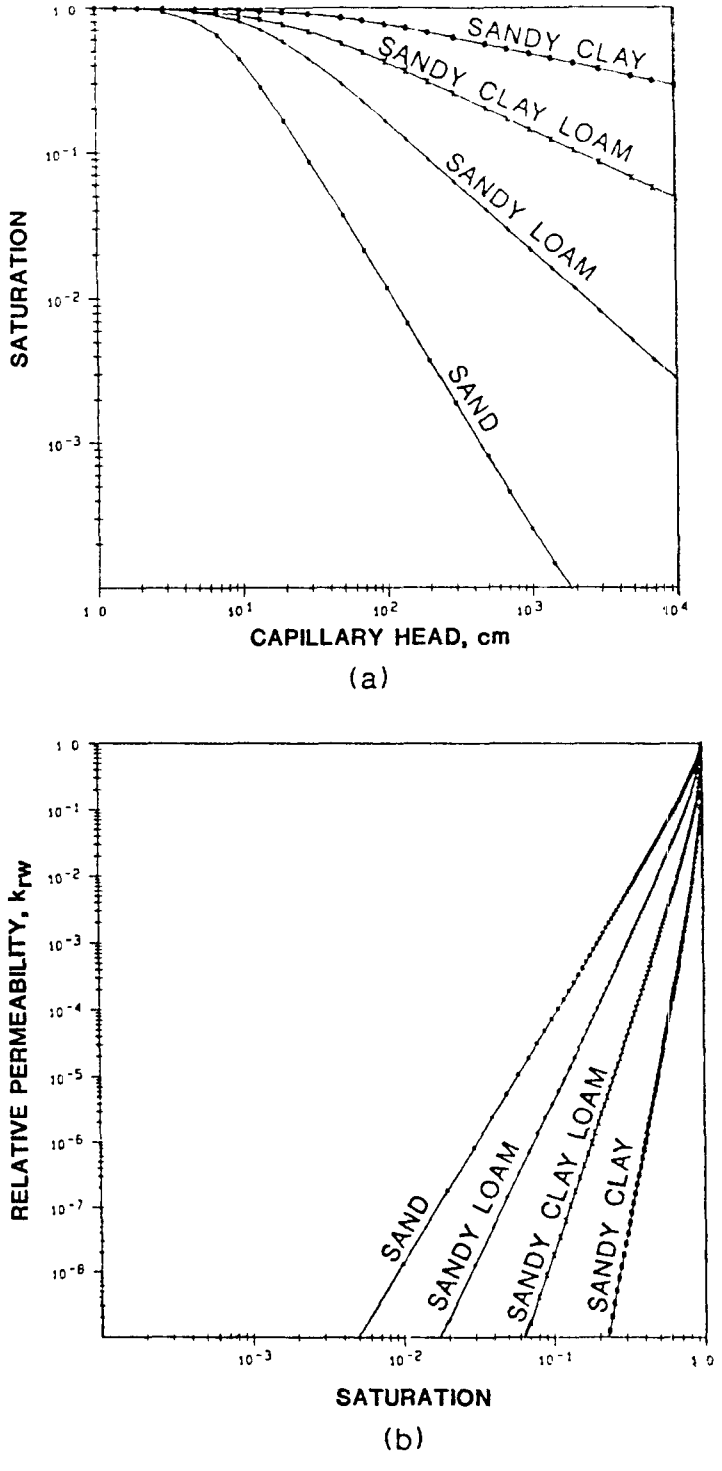

Figure 3.4. Logarithmic plot of constitutive relations for sandy clay, sandy clay loam, sandy loam and sand: (a) saturation vs. capillary head and (b) relative permeability vs. saturation.

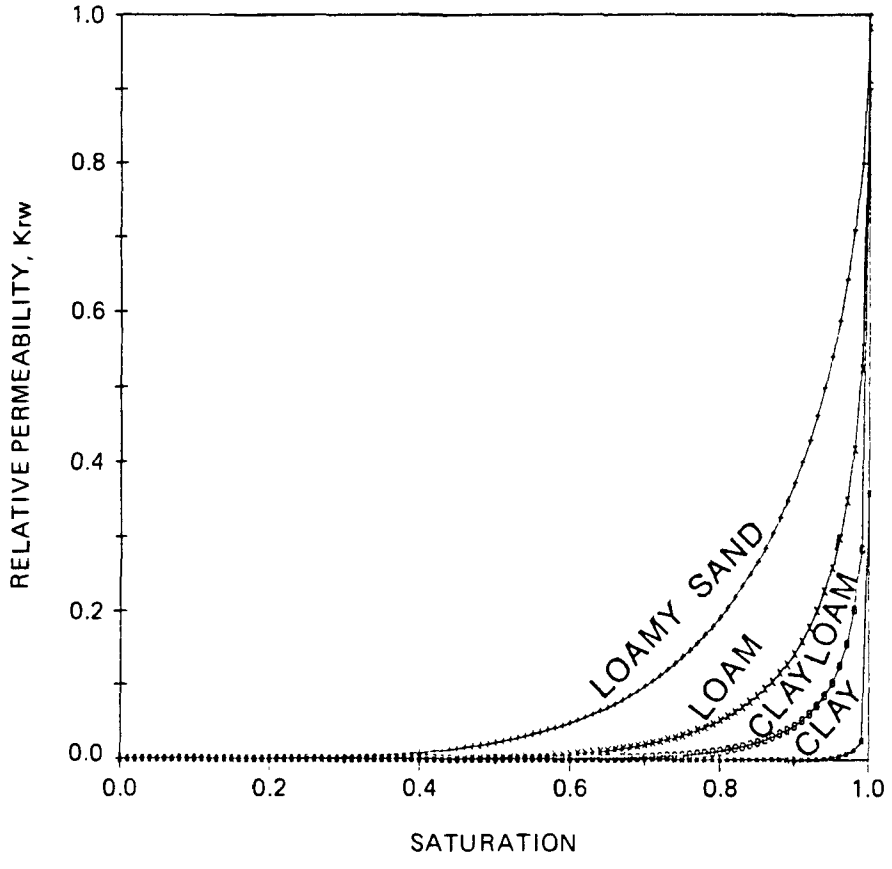

Figure 3.5. Standard plot of relative permeability vs. saturation for clay, clay loam, loam and loamy sand.

3.3.2 Numerical Solution

3.3.2.1 Numerical Approximation of the Flow Equation--
A numerical approximation of the one-dimensional flow equation in the vadose zone is obtained using a Galerkin finite-element formulation with spatial discretization performed using linear elements. Time integration is performed using a backward finite difference approximation. This leads to a system of nonlinear algebraic equations. For a typical node i in the finite-element grid (see Figure 3.8), the equation may be expressed as

$$\alpha_i \psi_{i-1}^{k+1} + \beta_i \psi_i^{k+1} + \gamma_i \psi_{i+1}^{k+1} = d_i \qquad (3\text{-}9)$$

where k+1 is the current time level, and α_i, β_i, γ_i, and d_i are given by

$$\alpha_i = \frac{-\{Kk_{rw}\}_{i-1}}{\Delta z_{i-1}} \qquad (3\text{-}10a)$$

$$\beta_i = \frac{\{Kk_{rw}\}_{i-1}}{\Delta z_{i-1}} + \frac{\{Kk_{rw}\}_i}{\Delta z_i} + \frac{\eta_i}{\Delta t_k}\left(\frac{\Delta z_{i-1} + \Delta z_i}{2}\right) \tag{3-10b}$$

$$\gamma_i = \frac{-\{Kk_{rw}\}_i}{\Delta z_i} \tag{3-10c}$$

$$d_i = \frac{\eta_i}{\Delta t_k}\left(\frac{\Delta z_{i-1} + \Delta z_i}{2}\right)\psi_i^k + \{Kk_{rw}\}_{i-1} - \{Kk_{rw}\}_i \tag{3-10d}$$

and Δz_i and Δt_k are the spatial and time increments, respectively. Note that the braces ({}) are used in the equations above (and below) to denote the value of the enclosed quantity at the element centroid. The nonlinear system of equations is solved for each time step. Three nonlinear schemes are provided in the VADOFT code. The first scheme is a Picard type iteration scheme, the second scheme is a Newton-Raphson scheme, and the third is a Newton-Raphson scheme modified by Huyakorn (1988, personal communication).

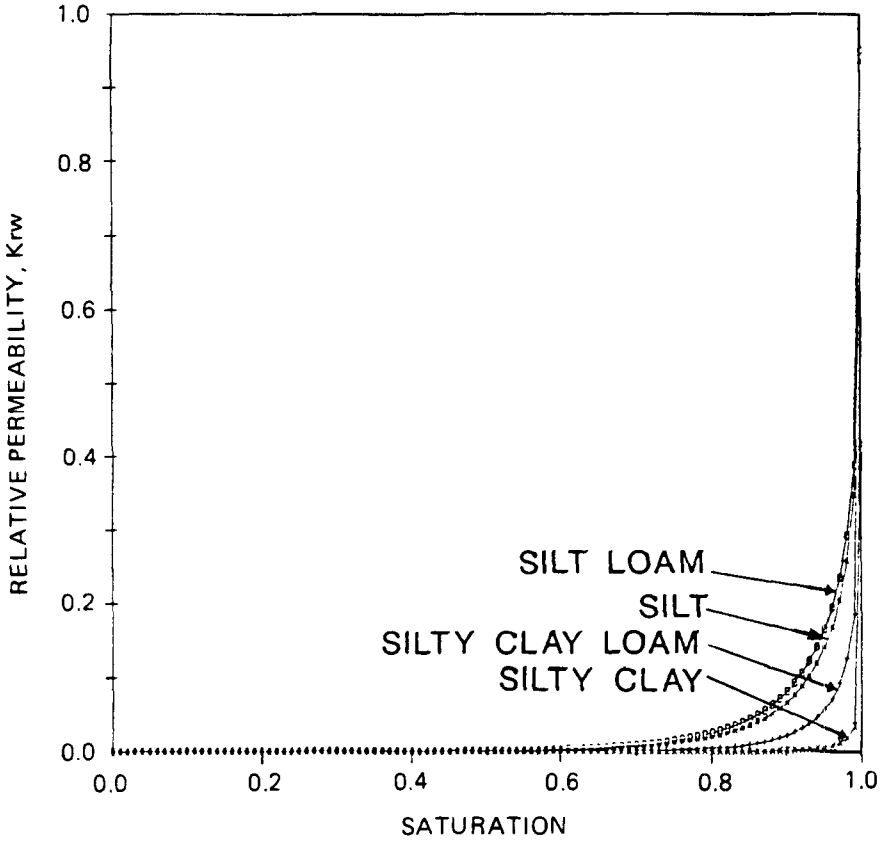

Figure 3.6. Standard plot of relative permeability vs. saturation for silt, silt clay loam, silty clay and silty loam.

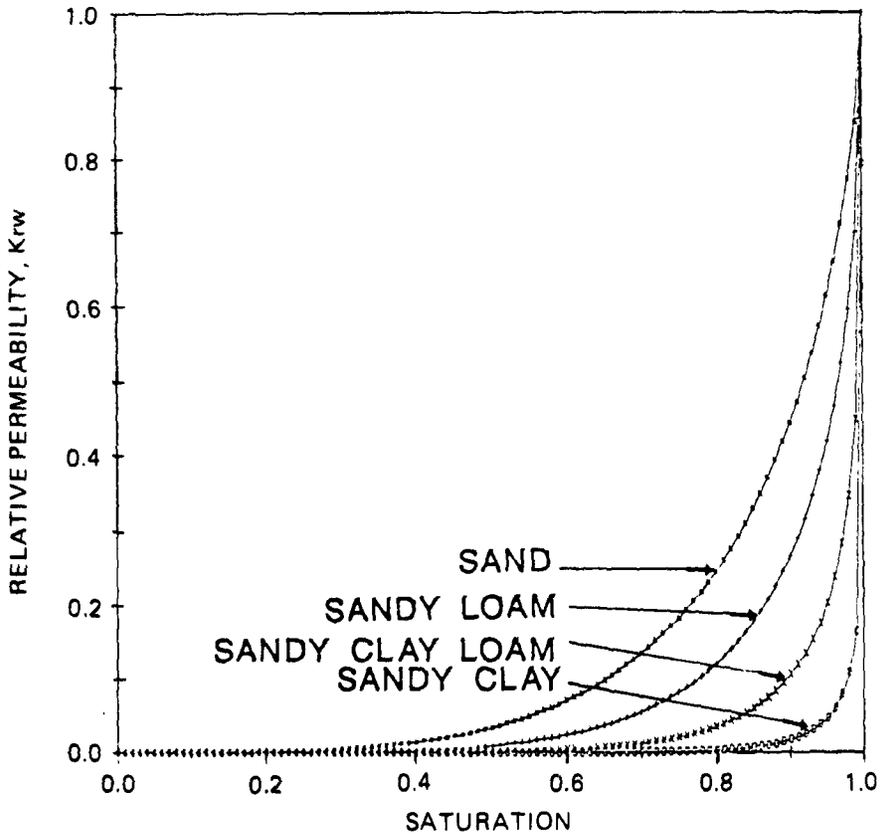

Figure 3.7. Standard plot of relative permeability vs. saturation for sandy clay, sandy clay loam, sandy loam and sand.

In the Picard scheme, the matrix coefficients, α_i, β_i, γ_i, and d_i, are first evaluated using an initial estimate of pressure head values, ψ_i^k. The resulting system of linearized equations is then solved for ψ_i^{k+1} using the Thomas algorithm. Updating of the matrix coefficient is performed by recomputing values of nonlinear soil parameters. Iterations are performed until the successive change in pressure head values is within a prescribed tolerance.

In the Newton-Raphson scheme, the nonlinear system of equations is treated by applying the Newton-Raphson technique (see Huyakorn and Pinder 1983, pp. 159-162) to Equation 3-9. This leads to the following system of linearized algebraic equations:

$$(\alpha_i + \alpha_i^*)^r \psi_{i-1}^{k+1} + (\beta_i + \beta_i^*)^r \psi_i^{k+1} + (\gamma_i + \gamma_i^*)^r \psi_{i+1}^{k+1} = (d_i + d_i^*)^r \qquad (3\text{-}11)$$

where superscript r is used to denote the r-th iterate; α_i, β_i, γ_i, and d_i are as defined previously; and α_i^*, β_i^*, γ_i^*, and d_i^* are given by

$$\alpha_i^* = \frac{1}{2}\left[-1 + \frac{(\psi_i - \psi_{i-1})^r}{\Delta z_{i-1}}\right]\left\{K\frac{dk_{rw}}{dS_w}\frac{dS_w}{d\psi}\right\}_{i-1}^r \tag{3-12a}$$

$$\beta_i^* = \alpha_i^* + \gamma_i^* + \frac{l_i}{\Delta t_k}\left[\frac{\partial l_i}{\partial \psi_i}\right]^r (\psi^r - \psi^k) \tag{3-12b}$$

$$\gamma_i^* = \frac{1}{2}\left[1 + \frac{(\psi_i - \psi_{i+1})^r}{\Delta z_i}\right]\left\{K\frac{dk_{rw}}{dS_w}\frac{dS_w}{d\psi}\right\}_i^r \tag{3-12c}$$

$$d_i^* = \alpha_i^* \psi_{i-1}^r + \beta_i^* \psi_i^r + \gamma_i^* \psi_{i+1}^r \tag{3-12d}$$

where $l_i = \frac{[\Delta z_{i-1} + \Delta z_i]}{2}$

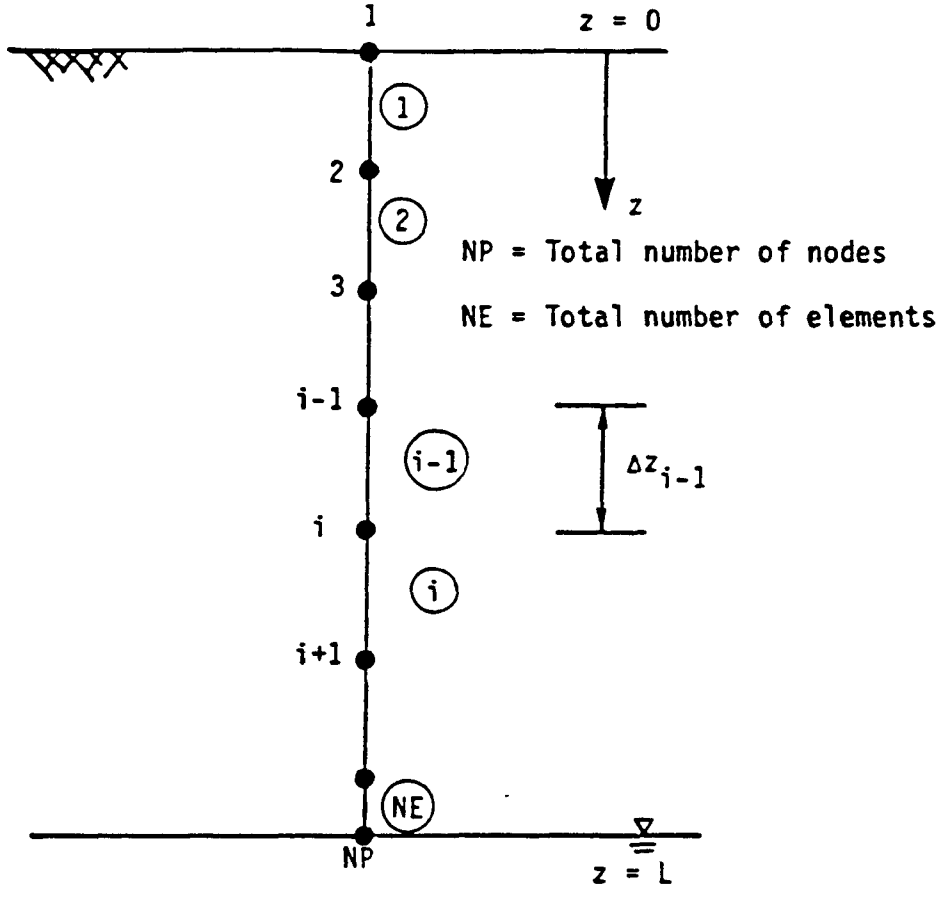

Figure 3.8. Finite element discretization of soil column showing node and element numbers.

The initial solution and subsequent iterations of the Newton-Raphson scheme are performed in the same manner as that described for the Picard scheme.

3.3.2.2 General Guidance on Selection of Grid Spacings and Time Steps, and the Use of Solution Algorithms--

In designing a finite-element grid for variably saturated flow simulations, one should select nodal spacings that will yield reasonable approximations to the expected moisture profiles.

In the analysis of the given variably saturated flow problem, small nodal spacings should be used in the zones where head gradients or moisture fronts are steep. The nodal spacings may be gradually increased in the zone where no abrupt changes in hydraulic conductivities occur and the head gradients are gradually sloping. The variably saturated flow simulation can be performed using either the Picard or either Newton-Raphson solution algorithm. For one-dimensional cases where convergence difficulties are not expected, the efficiency of these algorithms have been found to be similar. For certain steady-state cases involving highly nonlinear soil moisture characteristics, the use of either Newton-Raphson algorithm is preferable, particularly when the Picard algorithm fails to converge within a reasonable number of iterations (say between 10 and 20).

3.4 DESCRIPTION OF THE TRANSPORT MODULE

3.4.1 Transport Equation

The governing equation for one-dimensional transport of a nonconservative solute species in a variably saturated soil takes the form

$$\frac{\partial}{\partial z}\left(D\frac{\partial c}{\partial z}\right) - V\frac{\partial c}{\partial z} = \theta R\left(\frac{\partial c}{\partial t} + \lambda c\right) \tag{3-13}$$

where D is the apparent dispersion coefficient (L^2T^{-1}), c is the solute concentration (ML^{-3}), θ is the volumetric water content ($\theta = \phi S_w$), R is the retardation coefficient, and λ is the first-order decay constant (T^{-1}). Note that the apparent dispersion coefficient is defined as $D = \alpha_L V + \phi D^*$, where α_L is the longitudinal dispersivity, and D^* is the effective molecular diffusion coefficient.

The initial and boundary conditions of the one-dimensional transport problem may be expressed as:

$$c(z,0) = c_i \tag{3-14}$$

either

$$-D\frac{\partial c}{\partial z}(0,t) = V\,(c_o - c) \tag{3-15a}$$

or

$$c(0,t) = c_o \tag{3-15b}$$

$$\frac{\partial c}{\partial z}(L,t) = 0 \tag{3-16}$$

where c_i is the initial concentration (ML^{-3}), and c_o is the leachate concentration at the source (ML^{-3}).

3.4.2 Numerical Solution of the Transport Equation

3.4.2.1 Numerical Approximation of the Transport Equation--
A numerical approximation of the one-dimensional transport equation is obtained using an upstream-weighted finite-element formulation with spatial discretization performed using linear elements. Time integration is performed using a central finite-difference approximation. This leads to a system of linear algebraic equations. The equation corresponding to node i takes the form:

$$\alpha_i\, c_{i-1}^{k+1} + \beta_i\, c_i^{k+1} + \gamma_i\, c_{i+1}^{k+1} = d_i \tag{3-17}$$

where α_i, β_i, γ_i, and d_i are given by

$$\alpha_i = \tau\alpha_i^* + \{\theta R\}_{i-1}\,\Delta z_{i-1}/(6\Delta t_k) \tag{3-18a}$$

$$\beta_i = \tau\beta_i^* + [\{\theta R\}_i\,\Delta z_i + \{\theta R\}_{i-1}\,\Delta z_{i-1}]/(3\Delta t_k) \tag{3-18b}$$

$$\gamma_i = \tau\gamma_i^* + \{\theta R\}_i\,\Delta z_i/(6\Delta t_k) \tag{3-18c}$$

$$d_i = (\tau - 1)(\alpha_i^*\, c_{i-1}^k + \beta_i^*\, c_i^k + \gamma_i^*\, c_{i+1}^k) + \frac{\{\theta R\}_{i-1}}{6\Delta t_k}(c_{i-1}^k + 2c_i^k)\Delta z_{i-1} + \frac{\{\theta R\}_i}{6\Delta t_k}(c_{i+1}^k + 2c_i^k)\Delta z_i \tag{3-18d}$$

$$\alpha_i^* = -\frac{\{D\}_{i-1}}{\Delta z_{i-1}} - \frac{(1-\omega)}{2}\{V\}_{i-1} + \frac{\lambda\{\theta R\}_{i-1}\,\Delta z_{i-1}}{6} \tag{3-18e}$$

$$\beta_i^* = \left(\frac{\{D\}_{i-1}}{\Delta z_{i-1}} + \frac{\{D\}_i}{\Delta z_i}\right) + \frac{\lambda}{3}[\{\theta R\}_{i-1}\,\Delta z_{i-1} + \{\theta R\}_i\Delta z_i] + \frac{(1-\omega)}{2}\{V\}_{i-1} - \frac{(1+\omega)}{2}\{V\}_i \tag{3-18f}$$

$$\gamma_i^* = -\frac{\{D\}_i}{\Delta z_i} + \frac{(1+\omega)}{2}\{V\}_i + \frac{\lambda\{\theta R\}_i\,\Delta z_i}{6} \tag{3-18e}$$

with τ and ω denoting the time weighting factor and the upstream weighting factor, respectively.

To obtain a second-order temporal approximation, the value of τ is set equal to 1/2. This corresponds to using the Crank-Nicholson central difference time stepping scheme. The upstream weighting factor ω is introduced in the above numerical approximation to curb numerical oscillations that may occur when the selected finite-element grid is not sufficiently refined for a given value of longitudinal dispersivity. For each time step, the linear system of algebraic equations is solved using the Thomas algorithm.

Transport of a daughter species in a decay chain can also be handled by the VADOFT code. In this case, the right hand side of the governing equation for single species transport (3-13) is modified by adding a source term accounting for transformation of parent components. This source term is given by

$$m = -\sum_{\ell=1}^{n_p} \phi \; S_w \; \epsilon_\ell \; \lambda_\ell \; R_\ell \; c_\ell \tag{3-19}$$

where subscript ℓ is used to denote the parent species, n_p is the number of parent species, and ϵ_ℓ is the mass fraction of parent component that is transformed into the daughter species under consideration.

The numerical solution of the modified transport equation can be performed in the same manner as that described previously for a single species. The source term from Equation 3-19 is incorporated into the finite element matrix equation by adding d_i^* to the right hand side. The term d_i^* is given by

$$d_i^* = \frac{1}{2} \left[\sum_{\ell=1}^{n_p} \epsilon_\ell \; \lambda_\ell \; R_\ell \; c_{\ell i}^{k+1} \right] (\Delta z_i + \Delta z_{i-1})(\phi \; S_w)_i \tag{3-20}$$

In performing the solute transport analysis, the selection of nodal spacing (Δz) and time step value (Δt) should follow the so-called Peclet number and Courant number criteria where possible. These two criteria are given as follows:

$$\frac{\Delta z}{\alpha_L} \leq 4 \tag{3-21}$$

$$V_{sol} \; \Delta t/\Delta z \leq 1 \tag{3-22}$$

$$V_{sol} = V/\theta R \tag{3-23}$$

where α_L is the longitudinal dispersivity, V_{sol} is the solute velocity, V = Darcy velocity, θ = water content, and R = retardation coefficient.

The VADOFT code also provides the user with the option of using upstream weighting to curb numerical oscillations that may occur in solving the advective-dispersive transport equation. The recommended value of ω, the weighing factor, is determined by using the following formulae:

$$\omega = 1 - 4\alpha_L/\ell, \qquad \ell > 4\alpha_L \tag{3-24}$$

$$\omega = 0, \qquad \ell \leq 4\alpha_L \tag{3-25}$$

where α_L is the longitudinal dispersivity, and ℓ is the length of the element.

3.5 RESULTS OF VADOFT TESTING SIMULATIONS

Three sets of benchmark problems were used to test the VADOFT code. The first set consists of two steady and transient problems designed to test the variably saturated flow component of the code. The second set consists of four transient one-dimensional transport problems. The third set consists of two coupled flow-transport problems. Numerical results obtained from VADOFT are compared with analytical solutions and results obtained using two other finite-element codes, UNSAT2 and SATURN. These test problems were simulated using VADOFT before it was linked to the other RUSTIC modules.

3.5.1 Flow Module (Variably Saturated Flow Problems)

3.5.1.1 Transient Upward Flow in a Soil Column--

This problem concerns transient, vertically upward moisture movement in a soil column 20 cm in length. The soil column is subject to zero pressure head at the base and zero flux at the top. The initial distribution of pressure head is hydrostatic: $(t = 0) = -90 + z$ cm, where z is the depth below the top of the soil column. Soil properties and discretization data used in the simulation are presented in Table 3-1. The simulation was performed for 15 time steps with constant time step value of $t = 0.01$ d. Numerical results given by the Picard and the Newton-Raphson schemes are virtually identical. Both schemes require between 2 and 3 iterations per time step to converge to a head tolerance of 0.01 cm. The simulation results obtained from VADOFT are compared with those obtained from UNSAT2 and SATURN (the two-dimensional finite-element codes described by Davis and Neuman [1983], and Huyakorn et al. [1984]) respectively. Shown in Figures 3.9 and 3.10 are plots of distributions of pressure head and water saturation, respectively. As can be seen, the results of VADOFT are in good agreement with the results of the other two codes.

3.5.1.2 Steady Infiltration in a Soil Column--

This problem concerns steady-state infiltration in a soil column. The column is 550 cm in length and is subject to an infiltration rate of 4.07 cm/d at the top and zero pressure head at the bottom. Soil properties used in the simulation are presented in Table 3-2. Five cases of varying degree of nonlinearity of relative permeability function ($k_{rw} = S_e^n$) were simulated. Both the Picard and the Newton-Raphson schemes were used in conjunction with

Table 3-1. SOIL PROPERTIES AND DISCRETIZATION DATA USED IN SIMULATING TRANSIENT FLOW IN A SOIL COLUMN

Parameter	Value
Length of soil column, L	20 cm
Saturated hydraulic conductivity, K	10 cm d^{-1}
Porosity, ϕ	0.45
Residual water phase saturation, S_{wr}	0.333
Air entry value, ψ_a	0.0 cm
Constitutive relations:	
$k_{rw} = (S_w - S_{wr})/(1 - S_{wr})$	
$(\psi - \psi_a)/(\psi_r - \psi_a) = (1 - S_w/(1 - S_{wr})$	
where $\psi_r = -100$ cm.	
$\Delta z = 0.5$ cm	
$\Delta t = 0.01$ d	

a finite-element grid having constant nodal spacing, z = 10 cm. The performance of the two iterative schemes are illustrated in Table 3-3. Note that the Newton-Raphson scheme converges for all cases, whereas the Picard scheme fails to converge when the nonlinear exponent n exceeds 4. Simulated distributions of pressure head and water saturation are shown in Figure 3.11 and 3.12, respectively. These results of the VADOFT code are virtually identical to corresponding results obtained using the SATURN code.

3.5.2 Transport Module

3.5.2.1 Transport in a Semi-Infinite Soil Column--
This problem concerns one-dimensional transport of a conservative solute species in a saturated soil column of infinite length. The solute is introduced into the column at the inlet section where z = 0. The initial concentration is assumed to be zero, and the dimensionless constant inlet concentration is prescribed as 1. Values of physical parameters and discretization data used in the numerical simulation are given in Table 3-4. The finite-element grid representing the soil column was 400 cm in length. The simulation was performed for 20 time steps. Thus the duration of the simulation time of transport in the soil column was 50 hours. For this duration, the selected grid length is sufficient to avoid the end boundary effect. The numerical solution obtained from the VADOFT code was checked against the analytical solution of Ogata and Banks (1961). Shown in Figure 3.13 and Table 3-5 are concentration values at t = 25 hours and t = 50 hours. As can be seen, the numerical and analytical solutions are in excellent agreement.

Table 3-2. SOIL PROPERTIES USED IN SIMULATING STEADY-STATE INFILTRATION

Parameter	Value
Length of soil column, L	550 cm
Saturated hydraulic conductivity, K	25 cm d^{-1}
Porosity, ϕ	0.331
Residual water saturation, S_{wr}	0.0
Air entry value, ψ_a	0.0 cm
Constitutive relations:	
$k_{rw} = S_e^n$, n = 3, 4, 6, 8, 10	
$S_e = \frac{1}{[1 + (\alpha\lvert\psi - \psi_a\rvert)^\beta]^\gamma}$	
where $S_e = (S_w - S_{wr})/(1 - S_{wr})$, $\alpha = 0.014$ cm^{-1}, $\psi_a = 0$ cm,	
$\beta = 1.51$, $\gamma = 0.338$	

3.5.2.2 Transport in a Finite Soil Column--
In this problem, downward vertical transport of dissolved contaminants in a soil column above the water table of an unconfined aquifer is considered.

The length of the soil column is 20 m and the Darcy velocity and water content are assumed to be constant and equal to 0.25 m/d and 0.25, respectively. The initial concentration is zero, and water with dimensionless solute concentration of 1 enters the soil surface at a rate of 0.25 m/d. At the water table, a zero dispersive-flux boundary condition is assumed. A list of physical parameter values and discretization data used in the simulation is provided in Table 3-6. Two cases involving conservative and nonconservative species were simulated. Results obtained from the VADOFT code are compared in Figure 3.14 and Table 3-7 with the analytical solution given by van Genuchten and Alves (1982). There is excellent agreement between the numerical and analytical solutions for both cases.

3.5.2.3 Transport in a Layered Soil Column--
This problem concerns one-dimensional transport of a conservative solute species in a soil column consisting of three layers. The initial concentration in the soil column is assumed to be zero, and the two boundary conditions prescribed are a unit concentration at the top and a zero dispersive flux boundary condition at the bottom. A list of physical parameter values and discretization data used in the simulation is provided

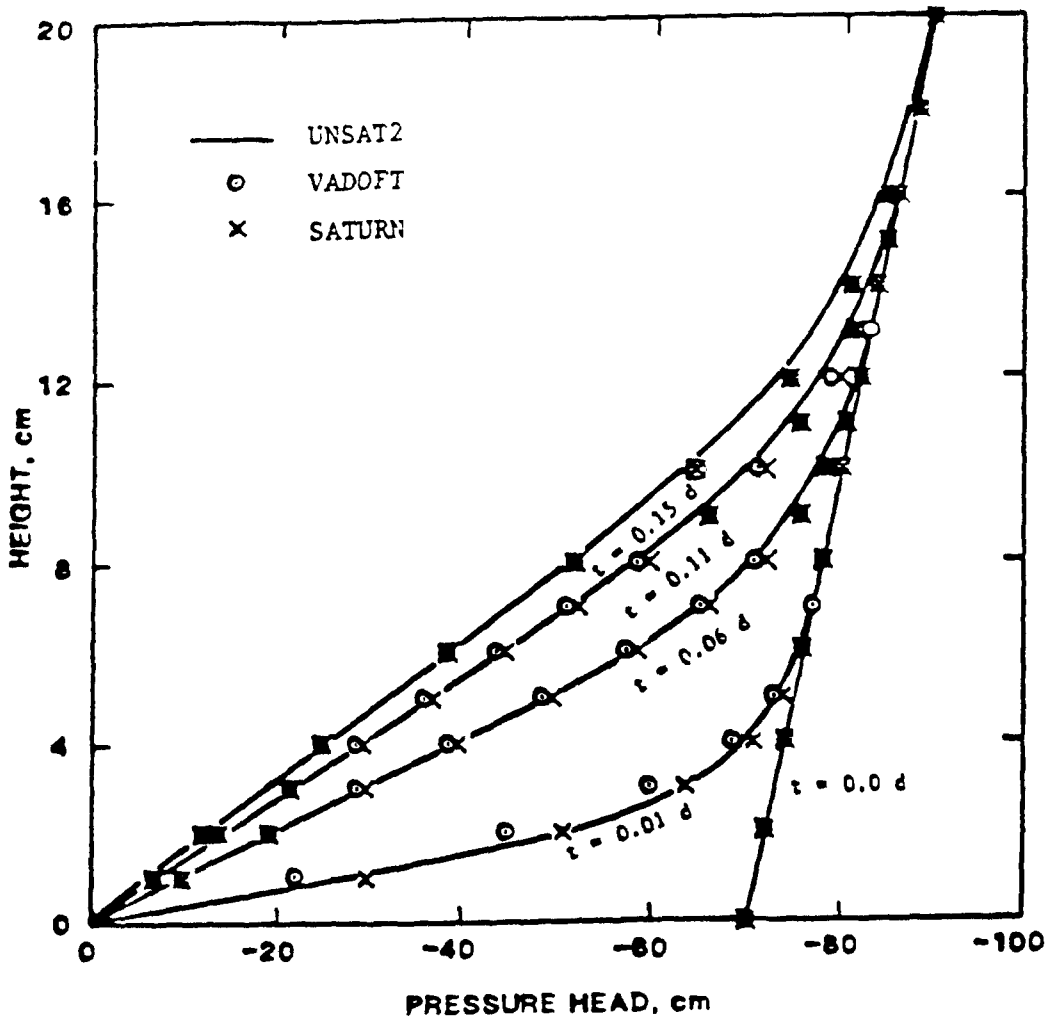

Figure 3.9. Simulated pressure head profiles for the problem of transient upward flow in a soil column. (Adapted from Battelle and GeoTrans, 1988).

in Table 3-8. Two cases corresponding to those considered by Shamir and Harleman (1967) were simulated. Both cases have contrasting longitudinal dispersivity values among the three layers. The dispersivity values of the second case are ten times those of the first case for the same layers. The intention here is to test the numerical scheme used in the VADOFT code, as well as to check the validity of an approximate analytical solution presented by Shamir and Harleman (1967) and Hadermann (1980). It should be noted here that the approximate solutions by Shamir and Harleman (1967) and Hadermann (1980) are valid only for relatively small values of dispersivity. Therefore, for a small dispersivity value, the solutions can be employed to verify the VADOFT code. Then with appropriate discretization, the VADOFT code could be used to determine the validity of the analytical solutions at large dispersivity values.

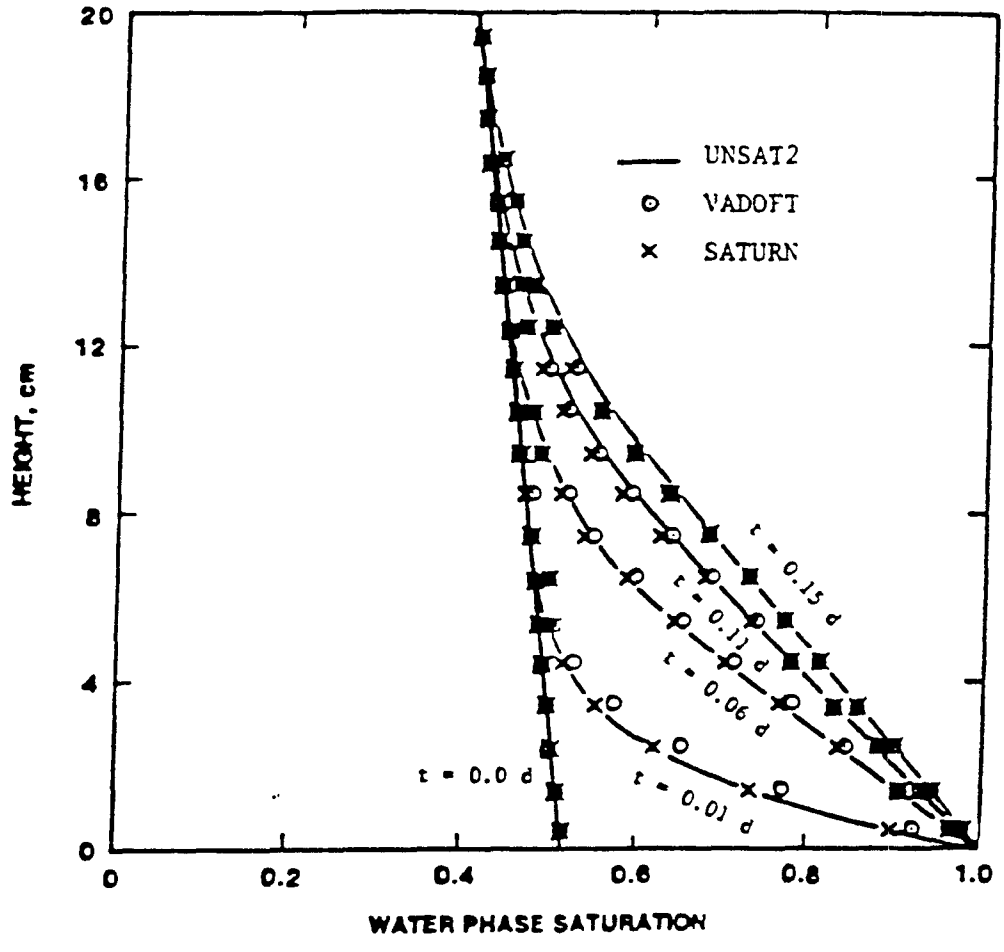

Figure 3.10. Simulated profile of water saturation for the problem of transient upward flow in a soil column. (Adapted from Battelle and GeoTrans, 1988).

Table 3-3. ITERATIVE PROCEDURE PERFORMANCE COMPARISON

Case	Number of Nonlinear Iterations	
	Newton-Raphson	Picard
n = 3	12	33
n = 4	13	56
n = 6	19	n.c.*
n = 8	27	n.c.
n = 10	31	n.c.

* No convergence. Head tolerance = 0.0001 cm. Grid spacing z = 10 cm.

Table 3-4. VALUES OF PHYSICAL PARAMETERS AND DISCRETIZATION DATA USED IN SIMULATING ONE-DIMENSIONAL TRANSPORT IN A SEMI-INFINITE SOIL COLUMN

Parameter	Value
Darcy velocity, V	1 cm hr^{-1}
Porosity, ϕ	0.25
Longitudinal dispersivity, α_L	5 cm
Concentration at the source, c_o	1
Δz = 10 cm	
Δt = 2.5 hr	

Using the discretization data given in Table 3-8, the VADOFT code was run for 180 time steps. Simulated breakthrough curves at the bottom end of the column (z = 86.1 cm) are presented in Figures 3.15 and 3.16 and in Tables 3-9 and 3-10. As can be seen, the numerical solution of the VADOFT code compares very well with the analytical solution for case 1: The small dispersivity case, where the analytical assumption of infinite ratio of layer thickness to layer dispersivity--i.e., each layer extends to infinity--is fairly accurate. There is a slight discrepancy of the analytical solution from the numerical solution for case 2, where the analytical assumption is less accurate.

3.5.3 Combined Nonlinear Flow and Transport Modules

3.5.3.1 Transport During Absorption of Water in a Soil Tube--
This problem is selected to provide simultaneous testing of the flow and the transport modules of VADOFT. The problem is depicted schematically in Figure 3.17. A conservative solute species has a uniform initial concentration and moisture content. The initial concentration is assumed to be zero, and the inlet concentration c_o is assumed to be 1 ppm. The solute is transported by dispersion and advection. Note that the solute front and the wetting front advance at different rates. The solute velocity, V_{sol}, was previously defined as Equation 3-23. The velocity of the wetting front is dependent upon the rate of water sorption into the soil, which is dependent on moisture diffusivity; thus, calculation of the wetting front velocity requires integration of the mass balance equation. For the sake of convenience, all physical data pertaining to the geometry of the soil tube and the physical parameter values are kept the same as those used in the paper by Huyakorn et al. (1985). The complete set of data is listed in Table 3-11. The simulation was performed in two stages. In the first stage, the transient water flow problem was analyzed to determine the distributions of Darcy velocity and water saturation for each time level. These results are written on an output file. In the second stage, the transient solute transport

problem was analyzed to determine concentration distributions using the velocity and water saturation data file obtained from the flow simulation.

The spatial and temporal discretization data used in running the VADOFT code are also given in Table 3-11. Both the flow and the transport analyses were performed for 50 time steps. Results of the flow analysis are plotted in Figure 3.18. The water saturation profiles given by VADOFT compare well with those obtained using the semi-analytical solution of Phillip (1955) and the UNSAT2 finite-element flow code. Results of the transport analysis are

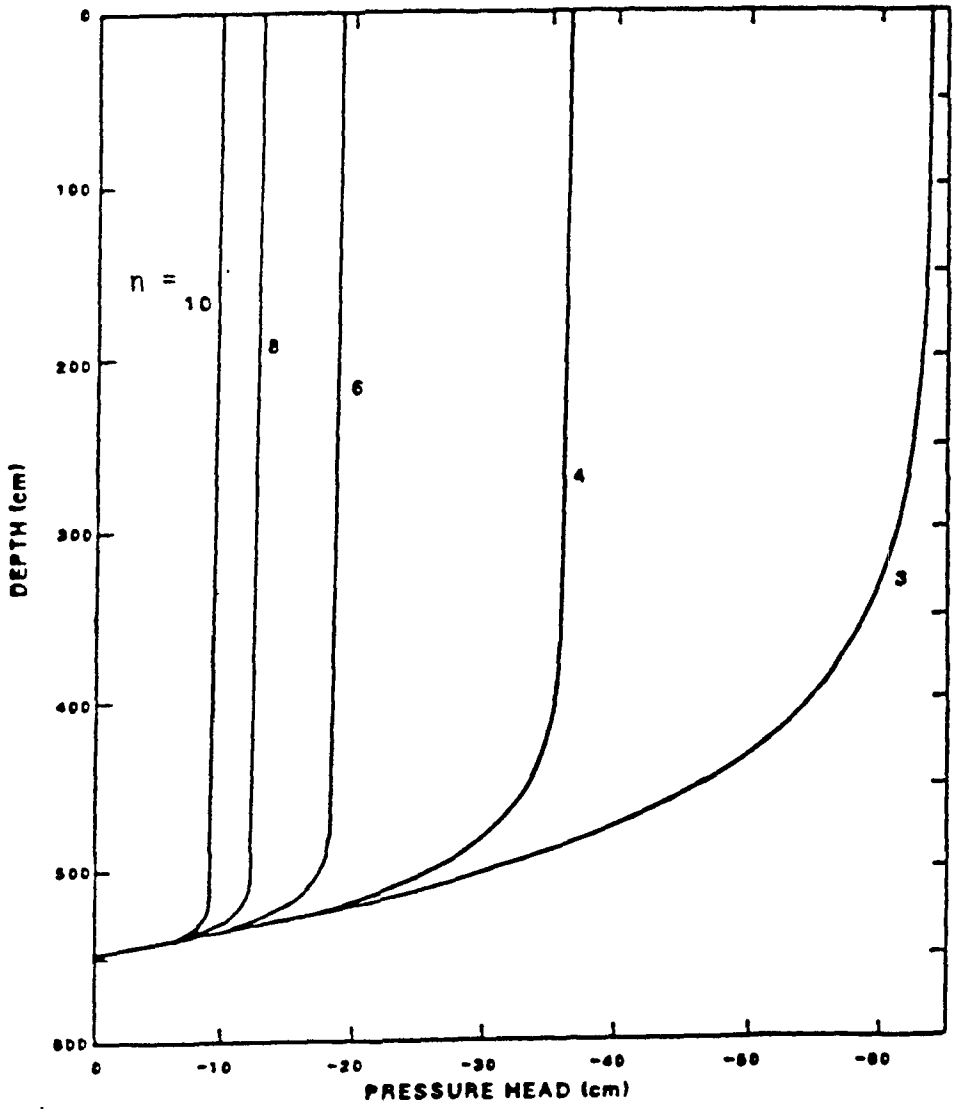

Figure 3.11. Simulated pressure head profiles for five cases of the problem of steady infiltration in a soil column. (Adapted from Springer and Fuentes, 1987).

plotted in Figure 3.19. The concentration distributions given by VADOFT also compare well with those obtained using the semi-analytical solution of Smiles et al. (1978) and the FEMWASTE finite-element transport code documented by Yeh and Ward (1981).

3.5.3.2 Transient Infiltration and Contaminant Transport in the Vadose Zone- This problem, schematically depicted in Figure 3.20, involves variable infiltration and contaminant transport in a layered system in which layer

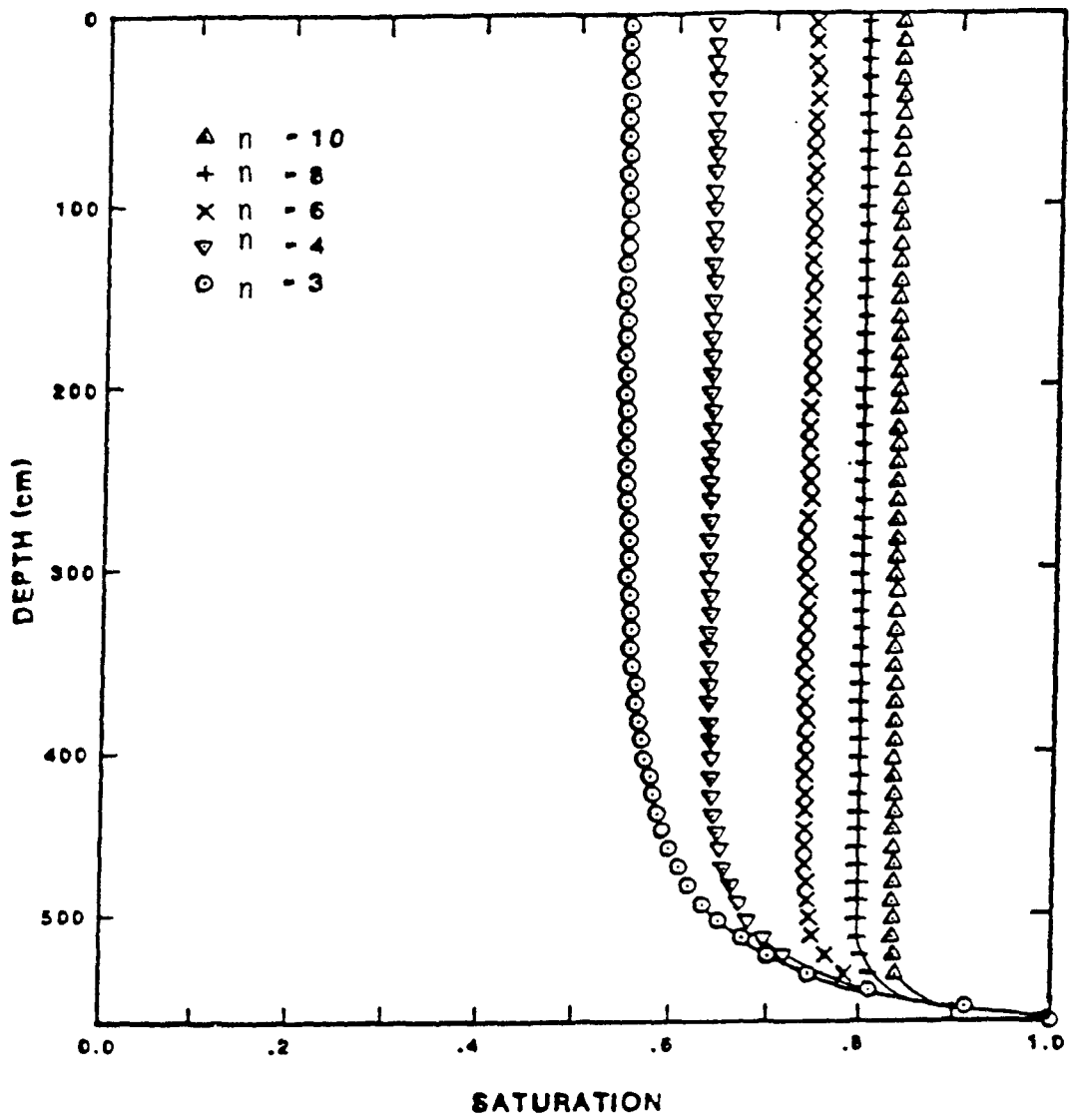

Figure 3.12. Simulated profiles of water saturation for five cases of the problem of steady infiltration in a soil column. (Adapted from Springer and Fuentes, 1987).

permeabilities differ by more than two orders of magnitude. The problem was chosen to demonstrate the capability of VADOFT to handle a higher nonlinear situation involving soil materials with sharp contrast in drainage properties. Shown in Table 3-12 are values of physical parameters and discretization data used in the flow and transport simulations. For the unsaturated flow simulation, the transient infiltration rates illustrated in Figure 3.21 were used. It was assumed that the initial condition corresponded to a hydrostatic pressure head distribution in the soil with pressure head values at the water table and the top of the soil equal to 0 and -420 cm, respectively. The simulation was performed for 20 time steps

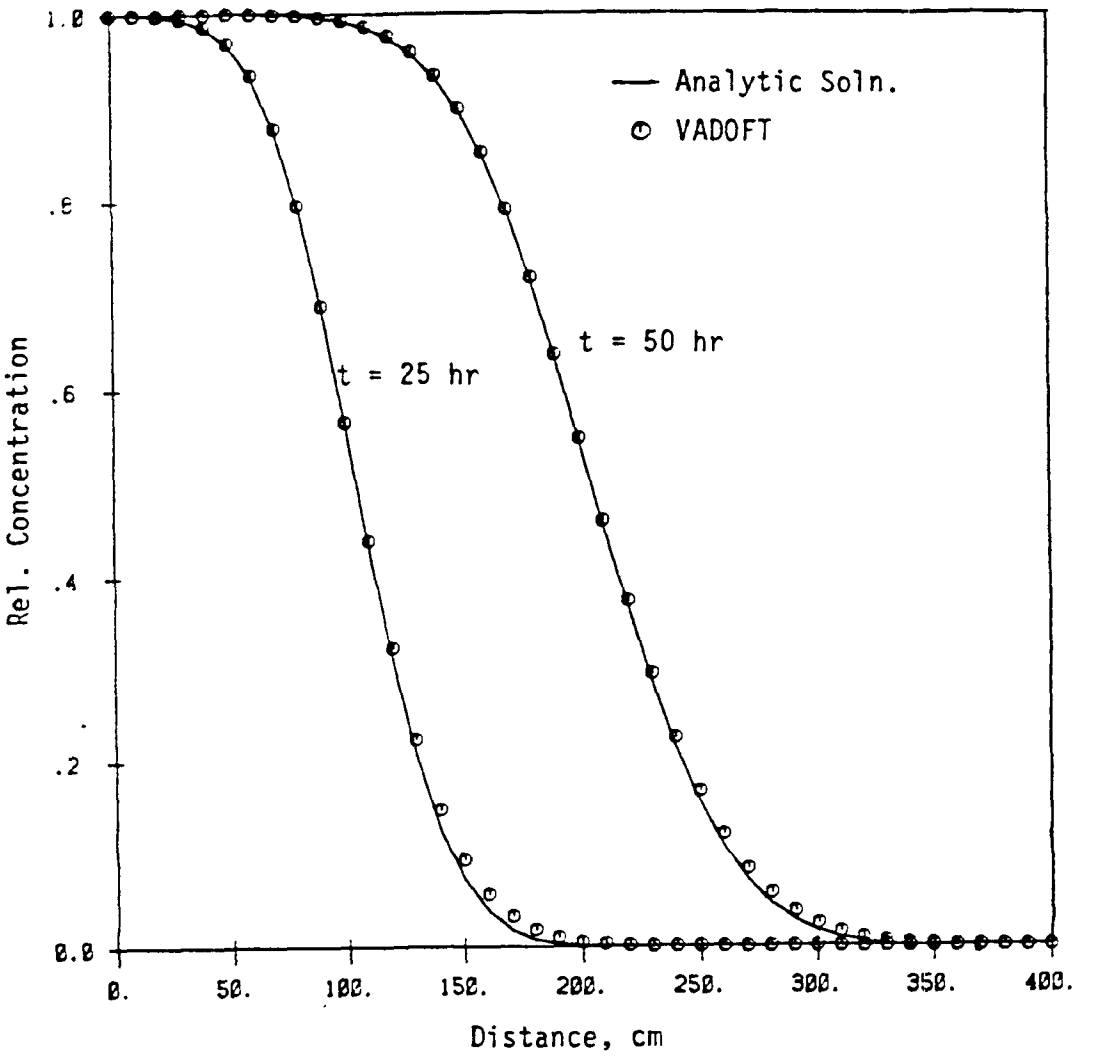

Figure 3.13. Simulated concentration profiles for the problem of solute transport in a semi-infinite soil column.

Table 3-5. CONCENTRATION PROFILE CURVES AT t = 25 hr AND t = 50 hr SHOWING COMPARISON OF THE ANALYTICAL SOLUTION AND RESULTS FROM VADOFT

z Distance (cm)	Concentration Values			
	t = 25 hr		t = 50 hr	
	Analytical	VADOFT	Analytical	VADOFT
00.0	1.0000	1.0000	1.0000	1.0000
10.0	0.9997	0.9998	1.0000	1.0000
20.0	0.9983	0.9987	1.0000	1.0000
30.0	0.9945	0.9954	1.0000	1.0000
40.0	0.9854	0.9870	0.9999	1.0000
50.0	0.9662	0.9688	0.9999	0.9999
60.0	0.9313	0.9346	0.9996	0.9997
70.0	0.8745	0.8781	0.9991	0.9994
80.0	0.7924	0.7956	0.9981	0.9985
90.0	0.6858	0.6889	0.9960	0.9967
100.0	0.5619	0.5660	0.9921	0.9933
110.0	0.4321	0.4394	0.9854	0.9871
120.0	0.3099	0.3222	0.9743	0.9767
130.0	0.2060	0.2235	0.9570	0.9599
140.0	0.1264	0.1474	0.9313	0.9348
150.0	0.0713	0.0928	0.8953	0.8991
160.0	0.0369	0.0560	0.8475	0.8513
170.0	0.0175	0.0327	0.7872	0.7908
180.0	0.0075	0.0184	0.7151	0.7186
190.0	0.0030	0.0101	0.6331	0.6368
200.0	0.0011	0.0054	0.5447	0.5491
210.0	0.0003	0.0029	0.4541	0.4598
220.0	0.0000	0.0015	0.3660	0.3736
230.0			0.2845	0.2942
240.0			0.2129	0.2246
250.0			0.1532	0.1662
260.0			0.1058	0.1193
270.0			0.0701	0.0831
280.0			0.0444	0.0563
290.0			0.0270	0.0371
300.0			0.0157	0.0239
310.0			0.0087	0.0150
320.0			0.0046	0.0092
330.0			0.0000	0.0055

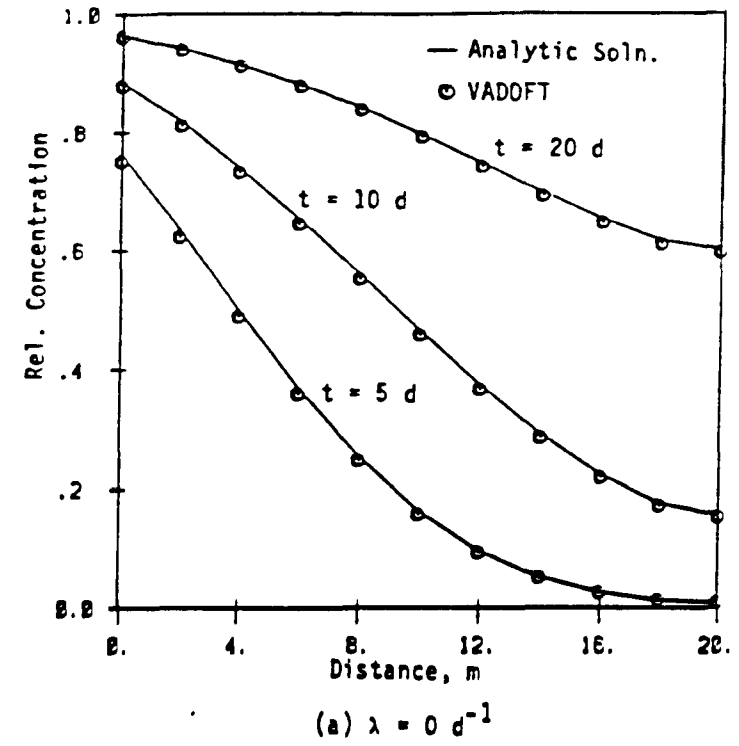

(a) $\lambda = 0\ d^{-1}$

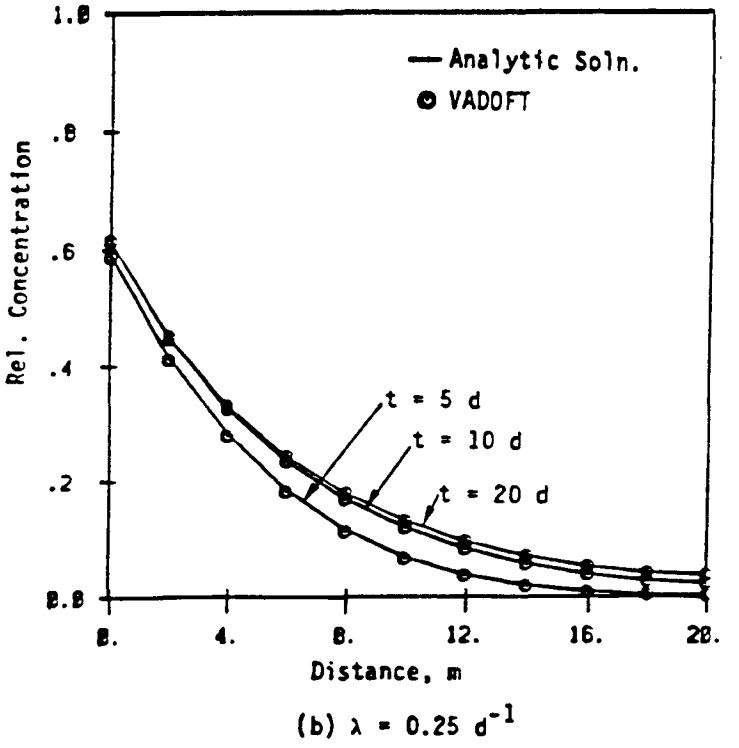

(b) $\lambda = 0.25\ d^{-1}$

Figure 3.14. Simulated concentration profiles for two cases of the problem of solute transport in a soil column of finite length, (a) $\lambda = 0\ d^{-1}$, and (b) $\lambda = 0.25\ d^{-1}$.

Table 3-6. VALUES OF PHYSICAL PARAMETERS AND DISCRETIZATION DATA USED IN SIMULATING ONE-DIMENSIONAL TRANSPORT IN A FINITE SOIL COLUMN

Parameter	Value
Thickness of soil column, L	20 m
Darcy velocity, V	0.25 m d^{-1}
Water content, θ	0.25
Retardation coefficient, R	1
Longitudinal dispersivity, α_L	4 m
Source leachate concentration, c_o	1
Case 1:	
Decay constant, λ	0 d^{-1}
Case 2:	
Decay constant, λ	0.25 d^{-1}
Δz = 1.0 m	
Δt = 0.5 d	

using Δt = 1 d. Shown in Figures 3.22 through 3.24 are simulated profiles of water saturation, pressure head, and vertical Darcy velocity, respectively. As expected, the two sand layers exhibit fast drainage response whereas the intervening clay-loam layer exhibits slow drainage response. This behavior is seen in Figure 3.22. The pressure head and velocity profiles depicted in Figures 3.23 and 3.24 directly reflect the effect of temporal change in the infiltration rate. Note that the values of Darcy velocity at the soil surface (Figure 3.24) are equal to the values of infiltration rate for the same time values. Following the unsaturated flow simulation, the transport simulation was performed using the Darcy velocity file from the flow computation as an input file for the transport computation. Concentration profiles determined by the code are plotted in Figure 3.25. As illustrated, the contaminant front exhibits slow movement through the clay loam layer.

Table 3-7. CONCENTRATION PROFILE CURVES SHOWING COMPARISON OF THE ANALYTICAL SOLUTION AND VADOFT

Case 1: $\lambda = 0\ d^{-1}$

Distance	t = 5 d		t = 10 d		t = 20 d	
z, (m)	Analytical	VADOFT	Analytical	VADOFT	Analytical	VADOFT
0.0	0.764	0.751	0.884	0.878	0.963	0.961
2.0	0.638	0.624	0.820	0.812	0.942	0.939
4.0	0.502	0.489	0.742	0.733	0.914	0.911
6.0	0.371	0.360	0.655	0.645	0.881	0.877
8.0	0.256	0.247	0.561	0.552	0.841	0.837
10.0	0.164	0.158	0.466	0.457	0.796	0.791
12.0	0.097	0.094	0.375	0.367	0.748	0.742
14.0	0 053	0.052	0.293	0.286	0.698	0.692
16.0	0.027	0.027	0.224	0.219	0.652	0.646
18.0	0.013	0.014	0.176	0.171	0.617	0.610
20.0	0.009	0.009	0.157	0.152	0.602	0.595

Case 2: $\lambda = 0.25\ d^{-1}$

Distance	t = 5 d		t = 10 d		t = 20 d	
z, (m)	Analytical	VADOFT	Analytical	VADOFT	Analytical	VADOFT
0.0	0.593	0.588	0.615	0.613	0.618	0.617
2.0	0.416	0.411	0.449	0.447	0.453	0.452
4.0	0.283	0.279	0.326	0.325	0.333	0.332
6.0	0.186	0.182	0.236	0.234	0.244	0.243
8.0	0.116	0.113	0.169	0.167	0.179	0.178
10.0	0.069	0.067	0.119	0.118	0.131	0.131
12.0	0.038	0.037	0.083	0.083	0.096	0.096
14.0	0.020	0.019	0.057	0.057	0.071	0.071
16.0	0.009	0.009	0.039	0.039	0.053	0.053
18.0	0.004	0.004	0.028	0.028	0.042	0.042
20.0	0.002	0.002	0.024	0.024	0.038	0.038

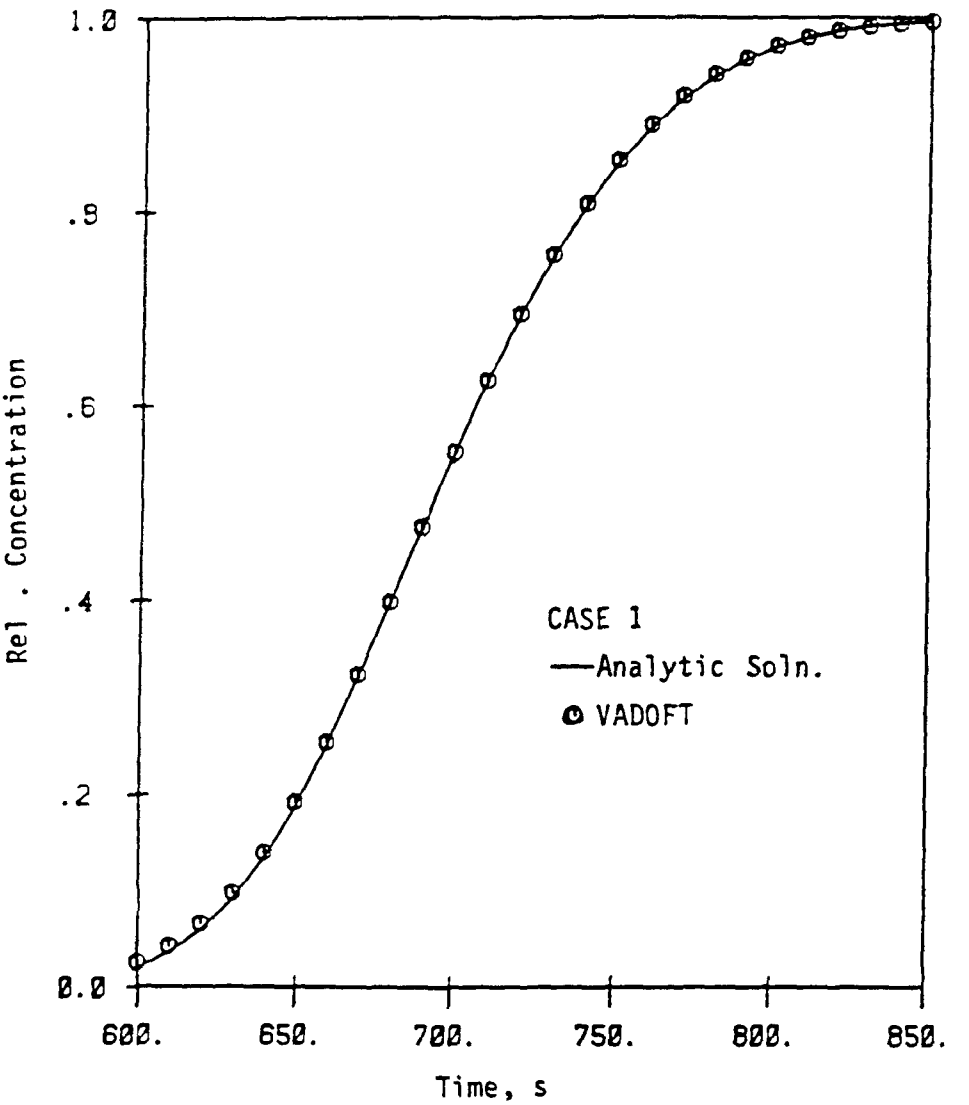

Figure 3.15. Simulated outflow breakthrough curve for case 1 of the problem of solute transport in a layered soil column.

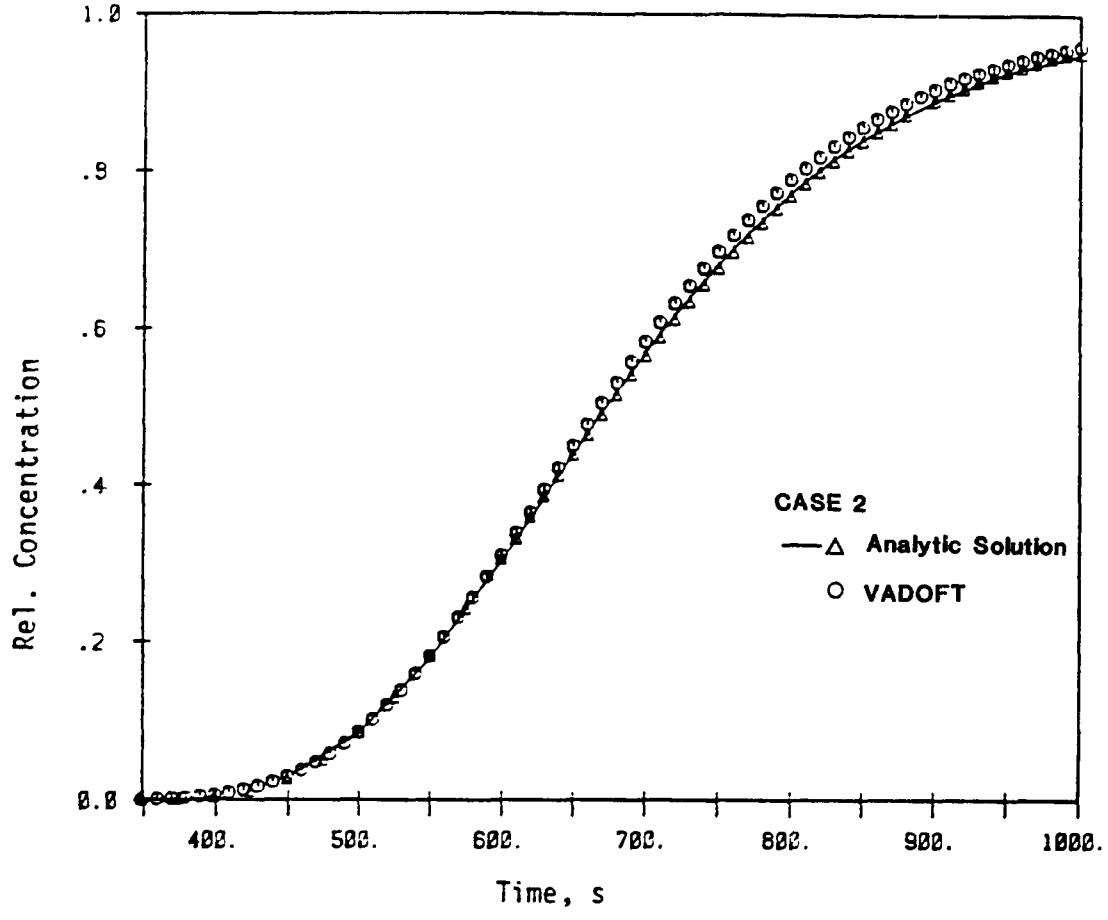

Figure 3.16. Simulated outflow breakthrough curve for case 2 of the problem of solute transport in a layered soil column.

Table 3-8. VALUES OF PHYSICAL PARAMETERS USED IN THE SIMULATION OF TRANSPORT IN A LAYERED SOIL COLUMN

Parameter	Value for Layer i		
	Layer 1	Layer 2	Layer 3
Layer thickness, ℓ_i	25.48	30.31	30.31 cm
Seepage velocity, u_i	0.127	0.123	0.121 cm s^{-1}
Retardation coeff., R_i	1.0	1.0	1.0
Decay constant, λ_i	0	0	0 s^{-1}
Source concentration, c_o	1.0		
Case 1:			
Dispersivity, α_{Li}	0.076	0.174	0.436 cm
Case 2:			
Dispersivity, α_{Li}	0.76	1.74	4.36 cm
Δz = 0.6888 cm			
Δt = 5 s			

Table 3-9. BREAKTHROUGH CURVES (at z = 86.1 cm) COMPUTED USING THE ANALYTICAL SOLUTION AND VADOFT: CASE 1

Time, t (s)	Concentration Values for Case 1	
	Analytical Solution	Numerical VADOFT
600	0.0204	0.0262
610	0.0361	0.0427
620	0.0596	0.0665
630	0.0923	0.0989
640	0.1354	0.1410
650	0.1887	0.1930
660	0.2514	0.2543
670	0.3217	0.3234
680	0.3971	0.3981
690	0.4748	0.4755
700	0.5518	0.5526
710	0.6255	0.6266
720	0.6935	0.6951
730	0.7544	0.7564
740	0.8072	0.8096
750	0.8517	0.8542
760	0.8881	0.8907
770	0.9172	0.9197
780	0.9400	0.9421
790	0.9573	0.9590
800	0.9704	0.9715
810	0.9800	0.9805
820	0.9870	0.9869
830	0.9919	0.9913
840	0.9950	0.9943
850	0.9970	0.9964

Table 3-10. BREAKTHROUGH CURVES (at z = 86.1 cm) COMPUTED USING THE ANALYTICAL SOLUTION AND VADOFT: CASE 2

Time, t (s)	Concentration Values for Case 2	
	Analytical Solution	Numerical VADOFT
600	0.303	0.310
610	0.330	0.337
620	0.357	0.365
630	0.384	0.394
640	0.412	0.422
650	0.439	0.450
660	0.466	0.478
670	0.493	0.505
680	0.519	0.532
690	0.544	0.558
700	0.569	0.584
710	0.593	0.608
720	0.617	0.632
730	0.639	0.655
740	0.661	0.677
750	0.681	0.698
760	0.701	0.718
770	0.720	0.737
780	0.738	0.755
790	0.755	0.772
800	0.771	0.788
810	0.787	0.804
820	0.801	0.818
830	0.815	0.831
840	0.828	0.844
850	0.840	0.856
900	0.889	0.904

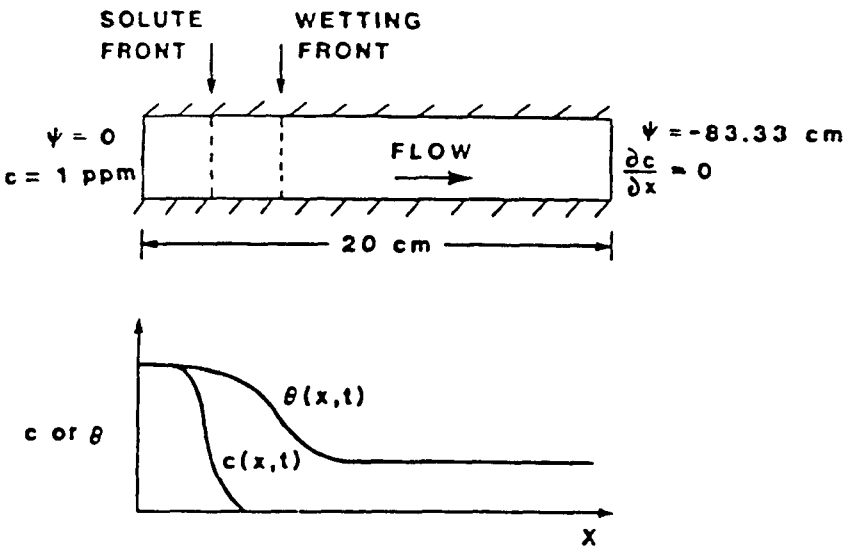

Figure 3.17. One-dimensional solute transport during absorption of water in a soil tube. (Adapted from Huyakorn et al., 1985).

Table 3-11. VALUES OF PHYSICAL PARAMETERS AND DISCRETIZATION DATA USED IN SIMULATING TRANSPORT IN A VARIABLY SATURATED SOIL TUBE

Parameter	Value
Length of soil column, L	20 cm
Saturated hydraulic conductivity, K	1 cm d^{-1}
Initial pressure head, ψ_i	-83.33 cm
Remaining flow parameters	See Table 3-2
Initial concentration, c_i	0 ppm
Longitudinal dispersivity, α_L	0 cm
Molecular diffusion, D^*	1 cm^2 d^{-1}
Decay constant, λ	0 d^{-1}
Retardation coefficient, R	1
Δz = 0.25 cm	
Δt = 0.0025 d	

Table 3-12. VALUES OF PHYSICAL PARAMETERS AND DISCRETIZATION DATA USED IN SIMULATING TRANSIENT INFILTRATION AND CONTAMINANT TRANSPORT IN THE VADOSE ZONE

Property	Material 1 (Sand)	Material 2 (clay loam)
Saturated conductivity, K	713	6.24 cm d^{-1}
Porosity, ϕ	0.43	0.41
Residual Water Saturation, S_{wr}	0.105	0.232
Air entry value, ψ_a	0.0	0.0 cm
Soil moisture parameter, α	0.145	0.019 cm^{-1}
Soil moisture parameter, β	2.68	1.31
Soil moisture parameter, γ	0.63	0.24
Longitudinal dispersivity, α_L	1.0	1.0 cm
Retardation coefficient, R	1.1	1.5
Decay coefficient, λ	0.00274	0.00274 d^{-1}
Δz = 4 cm		
Δt = 1 d		

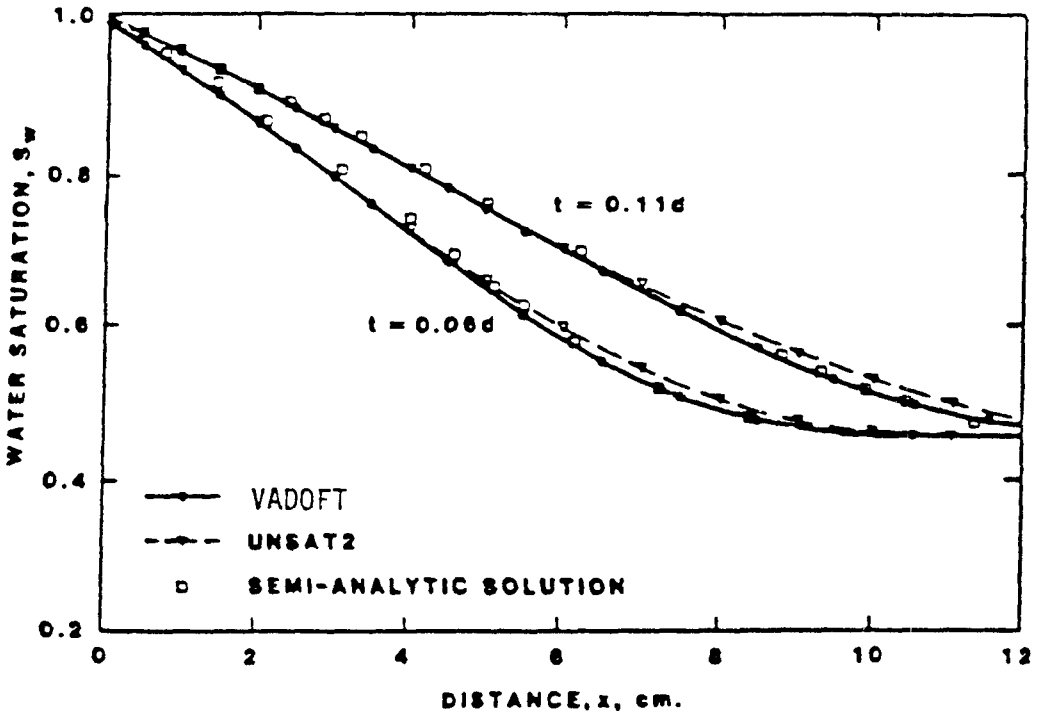

Figure 3.18. Simulated profiles of water saturation during absorption of water in a soil tube. (Adapted from Huyakorn et al., 1984a).

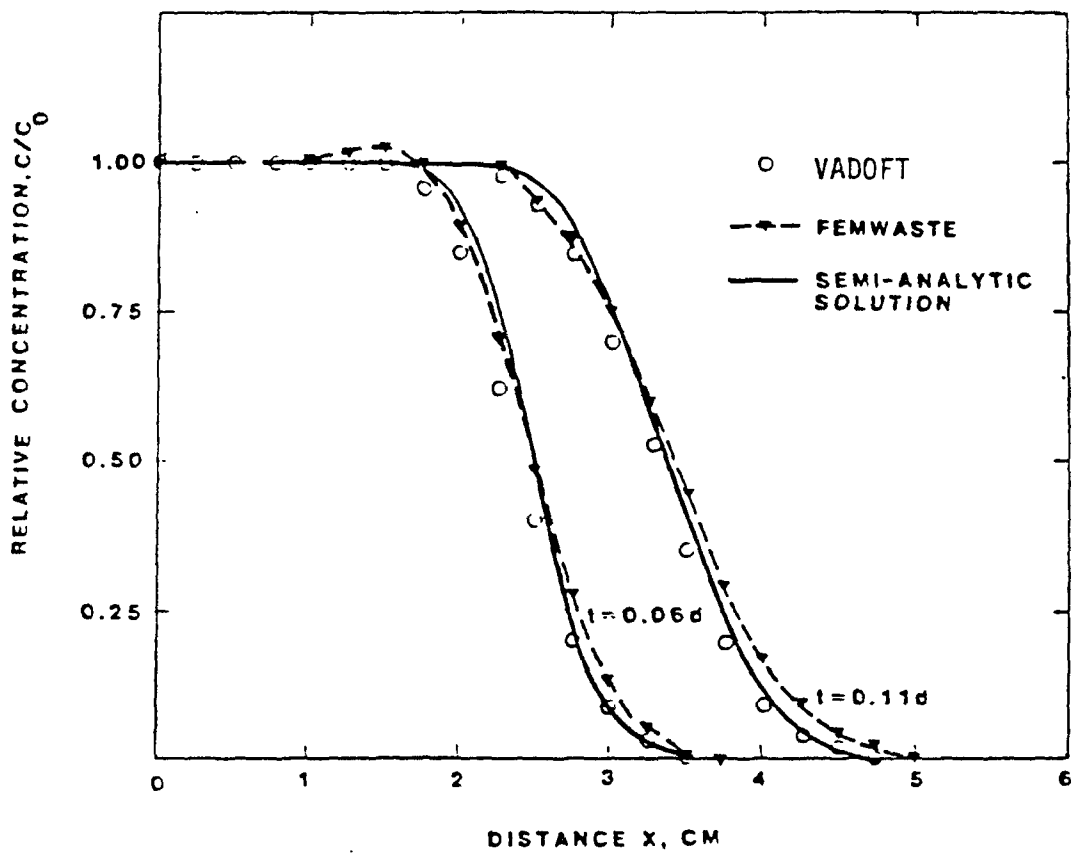

Figure 3.19. Simulated concentration profiles for the problem of one-dimensional solute transport during absorption of water in a soil tube. (Adapted from Huyakorn, et al., 1985).

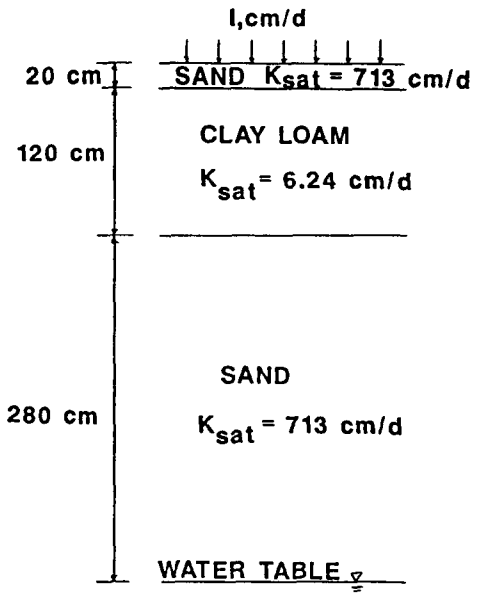

Figure 3.20. Problem description for transient infiltration and transport in the vadose zone.

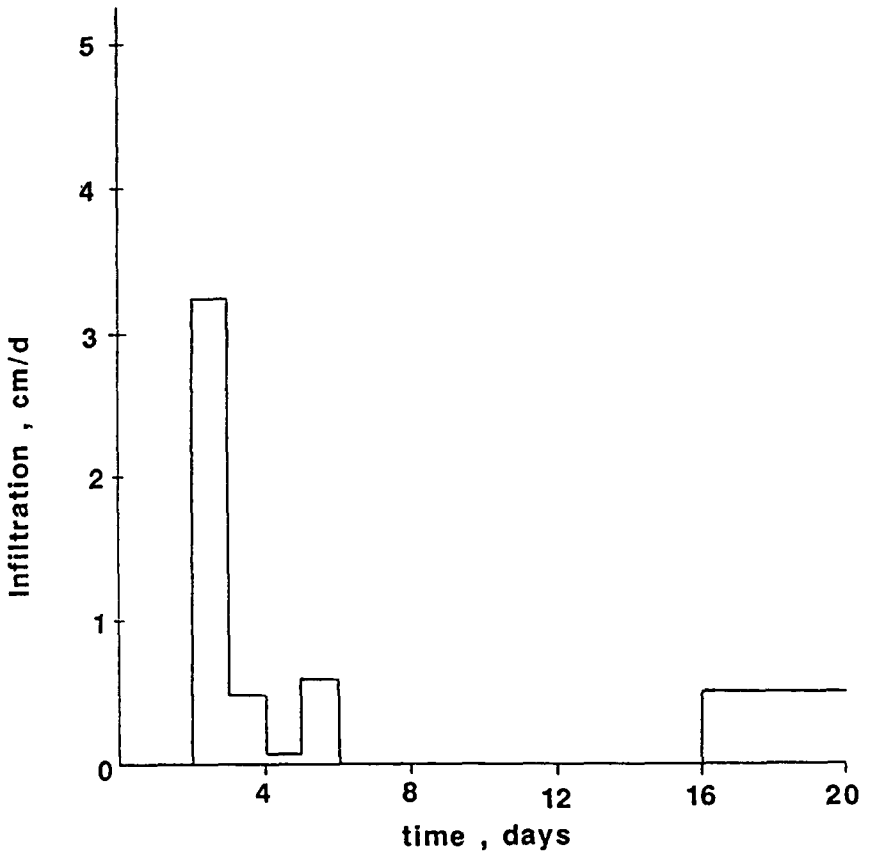

Figure 3.21. Infiltration rate vs. time relationship used in numerical simulation.

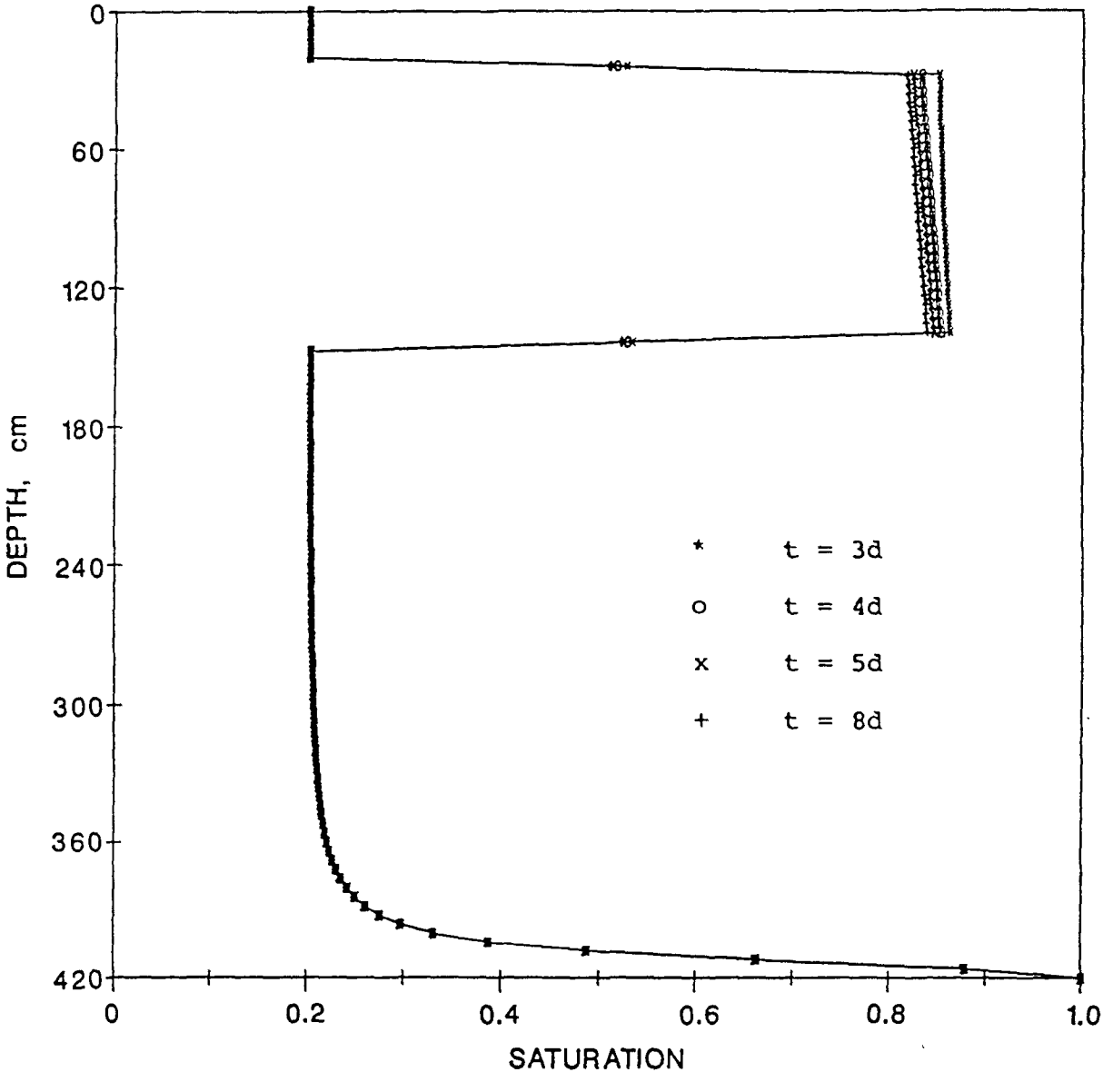

Figure 3.22. Simulated water saturation profiles.

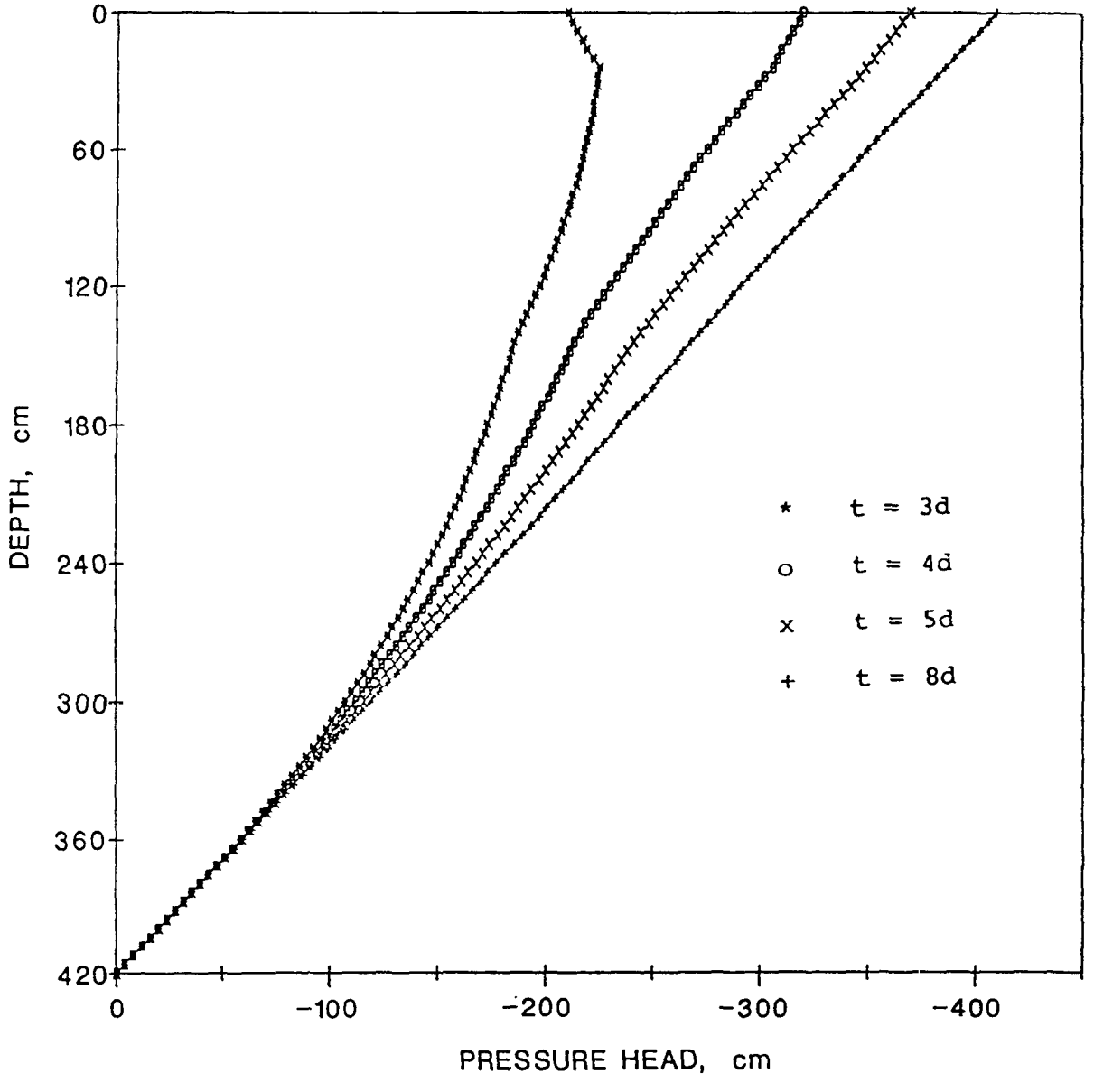

Figure 3.23. Simulated pressure head profiles.

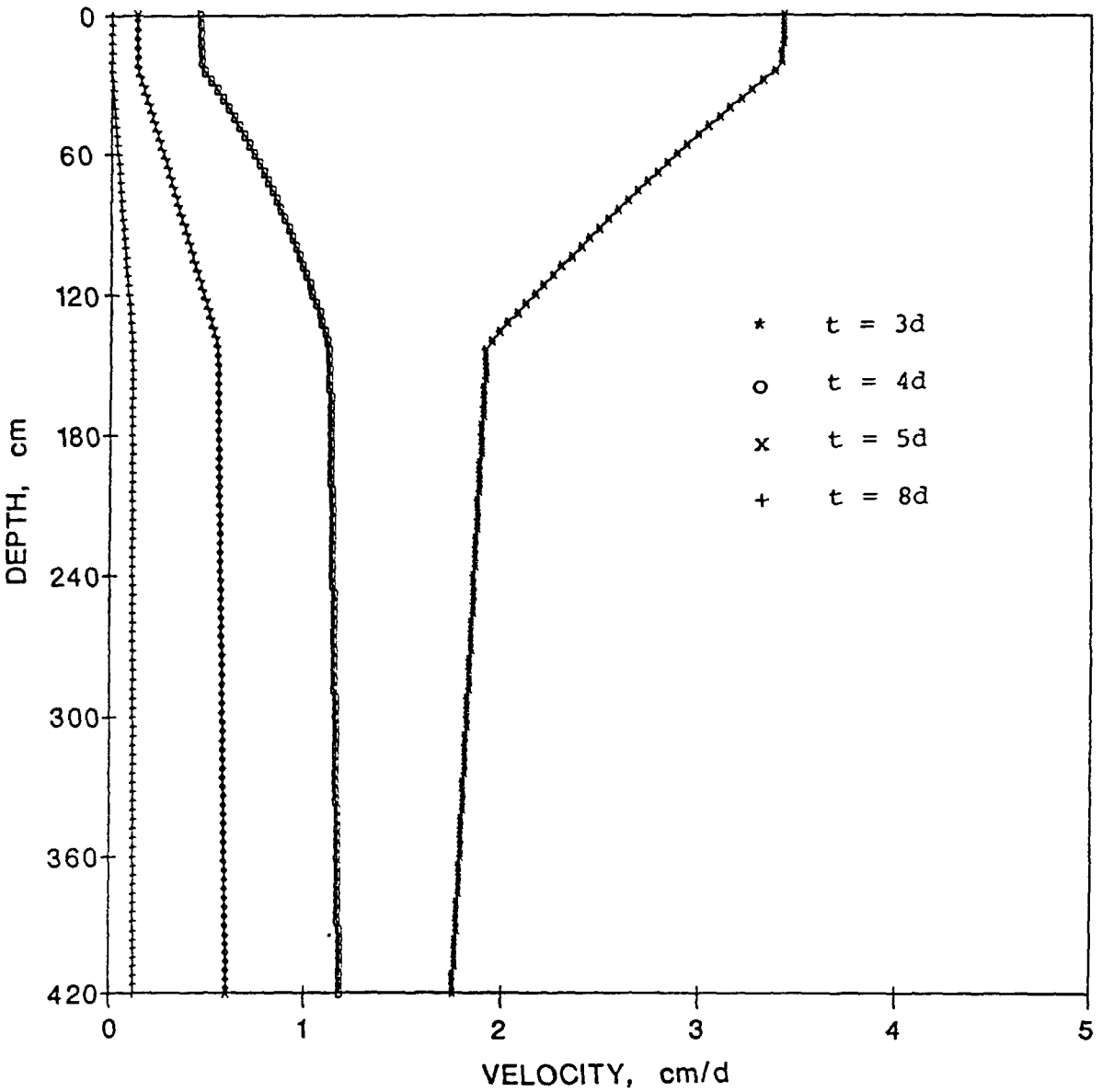

Figure 3.24. Simulated vertical Darcy velocity profiles.

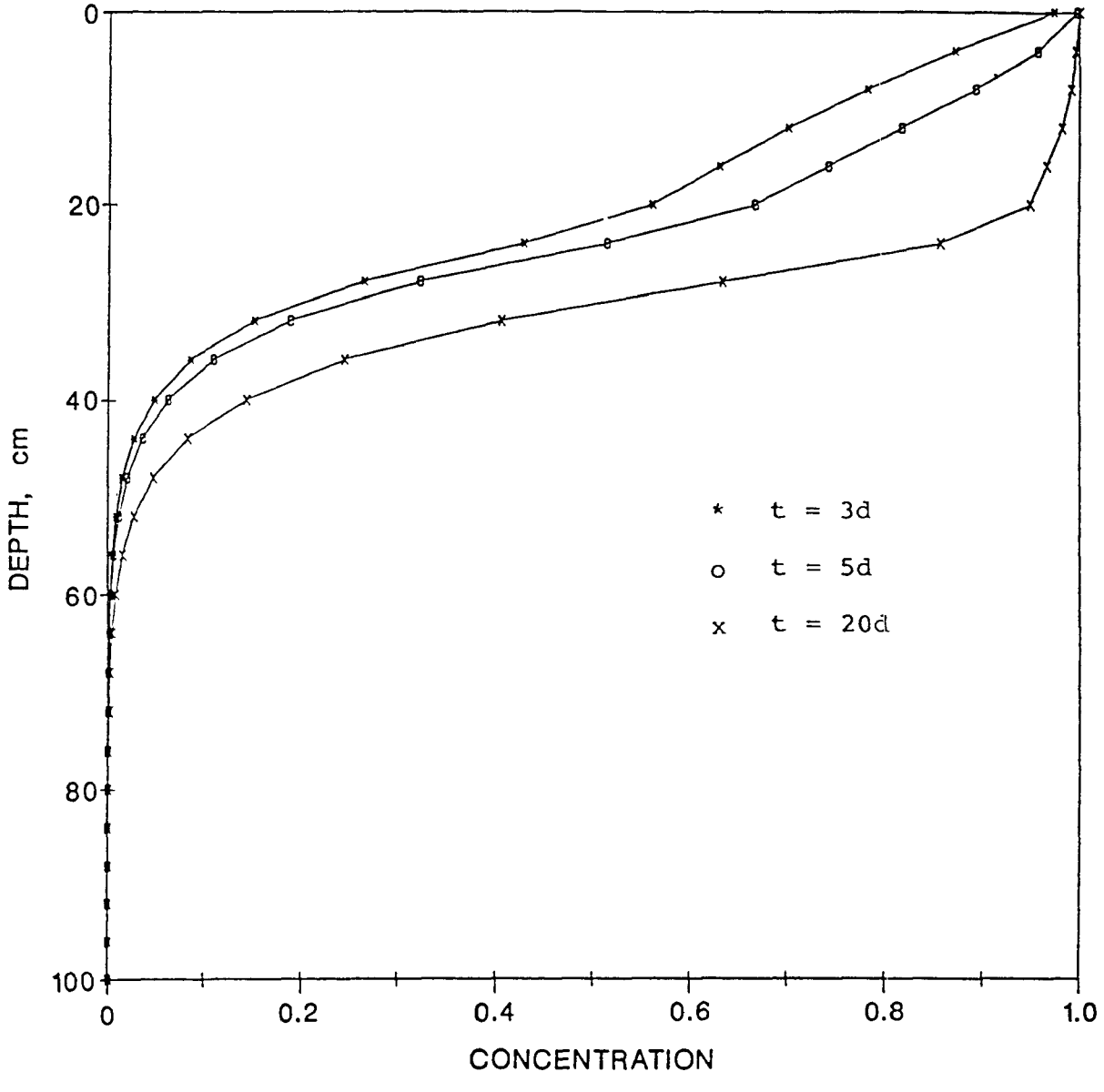

Figure 3.25. Simulated solute concentration profiles.

SECTION 4

SATURATED ZONE FLOW AND TRANSPORT MODEL (SAFTMOD)

4.1 INTRODUCTION

SAFTMOD is a finite-element code for simulating groundwater flow and solute transport in the saturated zone of an unconfined aquifer system. It is the third part of the three-component RUSTIC model for predicting the movement of pesticides within and below the plant root zone and assessing consequent groundwater contamination. SAFTMOD performs two-dimensional simulations in an areal plane or a vertical cross section. In addition, the code also performs axisymmetric simulations. Both single and leaky two-aquifer systems can be handled. The code considers only single-porosity media and ignores the effects of fracture flow in the aquifer system. Transport of dissolved contaminants may also be simulated within the same domain. Transport processes accounted for include hydrodynamic dispersion, advection, linear equilibrium sorption, and first-order decay. Parent/daughter transformations are also simulated.

4.2 OVERVIEW OF SAFTMOD

The SAFTMOD code may be used in conjunction with the root zone model, PRZM, and/or the vadose-zone model, VADOFT, to simulate groundwater flow and transport of dissolved contaminants in the saturated zone. SAFTMOD predicts groundwater velocity field, flow rates, concentration plumes, and temporal distributions of contaminant concentration at downstream locations.

4.2.1 Features

4.2.1.1 General Description--

The SAFTMOD code can be used to perform two-dimensional or axisymmetric modeling of groundwater flow and solute transport in the saturated zone of an unconfined aquifer system. For demonstrative purposes, we consider a situation involving the migration of pesticide in an aquifer subjected to well pumping (Figure 4.1). SAFTMOD can be used in three ways. First, the code can be used to perform either an axisymmetric or vertical cross-section analysis to assess the local well flow or migration of contaminants. Second, the code can be used to perform an areal analysis to assess flow and the migration of contaminants on a regional scale. SAFTMOD can be operated as a stand-alone code or operated in conjunction with PRZM and/or VADOFT. In the latter case, PRZM and/or VADOFT need to be run to obtain the necessary information pertaining to flux boundary conditions on the water table beneath the unsaturated soil column.

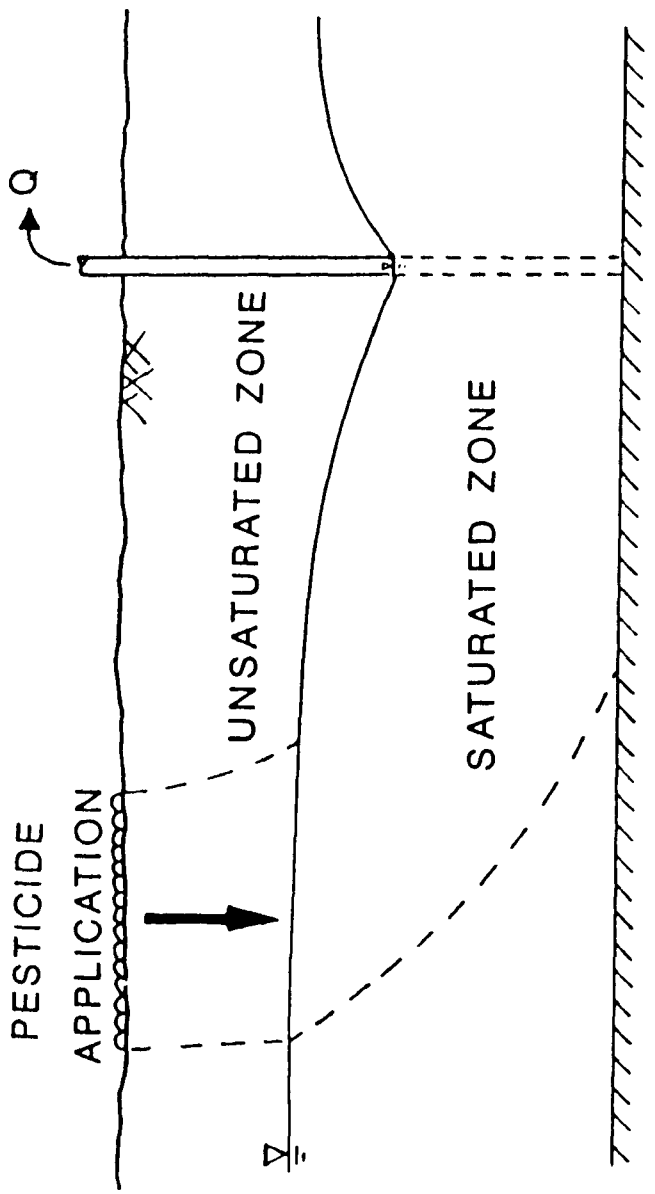

Figure 4.1. Schematic description of pesticide migration in unconfined aquifer system subject to pumping.

4.2.1.2 Processes and Geometry--
SAFTMOD performs two-dimensional and axisymmetric analysis of saturated groundwater flow and associated solute transport problems. The analyses can be done in a transient or steady-state mode. The code employs the Galerkin finite-element technique to approximate the governing equations for flow and transport. It handles single nonleaky aquifer systems as well as leaky aquifer systems having two aquifers separated by semi-permeable layers or aquitards. For groundwater flow simulations, the code accommodates water table conditions, recharge by infiltration or precipitation, and well pumping or injection. For solute transport simulations, the code accounts for various transport processes, including hydrodynamic dispersion, advection, linear equilibrium sorption, and first-order decay. Steady-state transport can not be simulated when decay is considered. Boundary conditions of the saturated flow problem are specified in terms of prescribed hydraulic head (defined as the sum of pressure head and elevation), or prescribed volumetric water flux. Boundary conditions of the solute transport problem are specified in terms of prescribed concentration or prescribed solute mass flux. All boundary conditions can be time dependent.

4.2.1.3 Assumptions--
The SAFTMOD code contains both saturated flow and solute transport models. Major assumptions of the flow model are as follows:

- Darcy's law is valid and hydraulic head gradients are the only significant driving mechanism for fluid flow.
- The porosity and hydraulic conductivity are constant with time.
- Gradients of fluid density, viscosity, and temperature do not affect the velocity distribution.
- For areal flow simulation in two-aquifer systems, vertical leakage in aquitards is assumed.

Major assumptions of the transport model are as follows:

- Fluid properties are independent of concentrations of contaminants.
- Contaminants are miscible with in-place fluids.
- For areal transport simulations, advection in aquitards is assumed to be negligible.
- Diffusive/dispersive transport in the porous-medium system is governed by Fick's law. The hydrodynamic dispersion coefficient is defined as the sum of the coefficients of mechanical dispersion and molecular diffusion.
- Adsorption and decay of the solute may be described by a linear equilibrium isotherm and a first-order decay constant.

4.2.2 Limitations

Major limitations of the SAFTMOD are summarized as follows:

- The code simulates only single-phase water flow and solute transport in saturated porous media. It does not consider unsaturated or fractured media.
- Non-Darcy flow that may occur near pumping wells is neglected.
- Only two-dimensional or quasi-three-dimensional problems can be simulated.
- The code does not take into account sorption nonlinearity or kinetic sorption effects which, in some instances, can be important.

4.3 DESCRIPTION OF FLOW MODULE

4.3.1 Flow Equation

The form of the flow equation used in SAFTMOD depends on the type of analysis. In a vertical cross-sectional analysis, the following equation is used:

$$\frac{\partial}{\partial x}\left(K_{xx}\frac{\partial h}{\partial x}\right) + \frac{\partial}{\partial z}\left(K_{zz}\frac{\partial h}{\partial z}\right) = S_s\frac{\partial h}{\partial t} - q \qquad (4\text{-}1)$$

where x and z are the horizontal and vertical coordinates, h is the hydraulic head (L), K_{xx} and K_{zz} are principal components of hydraulic conductivity tensor in the x and z directions, respectively (LT^{-1}), S_s is the specific storage (L^{-1}), t is time (T), and q is the volumetric flow rate of sources or sinks per unit volume of the porous medium ($L^3T^{-1}L^{-3}$).

In an axisymmetric analysis, the following equation is used:

$$\frac{1}{r}\frac{\partial}{\partial r}\left(rK_{rr}\frac{\partial h}{\partial r}\right) + \frac{\partial}{\partial z}\left(K_{zz}\frac{\partial h}{\partial z}\right) = S_s\frac{\partial h}{\partial t} - q \qquad (4\text{-}2)$$

where r and z are the radial and vertical coordinates of the cylindrical coordinate system, and K_{rr} and K_{zz} are the radial and vertical components of the hydraulic conductivity tensor (LT^{-1}).

In an areal analysis, flow in a horizontal plane (x-y) of each aquifer is described by the following vertically averaged equation:

$$\frac{\partial}{\partial x}\left(K_{xx}\,H\frac{\partial h}{\partial x}\right) + \frac{\partial}{\partial y}\left(K_{yy}\,H\frac{\partial h}{\partial y}\right) = \eta\frac{\partial h}{\partial t} - q^* - \gamma \qquad (4\text{-}3)$$

where q^* is the volumetric flow rate of sources or sinks per unit area (L^3T^{-1} L^{-2}), γ is the vertical leakage flux from aquitard to aquifer (LT^{-1}), H is the saturated thickness (L), and η is a storage coefficient defined as

$$\eta = \begin{cases} S_s\ H & \text{for a confined aquifer} \\ S_y + S_s\ H & \text{for an unconfined aquifer, where } S_y \gg S_s H \end{cases} \tag{4-4}$$

in which S_y is the specific yield of the aquifer.

The use of equations 4-1, 4-2, and 4-3 implies that the principal directions of anisotropy coincide with the grid coordinate axes.

In the areal analysis, flow in aquitards is described approximately by the following one-dimensional vertical leakage equation:

$$\frac{\partial}{\partial z}\left[K' \frac{\partial h'}{\partial z}\right] = S_s' \frac{\partial h'}{\partial t} \tag{4-5}$$

where K' and S_s' are the vertical hydraulic conductivity (LT^{-1}) and specific storage (L^{-1}) of the aquitard, and h' is the hydraulic head in the aquitard.

The initial and boundary conditions of the groundwater flow problem may be expressed as

$$h(x_i,0) = h_o(x_i) \tag{4-6}$$

$$h(x_i,t) = \bar{h} \text{ on } B_1 \tag{4-7a}$$

$$V_i n_i = V_n \text{ on } B_2 \tag{4-7b}$$

where h_o is the initial head (L), $\bar{h}$ is the prescribed head (L) on boundary portion B_1, n_i is the outward unit normal vector on boundary portion B_2, where the fluid flux is prescribed as $-V_n$ (LT^{-1}). The sign convention for V_n is positive for inflow and negative for outflow. x_i (i=1,2) are the coordinates that correspond to x and z for cross-sectional, x and r for axisymmetric, and x and y for areal simulation.

The SAFTMOD code performs a finite element solution of the stated flow problem, and determines values of the hydraulic head at nodal points of a two-dimensional finite-element grid. After the head distribution has been determined, values of Darcy velocity components at element centroids are evaluated using Darcy's law, which may be expressed as

$$V_x = -K_{xx} \frac{\partial h}{\partial x} \tag{4-8}$$

$$V_y = -K_{yy} \frac{\partial h}{\partial y} \tag{4-8a}$$

Equations (4-8) and (4-8a) are used in the areal analysis. They are also applicable in the vertical cross-sectional and axisymmetric analyses if the coordinate system (x,y) is replaced by (x,z) and (r,z), respectively.

4.3.2 Numerical Solution of Flow Problems

Numerical approximations of the groundwater flow equations describing cross-sectional, axisymmetric, and areal problems are obtained using the Galerkin finite element technique. In the Galerkin finite element approximation procedure, the flow region is first discretized into a network of finite elements, and an interpolating trial function is used to represent the unknown function (hydraulic head) over the discretized region. An integral approximation of the flow equation is then obtained using the Galerkin weighted residual criterion. Spatial integration is performed piecewise over each element. Upon assembly of the elements and incorporation of boundary conditions, a system of nodal equations is obtained. For a steady-state simulation, the nodal equations are algebraic equations. For a transient simulation, the nodal equations are first-order time differential equations that can be integrated using a finite difference approximation. For each time step, this gives rise to a system of algebraic equations that are solved using a direct Gaussian elimination procedure.

4.3.2.1 Cross-sectional and Axisymmetric Flow --
For a cross-sectional or an axisymmetric simulation, the flow system is modeled as one aquifer unit discretized into a number of elements. (Simple rectangular plane elements or axisymetric rectangular ring elements are used in SAFTMOD.) Heterogeneity of the flow system is treated by assigning different sets of hydraulic properties to individual elements. (A detailed description of the finite element technique can be found in standard finite element textbooks, e.g., Pinder and Gray 1977; Huyakorn and Pinder 1983.) In each case, the governing equation (4-1) or (4-2) is written in a general tensorial form as follows:

$$\frac{\partial}{\partial x_i} \left(K_{ij} \frac{\partial h}{\partial x_j} \right) - S_s \frac{\partial h}{\partial t} + q = 0 \tag{4-9}$$

where x_i (i=1,2) are coordinates as defined before, and K_{ij} is component ij of the hydraulic conductivity tensor.

A trial function h_T is used to approximate h. The expression for h_T is given by

$$h_T(x,z,t) = N_J(x,z)\, h_J(t), \quad J = 1,2, \ldots,n \tag{4-10}$$

where $N_J(x,z)$ and $h_J(t)$ are interpolating basis functions and nodal values of h_T at time t, respectively, n is the number of nodes in the finite element network, and repeated indicies imply nodal summation.

An integral approximation of (4-9) may be obtained using the Galerkin weighted residual criterion, which requires that the following condition be satisfied:

$$\int_R N_I \, L(h) \, dR = 0, \quad I = 1, 2, \ldots, n \tag{4-11}$$

where L(h) corresponds to the left-hand-side of (4-9) with h replaced by equation (4-10), R is the solution domain, and $dR = dx_1 \, dx_2$ for the plane case and $dR = 2\pi x_1 dx_1 dx_2$ for the axisymmetric case.

Combining equations (4-9) - (4-11) and using Green's theorem to transform the second derivative terms, one obtains

$$\int_R \left[K_{ij} \frac{\partial N_I}{\partial x_i} \frac{\partial N_J}{\partial x_j} h_J + S_s \, N_I \, N_J \frac{dh_J}{dt} \right] dR - \int_B K_{ij} \frac{\partial h}{\partial x_j} n_i \, dB$$

$$- \int_R N_I \, q \, dR = 0, \quad I = 1, 2, .., n \tag{4-12}$$

where B is the boundary of the solution domain, and n_i is the outward unit vector normal to the boundary.

Equation (4-12) can be written more concisely as

$$A_{IJ} \, h_J + B_{IJ} \frac{dh_J}{dt} = F_I, \quad I = 1, 2, \ldots, n \tag{4-13}$$

where

$$A_{IJ} = \sum_e \int_{R^e} K_{ij} \frac{\partial N_I}{\partial x_i} \frac{\partial N_J}{\partial x_j} \, dR \tag{4-13a}$$

$$B_{IJ} = \sum_e \int_{R^e} S_s \, N_I \, N_J \, dR \tag{4-13b}$$

$$F_I = \sum_e \left(\int_{B^e} V_n \, N_I \, dB + \int_{R^e} N_I \, q \, dR \right) \tag{4-13c}$$

in which R^e is the element subdomain with boundary B^e, and V_n denotes the normal velocity at the boundary. The sign convention for V_n is the same as for q. That is, V_n is positive for inward flow and negative for outward flow.

Equation (4-13) represents a system of n linear ordinary differential equations. Time integration is performed as follows:

$$\omega\, A_{IJ}\, h_J^{k+1} + (1-\omega)\, A_{IJ}\, h_J^k + \frac{B_{IJ}}{\Delta t_k}\,(h_J^{k+1} - h_J^k) = F_I^{k+\omega} \qquad (4\text{-}14)$$

where ω is a time-weighting factor, superscripts k and k+1 are used to denote the previous and current time level, respectively, and $\Delta t_k = t_{k+1} - t_k$. The value of ω is set to 0.5 for a centered-in-time scheme. A value of 1.0 for ω results in a fully implicit (backward difference) time scheme.

Equation (4-14) is a set of linear algebraic equations that may be rearranged in the form:

$$\left(\omega\, A_{IJ} + \frac{B_{IJ}}{\Delta t_k}\right) h_J^{k+1} = F_I^{k+\omega} + (\omega-1)\, A_{IJ}\, h_J^k + \frac{B_{IJ}}{\Delta t_k}\, h_J^k) \qquad (4\text{-}15)$$

In the SAFTMOD code, the value of ω is normally set equal to 1. The resulting set of algebraic equations is solved using a direct Gaussian solver that takes advantage of the symmetric and banded feature of the global coefficient matrix.

4.3.2.2 Areal Flow --
Consider an areal flow problem involving a general situation where the system consists of two aquifers separated by an intervening aquitard. SAFTMOD represents the domain of each aquifer by a two-dimensional areal grid with rectangular elements. Both aquifers are discretized in an identical manner. Vertical one-dimensional column grids are used to represent the aquitard flow domain. Each aquitard column has the two end nodes that coincide with aquifer nodes.

For each aquifer, the governing areal flow equation is written in a tensorial form as follows:

$$\frac{\partial}{\partial x_i}\left(T_{ij}\,\frac{\partial h}{\partial x_j}\right) = \eta\,\frac{\partial h}{\partial t} - q^* - \gamma \qquad (4\text{-}16)$$

where T_{ij} is the i-j component of the transmissivity tensor defined as $T_{ij} = K_{ij}H$ with K_{ij} and H being the component of the hydraulic conductivity tensor and the saturated thickness, respectively.

Applying the Galerkin procedure to (4-16) and performing a temporal approximation using finite differences yield a set of algebraic equations that can also be represented by equation (4-15) with A_{IJ}, B_{IJ}, and F_I being defined as follows:

$$A_{IJ} = \sum_e \int_{R^e} T_{ij} \frac{\partial N_I}{\partial x_i} \frac{\partial N_J}{\partial x_j} \, dR \tag{4-17}$$

$$B_{IJ} = \sum_e \int_{R^e} \eta \, N_I \, N_J \, dR \tag{4-17a}$$

$$F_I = \sum_e \left(\int_{B^e} V_n \, H \, N_I \, dB + \int_{R^e} N_I \, q^* \, dR + \int_{R^e} N_I \, \gamma \, dR \right) \tag{4-17b}$$

Because the right-hand side of (4-17b) contains the unknown aquitard leakage flux, γ, it is necessary to consider the one-dimensional governing equation for vertical leakage in the aquitard column intersecting aquifer node I. The equation corresponds to equation (4-5). To approximate (4-5), the aquitard column is discretized into a network of n'-1 one-dimensional linear elements. Next the Galerkin procedure and the finite difference temporal approximation technique are applied. This leads to a tridiagonal set of algebraic equations for a current time level k+1. The tridiagonal system can be represented by:

$$\begin{aligned}
&\beta_1 \, h'^{k+1}_1 + \xi_1 \, h'^{k+1}_2 && = d_1 \\
&\alpha_i \, h'^{k+1}_{i-1} + \beta_i \, h'^{k+1}_i + \xi_i \, h'^{k+1}_{i+1} && = d_i, \; i = 2, 3, \ldots, n'-1 \\
&\alpha_{n'} h'^{k+1}_{n'-1} + \beta_{n'} h'^{k+1}_{n'} && = d_{n'} - \gamma^{k+1}
\end{aligned} \tag{4-18}$$

where α_i, β_i, and ξ_i are tridiagonal matrix elements, and $d_i (i = 1, 2, \ldots, n')$ are elements of the right-hand-side vector.

For the general case of areal flow in a two-aquifer system, the solution scheme implemented in the SAFTMOD code is a sequential solution scheme that consists of three stages performed for each aquifer. Stage 1 involves using the Thomas algorithm to perform a forward elimination of the tridiagonal matrix equation (4-18), thereby allowing the vertical leakage flux γ^{k+1} to be expressed in terms of head value at node I of the aquifer domain. Stage 2 involves the direct solution of the aquifer matrix equation (with the incorporation of the aquitard leakage flux) to determine the head values in the aquifer. At this stage, Picard iterations are performed if the aquifer concerned is an unconfined aquifer. Stage 3 of the overall scheme involves performing back-substitution in the Thomas algorithm to determine nodal values of head in each aquitard column.

4.4 DESCRIPTION OF THE TRANSPORT MODULE

4.4.1 Transport Equation

The form of the advective-dispersive transport equation used in SAFTMOD also depends on the type of analysis. In a vertical cross-sectional analysis, the following equation is used:

$$\frac{\partial}{\partial x}\left[D_{xx}\frac{\partial c}{\partial x}\right] + \frac{\partial}{\partial z}\left[D_{zz}\frac{\partial c}{\partial z}\right] + \frac{\partial}{\partial x}\left[D_{xz}\frac{\partial c}{\partial z}\right] + \frac{\partial}{\partial z}\left[D_{zx}\frac{\partial c}{\partial x}\right]$$

$$- V_x\frac{\partial c}{\partial x} - V_z\frac{\partial c}{\partial z} = \phi R\left[\frac{\partial c}{\partial t} + \lambda c\right] - q(c^* - c) \qquad (4\text{-}19)$$

where c is the solute concentration (ML^{-3}), D_{xx}, D_{zz}, D_{xz}, and D_{zx} are components of the hydrodynamic dispersion tensor (L^2T^{-1}), V_x and V_y are components of the Darcy velocity vector (LT^{-1}), ϕ is effective porosity, R and λ are retardation and decay (T^{-1}) coefficients, respectively, q is the volumetric rate of fluid flow per unit volume of the porous medium (L^3T^{-1} L^{-3}), and c^* is the solute concentration in the inflowing fluid (ML^{-3}).

In an axisymmetric analysis, the following equation is used:

$$\frac{1}{r}\left[\frac{\partial}{\partial r}\left[rD_{rr}\frac{\partial c}{\partial r}\right] + \frac{\partial}{\partial r}\left[rD_{rz}\frac{\partial c}{\partial z}\right] + \frac{\partial}{\partial z}\left[rD_{zr}\frac{\partial c}{\partial r}\right]\right]$$

$$+ \frac{\partial}{\partial z}\left[D_{zz}\frac{\partial c}{\partial z}\right] - V_r\frac{\partial c}{\partial r} - V_z\frac{\partial c}{\partial z} = \phi R\left[\frac{\partial c}{\partial t} + \lambda c\right] - q(c^* - c) \qquad (4\text{-}20)$$

where subscripts r and z are used to denote the r and z components of a vectorial or tensorial quantity.

In an areal analysis, transport in a horizontal plane of each aquifer is described by the following equation:

$$\frac{\partial}{\partial x}\left[HD_{xx}\frac{\partial c}{\partial x}\right] + \frac{\partial}{\partial y}\left[HD_{yy}\frac{\partial c}{\partial y}\right] + \frac{\partial}{\partial x}\left[HD_{xy}\frac{\partial c}{\partial y}\right] + \frac{\partial}{\partial y}\left[HD_{yx}\frac{\partial c}{\partial x}\right]$$

$$- V_xH\frac{\partial c}{\partial x} - V_yH\frac{\partial c}{\partial y} = \phi RH\left[\frac{\partial c}{\partial t} + \lambda c\right] - q^*(c^* - c) - \Gamma \qquad (4\text{-}21)$$

Where Γ is the rate of solute mass transfer from aquitard to aquifer (ML^2 T^{-1}), and the remaining symbols have the same meaning as defined previously.

For areal transport in a system with aquitards, transport in each aquitard is described approximately by the following one-dimensional diffusion equation:

$$\frac{\partial}{\partial z}\left[D' \frac{\partial c'}{\partial z}\right] = \phi' R'\left[\frac{\partial c'}{\partial t} + \lambda c'\right] \tag{4-22}$$

where c' is the solute concentration in the aquitard (ML^{-3}), D', ϕ', and R' are the vertical diffusion coefficient (L^2T^{-1}), effective porosity, and the retardation coefficient for the aquitard, respectively.

For the sake of completeness, components of the hydrodynamic dispersion tensor also need to be defined. For the aquifer, the components of D_{ij}, where i and j denote coordinate subscripts, are defined as

$$D_{11} = \alpha_L V_1^2/|V| + \alpha_T V_2^2/|V| + D_o \tag{4-23}$$

$$D_{12} = D_{21} = (\alpha_L - \alpha_T) V_1 V_2/|V| \tag{4-23a}$$

where α_L and α_T are the longitudinal and transverse dispersivities, respectively, and D_o is the effective molecular diffusion coefficient.

The initial and boundary conditions of the transport problem are as follows:

$$c(x_i,0) = c_o \tag{4-24}$$

$$c(x_i,t) = \bar{c} \text{ on } B_1' \tag{4-24a}$$

$$D_{ij} \frac{\partial c}{\partial x_j} n_i = q_c^D \text{ on } B_2' \tag{4-24b}$$

$$\left(D_{ij} \frac{\partial c}{\partial x_j} - V_i\right) n_i = q_c^T \text{ on } B_3' \tag{4-24c}$$

where B_1' is the portion of the boundary where concentration is prescribed as $\bar{c}$, B_2' is the portion of the boundary where dispersive mass flux of solute is prescribed as q_c^D, and B_3' is the portion of the boundary where the total solute mass flux is prescribed as q_c^T. Note that the sign convention for q_c^D and q_c^T are positive for inward mass flux and negative for outward mass flux. x_i (i=1,2) and x_j (j=1,2) are coordinates defined earlier.

4.4.2 Numerical Solution of the Transport Problems

Numerical approximations of the solute transport equations are performed in a similar manner to that of the groundwater flow equations. For a cross-sectional or an axisymmetric flow simulation, the following set of linear algebraic equations is derived:

$$\left(\omega A_{IJ} + \frac{B_{IJ}}{\Delta t_k} + \omega\lambda B_{IJ}\right) c_J^{k+1} + \omega \bar{B}_{IJ} c_J^{k+1} = F_I^*, \quad I = 1, 2, .., n \tag{4-25}$$

where ω is the time weighting factor (set equal to ½ if the Crank-Nicholson time stepping scheme is required, and set equal to 1 if a fully-implicit scheme is desired), and

$$A_{IJ} = \sum_e \int_{R^e} \left(D_{ij} \frac{\partial N_I}{\partial x_i} \frac{\partial N_J}{\partial x_j} + V_i N_I \frac{\partial N_J}{\partial x_i} \right) dR \tag{4-26}$$

$$B_{IJ} = \sum_e \int_{R^e} \phi R N_I N_J dR \tag{4-26a}$$

$$\bar{B}_{IJ} = \sum_e \left(\int_{B^e} V_n N_I N_J dB + \int_{R^e} q N_I N_J dR \right) \tag{4-26b}$$

$$F_I^* = (\omega-1)(A_{IJ} + \lambda B_{IJ})c_J^k + \frac{B_{IJ}}{\Delta t_k} c_J^k + (\omega-1)\bar{B}_{IJ} c_J^k + \bar{B}_{IJ} c_J^{*k+1} \tag{4-26c}$$

For an areal flow simulation, the set of algebraic equations derived by the code can also be represented by equation (4-25) with the following definitions of the matrix elements:

$$A_{IJ} = \sum_e \int_{R^e} H \left(D_{ij} \frac{\partial N_I}{\partial x_i} \frac{\partial N_J}{\partial x_j} + V_i N_I \frac{\partial N_J}{\partial x_i} \right) dR \tag{4-27}$$

$$B_{IJ} = \sum_e \int_{R^e} \phi R H N_I N_J dR \tag{4-27a}$$

$$\bar{B}_{IJ} = \sum_e \left(\int_{B^e} H V_n N_I N_J dB + \int_{R^e} q^* N_I N_J dR \right) \tag{4-27b}$$

$$F_I^* = (\omega-1)(A_{IJ} + \lambda B_{IJ})c_J^k + \frac{B_{IJ}}{\Delta t_k} c_J^k + (\omega-1)\bar{B}_{IJ} c_J^k + \bar{B}_{IJ} c_J^{*k+1} + \sum_e \int_{R^e} N_I \Gamma dR \tag{4-27c}$$

Discretization of aquitard columns and numerical approximation of the one-dimensional transport equation in the aquitard are performed in the same manner as described previously for the areal flow problem. The overall sequential solution scheme for the areal transport problem is also performed in the same manner as described previously.

4.4.3 Treatment of a Decay Chain

Transport of a daughter species in a decay chain can also be handled by the SAFTMOD code. The governing equations used by the code to perform cross-sectional, axisymmetric and areal aquifer analyses correspond to equations (4-19), (4-20), and (4-21) with an additional source term on its right-hand side. This source term accounts for the rate of mass of the daughter species

that is generated by transformation of parent species. The source term required is given by

$$\dot{m} = -\sum_{\ell=1}^{n_p} \phi \, \xi_\ell \, R_\ell \, \lambda_\ell \, c_\ell \tag{4-28}$$

where subscript ℓ is used to identify the parent species, n_p is the number of parent species, and ξ_ℓ is the mass fraction of parent component ℓ that transforms into the daughter species under consideration.

The numerical solution of the transport equation for a daughter species of a decay chain can be performed in the same manner as that described previously for a single species. The source term from equation (4-28) is incorporated into the finite element matrix equation by modification of its right-hand side. The modified right-hand term of the finite element equation is given by

$$F_I^* = F_I + \sum_e \left(\int_{R^e} N_I \, \dot{m} \, dR \right) \tag{4-29}$$

where F_I and F_I^* are the original and modified right-hand terms, and $\dot{m}$ is given by equation (4-28).

For areal transport in a system with aquitards, it is also necessary to treat the aquitard diffusion equation (4-22) by adding the following source term to the right-hand side:

$$\dot{m}' = -\sum_{\ell=1}^{n_p} \phi' \xi_\ell \, R'_\ell \, \lambda'_\ell \, c'_\ell \tag{4-30}$$

In the finite element solution, $\dot{m}'$ is treated in a similar manner to $\dot{m}$.

4.4.4 Spatial and Temporal Discretizations

Spatial discretization of the solution region is performed automatically in the SAFTMOD code. A rectangular grid (Figure 4.2) is used to represent the modeled two-dimensional region. In a cross-sectional or an axisymmetric analysis, the modeled region corresponds to the entire system, which is considered as one unit where different materials are accommodated by assigning different sets of material properties for different elements. In an areal analysis, a distinction is made between aquifer and aquitard regions. Each aquifer region is discretized using a network of rectangular elements. The same nodal arrangement and element configuration are used for different aquifers. Nodes and elements are numbered sequentially as shown in

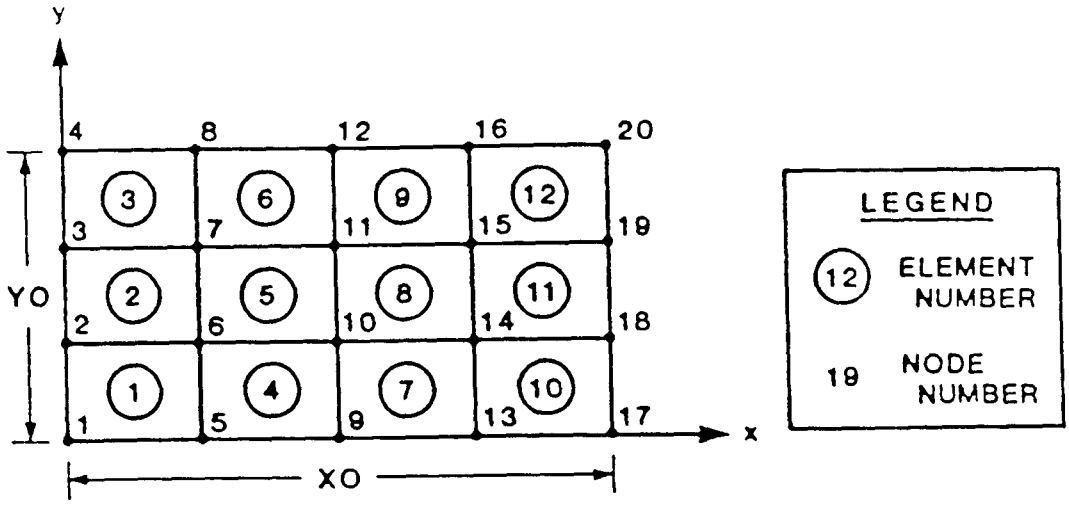

(a)

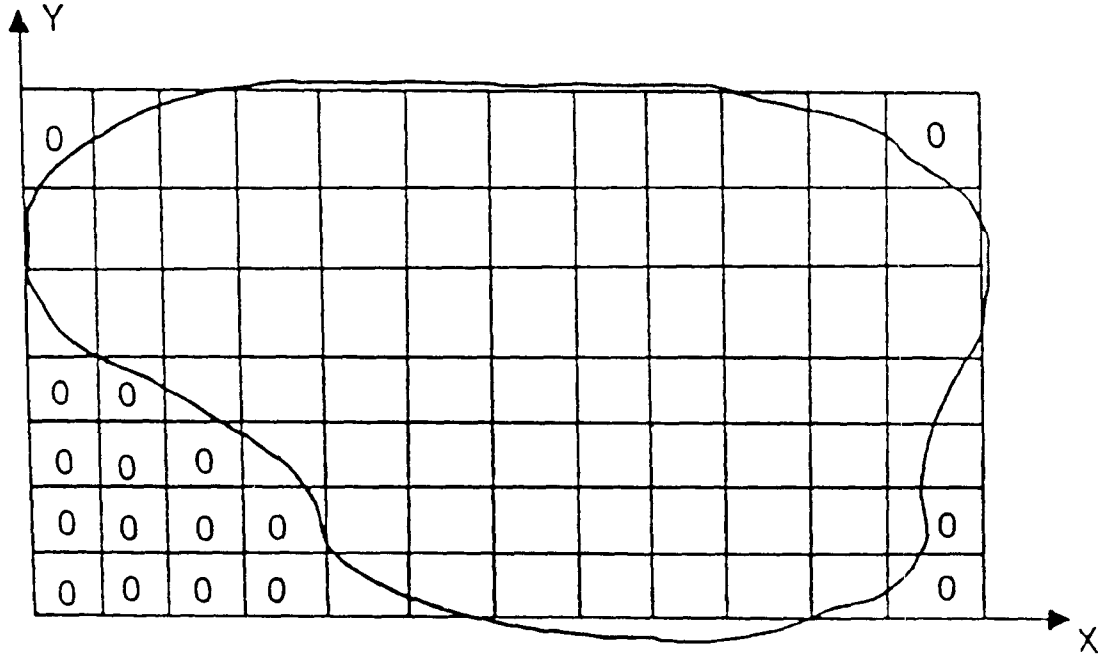

(b)

Figure 4.2. Discretization of aquifer regions: (a) regular region, and (b) irregular region.

Figure 4.2a. Irregular boundaries are accommodated by assigning zero material number to elements outside the region of interest (Figure 4.2b). In the areal simulation of a system comprising two aquifers separated by an aquitard, numbering of nodes and elements is performed aquifer by aquifer starting from the bottom aquifer. The confining aquitard region is treated as a series of vertical columns each of which is bounded at both ends by two opposite aquifer nodes. Each aquitard column is represented by a one-dimensional linear finite element grid. The one-dimensional grid is generated automatically using a local dimensionless vertical coordinate, ξ, defined as $\xi=z'/b'$, where z' is the height measured from the bottom of the aquitard, and b' is the thickness of the aquitard column. Aquitard nodes in the column are numbered sequentially from the bottom to top of the column.

In SAFTMOD, temporal discretization can also be performed automatically if required. Time steps and time values at the end of the time steps are generated using a simple algorithm: $\Delta t_k = f\Delta t_{k-1} \leq \Delta t_{max}$, and $t_{k+1} = t_k + \Delta t_k$, where f is the time multiplier and Δt_{max} is the maximum value of time step allowed. As an alternative to automatic time step generation, the time discretization data required for transient analysis can be supplied to the code by the user.

4.5 RESULTS OF SAFTMOD TESTING SIMULATIONS

Three sets of benchmark problems were used to test the SAFTMOD code. The first set consists of three steady and transient problems designed to test the flow component of the code. The second set consists of four transient two-dimensional transport problems. The third set consists of a coupled flow-transport problem designed to illustrate a field application of SAFTMOD. Numerical results obtained from SAFTMOD are compared with analytical solutions and results obtained using another finite element code, VAM3D (Huyakorn et al., 1986b). The SAFTMOD testing simulations were conducted before being linked to the other RUSTIC modules.

4.5.1 Flow Module

Three flow problems are presented which test various formulations of the flow module. The first problem is a well flow problem designed to check the areal and axisymmetric analyses as applied to two-aquifer systems. The second problem is a drain flow problem used to compare the areal and cross-sectional analyses of steady and transient flow in unconfined aquifers. The third problem is a confined flow problem used to test the incorporation of flux and head boundary conditions in the flow module.

1) Well Flow in a Two-Aquifer System with a Confining Aquitard

This problem concerns transient flow to a pumping well fully penetrating a system consisting of two aquifers separated by a confining aquitard (Figure 4.3). For such a system, the analytical solution of the problem can be found in Neuman and Witherspoon (1969). The case used to test SAFTMOD had been solved numerically by Huyakorn et al. (1986). Two alternative simulations were performed using the SAFTMOD code. In the first simulation, the axisymmetric grid shown in Figure 4.4a was used. This grid consists of 120 elements and 143 nodes. The elements that lie in the two identical aquifers

are assigned material number 1, and the elements that lie in the aquitard are assigned material number 2. In the second simulation, the areal grid shown in Figure 4.4b was used to represent the first (bottom) aquifer, and a second areal grid with identical nodal spacings to the first one was used to represent the second (top) aquifer. Node numbers of this second grid start from 170 and finish at 338, and element numbers start from 145 and finish at 288. Both the areal and the axisymmetric simulations were performed for 40 time steps using an identical set of time step values. The time step values were generated as follows: $\Delta t_1 = 36$ s, $\Delta t_k = 1.414 \Delta t_{k-1} \leq \Delta t_{max} = 3.6*10^6$ s. Numerical results obtained from SAFTMOD are compared with the analytical solution. Figure 4.5 shows the plot of time versus drawdown in the pumped aquifer. Agreement between the numerical and the analytical solutions is fairly good despite the fact that the numerical results were obtained using a rather coarse grid and large time steps. Note that the same degree of accuracy was obtained with the axisymmetric and areal numerical simulations.

2) Flow to Parallel Drains in an Unconfined Aquifer

This problem concerns flow to parallel drains in an unconfined aquifer receiving vertical recharge due to precipitation (Figure 4.6). A steady-state analytical solution can be found in Bear (1979). Both areal and cross-sectional simulations were performed using SAFTMOD. The simulations were transient and based on the areal and cross-sectional grids shown in Figure 4.7. The initial hydraulic head in the aquifer was assumed to be 50 ft. The hydraulic conductivity and effective porosity of the aquifer were assumed as 1 ft/day and 0.2, respectively. The aquifer was subjected to vertical

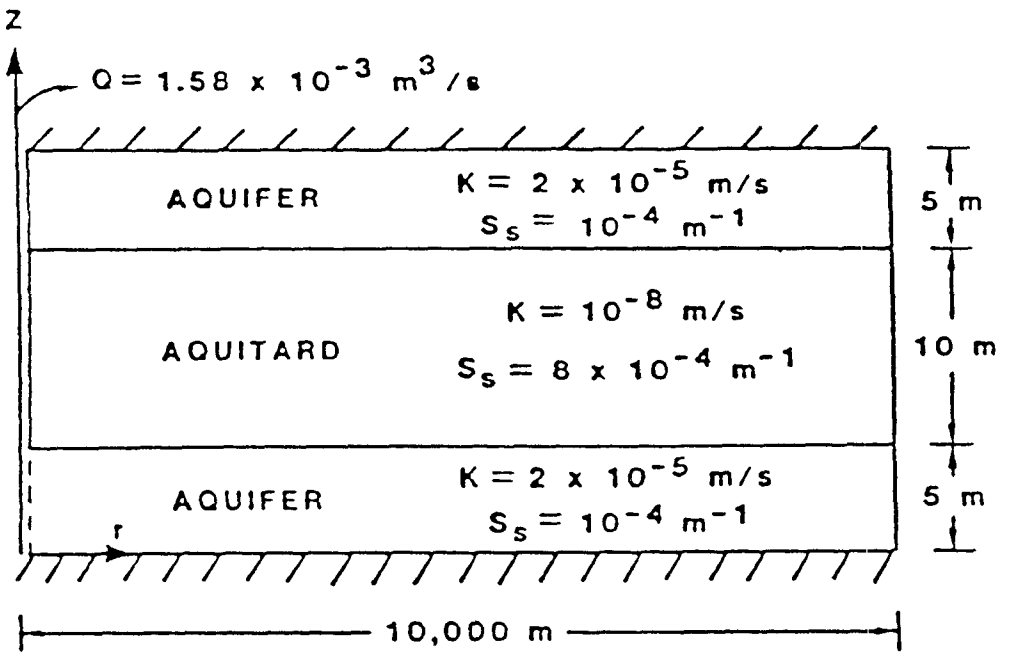

Figure 4.3. Problem description of flow to a well in a two-aquifer system with a confining aquitard.

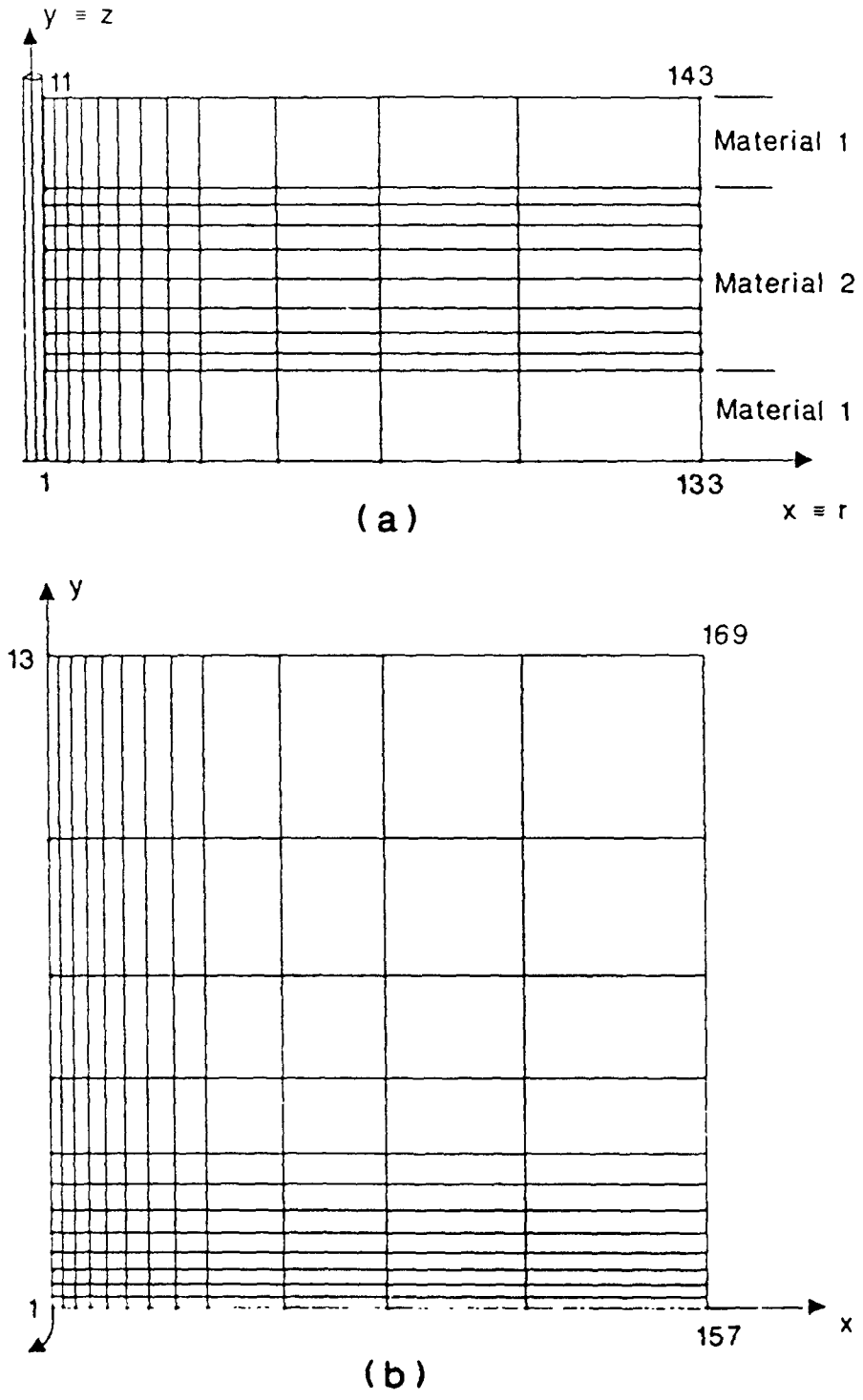

Figure 4.4. Finite element grids used in simulating well flow in two aquifer system: (a) axisymmetric grid, and (b) areal grid.

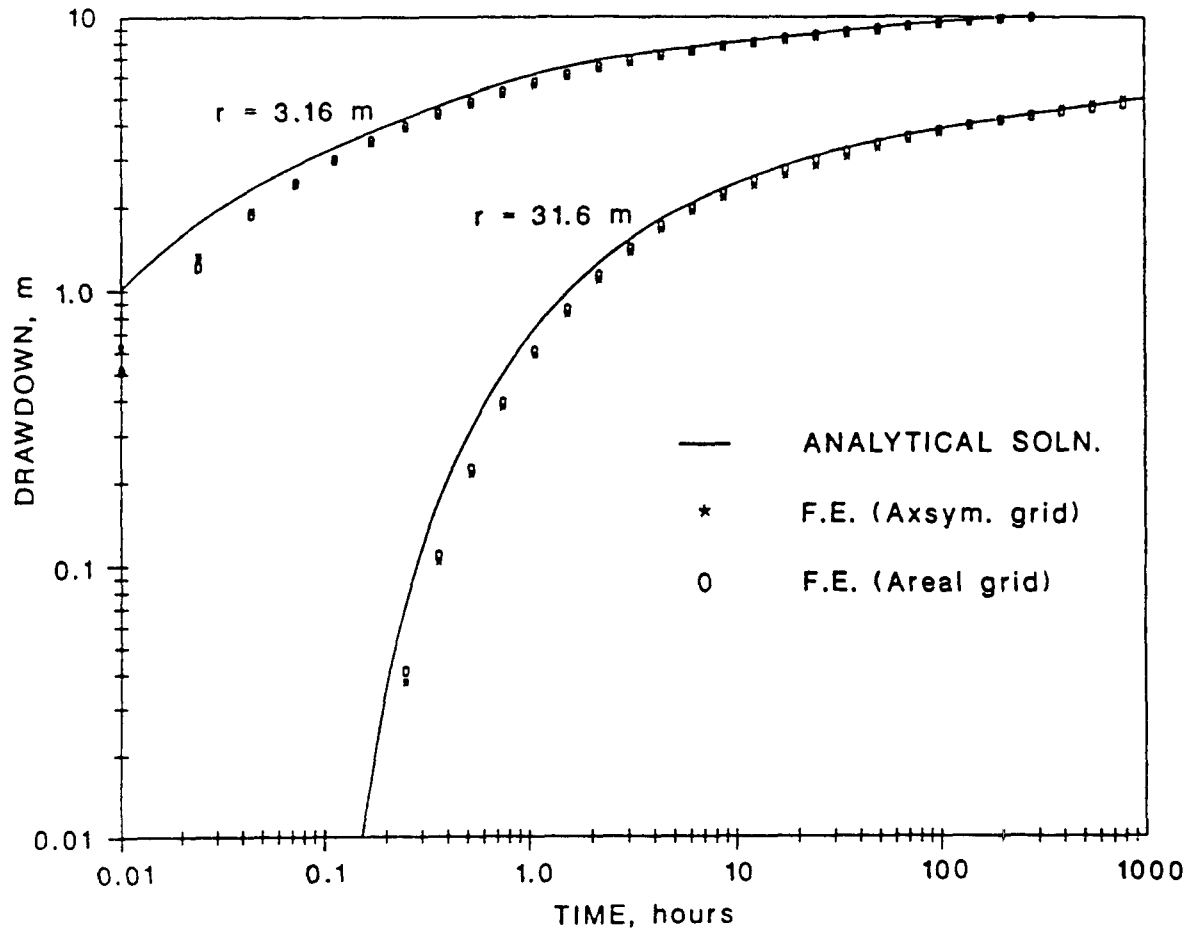

Figure 4.5. Simulated drawdown-time relationships for the pumped aquifer.

recharge at a rate of 0.01 ft/day. Note that it was sufficient to consider only half of the saturated flow region because of symmetry about the vertical axes midway between the drains. A constant head of 50 ft was prescribed at the drain where x = 0. Zero normal velocity was specified on the aquifer base and at x = 500 ft (midway between the two drains). Both simulations were performed for 35 time steps using the following time step values: Δt_1 = 1 day, $\Delta t_k = 1.4\Delta t_{k-1} \leq 100$ days, for k = 2, ..., 35. Results obtained from the simulation are plotted in Figure 4.8 for five typical time values. As expected, the plot shows a continuous water table mounding, and a steady-state condition at t ≥ 2000 days. There is excellent agreement between the steady-state analytical and numerical solutions.

3) Flow to a Gallery

This problem concerns flow to a gallery (horizontal well) penetrating a shallow confined aquifer system with two partially penetrating parallel drains (Figure 4.9). The aquifer is anisotropic with a 10 to 1 contrast in the horizontal versus vertical hydraulic conductivity. The gallery is

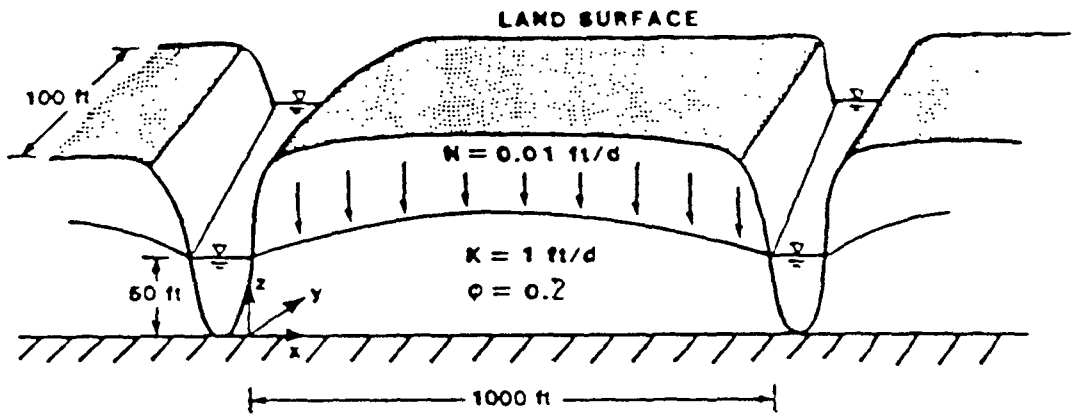

Figure 4.6. Problem description for flow to parallel drains in an unconfined aquifer.

pumping at a constant rate of 0.5 m^2/hr. The water levels in both drains are assumed to remain constant with time. No general analytical solution is available for the case considered. For this reason, numerical results from SAFTMOD were checked against corresponding results from another published numerical code, SATURN (Huyakorn et al., 1984). The transient flow problem was simulated with both codes using the cross-sectional grid shown in Figure 4.10. The simulations were performed for 20 time steps. Time step values were computed using the following algorithm: $\Delta t_1 = 0.1$ hr, $\Delta t_k = 1.414\Delta t_{k-1} \leq 10$ hr, $k = 2, \ldots, 20$. Numerical results obtained from both codes are compared in Figure 4.11, where hydraulic head profiles along the horizontal line passing through the gallery are plotted. As can be seen, the two numerical solutions are in excellent agreement.

4.5.2 Transport Module

Four transient solute transport problems were selected. The first problem is a one-dimensional problem used to check the cross-sectional formulation of the Galerkin finite element technique. The second and third problems are two-dimensional dispersion problems used to check the areal formulation and to assess the accuracy of the numerical approximations for cases involving conservative and nonconservative contaminants and source boundary conditions of continuous and instantaneous releases. The fourth problem is an injection well transport problem used to test the axisymmetric formulation applied to a situation involving aquifer-aquitard systems.

1) One-Dimensional Dispersion in Uniform Flow

This problem involves one-dimensional advection-dispersion of a conservative solute species through a semi-infinite porous medium (Figure 4.12a). As illustrated, the contaminant is released from a channel fully penetrating a shallow confined aquifer. The analytical solution of the problem was developed by Ogata and Banks (1961). This solution can also be found in Bear (1979). For the case simulated by SAFTMOD, the source concentration at the inlet was prescribed as 1 mg/m^3. The values of Darcy velocity, effective

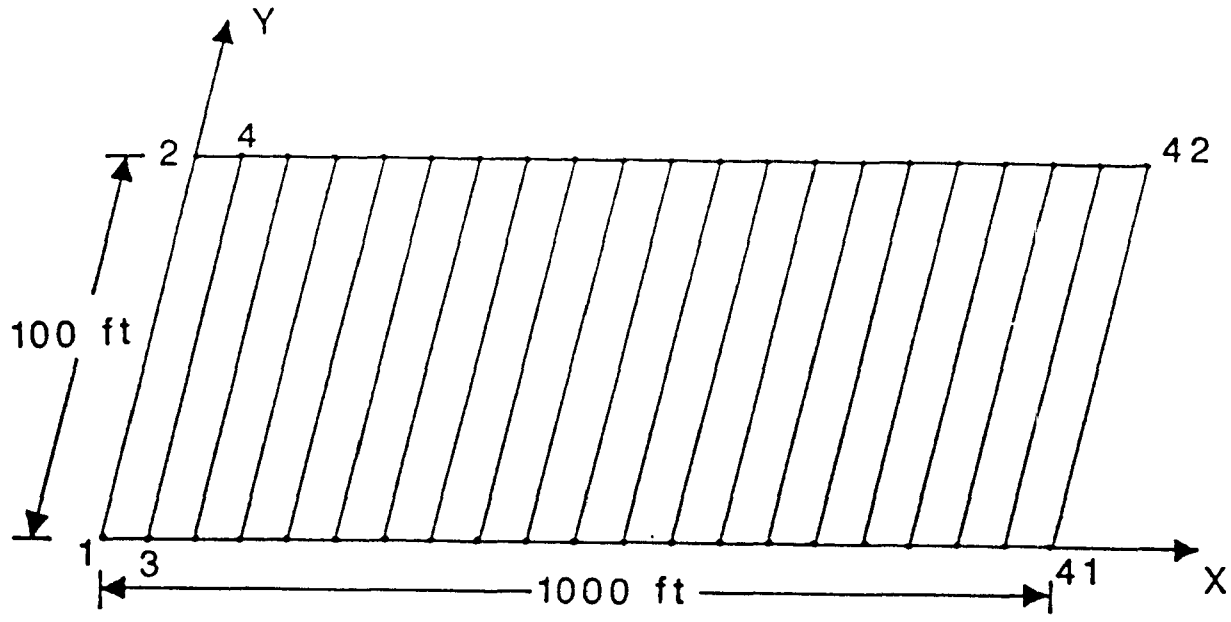

(a)

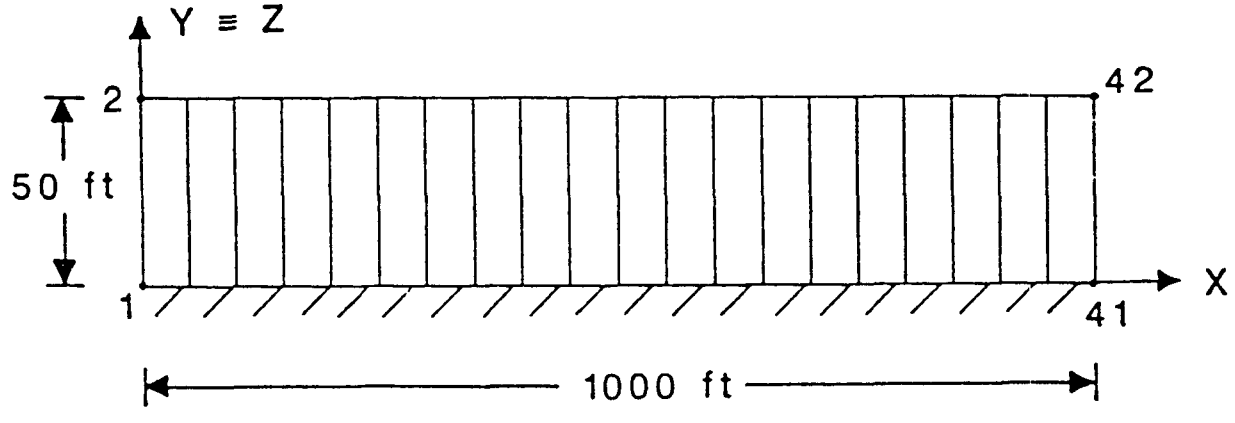

(b)

Figure 4.7. Finite element grids used in the simulation of flow through parallel drains: (a) areal grid, and (b) cross-sectional grid.

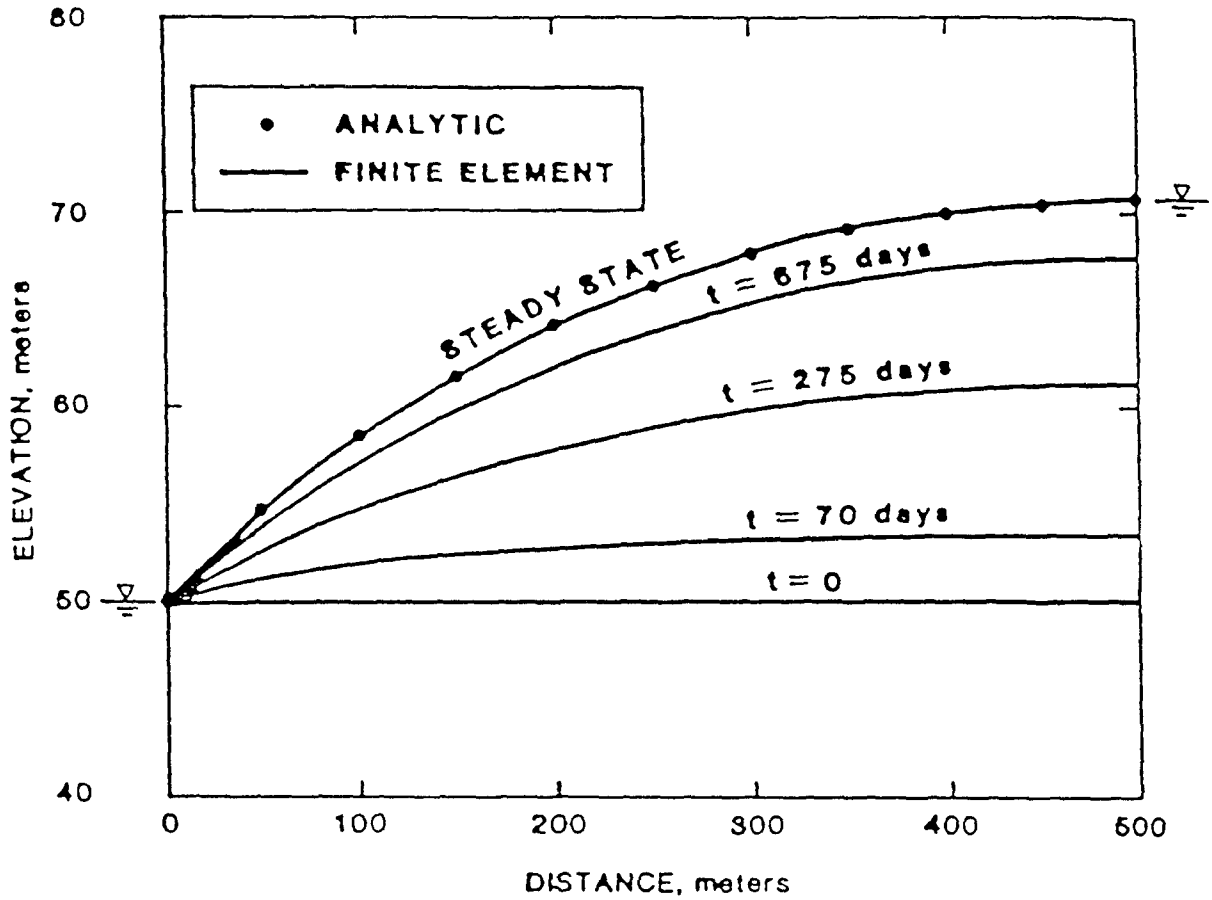

Figure 4.8. Simulated steady-state and transient water table profiles. (Adapted from Battelle and GeoTrans, 1988).

porosity, and longitudinal dispersivity were specified as 1 m/d, 0.25, and 5m, respectively. The modeled length of the aquifer domain was specified as 400 m. A uniform rectangular grid consisting of 82 nodes and 40 elements, each with Δx = 10 m, was used. The simulation was performed for 25 time steps with Δt kept constant and equal to 2.5 d. Simulated concentration distributions are plotted in Figure 4.12b for two typical timevalues. As can be seen, the numerical and analytical solutions are in excellent agreement.

2) Areal Dispersion in Uniform Flow

This problem concerns two-dimensional dispersion of solute in a uniform and steady groundwater flow field. In practice, the situation may correspond to that involving the areal migration of contaminants continually released into an extensive aquifer from an injection well treated as a point source in the areal plane (Figure 4.13a). Assuming that the injection rate is small so that the natural groundwater flow is undisturbed, the analytical solution of the problem can be found in Wilson and Miller (1978). Two cases involving conservative and non-conservative solute species were simulated using the SAFTMOD code with the parameter values shown in Table 4-1. The selected parameter values for Case 1 were based on data on the field study of the hexavalent chromium contamination problem reported by Perlmutter and Lieber

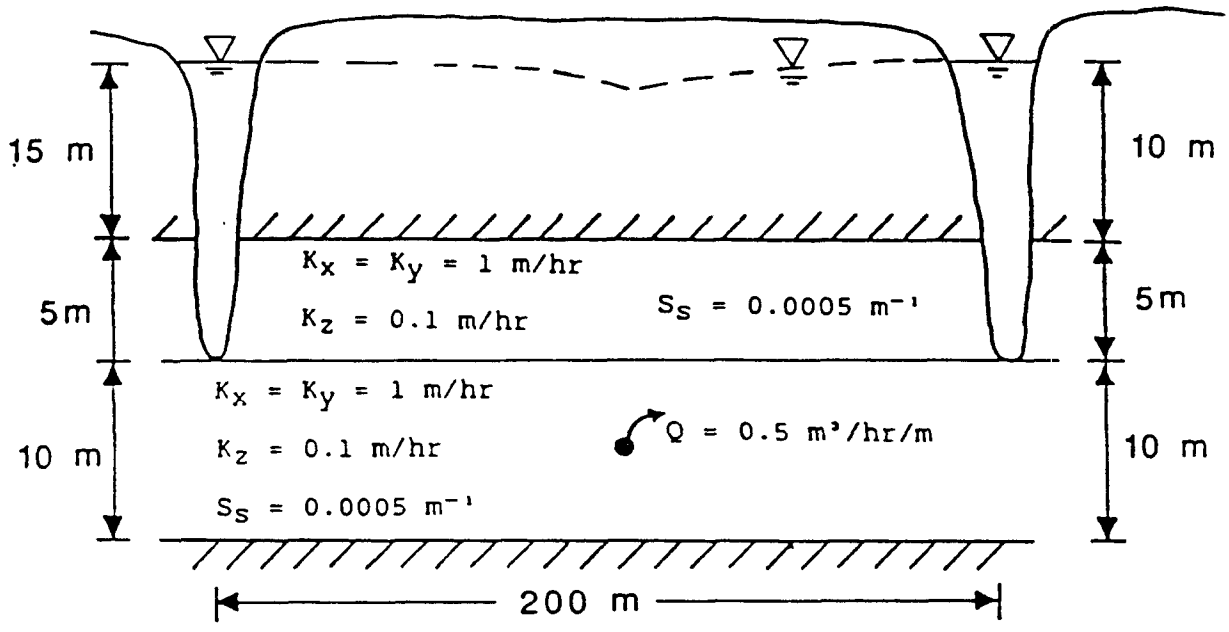

Figure 4.9. Problem description of flow to a gallery.

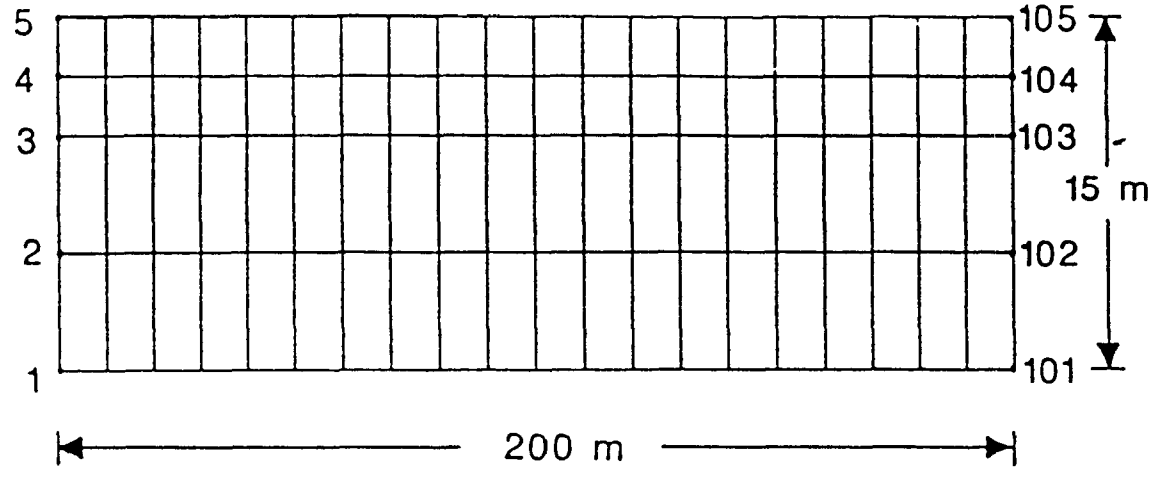

Figure 4.10. Finite element grid used in simulation of flow to a gallery.

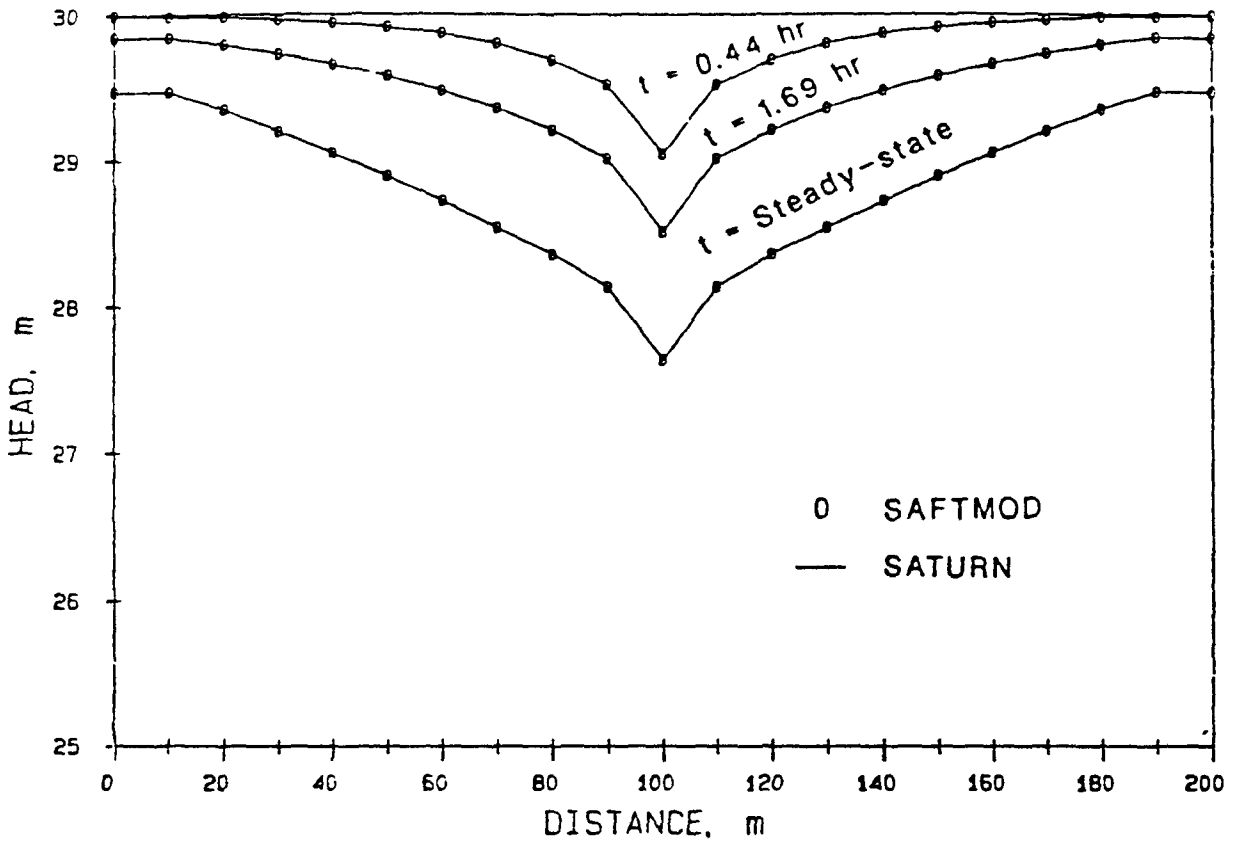

Figure 4.11. Simulated head profiles along the horizontal line passing through the gallery.

(1970), and Wilson and Miller (1978). For Case 2, the values of the retardation and decay constant were chosen arbitrarily to test the performance of SAFTMOD for a nonconservative species. Numerical simulations of both cases were performed using a rectangular grid that represents the domain shown in Figure 4.13b. Note that advantage was taken of the symmetry about the x-axis. The medium-mesh grid consisted of 440 nodes and 390 rectangular elements, each having $\Delta x = 60$ m, and $\Delta y = 30$ m. For both cases, the simulations were performed for 28 time steps with Δt kept constant and equal to 100 d. Concentration profiles along the x-axis are plotted in Figures 4.14 and 4.15 for Cases 1 and 2, respectively. The numerical results from SAFTMOD are in good agreement with the analytical solution.

3) Areal Dispersion of a Solute Slug in Uniform Groundwater Flow

This problem is similar to the preceding problem except for the boundary condition at the source. In the present case, an instantaneous injection of solute mass slug is considered (Figure 4.16a). The analytical solution of the problem was presented by Sauty (1980).

As in the preceding problem, simulation of only the upper half of the domain was necessary due to symmetry about the x-axis. The rectangular finite

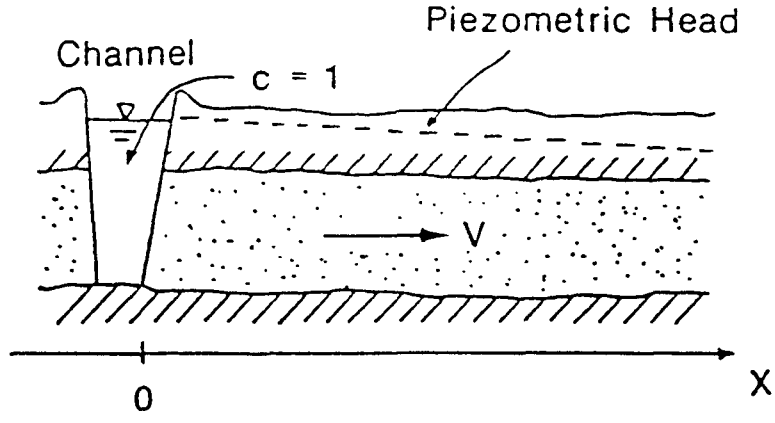

(a)

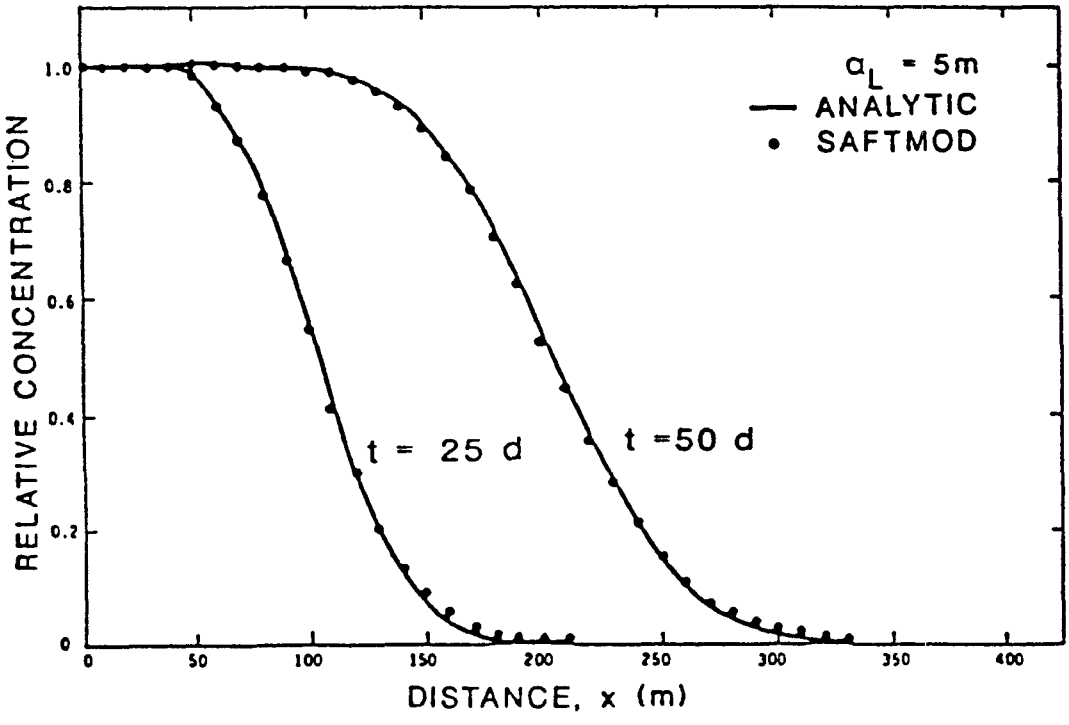

(b)

Figure 4.12. One dimensional dispersion in uniform flow: (a) problem description, and (b) simulated concentration profiles. (Adapted from Huyakorn et al., 1984b).

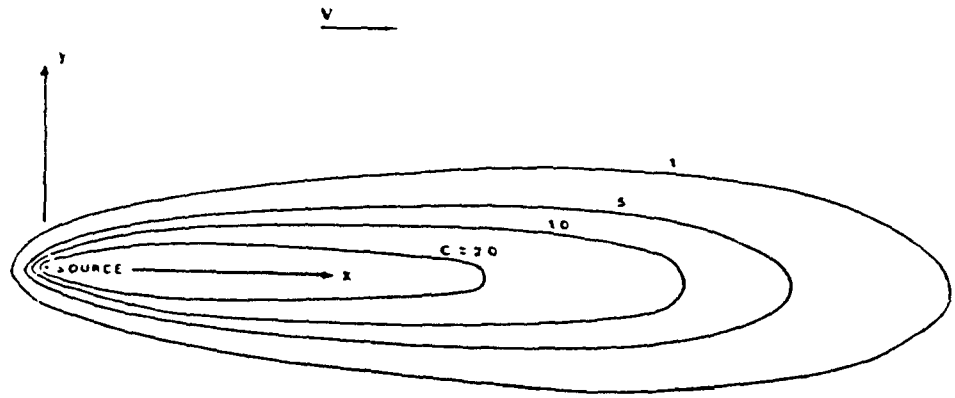

(a)

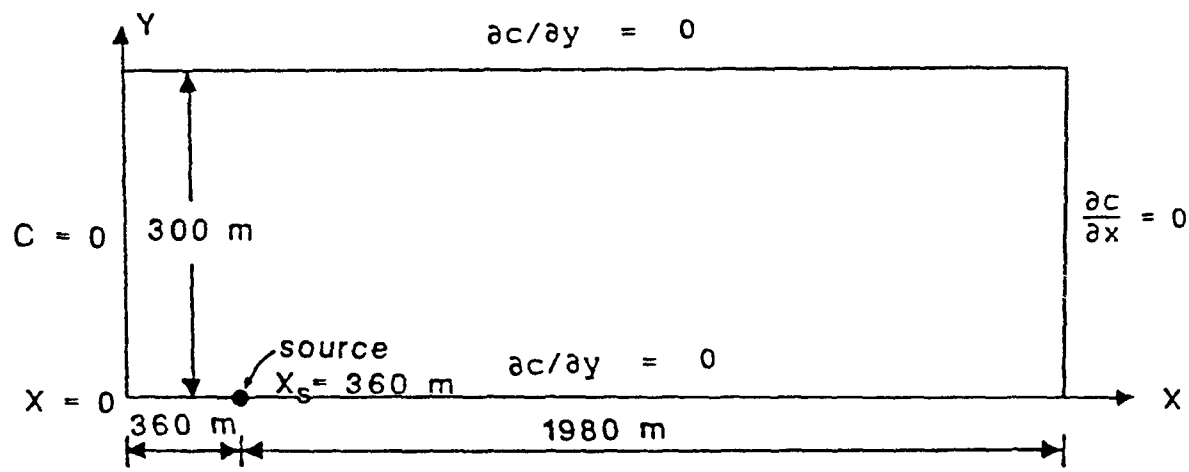

(b)

Figure 4.13. Areal dispersion in uniform flow: (a) problem description, and (b) modeled region and boundary conditions. (Figure 4.13(b) is a half-system representation and is not drawn to scale.)

TABLE 4-1. VALUES OF PHYSICAL PARAMETERS FOR PROBLEM 2

Parameter	Value
Darcy velocity, V	0.161 m d^{-1}
Porosity, ϕ	0.35
Longitudinal dispersivity, α_L	21.30 m
Transverse dispersivity, α_T	4.30 m
Aquifer saturated thickness, b	33.50 m
Contaminant mass flux, Qc_o (per unit thickness of aquifer)	704.0 g m^{-1} d^{-1}
Case 1:	
Retardation coefficient, R	1.0
Decay constant, λ	0.0 d^{-1}
Case 2:	
Retardation coefficient, R	2.0
Decay constant, λ	0.00019 d^{-1}
Selected grid	
Fine: Δx = 60 m, Δy = 15 m	
Medium: Δx = 60 m, Δy = 30 m	
Time steps	
Δt = 100 d (Use 28 time steps)	

element grid has 49 rows of nodes having variable spacing, and 11 columns of nodes having constant spacing of Δy = 5 m. The grid consisted of a total of 539 nodes and 480 elements. Values of the physical parameters used for the simulation and coordinates of the grid lines are provided in Table 4-2. One node located at x = y = 0 was used to represent the contaminant source.

Initially the concentration was specified as 400 mg/m^3 at this node and zero elsewhere. Considering that the total nodal area of the source node (counting the upper and the lower halves of the xy plane) is equal to 25 m^2 and the porosity is 0.35, this represents placing a finite contaminant slug at x = y = 0. The mass of this slug per unit aquifer thickness is equal to 3500 mg/m.

In order to accurately simulate movement of the dispersing slug, temporal discretization was performed using an automatic scheme (also presented in Table 4-2). The initial time step value was assigned as 1 day. Values of the remaining 29 time steps were generated using a multiplier of 1.2 and a maximum allowable time step value of 2 days. The problem was solved for 30 time steps and was subject to zero normal concentration gradient boundary conditions.

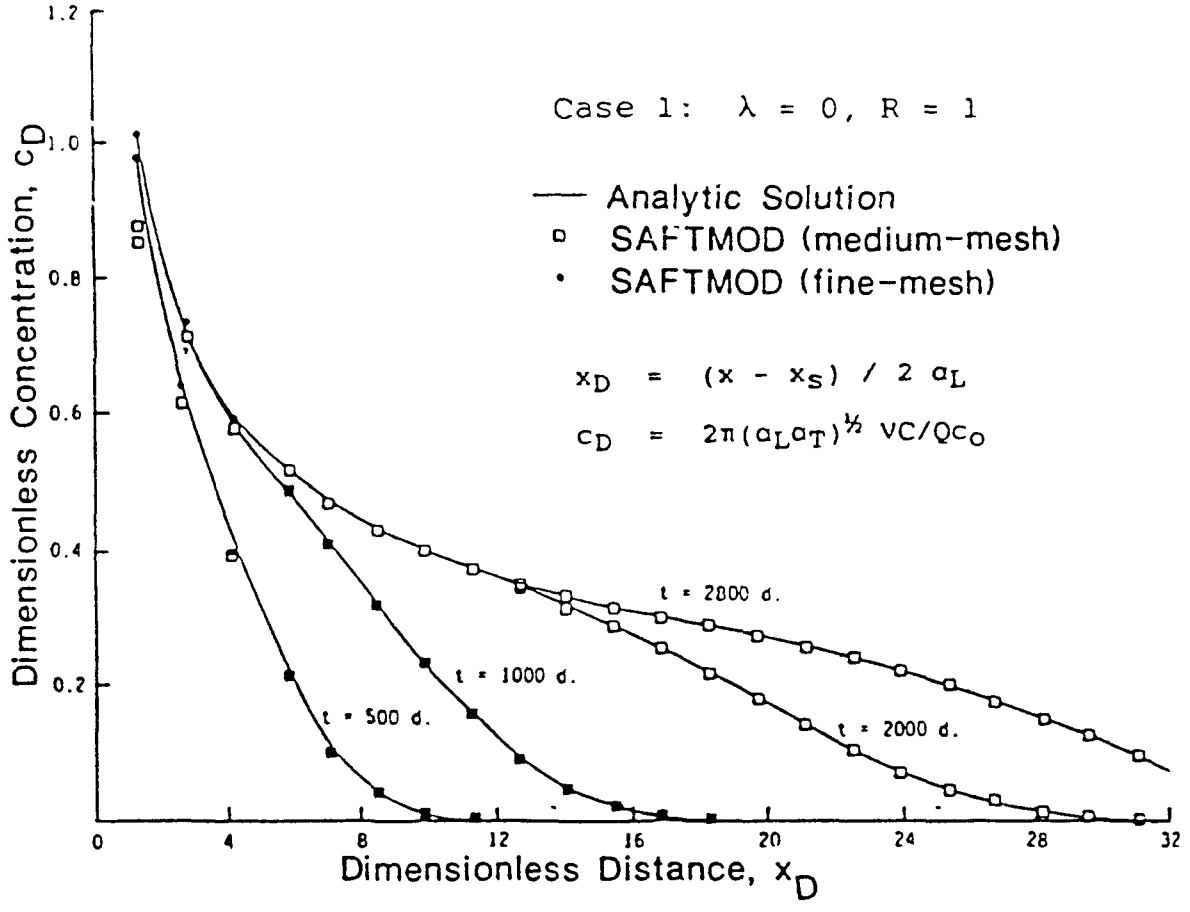

Figure 4.14. Simulated concentration profiles along the x-axis for case 1. (Adapted from Huyakorn et al., 1984b).

The numerical solution is compared in Figure 4.16b with the analytical solution computed by using equations (4.13) and (4.14). It can be seen that good predictions of the concentration distributions were achieved. At the early time value of 3.96 days, the numerical result deviates slightly from the analytical solution, particularly near the peak of the concentration curve.

4) Transport from an Injection Well in an Aquifer Confined by Aquitards

This problem concerns contaminant transport from a well in an aquifer confined by two very low permeability aquitards (Figure 4.17). The well injects a fluid containing dissolved contaminant of prescribed concentration, c_o. To make the problem amenable to analytical solution, it is assumed that the dispersion coefficient of the aquifer is constant and advection in the aquitard is insignificant. Based on these assumptions, the analytical solution for the case of infinite radial extent and infinite aquitard thickness can be obtained by converting the solution derived by Avdonin (1964) for the equivalent heat transport problem.

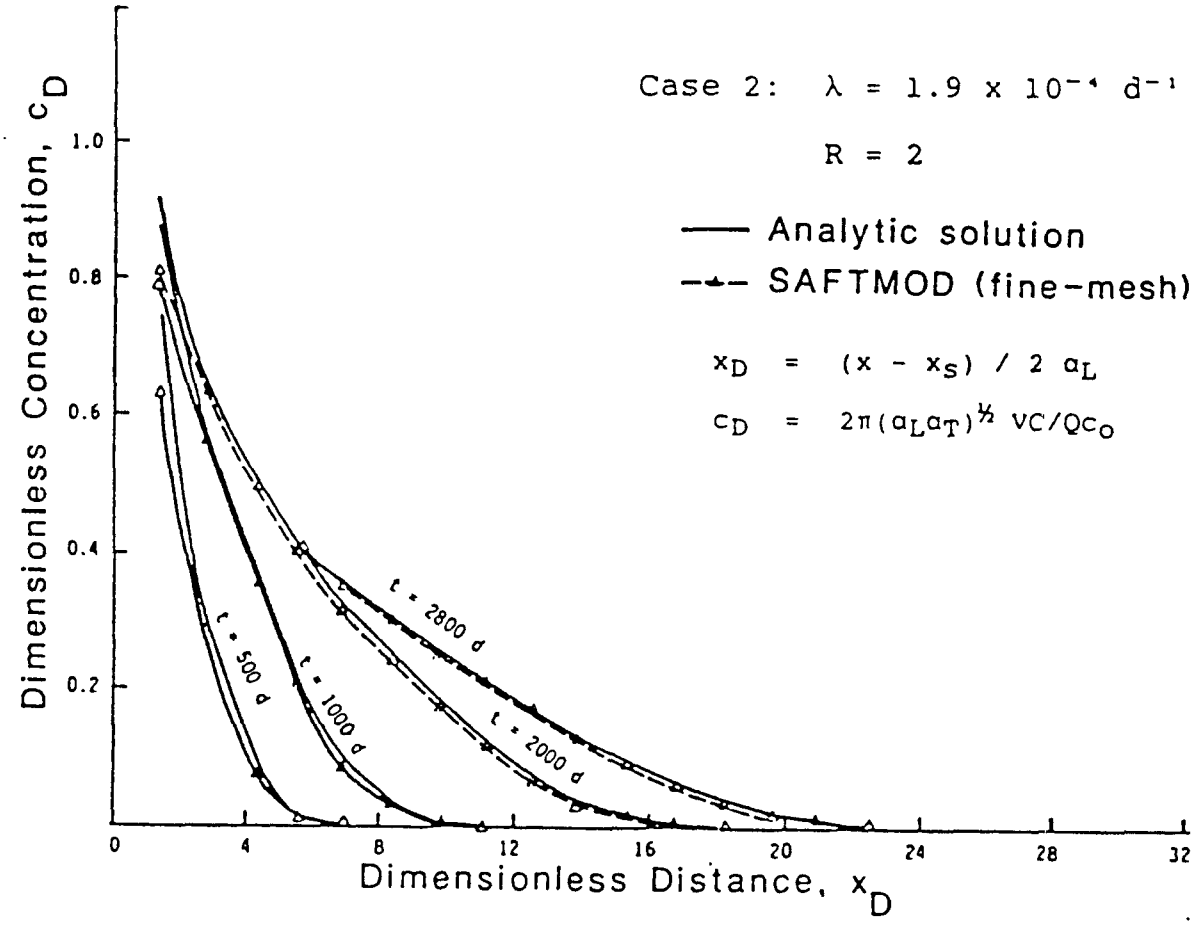

Figure 4.15. Simulated concentration profiles along the x-axis for case 2. (Adapted from Huyakorn et al., 1984b).

Two cases were simulated: (1) in which the aquitard is leaky, and (2) in a perfectly confined system. Values of the physical parameters used for both these cases are presented in Table 4-3. Both simulations were conducted in axisymmetric mode using a vertically-oriented, rectangular, finite element grid. Except for the first node, the other 40 nodal spacings in the radial direction were kept constant with $\Delta r = 0.5$ m. The 15 nodal grid lines in the vertical (z) direction were variable and equal to 0.0, 1.0, 2.0, 2.1, 2.25, 2.75, 3.0, 3.5, 4.0, 6.0, 10.0, 12.0, 20.0, 30.0, and 52.0 m, respectively. The grid thus consisted of 615 nodes and 560 elements. The simulations were run for 50 time steps using a constant Δt of 0.5 d.

The concentration breakthrough curves for case 1 (leaky system) and for case 2 (nonleaky system) are compared for t = 10 d and t = 25 d in Figure 4.18. In both cases there is excellent agreement between the numerical and analytical solutions.

The breakthrough curves for case 1 are steeper and more retarded than these for case 2 due to the influence of dispersion into the aquitard.

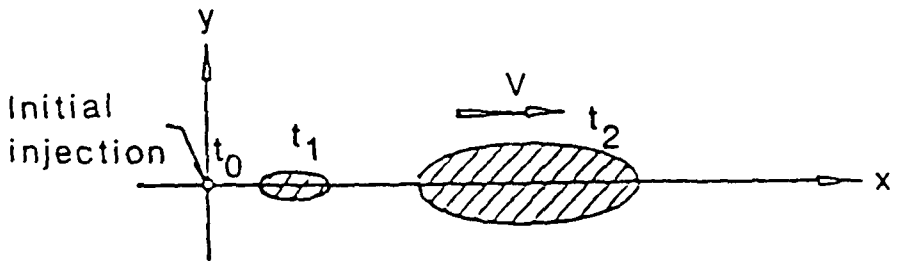

(a)

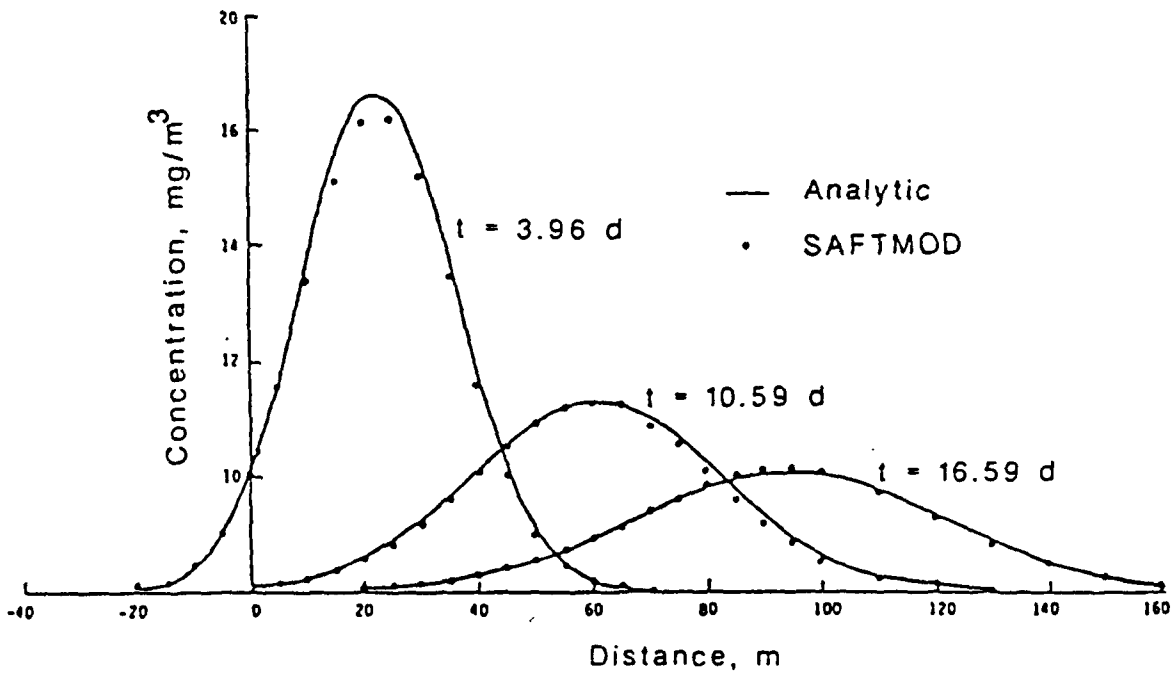

(b)

Figure 4.16. Areal dispersion of a solute slug in uniform groundwater flow: (a) problem description, and (b) simulated concentration profiles. (Adapted from Huyakorn et al., 1984b).

TABLE 4-2. VALUES OF PHYSICAL PARAMETERS AND DISCRETIZATION DATA FOR THE PROBLEM OF AREAL DISPERSION OF A SOLUTE SLUG IN UNIFORM GROUNDWATER FLOW

Parameter	Value
Darcy velocity, V	2 m d^{-1}
Porosity, ϕ	0.35
Longitudinal dispersivity, α_L	4 m
Transverse dispersivity, α_T	1 m
Retardation coefficient, R	1
Decay constant, λ	0.0 d^{-1}
Solute mass per unit aquifer thickness, m	3500 mg m^{-1}
x_i(m), i=1,...,49	-50., -40., -30., -25., -20., -15., -10., -5., 0., 5., 10., 15., 20., 25., 30., 35., 40., 45., 50., 55., 60., 65., 70., 75., 80., 85., 90., 95., 100., 110., 120., 130., 140., 150., 160., 170., 180., 190., 200., 210., 220., 230., 240., 250., 260., 270., 280., 290., 300.
y_j(m), j=1,...,11	0., 5., 10., 15., 20., 25., 30., 35., 40., 45., 50.
Δt_1 = 0.1 d	
$\Delta t_k = 1.2\ \Delta t_{k-1} \leq 2$ d, k = 2,...,30	

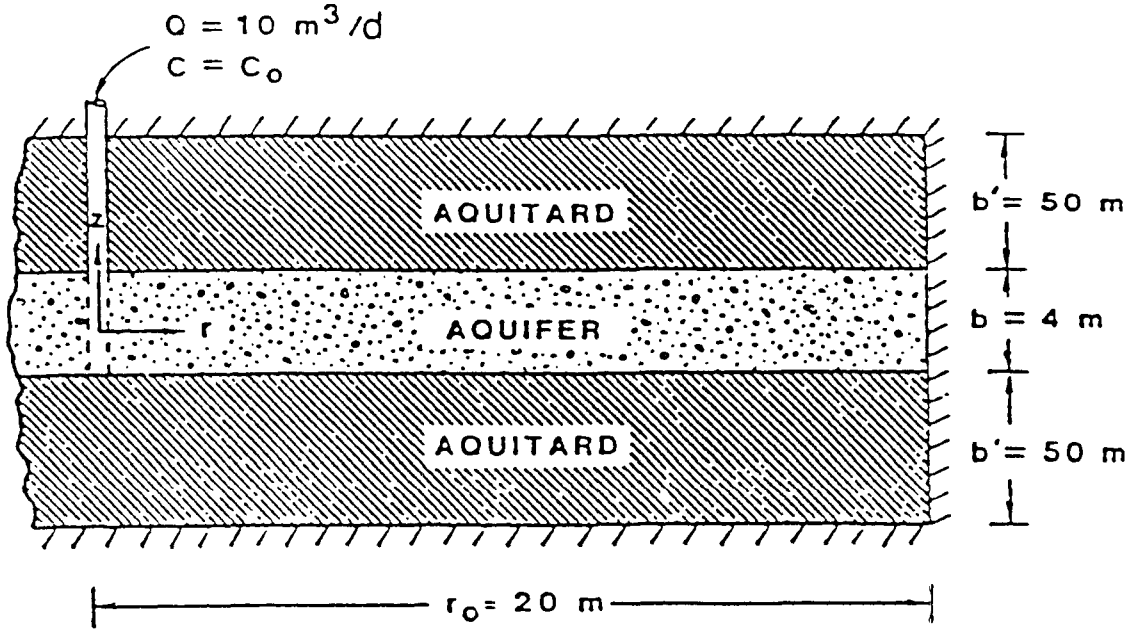

Figure 4.17. Solute transport from an injection well fully penetrating an aquifer overlain and underlain by aquitards.

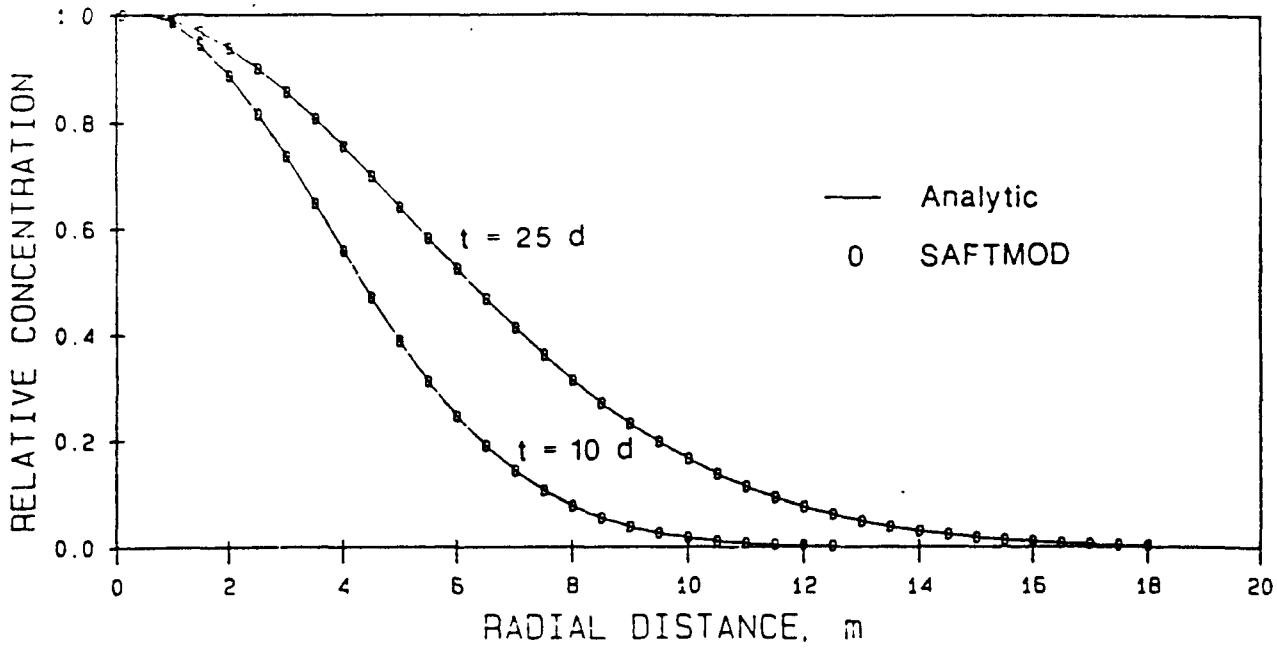

(a)

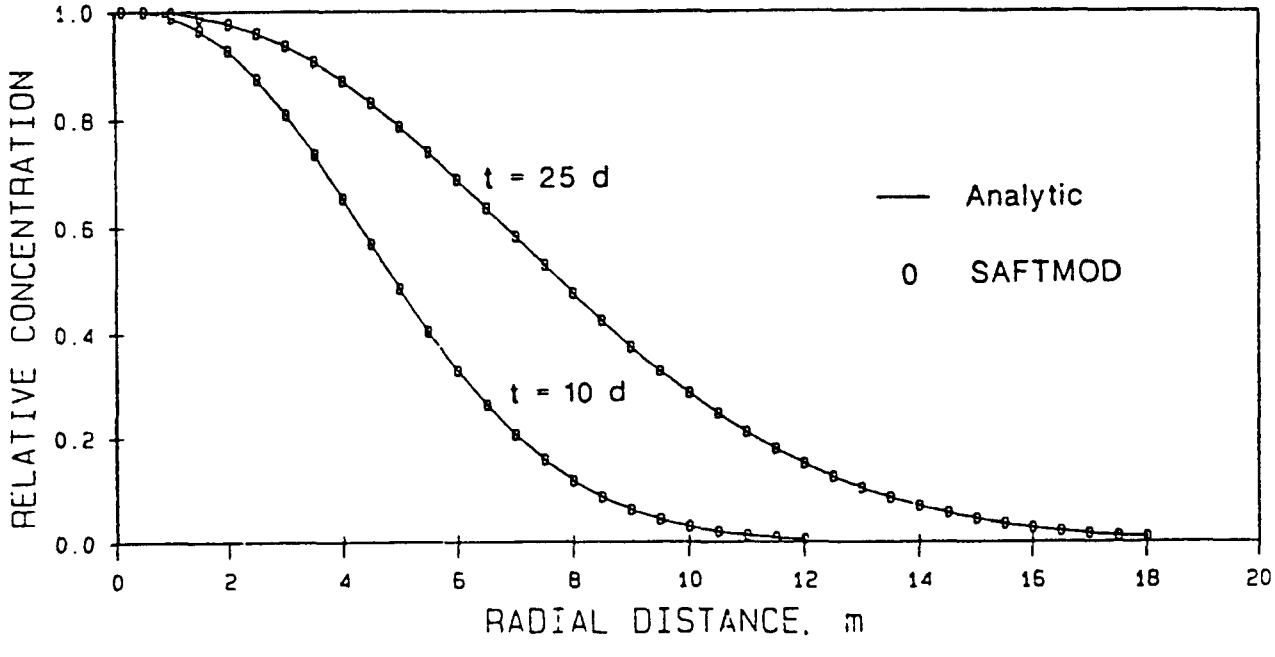

(b)

Figure 4.18. Simulated concentration profiles in the aquifer: (a) case 1, and (b) case 2.

TABLE 4-3. VALUES OF PHYSICAL PARAMETERS FOR THE PROBLEM OF SOLUTE TRANSPORT FROM AN INJECTION WELL

Parameter	Assigned Value	Unit
Fluid injection rate, Q	10.0	$m^3\ d^{-1}$
Solute concentration at the well, c_o	1.0	ppm
Well radius, r_w	0.1	m
External radius, r_o	20.0	m
Porosity of aquifer, ϕ	0.25	--
Radial dispersion coefficient for aquifer, D_o	0.152	$m^2\ d^{-1}$
Aquifer thickness, b	4.0	m
Case 1: Leaky System		
Vertical dispersion coefficient of aquitard, D'_o	0.152	$m^2\ d^{-1}$
Aquitard porosity, ϕ'	0.025	
Case 2: Nonleaky System		
No aquitard		

SECTION 5

LINKAGE OF VADOSE AND SATURATED ZONE MODELS

As stated earlier in this volume, the objective of RUSTIC is to simulate the fate and transport of chemicals applied in agricultural settings, from the source area, through the crop root zone, the vadose and saturated zones, and into drinking water wells. Instead of writing an entirely new computer code to meet this objective, it was decided early on in the development effort that existing software would be used where it was available and met, or could be modified to meet, the Agency's standards for computer codes. PRZM was selected to provide the simulation of the crop root zone, due to its degree of recognition and acceptability both to the Agency and the agricultural chemical industry.

Several options were studied for linkage of models to PRZM to provide the balance of the required simulation capabilities. The first involved use of PRZM and a saturated zone model only. In this configuration, PRZM would be used to represent both the root zone and the vadose zone. This option was eliminated because the assumptions of the elementary soil hydraulics in PRZM (i.e., drainage of the entire soil column to field capacity in one day) were not considered to be adequate for representing a thick vadose zone. The second involved the use of PRZM and a 2-D or 3-D variably saturated flow model. In this configuration, the latter model would represent both the vadose and saturated zones. Although the interface between the unsaturated and saturated zones would be more rigorously simulated, it was felt that the resulting code would be too computationally intensive for the intended application scenarios, especially when Monte Carlo simulation was involved. Therefore, this option was also dropped.

The combination of models finally selected is depicted in Figure 5.1. In this configuration, PRZM is linked to a two-dimensional (single or two-layer) saturated zone model through a one-dimensional vadose zone model. Both the vadose and saturated zone models simulate water flow and solute transport. Two new codes were written to provide the simulation of the vadose zone (VADOFT) and the two-dimensional X-Y, X-Z or axisymmetric simulation of the saturated zone (SAFTMOD). A significant problem associated with this type of linkage is difference between time domains of the individual models. While the vadose zone models are required to operate on a daily or less-than-daily time step, the time step of the saturated zone model could be from days to months. Another significant problem is the interfacing of the vadose and saturated zone models, where a fluctuating water table may require special handling of model spatial domains.

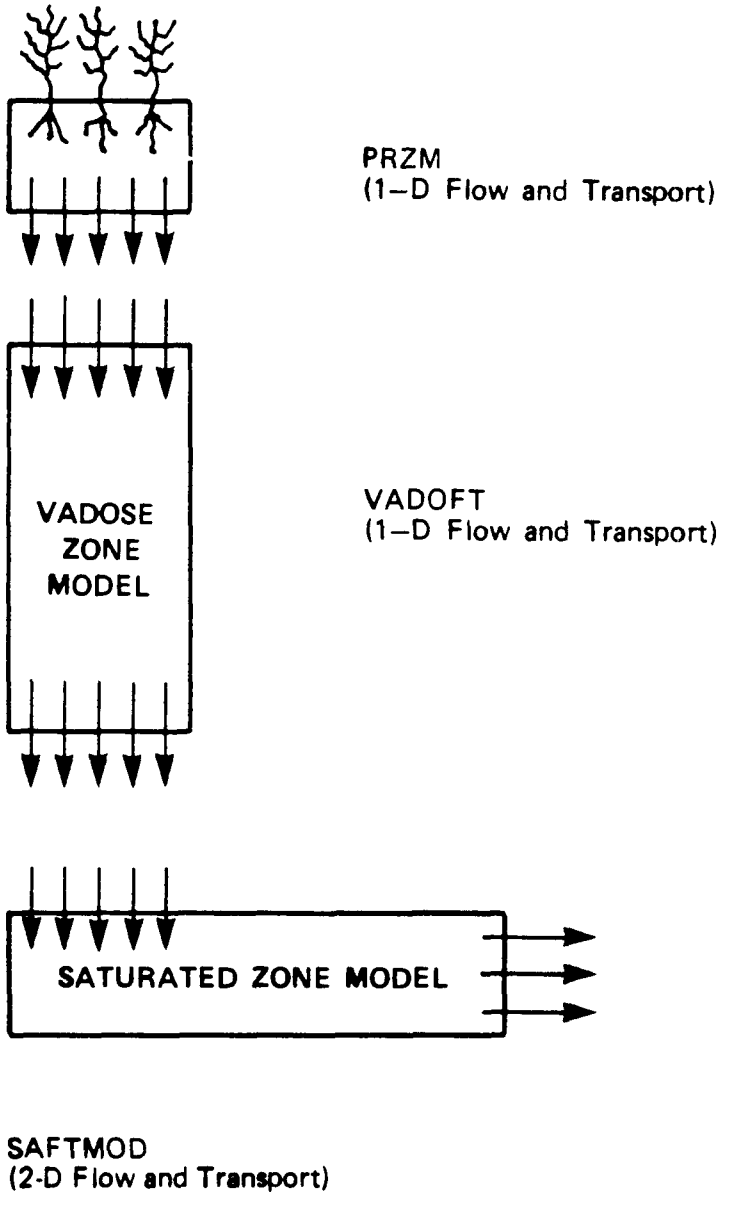

Figure 5.1. Linked modeling system configuration.

5.1 TEMPORAL MODEL LINKAGE

The resolution of the temporal aspects of the three models was straightforward. PRZM runs on a daily time step. The time stepping in VADOFT is dependent upon the properties of soils and the magnitude of the water flux introduced at the top of the column. In order for the non-linear Richard's equation to converge, VADOFT may sometimes require time steps on the order of minutes. The SAFTMOD time step, on the other hand, would normally be much longer than one day.

For simplicity, it was decided that the time step of SAFTMOD would always be an integer multiple of PRZM's daily time step. This makes the direct linkage of PRZM to SAFTMOD in a temporal sense very straightforward. PRZM is simply run for the number of days of the SAFTMOD time step, SAFTMOD is then run, and so forth. The water and pesticide fluxes from PRZM are summed and averaged over the length of the SAFTMOD time step. SAFTMOD receives the time-averaged fluxes as input.

For the linkage of PRZM, through VADOFT, to SAFTMOD, the resolution is not much more complicated. VADOFT is prescribed to simulate to a "marker" time value, specifically to the end of a day. The last computational time step taken by VADOFT is adjusted so that it coincides with the end of the day. This is depicted in Figure 5.2. PRZM's daily water fluxes are used as input to VADOFT. VADOFT utilizes this flux as a constant over the day and adjusts its internal computational time step in order to converge. PRZM and VADOFT execute for the number of days of the SAFTMOD time step. The output from VADOFT is then time averaged and used as input to SAFTMOD.

5.2 SPATIAL LINKAGES

The spatial linkages utilized for the models are more complex. The principal problem is that of the presence of a rising and falling water table, which complicates the interfacing of the vadose (or root zone) and saturated zone codes. A second problem is that of the incompatibility between the hydraulics in PRZM and VADOFT. Of course, any linking scheme utilized must provide a realistic simulation of the flow of water and transport of solutes at the interfaces and must provide for continuity (mass balance).

5.2.1 PRZM and VADOFT

The major problem with the interfacing of these two models is that while VADOFT solves the Richard's equation for water flow in a variably saturated medium, PRZM uses simple "drainage rules" to move water through the soil profile. Because of this incompatibility, there may be times when PRZM produces too much water for VADOFT to accommodate within one day. This is very likely to happen in agricultural soils, where subsoils are typically of lower permeability than those of the root zone, which have been tilled and perforated by plant roots and soil biota. The result of this would be water ponded at the interface which would belong neither to PRZM nor VADOFT. Several solutions were proposed to handle this situation, including:

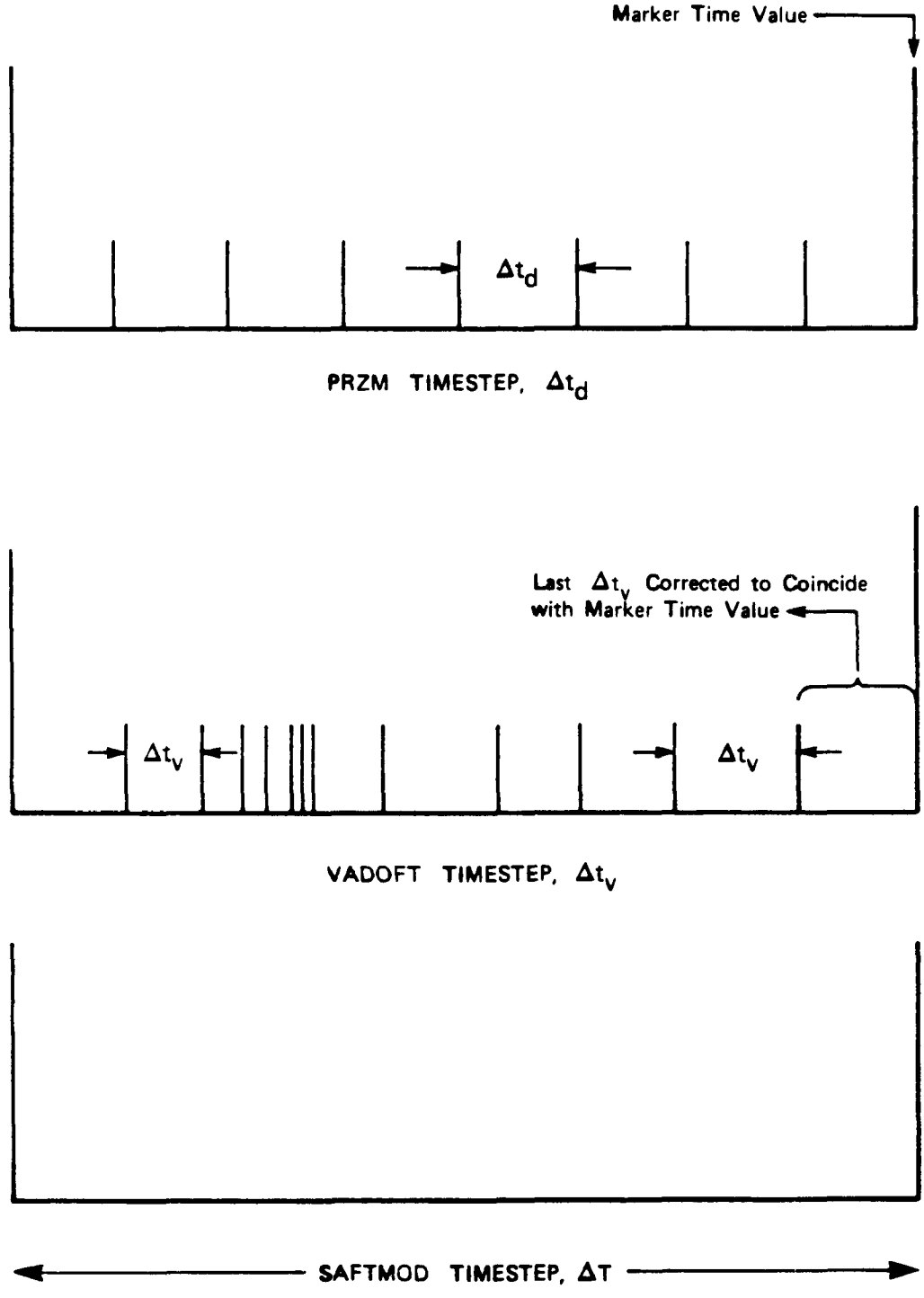

Figure 5.2. Resolution of component model timesteps.

- Automatically switching from a flux (unponded) condition to a head (ponded) condition in VADOFT at the top node if this latter condition occurs

- Changing PRZM hydraulics to a Green-Ampt formulation, which has a parameter for the saturated hydraulic-conductivity

- Applying the VADOFT flow and transport solutions to the root zone as well

- Checking the velocities coming out of PRZM to make sure that they are within an acceptable range and if not, using PRZM's restricted drainage option to correct them

For a variety of reasons, all of these proposals proved to be unattractive. In the end it was decided that the solution was to prescribe the flux from PRZM into VADOFT so that VADOFT accommodates all the water output by PRZM each day. This eliminates the problem of ponding at the interface. However, it does force more water into the vadose zone than might actually occur in a real system, given the same set of soil properties and meteorological conditions. The consequence is that water and solute are forced to move at higher velocities in the upper portions of the vadose zone. If the vadose zone is deep, then this condition probably has little impact on the solution. If it is shallow, however, it could overestimate loadings to groundwater, especially if chemical degradation rates are lower in the vadose zone than in the root zone.

5.2.2 VADOFT and SAFTMOD

The principal problem here is that of the presence of a dynamic boundary (rising and falling water table) between these models. There are two approaches available to handle the problem. The first is to expand or contract the spatial domains of the models to accommodate the moving boundary. This is not a particularly insurmountable problem for the vadose zone model; however, for the saturated zone model it would require the addition of nodes at the upper boundary. This would require a constant evaluation and switching of the set of nodes receiving fluxes from the vadose zone. This appeared undesirable.

The second option is to overlap the spatial domains of the models and interpolate values for fluxes based upon the position of the water table. This latter approach was ultimately utilized. It has the additional feature of eliminating the effects of the bottom boundary conditions prescribed for the vadose zone model on the simulation of solute transport just above the water table.

5.2.2.1 VADOFT/SAFTMOD (2-D, X-Y) Linkage

The following paragraphs describe the interface of VADOFT and SAFTMOD where a 2-D (X-Y) configuration is used for SAFTMOD. The linkage is depicted in Figure 5.3. The sequence in which the models are run is VADOFT flow, then SAFTMOD flow, VADOFT transport, then SAFTMOD transport.

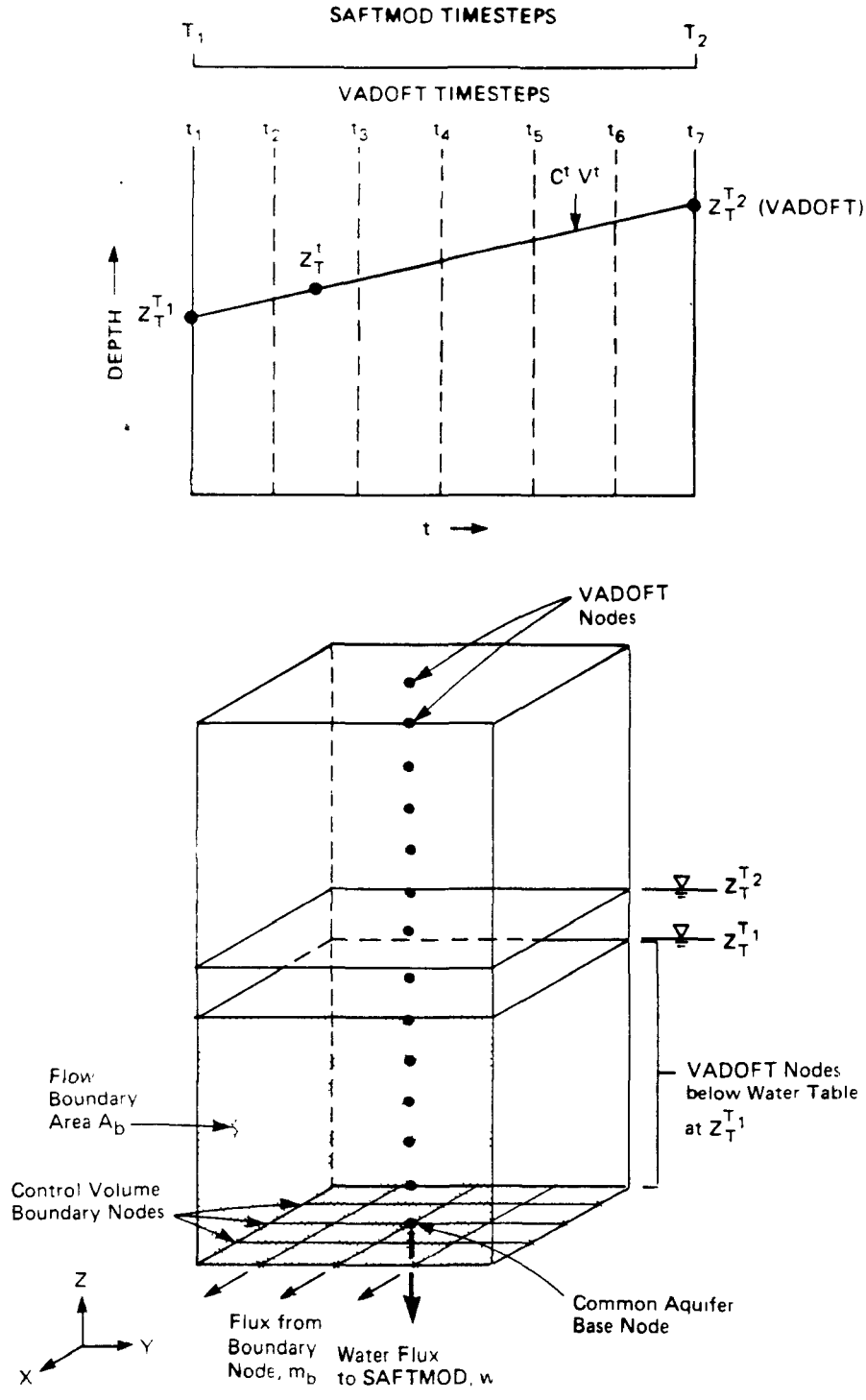

Figure 5.3. Definition sketch for a VADOFT/SAFTMOD control volume (x-y) configuration.

VADOFT and SAFTMOD are linked through the use of a common node at the base of the aquifer, thus ensuring continuity of pressure head and mass flux. The VADOFT flow model is run using Δt length time steps (7 in Figure 5.3), and the sum of the water flow predicted by VADOFT from the base of the aquifer is the water flux input to SAFTMOD. Next, SAFTMOD flow is run and a new pressure head at the aquifer base (ψ_β) and a new water table elevation (Z_T) are predicted (by SAFTMOD) at time T_2 (see Figure 5.3). The new water table elevation ($Z_T^{T_2}$) is used, along with ($Z_T^{T_1}$), to interpolate water table elevations (Z_T^t) for each VADOFT time step (Δt). Once these water table elevations and (V_T^t) are known, VADOFT transport is run to compute C_T^t, the contaminant concentrations at the water table. These results (V_T^t and C_T^t) can be used to compute the contaminant mass flux (M) to the water table over the interval ΔT. Once M is known, SAFTMOD transport can be run. Because SAFTMOD predicts a new mass in the control volume beneath the water table different from VADOFT, the concentrations at each VADOFT node 'i' beneath the water table, $C_i^{T_2}$, must be corrected. This is done in the next ΔT time step by multiplying concentrations at the VADOFT nodes beneath the water table by a correction factor which exactly conserves mass.

The steps which the model takes to achieve this linkage are outlined below:

(1) VADOFT flow is run for ΔT (T_1 to T_2) taking small time steps Δt with ψ_β (VADOFT) = ψ_β (SAFTMOD) as the initial condition.

(2) The water fluxes from the base node of the aquifer are summed and divided by ΔT. This scalar quantity, W, is the water flux to appropriate SAFTMOD nodes for ΔT. Each SAFTMOD node receives a total flux in each ΔT defined as the water flux times the area assigned to each node.

(3) SAFTMOD flow is run to obtain $Z_T^{T_2}$.

(4) Z_T^t is computed for each Δt by interpolating between $Z_T^{T_1}$ and $Z_T^{T_2}$.

(5) VADOFT transport is then run.

(6) M, the mass flux of contaminant to the water table, is determined by

$$M = \sum_{T_1}^{T_2} (C_T^t \, V_T^t \, \Delta t + \theta \, D \, \frac{\Delta c}{\Delta Z} \, \Delta t)/(T_2 - T_1) \qquad (5\text{-}1)$$

where

C_T^t = the concentration at the water table at time t (ML^{-3})

V_T^t = the vertical Darcy velocity at the water table at time t, as computed by VADOFT flow in Step (1) above (LT^{-1})

θ = the volumetric water content of the vadose zone just above the water table (L^3L^{-3})

D = the dispersion/diffusion coefficient in the vadose zone (L^2T^{-1})

Δc = the concentration difference in the vadose zone between the node at the water table and the node above (ML^{-3})

ΔZ = is the distance between the two nodes (L)

(7) SAFTMOD transport is run using M as the mass flux boundary condition at the appropriate SAFTMOD nodes. The actual flux to each node during ΔT is determined by multiplying M by the appropriate nodal area.

(8) The contaminant mass in the saturated control volume, $\forall$, at the end of ΔT is determined from:

$$M_L^{T_2} = \sum_{i=1}^{N} (C^{T_2} \phi R)_i \forall_i \qquad (5\text{-}2)$$

where

C^{T_2} = the SAFTMOD concentration values at node i at time value (ML^{-3})

$\forall_i$ = the portion of the saturated control volume assigned to node i (L^3)

ϕ_i = porosity of node i

R_i = retardation coefficient of node i

N = the number of SAFTMOD nodes in the control volume

(9) A mass correction is made to VADOFT nodes below the water table at the end of ΔT. The basis for the correction is

$$\underline{C}_i^{T_2} = C_i^{T_2} \frac{(M_L^{T_2})^S}{(M_L^{T_2})^V} \qquad (5\text{-}3)$$

where

$\underline{C}_i^{T_2}$ = the new concentration values at nodes below the water table at time T_2 (ML^{-3})

$C_i^{T_2}$ = the uncorrected values from VADOFT (ML^{-3})

$(M_L^{T_2})^S$ = the total mass in the control volume below the water table given by SAFTMOD at T_2 (M)

$(M_L^{T_2})^V$= the total mass in the control volume below the water table given by VADOFT at T_2 (M)

5.2.2.2 PRZM/SAFTMOD (2-D, X-Y) Linkage

The procedure for linking PRZM to SAFTMOD is very similar to that for linking VADOFT to SAFTMOD. The difference is that PRZM does not compute head values and, therefore, head continuity between PRZM and SAFTMOD can not be used as a common point. PRZM flow and transport are solved using a single-pass solution (i.e., unlike in VADOFT, flow and transport equations are solved in a single application of the model). The water flux to the water table is computed over time step ΔT. PRZM is initialized so that the water contents below the root zone are at field capacity (θ_{fc}). Therefore, the water flux below the root zone can be taken as the water flux$_{T_2}$ to the water table. SAFTMOD is run using this water flux to obtain $Z_T^{T_2}$ and values of the water table are interpolated for each Δt between T_1 and T_2. Values of mass flux to the water table are then interpolated from the midpoints of PRZM compartments on either side of the water table. From this point on, the procedure is exactly the same as for the VADOFT/SAFTMOD linkage.

5.2.2.3 VADOFT/SAFTMOD (2-D, X-Z) Linkage

This linkage is virtually the same as for the 2-D (X-Y) case. The difference is, of course, that SAFTMOD is capable of simulating vertical variations in pressures, velocities, and contaminant concentrations. The linkage is most easily accomplished if VADOFT and SAFTMOD nodes below the water table coincide.

First, VADOFT flow is run. The initial VADOFT pressure heads at nodes below the water table are equal to the average pressure heads across the SAFTMOD nodal rows within the two-dimensional control slice (see Figure 5.4). Then SAFTMOD flow is run to obtain $Z_T^{T_2}$. Following interpolation to obtain Z^t, VADOFT transport to the water table is computed, just as in the 2-D (X-Y) linkage. SAFTMOD transport is then run and the mass flux from the boundary of the control slice is computed. The VADOFT contaminant profile is adjusted exactly as in the 2-D (X-Y) case, over the next ΔT. The new average pressure heads for each row within the control slice become the new pressure heads for VADOFT nodes below the water table for the next VADOFT flow simulation.

5.2.2.4 PRZM/SAFTMOD (2-D, X-Z) Linkage

This link is accomplished in exactly the same way as that described for VADOFT and SAFTMOD except that, as in the 2-D, X-Y PRZM to SAFTMOD linkage, head continuity at the aquifer base is not maintained.

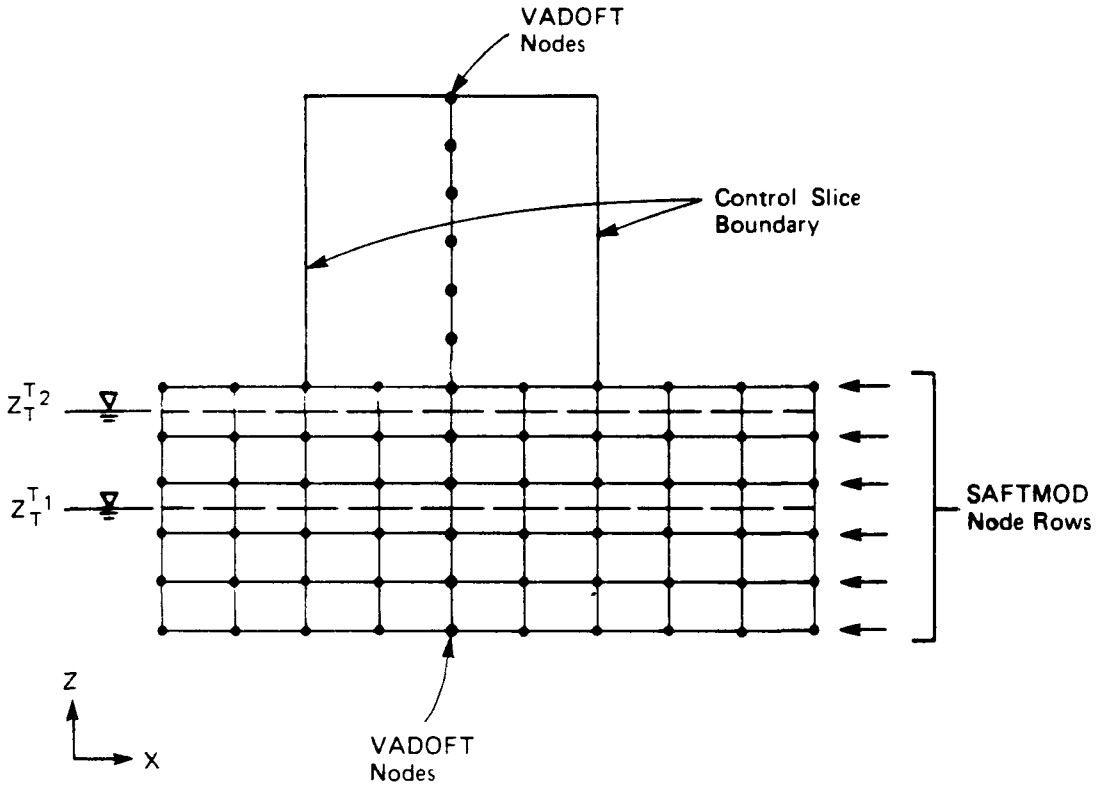

Figure 5.4. Schematic of VADOFT/SAFTMOD x-z configuration

SECTION 6

UNCERTAINTY PREPROCESSOR

6.1 INTRODUCTION

In recent years the use of quantitative models to assess the fate and transport of contaminants in the environment has increased significantly. Typically these models include a set of algorithms that simulate the fate and transport of a contaminant within a media (e.g., unsaturated zone, saturated porous media, air or a surface water body) based on a number of user-specified parameters. These parameters describe the properties of the chemical, the transport medium, and the effects that man has on the system.

Unfortunately, the values of these parameters are not known exactly due to measurement errors and/or inherent spatial and temporal variability. Therefore, it is often more appropriate to express their value in terms of a probability distribution rather than a single deterministic value and to use an uncertainty propagation model to assess the effect of this variability on the fate and transport of the contaminant.

This section describes the Monte Carlo method of uncertainty propagation and a Monte Carlo shell which is coupled with the RUSTIC model (subsequently referred to as the deterministic code in this report). The composite code (i.e., the uncertainty shell coupled with the deterministic code) can be used for the quantitative estimate of the uncertainty in the concentrations at the monitoring point due to uncertainty in the (fate and transport) model input parameters.

6.2 OVERVIEW OF THE PREPROCESSOR

The objective of the uncertainty analysis/propagation method is to estimate the uncertainty in model output (e.g., the concentration at a monitoring point) given the uncertainty in the input parameters and the fate and transport model. Alternatively stated, the objective is to estimate the cumulative probability distribution of the concentration at a receptor location given the probability distribution of the input parameters. If C_w represents the concentration at the receptor, then

$$C_w = g(\underline{X}) \tag{6-1}$$

where the function g represents the fate and transport model and $\underline{X}$ represents the vector of all model inputs. Note that some or all of the components of $\underline{X}$

may vary in an uncertain way, i.e. they are random variables defined by cumulative probability distribution functions. Thus the goal of an uncertainty propagation method is to calculate the cumulative distribution function $F_{C_w}(C'_w)$ given a probabalistic characterization of $\underline{X}$. Note that $F_{C_w}(C'_w)$ is defined as:

$$F_{C_w}(C'_w) = \text{Probability } (C_w \leq C'_w) \tag{6-2}$$

where C'_w is a given output concentration.

6.2.1 Description of the Method

Given a set of deterministic values for each of the input parameters, X_1, X_2, . . . X_n, the composite model computes the output variable (e.g., a downgradient receptor well concentration C_w) as:

$$C_w = g\ (X_1,\ X_2,\ X_3\ .\ .\ .\ X_n) \tag{6-3}$$

Application of the Monte Carlo simulation procedure requires that at least one of the input variables, X_1 . . . X_n, be uncertain and the uncertainty represented by a cumulative probability distribution. The method involves the repeated generation of pseudo-random number values of the uncertain input variable(s) (drawn from the known distribution and within the range of any imposed bounds) and the application of the model using these values to generate a series of model responses i.e. values of C_w. These responses are then statistically analyzed to yield the cumulative probability distribution of the model response. Thus, the various steps involved in the application of the Monte Carlo simulation technique involve:

i) Selection of representative cumulative probability distribution functions for describing uncertainty in the relevant input variables.

ii) Generation of pseudo-random numbers from the distributions selected in (i). These values represent a possible set of values for the input variables.

iii) Application of the model to compute the derived inputs and output(s).

iv) Repeated application of steps (ii) and (iii).

v) Presentation of the series of output (random) values generated in step (iii) as a cumulative probability distribution function (CDF).

vi) Analysis and application of the cumulative probability distribution of the output as a tool for decision making.

6.2.2 Uncertainty in the Input Variables

The parameters required by a fate and transport model can be broadly classified into two different sets that exhibit different uncertainty characteristics. These are:

- Chemical parameters. Examples of these variables include the octanol-water partition coefficient, acid, neutral, and base catalysed hydrolysis rate, soil-adsorption coefficient, Henry's Law Constant, etc.

- Media parameters. Examples of these variables include the groundwater velocity, soil porosity, organic carbon content, dispersivity values, etc.

- Meteorological parameters. Examples include precipitation, evaporation, solar radiation.

- Management parameters. Examples include irrigation timing, pesticide application timing, well pumping rates, etc.

Uncertainty in chemical parameters primarily arises due to laboratory measurement errors or theoretical methods used to estimate the numerical values. In addition to experimental precision and accuracy, errors may arise due to extrapolations from controlled (laboratory) measurement conditions to uncontrolled environmental (field) conditions. Further, for some variables, semi-empirical methods are used to estimate the values. In this case, errors in using the empirical relationships also contribute to errors/uncertainty in the model outputs.

Uncertainty in the second and third sets of parameters, identified above, may include both measurement and extrapolation errors. However, the dominant source of uncertainty in these is the inherent natural (spatial and temporal) variability. This variability can be interpreted as site-specific or within-site variation in the event that the fate and transport model is used to analyze exposure due to the use and/or the disposal of a contaminant at a particular site. Alternatively it can represent a larger scale (regional/national) uncertainty if the model is used to conduct exposure analysis for a specific chemical or specific disposal technology on a generic, nation-wide or regional basis. Note that the distributional properties of the variables may change significantly depending upon the nature of the application. Uncertainty in the fourth set of parameters may arise from a complex variety of factors including climate, sociology, economics, and human error.

Whatever the source of uncertainty, the uncertainty preprocessor developed here requires that the uncertainty be quantified by the user. This implies that for each input parameter deemed to be uncertain, the user select a distribution and specify the parameters that describe the distribution.

The current version of the preprocessor allows the user to select one of the following distributions:

i) Uniform
ii) Normal
iii) Log-normal
iv) Exponential
v) Johnson SB distribution
vi) Johnson SU distribution
vii) Empirical
viii) Triangular

Depending on the distribution selected, the user is required to input relevant parameters of the distribution. The first requires minimum and maximum values. The second and third distributions require the user to specify the mean and the variance. The fourth distribution requires only one parameter - the mean of the distribution. For the empirical distribution, the user is required to input the coordinates of the cumulative probability distribution function (minimum 2 pairs, maximum 20 pairs) which is subsequently treated as a piece-wise linear curve. For the triangular distribution the user is required to input the minimum, maximum and the most likely value. Finally, the Johnson SB and SU distribution requires four parameters - mean, variance, and the lower and upper bounds.

In addition to the parameters of the distribution, the user is required to input the bounds of each model parameter. These bounds may be based on available data or simply physical considerations e.g. to avoid the generation of negative values. Values generated outside these bounds are rejected.

Of the above eight distributions, the characteristics of the majority are easily available in literature (Benjamin and Cornell, 1970). The triangular distribution has been discussed in Megill (1977). Details of the Johnson system of distributions are presented in McGrath and Irving (1973) and Johnson and Kotz (1970). Additional details for each of these distributions are presented in the following discussion.

In some cases, it may be desirable to include correlations among the variables. For example there may be correlation between hydraulic conductivity and particle size or between adsorption and degradation coefficients. The uncertainty processor allows the generation of (linearly) correlated variables for cases where the underlying distribution of the variables is either normal and/or lognormal.

6.3 DESCRIPTION OF AVAILABLE PARAMETER DISTRIBUTIONS

The Monte Carlo Shell has the ability to generate data from a number of probability distributions listed above. A description of each of these distributions is provided in the following paragraphs, including parameters of the distributions, equations for the probability and cumulative density functions, and a brief discussion of the properties of each distribution.

6.3.1 Uniform Distribution

A uniform distribution is a symmetrical probability distribution in which all values within a given range have an equal chance of occurrence. A uniform

distribution is completely described by two parameters: 1) the minimum value (lower bound) A, and 2) the maximum value (upper bound) B. The equation for the uniform probability density distribution of variable x is given by:

$$f_u(x) = 1/(B - A) \tag{6-4}$$

where $f_u(x)$ is the value of the probability density function for x. The cumulative distribution F(x) is obtained by integrating Equation (6-4). This yields the probability distribution:

$$F_u(x) = (x - A)/(B - A) \tag{6-5}$$

where F(x) is the probability that a value less than or equal to x will occur.

6.3.2 Normal Distribution

The term normal distribution refers to the well known bell-shaped probability distribution. Normal distributions are symmetrical about the mean value and are unbounded, although values further from the mean occur less frequently. The spread of the distribution is generally described by the standard deviation. The normal distribution has only two parameters: the mean and the standard deviation. The probability density function of x is given by:

$$f_n(x) = \frac{1}{S_x \sqrt{2\pi}} \exp\left[-0.5 \left[\frac{x - m_x}{S_x}\right]^2\right] \tag{6-6}$$

where S_x is the standard deviation, and m_x is the mean of x. The cumulative distribution is the integral of the probability density function:

$$F_n(x) = \int_{-\infty}^{x} f_n(x)dx \tag{6-7}$$

The above integration must be performed numerically, but tables of numerically-integrated values of $F_n(x)$ are widely available in the statistical literature.

6.3.3 Log-Normal Distribution

The log-normal distribution is a skewed distribution in which the natural log of variable x is normally distributed. Thus, if y is the natural log of x,

then the probability distribution of y is normal with mean m_y, and standard deviation S_y and a probability density function similar to Equation (6-10). The mean and standard deviation of x (m_x and S_x) are related to the log-normal parameters m_y and S_y as follows:

$$m_x = \exp[m_y + 0.5(S_y)^2] \tag{6-8}$$

$$S_x^2 = m_x^2 \, [\exp(S_y^2) - 1] \tag{6-9}$$

To preserve the observed mean and standard deviation of x, the parameters of the log-normal distribution (m_y and S_y) are therefore selected such that the above relationships are satisfied. Note that m_y and S_y do not equal the natural logs of m_x and S_x respectively. Log-normal distributions have a lower bound of 0.0 and no upper bound, and are often used to describe positive data with skewed observed probability distributions.

6.3.4 Exponential Distribution

The probability density function for an exponential distribution is described by an exponential equation:

$$f_e(x) = \frac{\exp(-x/m_x)}{m_x} \tag{6-10}$$

where m_x is the mean of x. The cumulative distribution is given by:

$$F_e(x) = 1 - \exp(-x/m_x) \tag{6-11}$$

The exponential distribution is bounded by zero; the probability density function peaks at zero and decreases exponentially as x increases in magnitude.

6.3.5 The Johnson System of Distributions

The Johnson system involves two main distribution types: SB (Log-ratio or bounded) and SU (unbounded or hyperbolic arcsine). These two distribution types basically represent two different transformations applied to the random variable such that the transformed variable is normally distributed. The specific transformations are:

$$\text{SB:} \quad Y = \ln\left[\frac{(x-A)}{(B-x)}\right] \tag{6-12}$$

$$SB: \quad Y = \ln\left[\frac{x-A}{B-x} + \left(1 + \left(\frac{x-A}{B-x}\right)^2\right)^{0.5}\right] \tag{6-13}$$

where

ln = natural logarithm transformation

x = untransformed variable with limits of variation from A to B.

Y = the transformed variable with a normal distribution

Selection of a particular Johnson distribution for sample data set is accomplished by plotting the skewness and kurtosis of the sample data. The location of the sample point indicates the distribution for the sample data.

For additional details of the Johnson system of distributions, the reader is referred to McGrath and Irving (1973) and Johnson and Kotz (1970).

6.3.6 Triangular Distribution

A triangular distribution is a relatively simple probability distribution defined by the minimum value, the maximum value, and the most frequent value (i.e., the mode). Figure 6.1 shows an example triangular probability density function. The cumulative distribution for values of x less than the most frequent value, x_m, is given by:

$$F(x) = \frac{(x - x_1)^2}{(x_m - x_1)(x_2 - x_1)} \tag{6-14}$$

where x_1 is the minimum value and x_2 is the maximum value. For values of x greater than the most frequent value, the cumulative distribution is:

$$F(x) = 1 - \frac{\left(1 - \frac{x - x_1}{x_2 - x_1}\right)^2}{\left(1 - \frac{x_m - x_1}{x_2 - x_1}\right)} \tag{6-15}$$

6.3.7 Empirical Distribution

At times it may be difficult to fit a standard statistical distribution to observed data. In these cases it is more appropriate to use an empirical piecewise-linear description of the observed cumulative distribution for the variable of interest.

Cumulative probabilities can be estimated from observed data by ranking the data from lowest (rank = 1) to highest (rank = number of samples) value. The

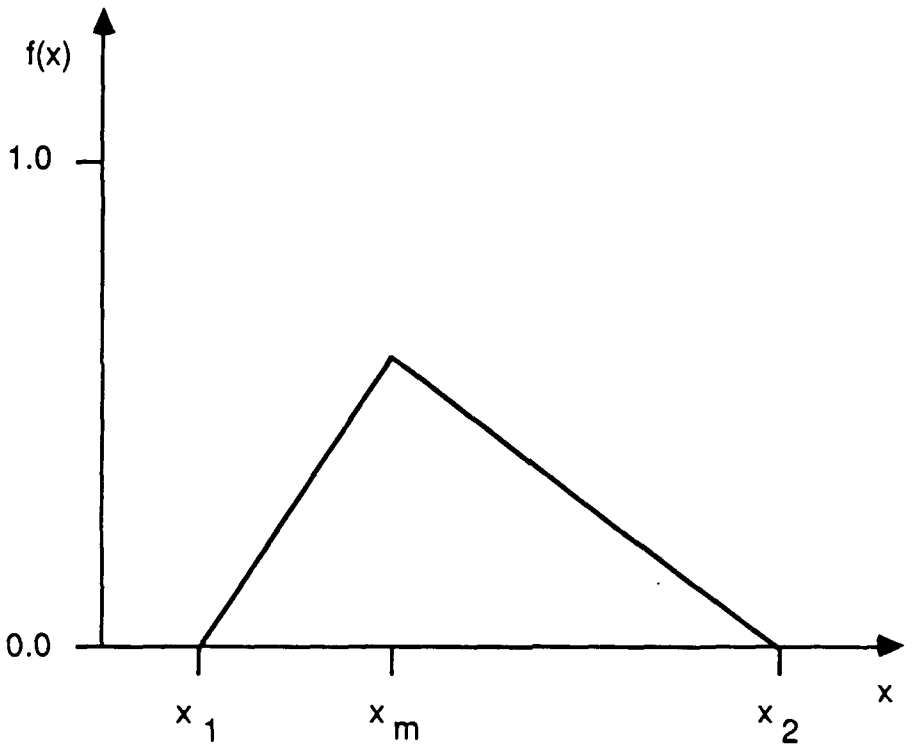

Figure 6.1. Triangular Probability Distribution

cumulative probability associated with a value of x is then calculated as a function of the rank of x and the total number of samples. The cumulative probabilities of values between observed data can be estimated by linear interpolation.

6.3.8 Uncertainty in Correlated Variables

In many cases model input variables are correlated due to various physical mechanisms. Monte Carlo simulation of such variables requires not only that parameters be generated from the appropriate univariate distributions, but also that the appropriate correlations be preserved in the generated input sequences. The Monte Carlo module currently has the ability to generate correlated normal, log-normal, Johnson SB, and Johnson SU numbers; the procedures used are described in the following paragraphs.

The correlation coefficient is a measure of the linear dependence between two random variables and is defined as:

$$\rho_{x,y} = \frac{\mathrm{cov}(x,y)}{\rho_x \, \rho_y} \tag{6-16}$$

where

$\rho_{x,y}$ = the correlation coefficient between random variables x any y
$\mathrm{cov}(x,y)$ = the covariance of x and y as defined below
ρ_x, ρ_y = the standard deviation for x and y.

The covariance of x and y is defined as:

$$\mathrm{cov}(x,y) = E\,[(x-m_x)(y-m_x)]$$

$$= \int_{-\infty}^{+\infty}\int (x-m_x)\,(y-m_y)\, f_{x,y}(x,y)\, dx\, dy \tag{6-17}$$

where

E = the expected value
m_x, m_y = the mean of the random variables x and y
$f_{x,y}(x,y)$ = the joint probability distribution of x and y.

Note that the linear correlation coefficient between x and y can be computed using

$$\rho_{x,y} = \frac{\sum_{i=1}^{n} x_i\, y_i - n\,\bar{x}\,\bar{y}}{\left[\sum_{i=1}^{n} (x_i^2 - n\bar{x}^2)\ \sum_{i=1}^{n} (y_i^2 - n\bar{y}^2)\right]^{0.5}} \qquad (6\text{-}18)$$

To generate correlated random variables three steps are required. First uncorrelated normally distributed random numbers are generated. This vector is then transformed to a vector of normally distributed numbers with the desired correlation. Finally, the normally distributed numbers are transformed to numbers with the desired distribution.

The transformation of uncorrelated to correlated normal numbers consists of multiplying the uncorrelated vector of numbers with a matrix B:

$$Y' = B\ e \qquad (6\text{-}19)$$

where

- e = the vector of uncorrelated, normally distributed random numbers.
- B = and N by N matrix
- Y' = a vector of standard normal deviates of mean zero and standard deviation of unity.

The matrix B is related to the variance-covariance matrix S as follows:

$$S = B\ B^T \qquad (6\text{-}20)$$

where B^T is the transpose of the B matrix. Since the normal variables Y' have means of zero and unit variances, the variance-covariance matrix is equivalent to the correlation matrix.

Thus, if the correlation matrix S is known, B can be found from Equation (6-20) by using a Choleski decomposition algorithm. This algorithm will decomposes a symmetric positive definite matrix, such as S, into a triangular matrix such as B (de Marsily, 1986, p. 381).

Having generated a vector of correlated normally distributed random numbers, the vector Y' can be converted, through appropriate transformations, to the distribution of choice. Thus for parameters X_i that have a normal distribution, the Y' numbers are transformed as follows:

$$X_i = m_x + \sigma_x(Y_i') \qquad (6\text{-}21)$$

For parameters that follow the lognormal distribution, the following transformation applies:

$$X_i = \exp[(Y_i') \ (\sigma_{ln,i}) + \mu_{ln,i}] \tag{6-22}$$

where

$\mu_{ln,i}$ = the log mean of the i^{th} parameter.

$\sigma_{ln,i}$ = the log standard deviation of the i^{th} parameter

For parameters with Johnson SB and SU distributions, the Y' are first transformed to normally distributed variables Y with mean M_y and standard deviation σ_y:

$$Y_i = M_y + \sigma_y \ Y_i' \tag{6-23}$$

Johnson SB numbers are then computed from Y_i as follows:

$$X_i = (B \exp(Y_i) - A)/(1 + \exp(Y_i)) \tag{6-24}$$

Johnson SU numbers are computed by:

$$X_i = A + (B-A)[\exp(Y_i) - \exp(-Y_i)]/2 \tag{6-25}$$

Other distributions can be easily incorporated into the analyses at a later time when suitable transformations from the normal distribution can be found. It is important to note that in using this technique, the correlations are maintained in normal space so if these correlations are estimated using actual data, the data should be transformed to a normal distribution before correlation coefficients are estimated.

For two correlated variables, one with a normal distribution (x_2) and the other with a log normal distribution (x_1), the following equation is used to transform correlations to normal space (Meija and Rodriguez-Iturbe, 1974):

$$\sigma_{y_1,y_2} = \frac{\sigma_{x_1,x_2}[\exp(\sigma_{y_1}^2) - 1]^{1/2}}{\sigma_{y_1}} \tag{6-26}$$

where

σ_{y_1,y_2} = the correlation coefficient between the two variables in the normal space

σ_{x_1,x_2} = the correlation coefficient between the two variables in the arithmetic space

$\sigma_{y_1}^2$ = the variance of y_1 derived from Equation (6-9)

If both x_1 and x_2 are log-normally distribution then the correlation coefficient is transformed using Meija and Rodriguez-Iturbe (1974):

$$\sigma_{y_1,y_2} = \frac{1}{S_{y_1} S_{y_2}} \ln \left[1 + \sigma_{x_1,x_2} \left|\frac{S_{x_1} S_{x_2}}{m_{x_1} m_{x_2}}\right|\right] \qquad (6\text{-}27)$$

where the relationships between $S_{x_1}(S_{x_2})$ and $S_{y_1}(S_{y_2})$ are given by Equations (6-8) and (6-9).

Thus, for log-normal variables the user enters the values of the correlation coefficients in log-normal space; Equations 6-26 and 6-27 are then used to transform the correlation coefficients into normal space.

No direct transformation of Johnson SB or SU correlations to normal correlations is currently known. For these distributions the user must therefore supply the correlation coefficients between normal-transformed numbers. This may be accomplished by first transforming Johnson SB and SU data to normal data using Equations 6-12 and 6-13. The covariance matrix S is then derived using only normal, log-normal, and normal-transformed SB and SU data.

6.3.9 Generation of Random Numbers

Having selected the distribution for the various input parameters, the next step is the generation of random values of these parameters. This requires the use of pseudo-random number generating algorithms for Normal and Uniform numbers. There exist numerous proprietary as well as non-proprietary subroutines that can be used to generate random numbers. A number of these are comparable in terms of their computational efficiency, accuracy, and precision. The performance of the algorithms included in this preprocessor has been checked to ensure that they accurately reproduce the parameters of the distributions that are being sampled (Woodward-Clyde Consultants, 1988).

6.4 ANALYSIS OF OUTPUT AND ESTIMATION OF DISTRIBUTION QUANTILES

Model output generally will consist of a volume of data that represents a sample of outcomes. Given the natural variability and the uncertainty of various model components, there will be variability in the output. All of the factors that were allowed to vary within the model contribute to variability in model predictions. Taken as a whole, the model output depicts

possible events in terms of their relative frequency of occurrence. Values produced by the model generally are treated as if they were observations of real field events. In interpreting these values, it is important to maintain the perspective dictated by the design and scope of the study.

Model output can be analyzed in various ways depending upon current objectives. Many features of the distribution may be characterized. Quite often, for example, it is of interest to estimate certain quantiles or percentiles of the distribution. Since the model output is treated as a sample from an unknown parent population, the methods of statistical inference normally are used to estimate distribution parameters and to associate with them measures of uncertainty.

One of the most frequently asked questions concerns the number of samples required for some given purpose. In modelling, this translates into the number of model runs needed. For the most part, since methods of basic inference are being applied in a Monte Carlo framework, resulting model output values are treated as observations forming a random sample. The sample size required to estimate a given parameter depends on a number of factors. These include the nature of the parameter that is being estimated, the form of the underlying distribution, the variability in the observations, the degree of precision and/or accuracy desired, the level of confidence to be associated with the estimate, and the actual statistical estimator used to provide the estimate.

Generally, if the output distribution is to be accurately characterized with respect to its many features, the number of model runs needed will be higher than if only a few parameters are to be estimated. The simulation strategy should be determined by the issues addressed by the modelling effort. It may be important, for example, to estimate the extreme upper percentiles of the output distribution. In this case, the choice of simulation design should account for the relative difficulty of obtaining such estimates. If it is not known exactly how the data will be utilized, then the problem becomes one of establishing a distributional representation that is as good as possible under the most extreme usage or estimation scenario. For example, if only a distribution mean were to be estimated, the sample size required could be determined without concern for estimating, say, the 99th percentile.

6.4.1 Estimating Distribution Quantiles

In the following section, a summary is given for statistical techniques used to estimate distribution quantiles. There are many such methods available to estimate a given percentile of an unknown distribution on the basis of sample data. In the RUSTIC code four such methods can be used. Among these are distribution-free or nonparametric techniques as described below. Others include methods specific to certain distributions that assume a knowledge of the distributional form. First, the point estimators are given, then the method for constructing a confidence interval is briefly described.

The order statistics of a sample are merely the ordered values denoted by $x_{(1)}, x_{(2)}, \ldots, x_{(n)}$, where n represents the sample size. The empirical cdf can be defined simply as

$$g(x) = \begin{cases} 0, & \text{if } x_{(1)} < x, \\ 1/n, & \text{if } x_{(i)} \le x < x_{(i+1)}, \text{ for } i=1, \ldots, n-1 \\ 1, & \text{if } x \ge x_{(n)}. \end{cases} \quad (6\text{-}28)$$

Mathematically, g(x) is a step function, discontinuous at each value $x_{(i)}$.

By definition, the 100p-th percentile (i.e., the p-level quantile) is given by u_p where

$$p = \Pr\{ X < u_p \} \quad (6\text{-}29)$$

If F(x) denotes the cumulative distribution function,

$$p = F(u_p) \text{ and } u_p = F^{-1}(p) \quad (6\text{-}30)$$

When only sample information is available, u_p is unknown, but it can be estimated by forming an appropriate function of the observations.

Nonparametric point estimates of u_p can be constructed as linear combinations of the order statistics. In particular, each of Y_1 through Y_3 below is an estimator of u_p. Let [z] denote the largest integer less than or equal to z. Define

$$j = [np], \qquad g = np - j \quad (6\text{-}31)$$

$$i = [np + 0.5], \quad r = (np + 0.5) - i \quad (6\text{-}32)$$

$$k = [(n+1)p], \quad h = (n+1)p - k \quad (6\text{-}33)$$

Then,

$$Y_1 = (1-h)\, X_{(k)} + h\, X_{(k+1)} \quad (6\text{-}34)$$

$$Y_2 = \frac{(X_{(j)} + X_{(j+1)})}{2}, \text{ if } g=0 \quad (6\text{-}35)$$

$$= X_{(j+1)}, \text{ if } g>0$$

$$Y_3 = (0.5+i-np)\, X_{(i)} + (0.5-i+np)\, X_{(i+1)} \quad (6\text{-}36)$$

$$= (1 - r)\, X_{(i)} + r\, X_{(i+1)}$$

In each of these definitions, only the values of n and p determine which order statistics are used in forming an estimate of u_p. Thus, the estimators

do not depend on the underlying distributions. However, the relative performance of these estimators is dependent upon several criteria involving the level p, the sample size n, the type of parent distribution from which samples are drawn, estimator bias, and the mean squared error. If the sample size is very large, the differences among the estimates are not very great. Of the estimators available, the three shown above exhibit the best performance in relatively small samples ($n \leq 50$) from normal and lognormal distributions.

Another simple estimator used in the model is calculated by constructing the cdf of the output

$$F(x) = i/n \tag{6-37}$$

in which i is the rank of the outcome in the sample. The specific quantile of interest is then determined by interpolation.

6.4.2 Confidence of u_p

Approximate confidence statements can be placed on u_p by selecting appropriate order statistics to serve as the upper and lower confidence bounds. The rationale is given as follows.

For a given distribution, the value u_p is such that exactly 100p% of all values of this distribution are less than u_p, and 100(1-p)% exceed this value. An individual value selected randomly from the distribution has probability p of being less than u_p. In a random sample of size n from this distribution, the probability of not exceeding u_p remains constant for each individual element of the sample. Thus, the number of values in the sample that are less than or equal to u_p is distributed binomially. The probability that the random interval $(X_{(j)}, X_{(j+1)})$ will contain u_p is equivalent to the probability that exactly i of the n elements of the sample will be less than u_p. Hence, this probability is

$$\binom{n}{i} p^i (1-p)^{n-1} \tag{6-38}$$

which is a simple binomial probability.

This expression can be calculated for each pair of consecutive order statistics $X_{(i)}$, $X_{(i+1)}$, for i=1, ..., n-1. However, it is more convenient to deal with these several intervals by calculating cumulative probabilities of the form

$$\Pr\{u_p \leq X_{(i+1)}\} = \sum_{j=0}^{i} \binom{n}{j} p_j (1-p)_{n-j} \tag{6-39}$$

For practical convenience, the normal approximation

$$F\{[(i+0.5)-np]/\sqrt{[np(1-p)]}\} \tag{6-40}$$

can be used, where F represents the cdf of the standard normal distribution.

All of this is utilized for determining two order statistics, denoted below with subscripts i and j, with the property

$$Pr\{X_{(i)} < u_p \leq X_{(j)}\} = 1 - \alpha \tag{6-41}$$

where $1-\alpha$ is the predetermined confidence coefficient; typically, $1-\alpha = 0.95$. Computationally, i and j can be determined by solving the equations

$$\alpha/2 = F\{[(i+0.5)-np]/\sqrt{[np(1-p)]}\} \tag{6-42}$$

and

$$1 - \alpha/2 = F\{[(j+0.5)-np]/\sqrt{[np(1-p)]}\} \tag{6-43}$$

This results in

$$i = (np-0.5) + \sqrt{[np(1-p)]}\ F^{-1}(\alpha/2) \tag{6-44}$$

$$j = (np-0.5) + \sqrt{[np(1-p)]}\ F^{-1}(1-\alpha/2) \tag{6-45}$$

where F^{-1} denotes the inverse cdf of the standard normal distribution (e.g., for $1-\alpha = 0.90$, $F^{-1}(1-\alpha/2) = 1.645$). For example, with n=100, p=0.95, and $1-\alpha=0.90$, i=90 and j=98, so that $(X_{(90)}, X_{(98)})$ forms the approximate 90% confidence interval on u_p.

Although the expressions for the confidence interval do not depend in any way on the underlying distribution, the expected width of the interval does. In particular, it depends on the expected values of the order statistics involved. In the example above, if the sample is from a standard normal distribution, $u_p = 1.645$ and the expected half-width of the interval is 0.349. If the sample is from a lognormal distribution based on a standard normal, $u_p = 5.180$ and the expected half-width is 1.858. Also, note that in normal sampling the expected confidence interval half-width for n=500 is 0.192 for the same estimate.

SECTION 7

REFERENCES

Avdonin, N.A. 1964. Some Formulas for Calculating the Temperature Field of a Stratom during Termal Injection. Izvestiya Vysshikh Uchebnykl Zavedenii Neft. Gaz. 7(3) 37-41.

Bassett, D.L., and D.W. Fitzsimmons. 1974. A Dynamic Model of Overland Flow in Border Irrigation. Am. Soc. Ag. Eng. Paper No. 74-2529, St. Joseph, MI.

Battelle, Pacific Northwest Laboratories, and GeoTrans. 1988. FASTCHEM Package Volume 2: User's Guide to the EFLOW Groundwater Flow Code. Electrical Power Rsearch Institute, EA-5870-CCM, Volume 2, Research Project 2485-2.

Bear, J. 1979. Hydraulics of Groundwater. McGraw-Hill, New York, NY.

Benjamin, J.R. and C.A. Cornell. 1970. Probability, Statistics, and Decision for Civil Engineers. McGraw Hill Book Company.

Bromilow, R.H., M. Richard and M. Leistra. 1980. Pesticide Sci. II:389-395.

Brooks, R.H. and A.T. Corey. 1966. Properties of Porous Media Affecting Fluid Flow. ASCE J. Irrig. Drain Div. 92 (IR2):61-68.

Brown, S.M., and S.H. Boutwell. 1986. Chemical Spill Exposure Assessment Methodology. RP 2634-1. Prepared for Electric Power Research Institute, Palo Alto, CA.

Carsel, R.F., and R.S. Parrish. 1988. Developing Joint Probability Distributions of Soil-Water Retention Characteristics. Water Resour. Res. 24(5):755-769.

Carsel, R.F., L.A. Mulkey, M.N. Lorber, and L.B. Baskin. 1985. The Pesticide Root Zone Model (PRZM): A Procedure for Evaluating Pesticide Leaching Threats to Ground Water. Ecological Modeling 30:49-69.

Carsel, R.F., C.N. Smith, L.A. Mulkey, J.D. Dean, and P. Jowise. 1984. User's Manual for the Pesticide Root Zone Model (PRZM): Release 1. U.S. Environmental Protection Agency, Environmental Research Laboratory, Athens, GA. EPA-600/3-84-109.

Chen, C.W., S.A. Cheriai, R.J.M. Hudson, and J.D. Dean. 1983. The Integrated Lake-Watershed Acidification Study. Vol. I. Model Principles and Application Procedures. Electric Power Research Inst. Rep. No. EA-3221, Vol. 1. Palo Alto, CA.

Cruse, R.M., D.R. Linden, J.K. Radke, W.E. Larson, and K. Larntz. 1980. A Model to Predict Tillage Effects on Soil Temperature. Soil Sci. Soc. Am. J. 44:378-383.

Davis, L.A., and S.P. Neuman. 1983. Documentation and User's Guide: UNSAT2 - Variably Saturated Flow Model. U.S. Nuclear Regulatory Commission Report, NUREG/CR-3390, Washington, D.C.

de Marsily, G. 1986. Quantitative Hydrogeology: Groundwater Hydrology for Engineers. Academic Press, San Diego, CA.

de Vries, D.A. 1963. Thermal Properties of Soils. In: Physics of the Plant Environment, ed. W.R. van Wijk, pp 210-235. New York: John Wiley and Sons, Inc.

Dean, J.D., and D.F. Atwood. 1985. Exposure Assessment Modeling for Aldicarb in Florida. EPA Contract No. 68-03-3116. Work Assignment No. 23, Final Report.

Donigian, A.S., Jr., C.S. Raju, and R.F. Carsel. 1986. Impact of Conservation Tillage on Environmental Pesticide Concentrations in Three Agricultural Regions. Prepared for U.S. EPA, Integrated Environmental Management Division, Office of Policy Analysis, Washington, D.C.

Dyer, A.J. 1974. A Review of Flux-Profile Relationships. Boundary-Layer Meteorology 7:363-372.

Dyer, A.J., and B.B. Hicks. 1970. Flux-Gradient Relationships in the Constant Flux Layer. Quarterly Journal of the Royal Meteorological Society 96:715-721.

Farrell, D.A., E.L. Greacen, and C.G. Gurr. 1966. Vapor Transfer in Soil Due to Air Turbulence. Soil Sci. 102:305-313.

Federal Register. 1984. Proposed Guidelines for Exposure Assessments: Request for Comments. U.S. Environmental Protection Agency. Vol. 49 (227), November 23.

Fok, Y.S., and A.A. Bishop. 1965. Analysis of Water Advance in Surface Irrigation. ASCE of Irrig. and Drainage 91(IR1):99-116.

Fukuda, H. 1955. Air and Vapor Movement in Soil Due to Wind Gustiness. Soil Science 79:249-258.

Grover, R., S.R. Shewchuk, A.J. Cessna, A.E. Smith, and J.H. Hunter. 1985. Fate of 2,4-D Iso-Octyl Ester after Application to a Wheat Field. J. Environ. Qual. 14:203-210.

Gupta, S.C., W.E. Larson, and R.R. Allmaras. 1984. Predicting Soil Temperature and Soil Heat Flux under Different Tillage-Surface Residue Conditions. Soil Sci. Soc. Am. J. 48:223-232.

Gupta, S.C., W.E. Larson, and D.R. Linden. 1983. Tillage and Surface Residue Effects on Soil Upper Boundary Temperatures. Soil Sci. Soc. Am. J. 47:1212-1218.

Gupta, S.C., J.K. Radke, W.E. Larson, and M.J. Shaffer. 1982. Predicting Temperature of Bare and Residue-Covered Soils from Daily Maximum and Minimum Air Temperatures. Soil Sci. Soc. Am. J. 46:372-376.

Gupta, S.C., J.K. Radke, and W.E. Larson. 1981. Predicting Temperature of Bare and Residue-Covered Soils with and without a Corn Crop. Soil Sci. Soc. Am. J. 45:405-412.

Hadermann, J. 1980. Radionuclide Transport Through Heterogeneous Media. Nuclear Technology 47:311-323.

Haith, D.A., and R.C. Loehr, eds. 1979. Effectiveness of Soil and Water Conservation Practices for Pollution Control. U.S. Environmental Protection Agency, Athens, GA. EPA-600/3-79-106.

Hanks, R.J., D.D. Austin, and W.T. Ondrechen. 1971. Soil Temperature Estimation by a Numerical Method. Soil Sci. Soc. Am. Proc. 35:665-667.

Harper, L.A., A.W. White, Jr., R.R. Bruce, A.W. Thomas, and R.A. Leonard. 1976. Soil and Microclimate Effects on Trifluralin Volatilization. J. Environ. Qual. 5:236-242.

Hasfurther, V.R., and R.D. Burman. 1974. Soil Temperature Modeling Using Air Temperature as a Driving Mechanism. Trans. ASAE 17:78-81.

Hunt, B. 1972. Dispersive Sources in Uniform Ground-Water Flow. ASCE Journal of the Hydraulics Division. 104(HYI).

Huyakorn, P.S., H.O. White, Jr., J.E. Buckley, and T.D. Wadsworth. 1988a. VADOFT: Finite Element Code for Simulating One-Dimensional Flow and Solute Transport in the Vadose Zone. Project Report to Woodward-Clyde Consultants. February.

Huyakorn, P.S., and J.E. Buckley. 1988b. SAFTMOD: Saturated Zone Flow and Transport Two-Dimensional Finite Element Model. Project Report to Woodward-Clyde Consultants. March.

Huyakorn, P.S., B.G. Jones, and P.F. Andersen. 1986a. Finite Element Algorithms for Simulating Three-Dimensional Groundwater Flow and Solute Transport in Multilayer Systems. Water Resour. Res. 22(3)361-374.

Huyakorn, P.S., E.P. Springer, V. Guvanasen, and T.P. Wadsworth. 1986b. A Three-Dimensional Finite-Element Model for Simulating Water flow in Variably Saturated Porous Media. Water Resour. Res. 22(13)1790-1808.

Huyakorn, P.S., J.W. Mercer, and D.S. Ward. 1985. Finite Element Matric and Mass Balance Computational Schemes for Transport in Variably Saturated Porous Media. Water Resour. Res. 21(3)346-358.

Huyakorn, P.S., S.D. Thomas, and B.M. Thompson. 1984a. Techniques for Making Finite Elements Competitive in Modeling Flow in Variably Saturated Porous Media. Water Resour. Res. 20(8):1099-1115.

Huyakorn, P.S., A.G. Kretschek, R.W. Broome, J.W. Mercer, and B.H. Lester. 1984b. Testing and Validation of Models for Simulating Solute Transport in Ground-Water. International Ground Water Modeling Center, Holcomb Research Inst., HRI No. 35.

Huyakorn, P.S., and G.F. Pinder. 1983. Computational Methods in Subsurface Flow. Academic Press. 473 pp.

Johnson, N.L., and S. Kotz. 1970. Distributions in Statistics: Continuous Univariate Distributions. Boston: Houghton Mifflin Company.

Jones, R.L. 1983. Movement and Degradation of Aldicarb Residues in Soil and Ground Water. Presented at the CETAC Conference on Multidisciplinary Approaches to Environmental Problems, November 6-9, Crystal City, VA.

Jones, R.L., P.S.C. Rao, and A.G. Hornsby. 1983. Fate of Aldicarb in Florida Citrus Soil 2. Model Evaluation. Presented at the Conference on Characterization and Monitoring of Vadose (Unsaturated) Zone, December 8-10, Las Vegas, NV.

Jury, W.A., W.F. Spencer, and W.J. Farmer. 1984. Behavior Assessment Model for Trace Organics in Soil: III. Application of Screening Model. 13: 573-579.

Jury, W.A., R. Grover, W.F. Spencer, and W.J. Farmer. 1983a. Behavior Assessment Model for Trace Organics in Soil: I. Model Description. J. Environ. Qual. 12:558-564.

Jury, W.A., R. Grover, W.F. Spencer, and W.J. Farmer. 1983b. Use of Models for Assessing Relative Volatility, Mobility, and Persistence of Pesticides and Other Trace Organics in Soil Systems. In: Harvard Assessment of Chemicals, ed. J. Saxena, pp. 1-43. New York: Academic Press.

Khalell, R., and D. Reddell. 1986. MOC Solutions of Convective-Dispersion Problems. Ground Water 24(6):798-807.

Konikow, L.F., and J.D. Bredehoeft. 1978. Computer Model of Two-Dimensional Solute Transport and Dispersion in Ground Water. Techniques of Water-Resources Investigations of the United States Geological Survey, Book 7, Chapter C2.

Kreysig, E. 1972. Advanced Engineering Mathematics, pp. 430-434. John Wiley and Sons Inc., New York, N.Y.

Lester, B.H., P.S. Huyakorn, H.O. White, Jr., T.D. Wadsworth, and J.E. Buckley. 1986. Analytical Models for Evaluating Leachate Migration in Groundwater Systems. Technical report prepared by GeoTrans, Inc., for U.S. Environmental Protection Agency, Office of Solid Waste, Washington, D.C. August.

Li, R., D.B. Simons, and M.A. Stevens. 1975. Non-linear Kinematic Wave Approximation for Water Routing. Water Res. Res. 11(2):245-252.

Liley, P.E., and W.R. Gambill. 1973. Section 3: Physical and Chemical Data. In: Chemical Engineers Handbook, eds. P.H. Perry and C.H. Chilton. New York: McGraw Hill.

Lo, A.K. 1977. An Analytical-Empirical Method for Determining the Roughness Length and Zero-Plane Displacement. Boundary-Layer Meteorology 12:141-151.

M. Baptista, A.E., E.E. Adams, and K.D. Stolzenbach. 1984. Eularian-Lagrangian Analysis of Pollution Transport in Shallow Water. MIT Report 296.

McGrath, E.J. and D.C. Irving. 1973. Techniques for Efficient Monte Carlo Simulation, Volume II. Random Number Generation for Selected Probability Distributions. Report prepared for Office of Naval Research. Project No. NR 366-076/1-5-72, Code 462.

Megill R. E. 1977. An Introduction to Risk Analysis. Tulsa, Oklahoma: Petroleum Publishing Company.

Mehlenbacher, L.A., and D.W.A. Whitfield. 1977. Modeling Thermal Eddy Diffusivity at Canopy Height. Boundary-Layer Meteorology 12:153-170.

Meija, J.M., and I. Rodriguez-Iturbe. 1974. On the Synthesis of Random Field Sampling From the Spectrum: An Application to the Generation of Hydraulic Spatial Processes. Water Resour. Res. 10(4), 705-712.

Mockus, V. 1972. Estimation of Direct Surface Runoff from Storm Rainfall. In: National Engineering Handbook. Section IV, Hydrology. U. S. Soil Conservation Report NEH-Notice 4-102. August.

Mualem, Y. 1976. A New Model for Predicting the Hydraulic Conductivity of Unsaturated Porous Media. Water Resour. Res. 12(3):513-522.

Neuman, S.P., R.A. Feddes, and E. Bresler. 1974. Finite Element Simulation of Flow in Saturated-Unsaturated Soils Considering Water Uptake by Plants. Hydrodynamics and Hydraulic Engineering Laboratory Report for Project No. ALO-SWC-77, Haifa, Israel.

Neumen, S.P., and P.A. Witherspoon. 1969a. Theory of Flow in a Confined Two-Aquifer System. Water Resource Res. 5(3), 803-816.

Neuman, S.P., and P.A. Witherspoon. 1969b. Applicability of Current Theories of Flow in Leaky Aquifers. Water Resour. Res. 5(4), 817-829.

Ogata, A., and R.B. Banks. 1961. A Solution of the Differential Equation of Longitudinal Dispersion in Porous Media. U.S. Geological Survey Professional Paper No. 411-A.

Oliver, H.R. 1971. Wind Profiles in and above a Forest Canopy. Quarterly Journal of the Royal Meteorological Society 97:548-553.

Papadopulos, I.S. 1965. Nonsteady Flow to a Well in an Infinite Anisstropic Aquifer. International Association of Scientific Hydrology Symposium of of Dubrovnik.

Parmele, L.H., E.R. Lemon, and A.W. Taylor. 1972. Micrometeorological Measurement of Pesticide Vapor Flux from Bare Soil and Corn under Field Conditions. Water, Air, and Soil Pollution 1:433-451.

Parton, W.J. 1984. Predicting Soil Temperature in a Shortgrass Steppe. Soil Sci. 138(2):93-101.

Perkins, H.C. 1974. Air Pollution. New York: McGraw-Hill, Inc.

Phillip, J.R. 1955. Numerical Solution of Equations of the Diffusion Type with Diffusivity Concentration-Dependent. Trans. Faraday Soc. 51:885-892.

Pinder, G.F., and W.G. Gray. 1977. Finite Element Simulation in Surface and Subsurface Hydrology. Academic Press, London.

Richards, L.A. 1931. Capillary Conduction of Liquids through Porous Mediums. Physics 1:318-333.

Rosenberg, N.J. 1974. Microclimate: The Biological Environment. New York: Wiley Interscience.

Salhotra, A.M. 1986. A Coupled Heat, Salt and Water Balance Model of Evaporation and Stratification in Saline Terminal Lakes: An Application to the Dead Sea. Ph.D. Dissertation. Massachusetts Institute of Technology, Department of Civil Engineering.

Sauty, J.P. 1980. An Analysis of Hydro Dispersive Transfer in Aquifers. Water Resour. Res. 16(1)145-158.

Scotter, D.R., and P.A.C. Raats. 1970. Movement of Salt and Water near Crystalline Salt in Relatively Dry Soil. Soil Sci. 109:170-178.

Shamir, U.Y., and D.R.F. Harleman. 1967. Dispersion in Layered Porous Media. J. of the Hydraulics Division, Amer. Soc. Civ. Engr. 93(HY5):237-260.

Smiles, D.E., J.R. Phillip, J.H. Knight, and D.E. Elrick. 1978. Hydrodynamic Dispersion During Absorption of Water by Soil. Soil Sci. Soc. Am. J. 42:229-234.

Smith, C.N., R.A. Leonard, G.W. Langdale, and G.W. Baily. 1978. Transport of Agricultural Chemicals from Small Upland Piedmont Watersheds. U.S. EPA, Environmental Research Laboratory, Athens, GA. EPA-600/3-78-056.

Springer, E.P., and H.R. Fuentes. 1987. Modeling Study of Solute Transport in the Unsaturated Zone. U.S. Nuclear Regulatory Commission, NUREC/CR-4615, LA-10730-MS, Volume 2.

Stamper, J.H., H.N. Nigg, and J.C. Allen. 1979. Organophosphate Insecticide Disappearance from Leaf Surfaces: An Alternative to First-Order Kinetics. Environ. Sci. and Tech. 13:1402-1405.

Stanhill, G. 1969. A Simple Instrument for the Field Measurement of Turbulent Diffusion Flux. J. Applied Meteorology 8:504-513.

Stewart, B.A., D.A. Woolhiser, W.H. Wischmeier, J.H. Caro, and M.H. Fere. 1976. Control of Water Pollution from Cropland, Volume II: An Overview. U.S. Environmental Protection Agency, Athens, GA. EPA-600/2-75-026b.

Streile, G.P. 1984. The Effect of Temperature on Pesticide Phase Partitioning, Transport, and Volatilization from Soil. Ph.D. dissertation, University of California, Riverside, CA.

Szeicy, G., G. Endrodi and S. Tajchman. 1969. Aerodynamic and Surface Factors in Evaporation. Water Resour. Res. 5(2):380-394.

Taylor, A.W. 1978. Post-Application Volatilization of Pesticides under Field Conditions. Journal of the Air Pollution Control Association 28:922-927.

Thibodeaux, L.J., C. Spencer, and L.M. Riley. 1982. Models of Mechanisms for the Vapor Phase Emission of Hazardous Chemicals from Landfills. Journal of Hazardous Materials 7:63-74.

Thibodeaux, L.J. 1979. Chemodynamics: Environmental Movement of Chemicals in Air, Water, and Soil. New York: John Wiley & Sons.

Thom, A.S., J.B. Stewart, H.R. Oliver, and J.H.C. Gash. 1975. Comparison of Aerodynamic and Energy Budget Estimates of Fluxes over a Pine Forest. Quarterly Journal of the Royal Meteorological Society 101:93-105.

van Bavel, C.H.M., and D.I. Hillel. 1976. A Simulation Study of Soil Heat and Moisture Dynamics as Affected by a Dry Mulch. In: Proceedings of 1975 Summer Computer Simulation Conference, San Francisco, California, pp. 815-821. Simulation Councils, Inc., La Jolla, CA.

van Bavel, C.H.M. and D.I. Hillel. 1975. Calculating Potential and Actual Evaporation from a Bare Soil Surface by Simulation of Concurrent Flow of Water and Heat. Agri. Meteorol. 17:453-476.

van Genuchten, M. T., and W.J. Alves. 1982. Analytical Solutions of the One-Dimensional Convective-Dispersive Solute Transport Equation. U.S. Technical Bulletin No. 1661. 151 pp.

van Genuchten, M. T. 1976. A Closed-form Equation for Predicting the Hydraulic Conductivity of Unsaturated Soils. Soil Sci. Soc. J. 44:892-898.

Wagenet, R.J., and J.W. Biggar. 1987. Measurement and Interpretation of DBCP Fate in Agricultural Soils. Journal of Environmental Quality (in press).

Wagenet, R.J., and J.L. Hutson. 1987. Leaching Estimation and Chemistry Model. Department of Agronomy, Cornell University, Ithaca, NY.

Wark, K., and C.F. Warner. 1976. Air Pollution: Its Origin and Control. New York: Harper and Row Publishers.

White, Jr., A.W., L.A. Harper, R.A. Leonard, and J.W. Turnball. 1977. Trifluralin Volatilization Losses from a Soybean Field. Journal of Environmental Quality 6:105-110.

Wilke, O., and E.T. Smerdon. 1965. A Solution of the Irrigation Advance Problem. ASCE Journal of Irrigation and Drainage 91(IR3):23-24.

Williams, J.R., C.A. Jones, and P.T. Dyke. 1984. A Modeling Approach to Determining the Relationship Between Erosion and Soil Productivity. Trans. ASAE 27:129-144.

Williams, J.R. 1975. Sediment Yield Prediction with Universe Equation Using Runoff Energy Factor In: Present and Prospective Technology for Predicting Sediment Yields and Sources. U.S. Department of Agriculture. AR5-5-40.

Willis, G.W., L.L. McDowell, L.A. Harper, L.M. Southwick, and S. Smith. 1983. Seasonal Disappearance and Volatilization of Toxaphene and DDT from a Cotton Field. J. Environ. Qual., 12:80-85.

Wilson, J.L., and P.J. Miller. 1978. Two-Dimensional Plume in Uniform Groundwater Flow. J. Hydraulics Div., ASCE 104,HY4.

Woodward-Clyde Consultants. 1988. Multimedia Exposure Assessment Model for Evaluating the Land Disposal of Hazardous Wastes. EPA Contract No. 68-03-6304. Work Assignment No. 1. Draft Report.

Wunderlich, W.O. 1972. Heat and Mass Transfer Between a Water Surface and the Atmosphere. Laboratory Rpt. No. 14 T.V.A. Eng. Lab., Norris, TN.

Yeh, G.T., and D.S. Ward. 1981. FEMWASTE: A Finite-Element Model of Waste Transport Through Saturated-Unsaturated Porous Media. Rep. ORNL-5601, Oak Ridge National Laboratory, Oak Ridge, TN. 137 pp.

SECTION 8

APPENDICES

8.1 QUALITY ASSURANCE

The quality assurance program for this model development program effort was broken down into two phases:

- Algorithms
- Software

The quality assurance aspects for these entities are discussed in the following sections.

8.1.1 Algorithms

The purpose of the quality assurance program for model algorithm development is to reduce or eliminate "model error" caused by the use of algorithms that are inappropriate, have assumptions which are frequently violated, have extensive data requirements, or produce biased results. A second purpose is to ensure that algorithms which are appropriate are implemented properly in the computer. The final purpose is to ensure that the code developed is capable of simulating results that are physically realistic and meaningful.

The quality assurance plan for algorithm development has three facets:

- Selection
- Implementation
- Testing

Algorithm selection was initially done by the individual or organization responsible for its development. Normally, the selection process was initiated by a literature review. The key criterion for initial selection was that the algorithms be physically based with parameters which could be easily estimated from readily available information. In addition, it was desirable that the algorithms had been tested against field or laboratory data and shown to be robust under a wide variety of circumstances. These initially selected algorithms were then proposed in a memorandum or oral presentation format to the model development team at one of a series of technical meetings which were held every 6 to 8 weeks during project execution. Changes suggested by reviewers were considered before committing the algorithms to a FORTRAN format.

Algorithm implementation was carried out by the same individual(s) who selected the algorithm. Each algorithm implemented was tested in one of several ways. First, if mass balance was a consideration, an acceptable closure for mass had to be obtained. Second, the "realism" of simulation was checked. This was done, under the most favorable circumstances, by checking the results of the simulations against published results of other similar models, analytical solutions, or data with which other models were developed. If other results were not available, algorithms were checked simply to see if they produced results which were reasonable based on the judgment of the developer and the rest of the model development team. Results of implementation testing were often reperformed or at least reviewed by other members of the model development team, often on different computer systems.

The final phase of algorithm QA was testing. Once all the individual pretested modules of code were assembled, the complete package was tested for mass balance realism. "Realism" was judged by comparing the simulation results to observed field data. In this case, the observed data were for the pesticide aldicarb in a contaminated, unconfined aquifer in Long Island, New York. The final testing was done by Woodward-Clyde Consultants, while model algorithm and software development were done primarily by Woodward-Clyde, HydroGeologic, and Aqua Terra Consultants. Thus, a high degree of objectivity was maintained in the initial code testing phase, included in the development effort. Continued model testing and evaluation is being performed under the support of the EPA Center for Exposure Assessment Modeling (CEAM) in Athens, GA by EPA scientists, contractors, and selected 'beta' test sites/organizations across the country.

8.1.2 Software

Given the large amount of new computer code required for this project, combined with the fact that several different firms were involved in code development, there was a great need for a systematic approach to software development and testing. Our software quality assurance program consisted of the following activities:

Software Development

- Use of structured code
- Use of standardized coding conventions

Software Testing

- Review of code capabilities versus project specifications
- Code analysis using Maintainability Analysis Tool (MAT)
- Testing as many code options as possible
- Compilation and testing of code on different machines

8.1.2.1 Quality Assurance in Software Development

In developing the RUSTIC program, the use of structure in design, implementation, and documentation was emphasized. The concepts of "structured programming technology" (IBM 1974) have been used extensively. It has been found that the use of these methods leads to computer programs

and documentation which are easier to understand than those produced by conventional methods. Also, the software has a unified underlying structure and is easier to maintain.
Coding conventions are particularly useful when different groups are jointly developing software and when groups that support the software are different from the groups that develop the software. With the use of conventions, the software can more easily be read, understood, debugged, and maintained. We have used the USGS Office of Surface Water's FORTRAN coding conventions (Kittle et al. 1986) as the basis for code development related to this project.

8.1.2.2 Quality Assurance in Software Testing
Considerable effort was expended to ensure the functional capabilities of the RUSTIC code prior to its release. Throughout the project, the code capabilities were reviewed to ensure that the evolving code was capable of performing according to the project goals and requirements. The quality of new subroutines and progress was assessed by applying the Maintainability Analysis Tool (Berns 1987) to completed code. The use of this FORTRAN static analyzer allows the checking of new or modified code after it has been successfully compiled. It supplements the compiler by analyzing the program as a whole rather than as individual source modules. By having this viewpoint, it identifies problems with common blocks and argument lists. Additionally, it notes bad programming practices, possible logic errors (i.e., variables referenced but not set), and deviations from standard FORTRAN.

After improving the code based on the suggestions of the static analyzer, a series of tests were performed which exercised as many program options as possible. While this testing resulted in the correction of many problems, it is anticipated that initial application studies using the new RUSTIC program will uncover additional oversights. As with any computer program, the user should carefully review input and results. Output review by the user should always include analysis of mass balance summaries reported by the RUSTIC process modules.

A final concern in software development is code portability. The RUSTIC code has been compiled and run on the IBM personal computer and the Prime computer running PRIMOS. Implementation of the current version on the IBM-PC requires greater than 640 K RAM. Adaptation to other machines should require minimal changes due to the coding conventions which were enforced during program development.

8.1.3 REFERENCES

Berns, G.M. 1987. "Reliable FORTRAN with MAT," Computer Language, Vol. 4, No. 6.

International Business Machines Inc. 1974. Structured Programming Textbook & Workbook -- Independent Study Program.

Kittle, J.L., Jr., A.L. Lumb, and T.D. Barnwell. 1986. ANNIE/WDMS FORTRAN Coding Convention and Documentation Software. U.S. Geological Survey Open File Report XXXX (Draft). Reston, VA.

☆U.S. GOVERNMENT PRINTING OFFICE:1989 -648-163/ 00324